ATTACHMENT I – UZ Data and Associated Data Tracking Numbers (DTNs)

I.1 Available Site Data

This section summarizes the data used in the AMRs supporting the UZ Flow and Transport PMR. The input data represent the current understanding of UZ flow and transport processes. Tables are presented to summarize the different data reviewed, analyzed, and developed in associated Analysis/Model Reports (AMRs). Some data sets are used in multiple analyses. The discussions associated with the tables cross-reference the relationships among data sets and AMRs. The details of analysis and modeling are given in individual AMRs and in Section 3. The Q-status of these data is provided in the DIRS database for the associated AMR. It should be noted that this Attachment is only intended to give the main data sets and the associated DTNs for the unsaturated zone, and is therefore not necessarily complete.

I.2 Geologic Data

The major inputs and outputs of the CRWMS M&O (2000, U0000), *Development of Numerical Grids for UZ Flow and Modeling*, are summarized in Table I-1 (with outputs presented in *italic*).

Table I-1. Geologic Data for the UZ Model

Data Description	DTN or ACC
Geologic Framework Model, GFM3.1	MO9901MWDGFM31.000
Integrated Site Model, components	MO9901MWDISMRP.000 MO9804MWDGFM03.001
Repository layout configuration	MOL.19990409.001
Mesh files for model calibrations, CRWMS M&O 2000, U0000	
Tables supporting UZ Model grid development	*LB990501233129.001*
1-D hydrogeologic property set inversions and model calibration	*LB990501233129.002*
2-D fault hydrogeologic property calibration	*LB990501233129.003*
3-D UZ Model calibration	*LB990501233129.004*
3-D UZ Model calibration grid for non-water-perching mode	*LB990701233129.002*
Mesh file for generating 3-D UZ flow fields, CRWMS M&O 2000, U0000	*LB990701233129.001*

The primary data input for UZ Flow and Transport Model grids is GFM3.1 (Geological Framework Model) for lithostratigraphic layering and major fault geometry at Yucca Mountain. The GFM contains information about layer thickness and layer contact elevation, and defines fault orientation and displacement. Approximately 40 geologic units and 18 faults are incorporated into the 3-D UZ Flow and Transport Model grids. RPM3.0 (Rock Properties Model) files are used to further define the units, especially the zeolitic zones of CHn. The repository layout data are used to locate areas for enhanced grid resolution.

CRWMS M&O (2000, U0000) also uses inputs of hydrologic unit definitions, fracture data for hydrologic units, and elevation data on the water table and perched water bodies. The hydrologic unit definitions are based on matrix properties (Flint 1998) discussed in Section 2.2.3. Fracture data, discussed in Section 2.2.4, are used to formulate the dual-permeability (dual-k) meshes. The vertical columns in the meshes are from the TCw bedrock to the water table. Water table and perched water elevation data for the lower UZ boundary are discussed in Section 2.2.10.

The final 3-D mesh files for UZ flow fields in Table I-1 are developed with inputs from calibrated property sets, summarized in Section 2.2.11. The areal domain of the UZ models encompasses approximately 40 km^2 of the Yucca Mountain area. The areal grids are constructed with centers coinciding as close as practical with locations of surface-based boreholes, alcoves and niches, faults, ESF and ECRB drifts, and other domain nodes.

I.3 Infiltration/Climate Data

The USGS (2000, U0005) refines the climate estimates for the next 10,000 years. The climate AMR provides input to the USGS (2000, U0010), *Simulation of Net Infiltration for Modern and Potential Future Climates*. The major inputs and outputs are summarized in Table I-2.

Table I-2. Infiltration/Climate Data for the UZ Model

Data Description	DTN or ACC
Daily precipitation input for 1980-1995 calibration (file MOD3-PPT.DAT)	GS950208312111.001 GS950208312111.002 GS960908312111.004 GS970108312111.001
Summary of the Day Data from the National Climatic Data Center (NCDC) for the Period Ending in 1995: for California, Nevada, Utah, Arizona, New Mexico, Colorado, and Wyoming.	MO9811NCDCSDD0.000
Streamflow records for 5 Yucca Mountain gauging stations (Upper Pagany Wash, Lower Pagany Wash, Wren Wash, Drill Hole Wash, Upper Split Wash).	NWIS Database ATS#YD-200000269
Parameters for SOLRAD subroutine for equations defined in Flint et al. (1996).	GS960908312211.003
Soil-depth-class map (Figure 13, Flint et al., 1996).	GS960908312211.003
Geospatial input parameters acquired from Flint et al. (1996) (elevation, slope, aspect, latitude, longitude, soil type, soil-depth class) (file 30MSITE.INP).	GS960908312211.003
100-year stochastic daily precipitation input (files 4JA.S01 and AREA12.S01).	GS960908312211.003
Calculated flux rates from neutron holes	GS960508312212.008
SO4 infiltration flux	GS910908315214.003 GS931008315214.032
Infiltration map - base case, lower bound, upper bound, CRWMS M&O 2000, U0010	GS000399991221.002

The climate USGS (2000, U0005) also used diatom and ostracode data from Owens Lake 1984-1992 cores, radiometric dating and $\delta^{18}O$ data from Devils Hole, and earth orbital parameter data for the last 10 million years and the next 100,000 years. The three climate states in VA are replaced by (1) the modern interglacial climate for about the next 400 to 600 years, (2) the monsoon climate for the duration of 900 to 1,400 years, and (3) the glacial-transition climate for the duration of 8,000 to 8,700 years. The modern climate uses data from site and regional meteorological stations. The monsoon climate uses data from Nogales, Arizona, and Hobbs, New Mexico, as upper-bound analogs and present-day site data as lower bound analog. The glacial transition climate uses data from Spokane, Rosalia, and St. John, all in Washington state, as upper-bound analogs and data from Beowawe, Nevada, and Delta, Utah, as lower-bound analogs.

The infiltration USGS (2000, U0010) also used elevation data, bedrock permeability and property data, geology maps, and soil properties as documented in the AMR. Simulation results and averaged values were presented for 123.7 km^2 area for the net infiltration model domain, for the 38.7 km^2 area of the UZ Flow and Transport Model domain, and for the 4.7 km^2 area of the 1999 design potential repository area. Over the potential repository area, the mean net infiltration is 4.7 mm/yr for the modern climate (with 0.4 mm/yr for the mean lower bound and 11.6 mm/yr for the mean upper bound), 12.5 mm/yr for the monsoon climate (with 4.7 mm/yr for the mean lower bound and 20.3 mm/yr for the mean upper bound), and 19.8 mm/yr for the glacial-transition climate (with 2.2 mm/yr for the mean lower bound and 37.3 mm/yr for the mean upper bound).

I.4 Matrix Properties

Matrix properties include permeability, porosity, residual saturation, and the van Genuchten α and m parameters used to describe water retention and relative permeability relationships (van Genuchten 1980, pp. 892–898). The input to the matrix properties for UZ Flow and Transport Model layers to the CRWMS M&O (2000, U0090), *Analysis of Hydrologic Property Data,* is based on the data transmittal listed in Table I-3. The data of Busted Butte cores are used in CRWMS M&O (2000, U0060), *Radionuclide Transport Models under Ambient Conditions.*

Table I-3. Matrix Properties for the UZ Model

Data Description	DTN or ACC
Matrix hydrologic property data	GS960908312231.004
Matrix saturation, water potential and hydrologic property data	GS000399991221.004
Physical and hydraulic properties of core samples from Busted Butte	GS990308312242.007 GS990708312242.008

The sample collection and laboratory measurement methodologies are described by Flint (1998, pp. 11–19) and Rousseau et al. (1999, pp. 19–46). Core samples are grouped and analyzed according to the hydrogeologic units characterized by matrix properties (Flint 1998, pp. 19–46, CRWMS M&O 2000, U0000, Section 6.3, CRWMS M&O 2000, U0090, Section 6.2). Matrix permeability has been measured on 750 core samples from eight surface-based boreholes. Some

samples with permeabilities too low to measure (nondetect results) were retested with a low-detection-limit permeameter. The nondetect results were included in defining the low-permeability units, especially the zeolitic zones of CHn. Matrix porosity values are based on 105°C oven-dried measurements of 4,888 core samples, from 23 shallow boreholes and eight deep boreholes. The residual saturation is determined by relative humidity (RH) porosity and total porosity, with RH porosity determined in a 65°C and 65% RH oven. The RH drying process is designed to remove water contributing flow, leaving only bound water and water in the smallest pores (Flint 1998, p. 17). The van Genuchten parameters are based on desaturation data from 75 samples. Desaturation data, with water potential and saturation measured several times while a core sample is drying, are used to calculate α and m by least-square fitting.

I.5 Fracture Properties, Air Permeabilities, and Liquid Release/Seepage Data

Fracture properties include fracture permeability, fracture porosity, van Genuchen fracture α and m parameters, fracture frequency, intensity, fracture interface area, and fracture aperture. Fracture properties are developed from analyzing fracture survey data and air-injection test data in CRWMS M&O (2000, U0090), *Analysis of Hydrologic Property Data*. The fracture permeability and van Genuchten parameters are updated in CRWMS M&O (2000, U0035), *Calibrated Properties Model*, after calibrations together with core saturation and *in situ* potential data, as summarized in Section 2.2.11. The fracture van Genuchten parameters and porosities are compared with ESF seepage test results for confirmation purposes. The seepage test results and other drift-scale hydrologic testing and air-permeability data are summarized in CRWMS M&O (2000, U0015), *In Situ Field Testing of Processes*. The seepage test results are used in CRWMS M&O (2000, U0080), *Seepage Calibration Model and Seepage Testing Data*. The major inputs and outputs from these AMRs related to fracture properties are tabulated in Table I-4.

Table I-4. Fracture Geometry, Air Permeability, and Liquid Release/Seepage Data

Data Description	DTN or ACC
Fracture type (location, strike, dip, length):	
Sta. 0+60 to 4+00	GS971108314224.020
Sta. 4+00 to 8+00	GS971108314224.021
Sta. 8+00 to 10+00	GS971108314224.022
Sta. 10+00 to 18+00	GS971108314224.023
Sta. 18+00 to 26+00	GS971108314224.024
Sta. 26+00 to 30+00	GS971108314224.025
Sta. 30+00 to 35+00	GS960708314224.008
Sta. 35+00 to 40+00	GS960808314224.011
Sta. 40+00 to 45+00	GS960708314224.010
Sta. 45+00 to 50+00	GS971108314224.026
Sta. 50+00 to 55+00	GS960908314224.014
Sta. 55+00 to 60+00	GS971108314224.028
Sta. 60+00 to 65+00	GS970208314224.003
Sta. 65+00 to 70+00	GS970808314224.008
Sta. 70+00 to 75+00	GS970808314224.010
Sta. 75+00 to 78+77	GS970808314224.012
Sta. 4+00 to 28+00, Alcoves 3 and 4	GS960908314224.020
Alcove 5	GS960908314224.018
Alcove 6	GS970808314224.014
ECRB Cross Drift	GS990408314224.001
	GS990408314224.002
Fracture frequency:	
15 model units from 14 borehole locations	GS970408314222.003
NRG-7a	SNF29041993002.084
SD-12	TM000000SD12RS.012
Fracture type:	
Outcrop survey of Calico Hills formation	GS970308314222.001
Line surveys in the Bullfrog Member of the Crater Flat Tuff from Raven Canyon	GS930608312332.001
Line surveys in the Bullfrog Member of the Crater Flat Tuff from east side of Little Skull Mountain in Yucca Mountain Area	GS930608312332.002

Table I-4. Fracture Geometry, Air Permeability, and Liquid Release/Seepage Data (Continued)

Data Description	DTN or ACC
Air-injection test data:	
surface-based boreholes	GS960908312232.012
	GS960908312232.013
Alcoves 1, 2, 3 (upper TCw, Bow Ridge fault, upper PTn)	GS970183122410.001
Alcove 4 lower PTn fault-matrix interaction test bed	LB980901233124.009
Alcove 5 – single heater test area	LB960500834244.001
Alcove 5 – drift scale test area	LB970600123142.001
	LB980120123142.004
	LB980120123142.005
Alcove 6 fracture-matrix interaction test bed	LB980901233124.004
Niches 3566 and 3650, pre-excavation and post-excavation data	LB980001233124.002
Niches 3107 and 4788, pre-excavation and post-excavation data	LB980901233124.001
Niches, pre-excavation and post-excavation analyses	LB990601233124.001
Niche 4788, Alcoves 4 and 6, cross-hole analyses, and	LB990901233124.004
4 niches and 2 alcoves, statistical analyses	
Niche 3107 and Alcove 5, air-injection , tracer test and fracture porosity data	LB980912332245.002
Fracture properties for the UZ Model grids and uncalibrated fracture and matrix properties for the UZ model layers, CRWMS M&O 2000, U0090	*LB99050501233129.001*
Seepage and liquid release data:	
Niches 3566 and 3650, pre-excavation liquid-release data, and	LB980001233124.003
Niche 3566, post-excavation seepage data	
Niches 3566, 3650, 3107 and 4788, pre-excavation liquid-release data and analyses, and	LB980901233124.003
Niche 3566, post-excavation seepage analyses	
Niche 3107, post-excavation seepage test data	LB990601233124.002
Seepage Calibration model, software routines and files, CRWMS M&O 2000, U0080	*LB990831012027.001*

Table I-4. Fracture Geometry, Air Permeability, and Liquid Release/Seepage Data (Continued)

Data Description	DTN or ACC
Infiltration and seepage data, Alcove 1 upper TCw El Nino test	GS000399991221.003
Water intake rate and wetting front detection data	
Alcove 4 lower PTn fault-matrix interaction test bed	LB990901233124.005
Alcove 6 fracture-matrix interaction test bed	LB990901233124.002

The precalibrated fracture permeabilities are based on air permeabilities from air-injection tests in vertical boreholes and ESF alcoves. For TCw, fracture permeabilities were based on tests in four vertical boreholes (NRG-7/7A, NRG-6, SD-12, and UZ-16) and Alcoves 1, 2, and 3. For PTn, permeability data are from one borehole (NRG-7/7A) and Alcove 3. For TSw, the permeability data are from the four boreholes and the tests at the Single Heater Test and the Drift Scale Test areas in Alcove 5. For CHn, permeability data are from a single sampled interval in borehole UZ-16. No air-injection data are available for the Prow Pass, Bullfrog, and Tram units. For model layers where no data are available, analogs to other units are used. The fracture properties in faults are based on air-injection tests in Alcove 2 for the Bow Ridge fault and in Alcove 6 for the Ghost Dance fault. The fracture permeabilities are used as prior information for the calibrated properties model CRWMS M&O (2000, U0035).

The test-interval lengths between packers were approximately 4 m for vertical boreholes, 1 to 3 m for Alcoves 1, 2, and 3, and 5 to 12 m in the Alcove 5 SHT and DST areas. Extensive air-permeability data on the scale of 0.3 m were measured in the niches (CRWMS M&O 2000, U0015). For Tptpmn, the niche data sets have approximately one order of magnitude lower mean values and two orders of magnitude higher range than the vertical borehole values. In this comparison, only the pre-excavation permeability values from the niche sites are used. The post-excavation data are used in the seepage calibration model CRWMS M&O (2000, U0080).

The detailed line survey (DLS) data along ESF, together with air-permeability data, are the primary data sets used to derive other fracture properties. Borehole fracture data were used only when no data or incomplete data were available from the ESF DLS. Fracture spacing and frequency are calculated from averaging the DLS. The fracture intensity is calculated by dividing the trace length of the fracture by the area surveyed. Fracture interface area is calculated by dividing the fracture area by the volume of the interval surveyed. Fracture apertures are calculated by the cubic law relationship. The van Genuchten fracture m parameter is determined by fitting an analytical solution resulting from the aperture size distribution to the fracture saturation-capillary pressure curve. The fracture alpha parameter (α_f) is related to the aperture by the Young-LaPlace equation. For Tptpmn, the average of $\log(\alpha_f)$ value is -3.17 from the fracture network estimation, compared to the value of -3.16 from averaging over seepage tests in five niche borehole intervals.

Fracture porosities are derived from a combination of field gas-tracer-test data and estimates from the geometry of fracture network. The porosities from gas-tracer tests range from 0.6% to

2%. The porosities from drift seepage tests have the average value of 1.3% from three water-content values determined from seepage front arrival times. The value of 1% is used as an order-of-magnitude estimate for Tptpmn (model layer tsw34). For model layers without field test data, fracture porosities are estimated from aperture and frequency of the fracture network, and relative values are scaled to the tsw34 value.

I.6 Pneumatic Data

The CRWMS M&O (2000, U0035), *Calibrated Properties Model*, uses the borehole pneumatic data in the inversions to calibrate the tuff model-layer and fault properties. The CRWMS M&O (2000, U0015), *In Situ Testing of Processes*, compiled the moisture monitoring data collected along the drifts and in alcoves for the evaluation of moisture removal induced by ventilation operations. Both data sets are summarized in Table I-5.

Table I-5. Pneumatic Data for the UZ Model

Data Description	DTN or ACC
In situ data in surfaced-based boreholes:	
NRG-6 and NRG-7a, pneumatic pressure and temperature	GS950208312232.003 GS951108312232.008 GS960308312232.001 GS960808312232.004
NRG#5, pneumatic pressure	GS960208312261.001
SD-7, pneumatic pressure	GS960908312261.004
UZ-7a, NRG-6, NRG-7a, and SD-12, pneumatic pressure and temperature	GS960308312232.001
UZ#4, UZ#5, UZ-7a, NRG-6, NRG-7a, and SD-12, pneumatic pressure, temperature, and water potential	GS970108312232.002
UZ#4, UZ#5, UZ-7a, NRG-7a, and SD-12, pneumatic pressure, temperature, and water potential:	
1/1/97 - 6/30/97	GS970808312232.005, MOL.19980226.0042-0045
7/1/97 - 9/30/97	GS971108312232.007, MOL.19980226.0607-0614
10/1/97 - 3/31/98	GS980408312232.001, MOL. 19980706.0269

Table I-5. Pneumatic Data for the UZ Model (Continued)

Data Description	DTN or ACC
Moisture monitoring data in underground drifts:	
21+00/LB20, 28+30/LB50, 35+00/LB40	LB960800831224.001
21+00/LB20, 28+30/LB50, 35+00/LB40, 42+50/LB60, 47+00/LB70, 51+73/LB80, 57+50/LB90, 64+59, 67+00, 73+50 10/1/96 – 1/31/97	LB970300831224.001
Before and After the Completion of the ESF	LB970801233124.001
	LB970901233124.002
7+20/GS#3, 10+93/GS#4, 28+93, 51+64, 67+20, 10/1/96 – 1/31/97	GS970208312242.001
2/1/97 – 7/3197	GS970708312242.002
8/1/97 – 7/31/98	GS980908312242.024
ECRB Cross Drift 0+25, 2+37, 2+88, 3+38, 10+03, 21+07, 24+75, 4/8/98 – 7/31/98	GS980908312242.035
ECRB Cross Drift 14+35, 21+40, 25+55	LB990901233124.006

Pneumatic pressure data measured *in situ* in five boreholes (NRG#5, NRG-6, NRG-7a, SD-7, and SD-12) are used in the 1-D inversion. These boreholes do not intersect known large faults, and thus the pneumatic pressure data are representative of the formation rock of Yucca Mountain. Pneumatic pressure data measured in borehole UZ-7a are used in the 2-D inversion for fault properties. This borehole intersects the Ghost Dance fault, and thus the pneumatic pressure data are representative of the faulted rock of Yucca Mountain.

Thirty days of data from each borehole are used for either the simultaneous inversion of five borehole columns or for the 2-D inversion for fault properties. The data are selected from the time period prior to detection of any influence associated with construction of the ESF. Most of the attenuation and lag of barometric signal occurs within the PTn and not in the fractured TCw or TSw. The data from all PTn instrument stations or ports, along with data from one TCw port (nearest to the bottom) and two TSw ports (uppermost and lowest), are used in the inversions. PTn contains multiple layers and has heterogeneous permeability distributions calibrated by pneumatic inversion.

With the penetration of the ESF drifts underground, atmospheric conditions were introduced into deep tuff units along the drifts. The barometric signals in the TSw ports became less attenuated as the ESF passed by the boreholes. In addition to barometric pressure, relative humidity, temperature, and/or air velocities are monitored along the drifts and in the alcoves, as summarized in Table I-5. The moisture conditions in the drifts are sensitive to the ventilation operations. Ventilation can remove the moisture, dry up the rock, and suppress the seepage. The perturbation to the ambient UZ conditions by the ESF drifts is *de facto* a mountain scale test at Yucca Mountain. UZ model calibration for the ambient conditions does not use the post-penetration data. Detected changes in pneumatic and moisture conditions can be used to validate

the models, assess the impacts of drift construction and operation, and provide inputs to repository design.

I.7 Saturation Data

The CRWMS M&O (2000, U0035), *Calibrated Properties Model*, uses the core saturation data summarized in Table I-6 in the inversions to calibrate the tuff model-layer and fault properties. The CRWMS M&O (2000, U0015), In Situ *Testing of Processes*, compiled the saturation data collected in alcoves and niches. The saturation data sets are summarized in Table I-6.

Table I-6. Saturation Data for the UZ Model

Data Description	DTN or ACC
Saturation data from surface-based borehole cores:	
UZ-7a, UZ-14, UZ#16, SD-7, SD-9, and SD-12	GS000399991221.004
SD-6	GS980808312242.014
WT-24	GS980708312242.010
Saturation data from underground borehole cores	
Alcove 3, 1 borehole	GS980908312242.033
Alcove 4, 2 boreholes	GS980908312242.032
North Ramp, 7+27 – 10+70	GS980308312242.005
South Ramp, 59+65 – 76+33	GS980308312242.003
3 boreholes in Alcove 6,	GS980908312242.029
1 borehole in Alcove 7	GS980908312242.028
Niche 3566, 3 main boreholes, 6 lateral boreholes	GS980908312242.018
Niche 3650, 7 main boreholes	GS980908312242.020
ECRB Cross Drift Starter tunnel, 1 slant borehole below the invert	GS980908312242.030
Time domain reflectometry measurements:	
South Ramp, 8/1/97 - 1/4/98	GS980308312242.001
Crossover point, ESF Main Drift 30+62 below the ECRB Cross Drift, 6/19/98 - 7/16/98	LB980901233124.014

Saturation data measured on core from seven deep boreholes (SD-6, SD-7, SD-9, SD-12, UZ-14, UZ#16, and WT-24) are used for the 1-D inversions. Saturation data measured on core from borehole UZ-7a are used for the 2-D inversions.

Some of the cores from shallow boreholes in alcoves and niches are affected by the drying process, which can decrease the saturation several meters into the rock from the drift walls. The dry samples are not used in UZ model calibrations. The time-domain reflectometry (TDR) sensors are widely used in soil studies and are applied in the ESF boreholes or walls for detection

of saturation changes and wetting front arrivals. Not included in Table I-6 are neutron-hole surveys in the ESF, which were widely used in the infiltration study.

I.8 Water Potential Data

The CRWMS M&O (2000, U0035), *Calibrated Properties Model*, uses the borehole water potential data in the inversions to calibrate the tuff model-layer and fault properties. The CRWMS M&O (2000, U0015), In Situ *Testing of Processes*, compiled the water-potential data in the ESF to evaluate the extent of the drying into the rock and *in situ* profiles along the drifts. The water-potential data sets are summarized in Table I-7.

Table I-7. Water-Potential Data

Data Description	DTN or ACC
In situ water-potential data with psychrometer in surface-based boreholes	
UZ#4, NRG-6, NRG-7a, SD-12, and UZ-7a	GS950208312232.003 GS951108312232.008 GS960308312232.001 GS960808312232.004 GS970108312232.002 GS970808312232.005 GS971108312232.007 GS980408312232.001
Psychrometer data in underground drifts	
Niche 3566, 3 main boreholes, 5 lateral boreholes, 5/9/97–10/21/97	LB980001233124.001
Niche 3650, 6 main boreholes, 7/1/97–7/28/97	
Niche 3107, 3 main boreholes, 12/22/97–1/8/98	
Cross over point, ESF Main Drift 30+62 below the ECRB Cross Drift, 6/19/98–7/16/98	LB980901233124.014
ECRB Cross Drift Starter tunnel, 1 slant borehole below the invert	LB980901233124.014
Heat dissipation probe (HDP) data in underground drifts:	
Niche 3566, 21 HDP, 11/4/97–7/31/98	GS980908312242.022
Alcove 7, 12/9/97–1/31/98	GS980308312242.007
South Ramp, 8/1/97–1/4/98	GS980308312242.002
ECRB Cross Drift 0+50–7+75, 6 HDP, 4/23/98–7/31/98	GS980908312242.036
ECRB Cross Drift	GS000399991221.001
Filter paper data on cores in underground drifts:	
Alcove 3, 1 core hole	GS980908312242.033
Alcove 4, 2 core holes	GS980908312242.032
North Ramp, 18 boreholes, Alcove 4, 3 boreholes, and South Ramp, 46 boreholes, HQ, 2-m length	GS980308312242.004

Five surfaced-based boreholes have enabled continuous measurements of *in situ* water potential with psychrometer since 1997 (see also Table I-5 on pneumatic pressure data). Data measured in four boreholes (UZ#4, NRG-6, NRG-7a, and SD-12) are used in the 1-D inversions for rock formation outside the fault zones. Data from UZ-7a intercepting the Ghost Dance fault are used in the 2-D inversions. The inversions use the *in situ* water-potential data summarized in the first entry of Table I-7 and the core saturation data of Table I-6.

Water-potential data measured in the ESF short boreholes and on cores generally have values substantially different from *in situ* values because of drying by drift ventilation or drying during drilling and/or handling. Drift-ventilation effects are minimized by bulkhead sealing in niches, Alcove 7, and in the second half of the ECRB Cross Drift. Preliminary data indicate that the water-potential values in the lower tuff units are in the range of -1 bar, substantially higher than values measured in the ESF Main Drift and/or sealed intervals in surface-based boreholes.

I.9 Geochemical Data

The CRWMS M&O (2000, U0085), *Analysis of Geochemical Data for the Unsaturated Zone*, and CRWMS M&O (2000, U0100), *Unsaturated Zone and Saturated Zone Transport Properties*, analyze and evaluate the UZ sorption and diffusion parameters for the UZ transport processes.

Table I-8. Geochemical Data for the UZ Model

Data Description	DTN or ACC
Mineralogic data:	
Model input and output files for mineralogic Model "MM3.0" Version 3.0.	LA9908JC831321.001
Mineralogic characterization of the ESF SHT Block	LASL831151AQ98.001
Chloride, chlorine-36, bromide, sulfate data:	
Deep boreholes, halide and ^{36}Cl analyses NRG-4, NRG-6, and NRG-7/7A UZ#16 UZ-14 SD-12	 LAJF831222AQ96.005 LAJF831222AQ96.014 LAJF831222AQ96.015 LAJF831222AQ97.007
ESF, Cl, ^{36}Cl, Br, S	LA9909JF831222.010 LA9909JF831222.005 LAJF831222AQ98.004
ESF, CWAT#1, #2, and #3, Cl, Br, S	LAJF831222AQ98.007
Niches 3566 and 3650, Cl, Br, S	LA9909JF831222.012
Tritium data:	
SD-7, SD-9, UZ-14, NRG-7a Alcoves 2 and 3 Alcove 5 SHT UZ-14, C#2, C#3, WT##, WT#17, WT-24, 10/06/97 – 07/01/98	GS951208312272.002 GS961108312261.006 GS970608312272.005 GS991108312272.004

Table I-8. Geochemical Data for the UZ Model (Continued)

Data Description	DTN or ACC
DST water and gas chemistry data:	
CO_2 gas analyses	LB991215123142.001
DST, 4th, 5th, and 6th Qtr. CO_2 data	LB990630123142.003
UZ diffusion and dispersivity coefficients:	MO9807SPAAREST.000 MO9810SPA00026.000 MO9807SPATBDOC.000
UZ retardation data:	
Np sorption column measurements	LA000000000034.002
Radionuclide elution data through crushed tuff columns and through fractured tuff columns	LAIT831341AQ95.001 LAIT831341AQ97.001
Radionuclide retardation measurements of Ba, CE, Se, Sr, U, Pu, and. Np	LAIT831341AQ96.001
Kd for zeolitic rocks in UZ transport model	LABR831371DN98.002
Busted Butte UZ transport test data:	
Tracer Breakthrough Concentrations	LA9909WS831372.001 LA9909WS831372.002
Radionuclide sorption coefficients of Np, Pu, U, Se	LA9909WS831372.003
Ground penetrating radar	LB990423123112.001 LB990423123112.002 LB000123123112.001
ESF tracer field test data:	
Alcove 6 fracture-matrix interaction test bed	LB990901233124.001
Niche 3650 drift seepage test	LB990601233124.003
Surface water data:	
Southern Nevada, 8/83 – 8/86, isotope content and temperature of precipitation	GS920908315214.032
Fortymile Wash, 1993 water year, water quality data	GS940308312133.002
Fortymile Wash, 1995 water year , water quality data	GS960308312133.001

Table I-8. Geochemical Data for the UZ Model (Continued)

Data Description	DTN or ACC
Pore water data:	
Triaxial-Compression Extraction	GS90090123344G.001
NRG-6, NRG7/7a, UZ-14 and UZ-N55, and UZ#16, chemical data from cores	GS950608312272.001
UZ-1, UZ-14, UZ#16, NRG-6, NRG-7a, SD-7, SD-9, Alcove 3 RBT#1, RBT#4, ESF rubble, 94-96	GS961108312271.002
10/1/96 – 1/31/97	GS970208312271.002
NRG-7a, SD-7, SD-9, SD-12, UZ-14, 2/1/97 – 8/31/97	GS970908312271.003
UZ-7a, WT-24, SD-6, SD-7, SD-12, 97 – 98	GS980108312272.004
UZ-14 and UZ-16	GS990208312271.001
Uranium isotopic data:	
SW Nevada–SE California, U isotopic analyses	GS930108315213.004
U and Th analyzed 1/94 – 9/96	GS960908315215.013
Alcove 5, 4/97 – 5/97	GS970508312271.001
12/96 – 12/97	GS980108312322.003
5/89 – 8/97	GS980208312322.006
1/15/98 – 8/15/98	GS980908312322.009
Strontium isotope data:	
4/8/88 – 5/2/89	GS920208315215.012
5/3/89 – 5/9/91	GS910508315215.005
5/10/91 – 2/28/92	GS920208315215.008
11/19/92 – 12/3/93	GS931008315215.029
12/6/93 – 8/17/94	GS941108315215.010
9/7/94 – 5/4/95	GS950608315215.002
SD-7 and ESF calcite	GS970908315215.011
WT-24 and J-13	GS981008315222.004
SD-9 and Sd-12	GS990308315215.004
SD-9 and SD-12, X-ray fluorescence elemental compositions	GS990308315215.003
UZ-1 carbon and oxygen data:	
UZ-1, ^{14}C	GS911208312271.009 GS930108312271.010 GS930408312271.020 GS940408312271.005 GS940408312271.008
UZ-1, $^{13}C/^{12}C$	GS911208312271.010 GS930108312271.009 GS930408312271.019
UZ-1, $^{13}C/^{12}C$ and $^{18}O/^{16}O$	GS940408312271.004

Geochemical data are used in the ambient geochemical model for CRWMS M&O (2000, U0050), *UZ Flow Models and Submodels.* Pore-water samples are mainly collected from eight boreholes (NRG-6, NRG-7A, SD-7, SD-9, SD-12, UZ#4, UZ-14, and UZ#16). Chloride concentrations are used in water-infiltration calibration to match the chloride distributions along the ESF and the ECRB Cross Drift. Hydro-geochemical simulations are carried out for the NRS-7A column and for the WT-24 column, with the calcite data available in the second borehole.

The transport properties are used in the CRWMS M&O (2000, U0060), *Unsaturated Zone Radionuclide Transport Model.* The K_d values for radionuclides ^{99}Tc, ^{237}Np, ^{239}U, and its daughter products (including the ^{235}U with modest absorption and long half-life) are among the important parameters used for the transport calculations. Colloidal transport is sensitive to filtration mechanisms, which are evaluated in the CRWMS M&O (2000, U0070), *Unsaturated Zone Colloid Transport Model.*

I.10 Temperature Data

The CRWMS M&O (2000, U0050), *UZ Flow Models and Submodels*, uses temperature profiles for calibration.

Table I-9. Temperature Data for the UZ Model

Data Description	DTN or ACC
In situ temperature data in surface-based boreholes NRG-6, NRG-7a, UZ#4, SD-12, and UZ-7a	GS950208312232.003 GS951108312232.008 GS960308312232.001 GS960808312232.004 GS970108312232.002 GS970808312232.005 GS971108312232.007 GS980408312232.001
Thermal conductivity, grain specific heat	SNT05071897001.012
Heat load data and repository footprint	SN9907T0872799.001
Hydrologic and thermal properties of drift design elements	SN9908T0872799.004
Effective thermal conductivity	SN9907T0872799.002

The recent data from six boreholes (NRG-6, NRG-7A, SD-12, UZ#4, UZ#5, UZ-7) are used for the calibration. The temperature profile data set (Sass et al. 1988) is one of the first sets of data used to indicate that the percolation flux is higher than the low value in the sub-mm/yr range. With low percolation flux, the convective contribution to heat transfer is suppressed. The deviation from conduction-only profiles is used to determine percolation flux.

I.11 Perched Water Data

The CRWMS M&O (2000, U0050), *UZ Flow Models and Submodels*, uses perched water data for calibration.

Table I-10. Perched Water Data for the UZ Model

Data Description	DTN or ACC
Water Table Elevations	MO9609RIB00038.000
Perched Water Elevations	
UZ-14	GS960308312312.005
WT-24	GS98058312313.001
G-2	GS970208312312.003
G-2	GS981008312313.003
SD-9 and NRG-7a	MOL.19980220.0164
SD-7	MOL.19971218.0442

The perched water elevations are used together with matrix liquid saturations and water potentials for the calibration. Perched water may occur where percolation flux exceeds the capacity of the tuff units to transmit vertical flux in the UZ. A permeability-barrier model and an unfractured zeolite model are used to determine the calibrated parameters for the perched water zones.

I.12 Calibrated Property Sets

The CRWMS M&O (2000, U0035), *Calibrated Properties Model*, uses the saturation-potential inversion described in Section 2.3.7 and the pneumatic inversion in Section 2.3.5 to generate the calibrated properties sets summarized in Table I-11. The calibrated property sets are used as inputs to the AMRs on UZ Flow and Transport Field.

Table I-11. Property Sets for the UZ Model

Data Description	DTN or ACC
Flow fields and calibrated hydrologic property set	LB971212001254.006
Top and bottom boundary temperatures, pressure, and boundary elevations	LB990701233129.002
Calibrated 1-D parameter set for the UZ Flow and Transport Model, FY99	
for basecase infiltration	*LB997141233129.001*
for upper-bound infiltration	*LB997141233129.002*
for lower-bound infiltration	*LB997141233129.003*
Drift scale calibrated 1-D property set, FY99	
for basecase infiltration	*LB990861233129.001*
for upper-bound infiltration	*LB990861233129.002*
for lower-bound infiltration	*LB990861233129.003*

Table I-11. Property Sets for the UZ Model (Continued)

Data Description	DTN or ACC
Calibration for CRWMS M&O 2000, U0035 Calibrated Properties Model	
for 1-D, mountain-scale calibration	*LB991091233129.001*
for 1-D, draft-scale calibration	*LB991091233129.002*
for 2-D, fault calibration	*LB991091233129.003*
for 1-D, calibrated fault properties for the UZ Flow and Transport Model	*LB991091233129.001*

Calibration of the UZ Flow and Transport Model is carried out in a series of steps. For the 1-D, mountain-scale calibration of formation rock (nonfault) parameters and the 2-D fault calibration, first, saturation and potential data are inverted, with permeabilities fixed. Second, the pneumatic data are inverted to calibrate the permeabilities. Third, the calibrated parameters are checked against the saturation and potential data and calibrated if necessary. And fourth, a "final" check against the pneumatic data is performed. The iteration can in principle be carried out with repeated cycles. As a result of the pneumatic inversion, site-scale fracture permeabilities in most of the TSw model layers are increased by almost two orders of magnitude compared to the prior information determined from air-injection tests. The air-injection tests use packed intervals with length a few meters or less, which is closer to the range of drift scale than site scale. In drift-scale calibration, the pneumatic pressure data are excluded. The drift-scale calibrated permeabilities are closer to drift-scale measured values.

The calibrated property sets are used as the starting point in other calibration models for different processes in different scales. The CRWMS M&O (2000, U0050), *UZ Flow Models and Submodels*, uses additional chloride, calcite, temperature and perched water data to formulate the UZ 3-D flow fields. The CRWMS M&O (2000, U0080), *Seepage Calibration Model and Seepage Testing Data*, uses UZ site-scale flow field as boundary conditions for additional drift scale calibration against niche seepage data. The CRWMS M&O (2000, N0120/U0110), *Drift-Scale Coupled Processes (DST and THC Seepage) Models*, uses the calibrated property and is validated against DST results. The CRWMS M&O (2000, U0060), *Unsaturated Zone Radionuclide Transport Model*, uses additional transport properties to evaluate radionuclide and colloid transport.

ATTACHMENT II – List of DTNs for Figures and Tables

The Q-status of the data listed in Tables II-1 and II-2 is provided in the DIRS database for this PMR.

Table II-1. DTNs for Figures

Figure Number	Data Tracking Number (DTN)
1-1.	N/A
1-2.	N/A
2.1-1.	N/A
2.1-2.	MO9901MWDGFM31.000
2.1-3.	MO9901MWDGFM31.000
2.1-4.	MO9901MWDGFM31.000
2.2-1.	LB980930123112.001
2.2-2.	(a) N/A (b) GS000399991221.002
2.2-3.	N/A
2.2-4.	(a) N/A (b) N/A (c) LAJF831222AQ98.004 LA9909JF831222.005 LA9909JF831222.010
2.2-5.	N/A
2.2-6.	(a) N/A (b) N/A (c) N/A (d) LB990901233124.002
2.2-7.	(a) N/A (b) N/A (c) N/A (d) LB990901233124.005
2.2-8.	(a) N/A (b) N/A (c) LB991131233129.002 GS000399991221.003
2.2-9.	N/A
2.2-10.	(a) GS000399991221.002 LB990801233129.003 (b) LB991131233129.001 (c) GS991299992271.001
2.2-11.	(a) N/A (b) GS980908315215.015 GS960908315215.014 (c) LAJF831222AQ98.011 GS991299992271.001
2.2-12.	(a) LB00032412213U.001 (b) N/A (c) N/A
2.2-13.	(a) N/A (b) N/A (c) LB980901123142.006
2.2-14.	N/A
2.4-1.	N/A [a]
2.4-2.	N/A [a]

[a] For historical perspective only.

Table II-1. DTNs for Figures (Continued)

2.4-3.	N/A [a]
2.4-4.	N/A [a]
3.2-1.	MO9901MWDGFM31.000
3.2-2.	N/A
3.2-3.	MO9901MWDGFM31.000
3.2-4.	N/A
3.2-5.	N/A
3.2-6.	MO9901MWDGFM31.000
3.2-7.	MO9910MWDISMMM.003
3.3-1.	N/A
3.3-2.	N/A
3.3-3.	N/A
3.3-4.	N/A
3.3-5.	N/A
3.3-6.	N/A
3.3-7.	N/A
3.3-8.	N/A
3.4-1.	N/A
3.4-2.	N/A
3.4-3.	(a) MO9901MWDISMMM.000 (b) MO9910MWDISMMM.003
3.4-4.	(a) MO9901MWDISMRP.000 (b) MO9910MWDISMRP.002
3.4-5.	LB990051233129.001
3.4-6.	(a) N/A (b) LB990501233129.004 (c) LB990701233129.001
3.4-7	(a) MO9901MWDGFM31.000 (b), (c) LB990701233129.001
3.4-8	(a) MO9901MWDGFM31.000 (b), (c) LB990701233129.001
3.4-9	(a) MO9901MWDGFM31.000 (b), (c) LB990501233129.004
3.5-1.	N/A
3.5-2.	(a) N/A (b) GS000399991221.002 (c) N/A
3.5-3.	N/A
3.5-4.	GS000399991221.002
3.5-5.	GS000399991221.002
3.5-6.	SN0003T0503100.001
3.6-1.	N/A
3.6-2.	N/A
3.6-3.	N/A
3.6-4	LB991091233129.001
3.6-5	LB991091233129.003
3.6-6.	LB997141233129.001
3.6-7.	LB997141233129.001
3.6-8.	GS960308312232.001 GS980908312242.036 LB990801233129.003 LB991121233129.007
3.6-9.	N/A
3.7-1.	N/A
3.7-2.	N/A
3.7-3.	LB990701233129.001

Table II-1. DTNs for Figures (Continued)

3.7-4.	(a) LB990801233129.003 (b) LB990801233129.015 (c) LB990801233129.009
3.7-5.	N/A
3.7-6.	MO9901MWDGFM31.000
3.7-7.	LB990801233129.003
3.7-8.	(a) LB990801233129.003 (b) LB990801233129.003
3.7-9.	LB990801233129.025
3.7-10.	(a) LB990801233129.003 (b) LB990801233129.003 (c) LB990801233129.004
3.7-11.	(a) LB990801233129.003 (b) LB990801233129.015 (c) LB990801233129.009
3.7-12.	(a) LB990801233129.003 (b) LB990801233129.015 (c) LB990801233129.009
3.7-13.	(a) LB990801233129.003 (b) LB990801233129.003
3.7-14	LB990801233129.003 LB990801233129.009 LB990801233129.015 GS000399991221.004
3.7-15	LB991121233129.007 GS960308312232.001
3.7-16.	SN9912T0581699.003 SN0001T0581699.004
3.7-17.	SN9912T0581699.003
3.7-18.	SN9912T0581699.003 SN0001T0581699.004
3.7-19	N/A
3.8-1.	N/A
3.8-2.	N/A
3.8-3	GS000399991221.002 LB990801233129.003
3.8-4.	LB991131233129.003
3.8-5	LB991131233129.003
3.8-6.	LB991131233129.001
3.8-7.	LB991131233129.003
3.8-8	N/A
3.9-1.	N/A
3.9-2.	N/A
3.9-3.	N/A
3.9-4.	LB990831012027.001
3.9-5.	LB990831012027.001
3.9-6.	LB980001233124.003 LB990831012027.001
3.9-7.	N/A
3.9-8.	N/A
3.9-9.	N/A
3.9-10.	SN9912T0511599.002
3.9-11.	SN9912T0511599.002
3.9-12.	N/A
3.10-1.	N/A
3.10-2.	N/A
3.10-3.	N/A

Table II-1. DTNs for Figures (Continued)

3.10-4	LB991200DSTTHC.002
3.10-5	LB991200DSTTHC.002
3.10-6.	LB991200DSTTHC.002
3.10-7.	LB991200DSTTHC.002
3.10-8.	LB991200DSTTHC.002
3.10-9.	LB991200DSTTHC.002
3.10-10.	LB991200DSTTHC.002
3.10-11.	LB991200DSTTHC.002
3.10-12.	LB991200DSTTHC.002
3.10-13.	N/A
3.11-1.	N/A
3.11-2.	N/A
3.11-3.	N/A
3.11-4.	LB991220140160.012
3.11-5.	LB991220140160.012
3.11-6.	LB991220140160.012
3.11-7.	LB991220140160.017
3.11-8.	LB9908T1233129.001
3.11-9.	LB9908T1233129.001
3.11-10.	LB991220140160.012 LB991220140160.017
3.11-11.	N/A
3.11-12.	SN9908T0581699.001 LB990901233129.001
3.11-13.	SN9908T0581699.001 LB990901233129.001
3.11-14.	SN9908T0581699.001 LB990901233129.001
3.11-15.	SN9908T0581699.001 LB990901233129.001
3.11-16.	N/A
3.12-1.	N/A
3.12-2.	N/A
3.12-3.	LB990701233129.001
3.12-4.	LB991201233129.001
3.12-5.	LB991201233129.001
3.12-6.	LB991201233129.001
3.12-7.	LB991201233129.001
3.12-8.	LB991201233129.001
3.12-9.	LB991201233129.001
3.12-10.	LB991201233129.001
3.12-11.	LB991201233129.001
3.12-12.	LB991201233129.001
3.12-13.	LB991201233129.001
3.12-14.	LA0004WS831372.002
5.1-1.	N/A
5.1-2.	N/A
5.1-3.	N/A
5.1-4.	N/A
5.1-5.	N/A

Table II-2. DTNs for Tables

Table	Data Tracking Number (DTN)
1-1.	N/A
1-2.	N/A
1.2-1	N/A
1.2-2.	N/A
1.2-3.	N/A
1.3-1.	N/A
2.3-1.	N/A
2.5-1.	N/A
3.2-1.	N/A
3.2-2.	N/A
3.4-1.	N/A
3.5-1.	N/A
3.5-2.	GS000399991221.002
3.5-3.	GS000399991221.002
3.5-4.	GS000399991221.002
3.7-1.	GS000399991221.002
3.7-2.	LB990801233129.003 LB990801233129.009 LB990801233129.015
3.7-3.	LB990801233129.003 LB990801233129.009 LB990801233129.015
3.7-4.	LB990801233129.003 LB990801233129.009 LB990801233129.015
3.7-5.	LB990801233129.001 LB990801233129.003 LB990801233129.005 LB990801233129.007 LB990801233129.009 LB990801233129.011 LB990801233129.013 LB990801233129.015 LB990801233129.017
3.8-1.	LB991131233129.001
3.9-1.	LB991101233129.001
3.9-2.	SN9912T0511599.002
3.10-1.	LB991200DSTTHC.001
3.10-2.	N/A
3.10-3.	MO9912SPAPAI29.002
3.11-1.	LA0003AM831341.001
3.11-2.	LA0003JC831362.001
3.11-3.	LB991220140160.012
3.11-4.	LA0004WS831372.002
3.12-1.	N/A
3.13-1.	N/A
4.2-1.	N/A
4.3-1.	N/A
5.2-1.	N/A

REFERENCES FOR ATTACHMENT II

CRWMS M&O 2000 (U0100). *Unsaturated Zone and Saturated Zone Transport Properties.* ANL-NBS-HS-000019. Input Transmittal 00104.T. Las Vegas, Nevada: CRWMS M&O. ACC: 20000310.0366.

CRWMS M&O 2000 (U0095). *Analysis of Infiltration Uncertainty.* ANL-NBS-HS-000027 REV 00. Input Transmittal 00113.T. Las Vegas, Nevada: CRWMS M&O. ACC: MOL.20000313.0632.

DTN: GS000399991221.002. Rainfall/Runoff/Runon 1999 Simulations. Submittal date: 03/10/2000.

DTN: GS000399991221.003. Preliminary Alcove 1 Infiltration Experiment Data. Submittal date: 03/10/2000.

DTN: GS000399991221.004. Preliminary Developed Matrix Properties. Submittal date: 03/10/2000.

DTN: GS960308312232.001. Deep Unsaturated Zone Surface-Based Borehole Instrumentation Program Data from Boreholes USW NRG-7A, USW NRG-6, UE-25 UZ#4, UE-25 UZ#5, USW UZ-7A, and USW SD-12 for the Time Period 10/01/95 through 3/31/96. Submittal date: 04/04/1996.

DTN: GS960908315215.014. Uranium and Thorium Isotope Data for ESF Secondary Minerals Collected Between March 1996 and July 1996. Submittal date: 09/25/1996.

DTN: GS980908312242.036. Water Potentials Measured With Heat Dissipation Probes in ECRB Holes from 4/23/98 to 7/31/98. Submittal date: 09/22/1998.

DTN: GS980908315215.015. Uranium and Thorium Isotope Data Including Calculated 230TH/U Ages and Initial 234U/238U Activity Ratios for in Situ Microdigestions of Outermost Opal-Rich Mineral Coatings from the Exploratory Studies Facility Analyzed Between 12/01/97 and 09/15/98. Submittal date: 09/23/1998.

DTN: GS991299992271.001. Preliminary Unsaturated Zone Borehole Hydrochemistry Data. Submittal date: 12/23/1999.

DTN: LA0003AM831341.001. Preliminary Revision of Probability for Sorption Coefficients (K_DS). Submittal date: 03/29/2000. Submit to RPC URN-0267

DTN: LA0003JC831362.001. Preliminary Matrix Diffusion Coefficients for Yucca Mountain Tuffs. Submittal date: 4/10/2000.

DTN: LA9909JF831222.005. Chlorine-36 Analyses of ESF and Busted Butte Porewaters in FY99. Submittal date: 09/29/1999.

DTN: LA9909JF831222.010. Chloride, Bromide, Sulfate, and Chlorine-36 Analyses of ESF Porewaters. Submittal date: 09/29/1999.

DTN: LA0004WS831372.002. Sorption of Np,Pu, and Am on Rock Samples From Busted Butte, NV. Submittal date: 04/19/2000. Submit to RPC.

DTN: LAJF831222AQ98.004. Chloride, Bromide, Sulfate, and Chlorine-36 Analyses of Salts Leached from ESF Rock Samples. Submittal date: 09/10/1998.

DTN: LAJF831222AQ98.011. Chloride, Bromide, Sulfate and Chlorine-36 Analyses of Springs, Groundwater, Porewater, Perched Water and Surface Runoff. Submittal date: 09/10/1998.

DTN: LB980001233124.003. Liquid Release Tests Performed to Determine if a Capillary Barrier Exists in Niches 3566 and 3650. Submittal date: 04/23/1998.

DTN: LB00032412213U.001. Busted Butte Ground Penetrating Radar Data Collected June 1998 through February 2000 at the Unsaturated Zone Transport Test (UZTT): GPR Velocity Data. Submittal date: 03/24/2000. Submit to RPC

DTN: LB980901123142.006. Laboratory Test Results of Hydrological Properties from Post-Test Dry-Drilled Cores in the Single Heater Test Area for the Final TDIF Submittal for the Single Heater Test. Submittal date: 08/31/1998.

DTN: LB980930123112.001. Surface to ESF Seismic Tomography. Submittal date: 09/30/1998.

DTN: LB990051233129.001. Extent of Vitric Region Used to Assign Material Properties in FY 9 UZ Model Layers; Figure 5 From AMR U0000, "Development of Numerical Grids for UZ Flow and Transport Modeling." Submittal date: 09/24/99.

DTN: LB990501233129.004. 3-D UZ Model Calibration Grids for AMR U0000. "Development of Numerical Grids of UZ Flow and Transport Modeling." Submittal date: 09/24/1999.

DTN: LB990701233129.001. 3-D UZ Model Grids for Calculation of Flow Fields for PA for AMR U0000, "Development of Numerical Grids for UZ Flow and Transport Modeling." Submittal date: 09/24/1999.

DTN: LB990801233129.001. TSPA Grid Flow Simulations for AMR U0050, "UZ Flow Models and Submodels." (Flow Field #1). Submittal date: 11/29/1999.

DTN: LB990801233129.003. TSPA Grid Flow Simulations for AMR U0050, "UZ Flow Models and Submodels." (Flow Field #3). Submittal date: 11/29/1999.

DTN: LB990801233129.004. TSPA Grid Flow Simulations for AMR U0050, "UZ Flow Models and Submodels." (Flow Field #4). Submittal date: 11/29/99.

DTN: LB990801233129.005. TSPA Grid Flow Simulations for AMR U0050, "UZ Flow Models and Submodels." (Flow Field #5). Submittal date: 11/29/1999.

DTN: LB990801233129.007. TSPA Grid Flow Simulations for AMR U0050, "UZ Flow Models and Submodels." (Flow Field #7). Submittal date: 11/29/1999.

DTN: LB990801233129.009. TSPA Grid Flow Simulations for AMR U0050, "UZ Flow Models and Submodels." (Flow Field #9). Submittal date: 11/29/1999.

DTN: LB990801233129.011. TSPA Grid Flow Simulations for AMR U0050, "UZ Flow Models and Submodels." (Flow Field #11). Submittal date: 11/29/1999.

DTN: LB990801233129.013. TSPA Grid Flow Simulations for AMR U0050, "UZ Flow Models and Submodels." (Flow Field #13). Submittal date: 11/29/1999.

DTN: LB990801233129.015. TSPA Grid Flow Simulations for AMR U0050, "UZ Flow Models and Submodels." (Flow Field #15). Submittal date: 11/29/1999.

DTN: LB990801233129.017. TSPA Grid Flow Simulations for AMR U0050, "UZ Flow Models and Submodels." (Flow Field #17). Submittal date: 11/29/1999.

DTN: LB990801233129.025. TSPA Grid Flow Simulations for AMR U0050, "UZ Flow Models and Submodels." Flow Field #25: Present Day Mean Infiltration for Flow-Through Perched-Water Conceptual Model. Submittal date: 3/11/00.

DTN: LB990831012027.001. Input to Seepage Calibration Model AMR U0080. Submittal date: 08/31/1999.

DTN: LB9908T1233129.001. Transport simulations for the low, mean, and upper infiltration scenarios of the present-day, monsoon, and glacial transition climates. Submittal date: 3/11/00.

DTN: LB990901233124.002. Alcove 6 Flow Data for AMR U0015, "In Situ Field Testing of Processes." Submittal date: 11/01/99.

DTN: LB990901233124.005. Alcove 4 Flow Data for AMR U0015, "In Situ Field Testing of Processes." Submittal date: 11/01/99.

DTN: LB990901233129.001. Input and Output Data for Verification of Dual-Continua Particle Tracker (DCPT) for AMR U0155, " Analysis Comparing Advect-Dispersion Transport Solution to Particle Tracking." Submittal date: 10/26/99.

DTN: LB991091233129.001. One-Dimensional, Mountain-Scale Calibration for AMR U0035, "Calibrated Properties Model." Submittal date: 10/22/1999.

DTN: LB991091233129.003. Two-Dimensional Fault Calibration for AMR U0035, "Calibrated Properties Model." Submittal date: 10/22/99.

DTN: LB991101233129.001. Model Input/Output Files Supporting Seepage Model for PA in AMR U0075, "Seepage Model for PA Including Drift Collapse." Submittal date: 11/30/99.

DTN: LB991121233129.007. Calibrated parameters for the present-day, mean infiltration scenario, used for simulations with perched water conceptual model #3 (non-perching) for the mean infiltration scenarios of the present-day, Monsoon and Glacial transition climates. Submittal date: 3/11/00.

DTN: LB991131233129.001. Modeling calcite deposition and percolation. Submittal date: 3/11/00.

DTN: LB991131233129.002. Modeling seepage and tracer tests at Alcove 1. Submittal date: 3/11/00.

DTN: LB991131233129.003. Analytical and Simulation Results of Chloride and Chlorine-36 Analysis. Submittal date: 3/11/00.

DTN: LB991200DSTTHC.001. Pore water composition and CO2 partial pressure input into THC simulations of the Drift Scale Test and the THC Seepage Model, Table 3 of AMR U0110/N0120. Submittal date: 3/11/00.

DTN: LB991200DSTTHC.002. Model Input and Output Files, Excel Spreadsheets and Resultant Figures which are Presented in AMR N0120/U0110, "Drift-Scale Coupled Processes (Drift-Scale Test and THC Seepage) Models." Submittal date: 12/15/99.

DTN: LB991201233129.001. The Mountain-Scale Thermal-Hydrologic Model Simulations for AMR U0105, "Mountain-Scale Coupled Processes (TH) Models." Submittal date: 12/15/99.

DTN: LB991220140160.012. Model Prediction of 3-D Transport, Present-Day Infiltration, #1 Perched Water Model, using EOS9nT Input and Output files. Submittal date: 3/11/00.

DTN: LB991220140160.017. Model Prediction of 3-D Colloid Transport, Present-Day Infiltration, #1 Perched Water Model, using EOS9nT Input and Output files. Submittal date: 3/11/00.

DTN: LB997141233129.001. Calibrated Base-case Infiltration 1-D Parameter Set for the UZ Flow and Transport Model FY99. Submittal date: 07/21/1999.

DTN: MO9901MWDGFM31.000. Geologic Framework Model. Submittal date: 01/06/1999.

DTN: MO9901MWDISMMM.000. Mineralogy Models. Submittal date: 01/22/1999. Submit to RPC.

DTN: MO9910MWDISMMM.003. ISM3.1 Mineralogic Models. Submittal date: 10/01/99.

DTN: MO9901MWDISMRP.000. ISM3.0 Rock Properties Models. Submittal date: 01/22/1999. Submit to RPC.

DTN: MO9910MWDISMRP.002. Rock Properties Model (RPM3.1). Submittal date: 10/06/1999.

DTN: MO9912SPAPAI29.002. PA Initial Abstraction of THC Model Chemical Boundary Conditions. Submittal date: 01/11/2000. Submit to RPC URN-0282.

DTN: SN0001T0581699.004. Supplemental Files to Support Base-case Particle-tracking Analysis for TSPA-SR (Total System Performance Assessment-Site Recommendation) (In Analysis/Model Report U0160, ANL-NBS-HS-000024). Submittal date: 01/06/2000.

DTN: SN0003T0503100.001. Weighting Factors for Low, Middle and High Climate Infiltration Rate Maps. Submittal date: 03/20/2000.

DTN: SN9908T0581699.001. Files to Support 1-D Comparison Between FEHM Particle Tracking and T2R3D Advective-Dispersive Transport Simulations along SD-9. Submittal date: 08/16/99.

DTN: SN9912T0511599.002. Revised Seepage Abstraction Results for TSPA-SR (Total System Performance Assessment-Site Recommendation). Submittal date: 12/15/99.

DTN: SN9912T0581699.003. Files to Support Base-case Particle-tracking Analyses (AMR U0160) for TSPA-SR. Submittal date: 12/13/99.

ATTACHMENT III – FIGURES

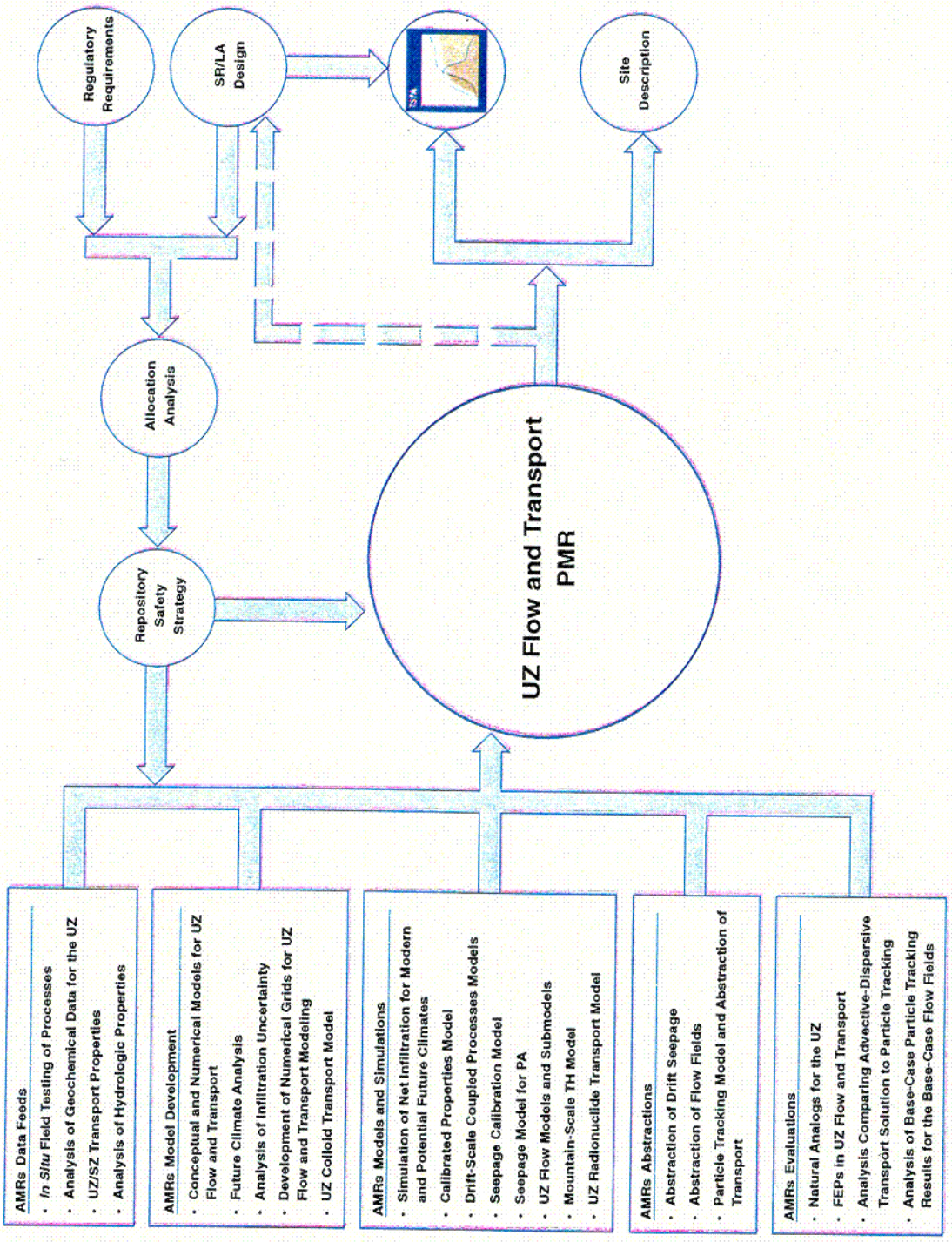

Figure 1-1. Schematic Diagram Showing the Relationships among Major YMP Documents, Including Analysis/Model Reports (AMRs), PMRs, SDs, SRR, and TSPA Documents

C001

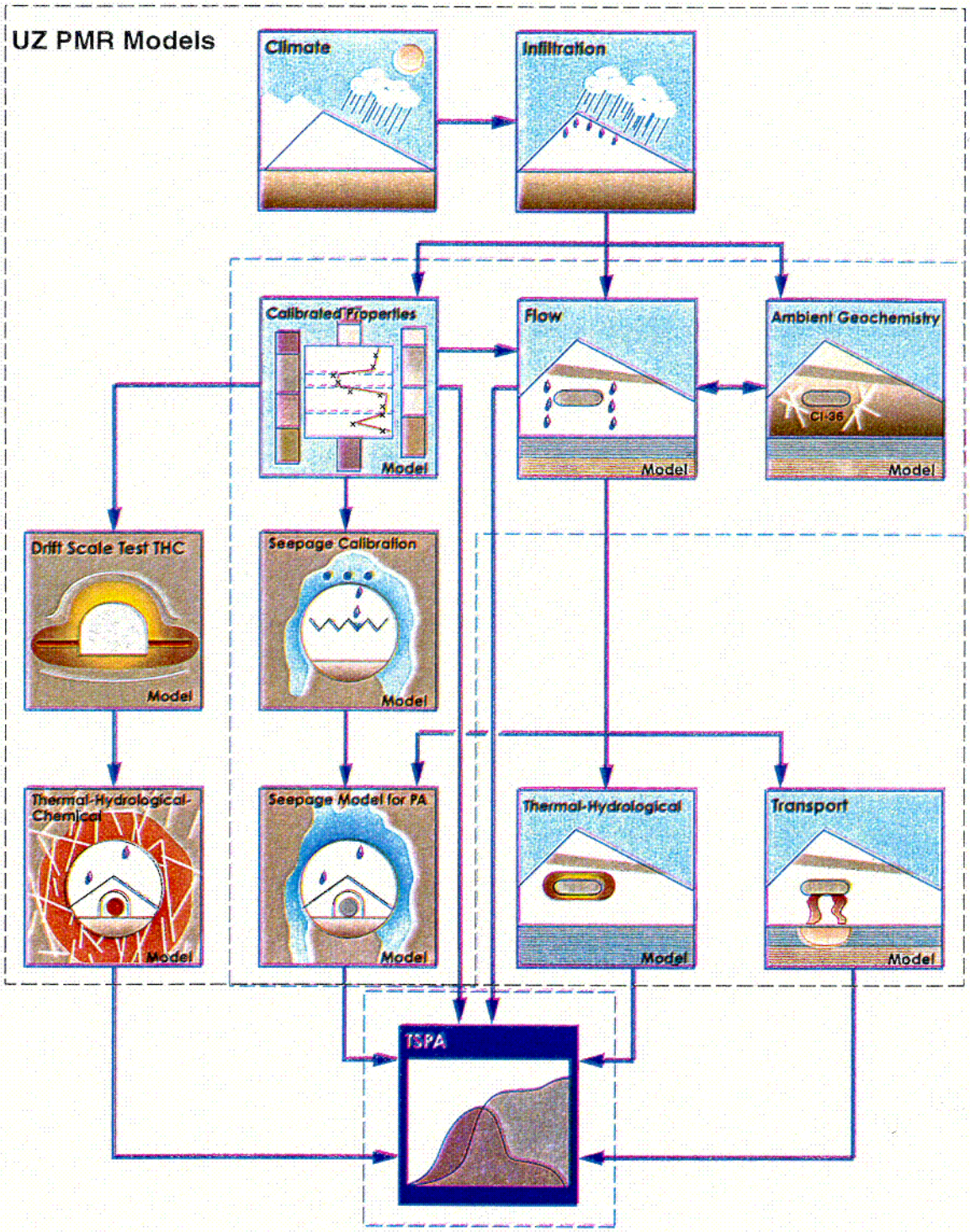

Figure 1-2. Main Models Included in the UZ PMR, Their Interrelations, and Their Connections to TSPA

C002

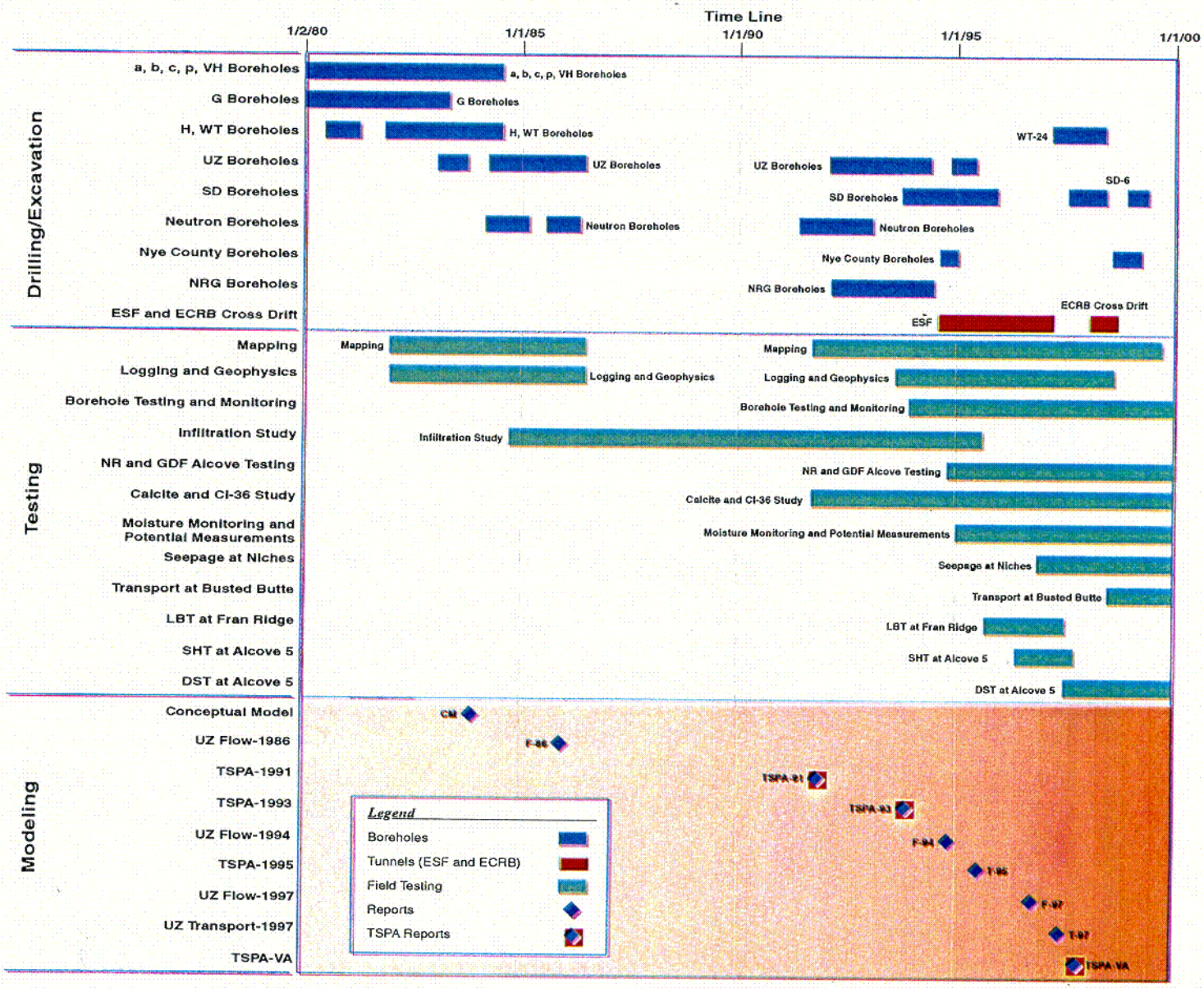

Figure 2.1-1. Chronology of Drilling/Excavation, Testing, and Modeling Activities of the UZ Site Characterization Program at Yucca Mountain

C003

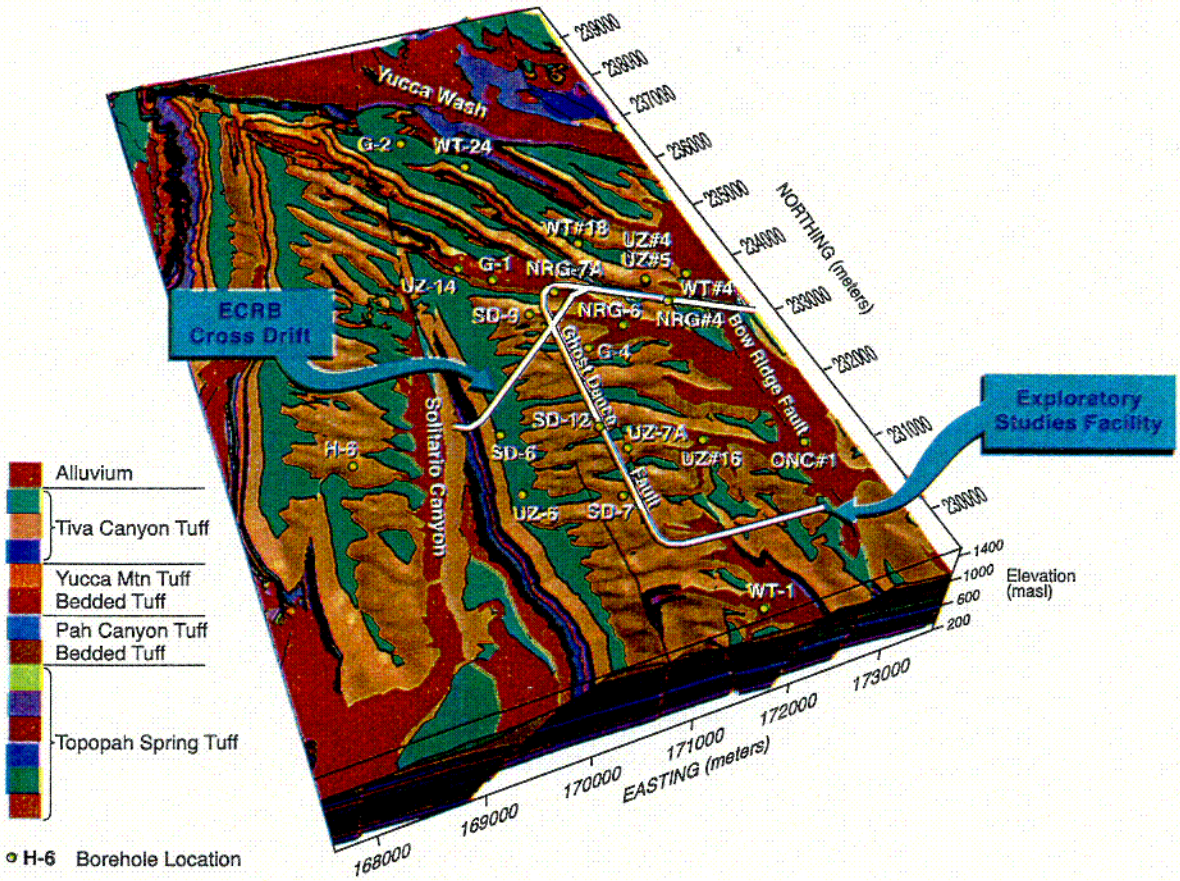

Figure 2.1-2. Schematic Illustration of the Main Surface-Based Deep Boreholes and Underground Drifts of the ESF, and the Major Faults in the Vicinity of Yucca Mountain

C004

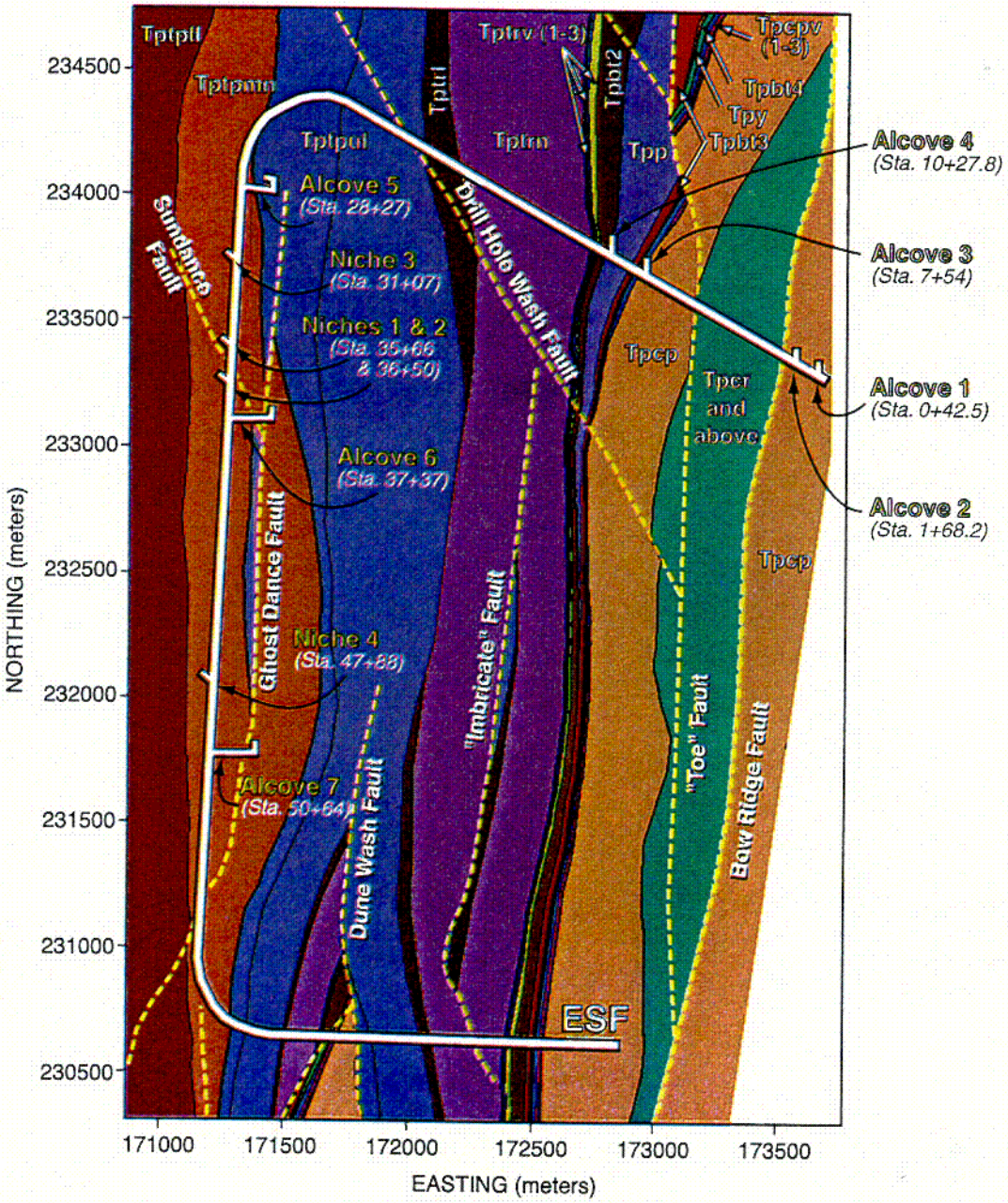

Figure 2.1-3. Schematic Illustration of Alcove and Niche Locations in the Exploratory Studies Facility at Yucca Mountain

C005

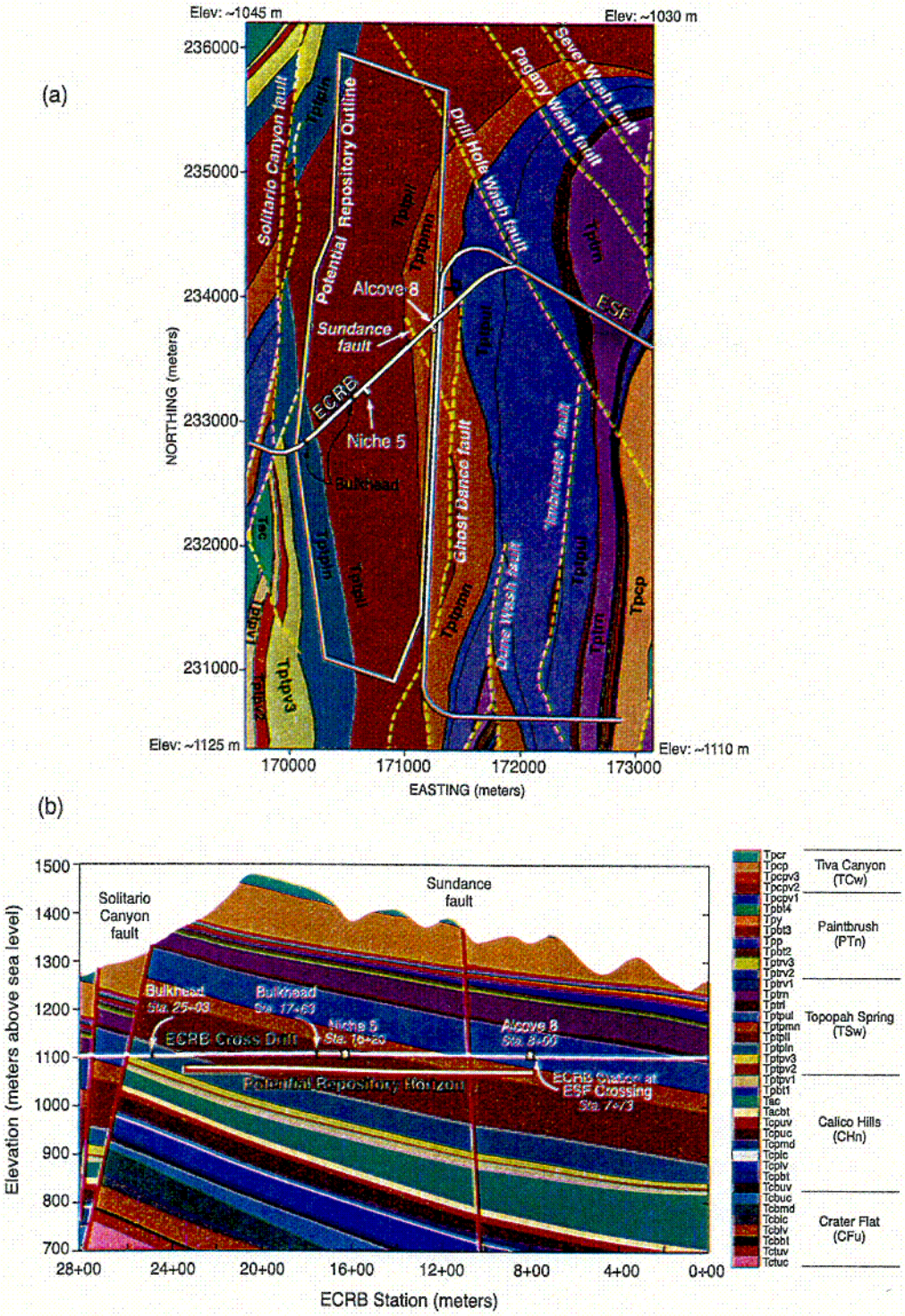

Figure 2.1-4. Schematic Illustration of the ECRB Cross Drift, Geological Units and Test Sites. (a) Generalized geological map at the Cross Drift level. (b) Generalized geological cross-section along the ECRB Cross Drift, showing the potential repository horizon.

C006

Geologic Mapping and Geophysical Studies on Surface and in ESF

(a) Drilling of Borehole SD-6 on the Crest of Yucca Mountain

(b) Pavement Cleared for Ghost Dance Fault Mapping

Objectives:

- Determine lithology and structural features of tuff units.
- Evaluate distribution of fractures and faults.

Approaches:

- Map features on bedrock, in trenches, and along ESF drifts.
- Conduct geophysical logging along boreholes.
- Deploy geophysical tomographic imaging techniques on the surface and in underground drifts.

Results:

- Refined geological maps of bedrock, washes and faults.
- Improved geological framework of tuff layers and fault offsets.
- Detailed line surveys and full peripheral maps along drifts.
- Interpreted fracture density distributions between surface and underground drifts.

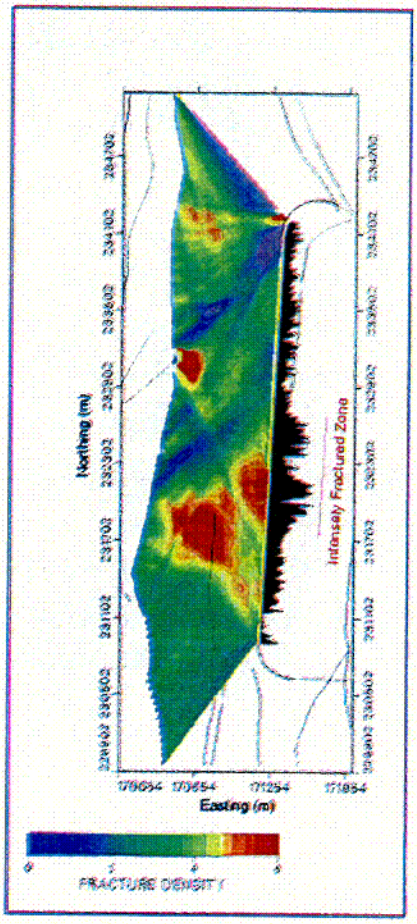

(c) Fracture Density Distributions by Detailed Line Survey and Seismic Tomograph

Figure 2.2-1. Geological and Geophysical Studies on the Surface and along the ESF

C 007

Infiltration Study on the Bedrock and in Washes

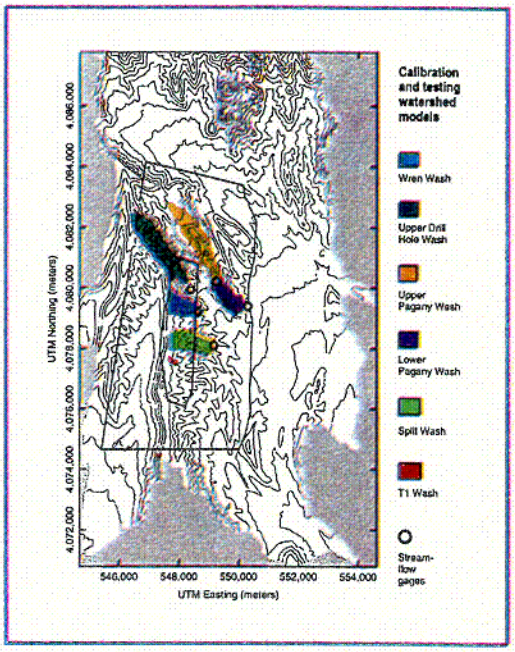

(a) Location of Washes Instrumented for Watershed Study

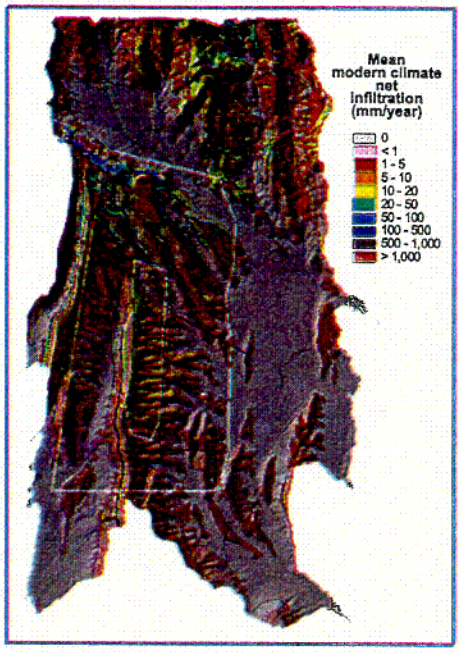

(b) Estimated Net Infiltration (mm/yr) for the Mean Modern Climate Scenario

Objectives:

- Provide upper boundary conditions for UZ Flow and Transport Model.
- Evaluate infiltration processes and mechanisms for determining net infiltration under current dry and future wet conditions.

Approaches:

- Conduct periodic neutron logging in network of shallow boreholes.
- Record climate changes and evaluate evapotranspiration potentials.
- Instrument washes to evaluate run-on and run-off processes.

(c) Neutron Logging at Pagany Wash

Results:

- Improved infiltration maps for current, monsoon, and glacial-transition climates.
- Quantification of relationships between precipitation and net infiltration.
- Quantification of downward flux and lateral run-on and run-off processes.

Figure 2.2-2. Infiltration Study on the Bedrock and in Washes (USGS 2000, U0010, Sections 6.3 and 7.1)

C008

Drift Seepage Test at Niche 3650

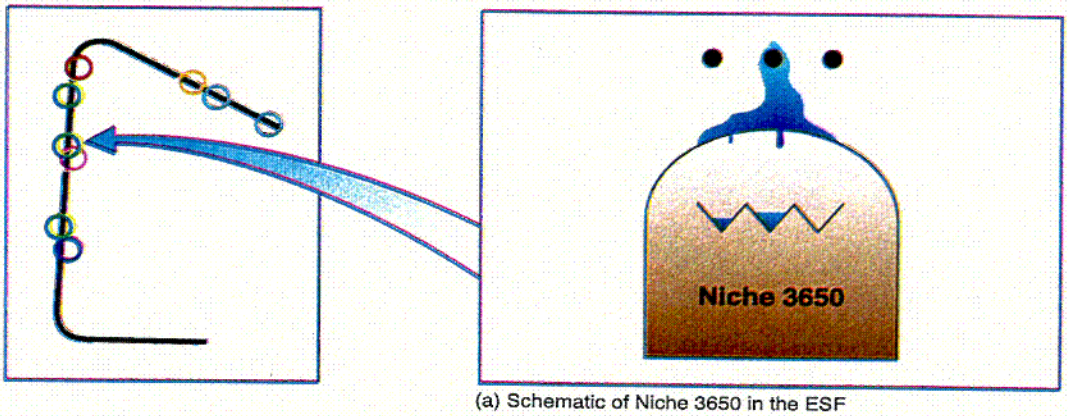

(a) Schematic of Niche 3650 in the ESF

Objectives:
- Quantify seepage threshold below which no seepage occurs.
- Evaluate capillary barrier mechanism and measure drift-scale parameters.

Approaches:
- Use air injection tests to characterize the niche site with resolution of 0.3-m scale (one tenth of drift dimensions).
- Use pulse releases to represent episodic percolation events.
- Determine seepage thresholds by sequences of liquid releases with reducing rates.
- Derive in situ fracture characteristic curves with wetting front arrival analyses.

Results:
- Measured seepage threshold ranges from 200 mm/yr to 136,000 mm/yr at localized release intervals.
- Six out of sixteen tested intervals did not seep.
- Observed both flow along high-angle fractures and flow through fracture network.
- Derived fracture capillary parameters and characteristic curves, with equivalent fracture porosity as high as 2.4%.

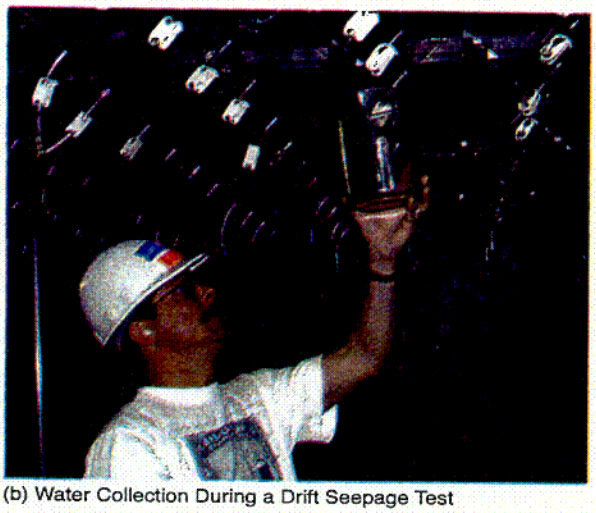

(b) Water Collection During a Drift Seepage Test

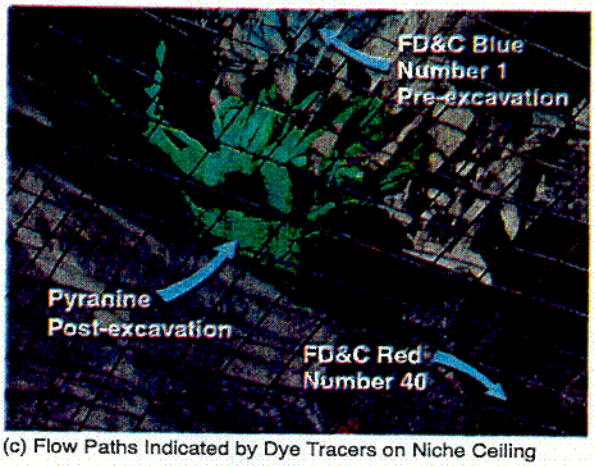

(c) Flow Paths Indicated by Dye Tracers on Niche Ceiling

Figure 2.2-3. Drift Seepage Test at Niche 3650 (CRWMS M&O 2000, U0015, Section 6.2.)

C009

In Situ Wet Feature Observed at Niche 3566

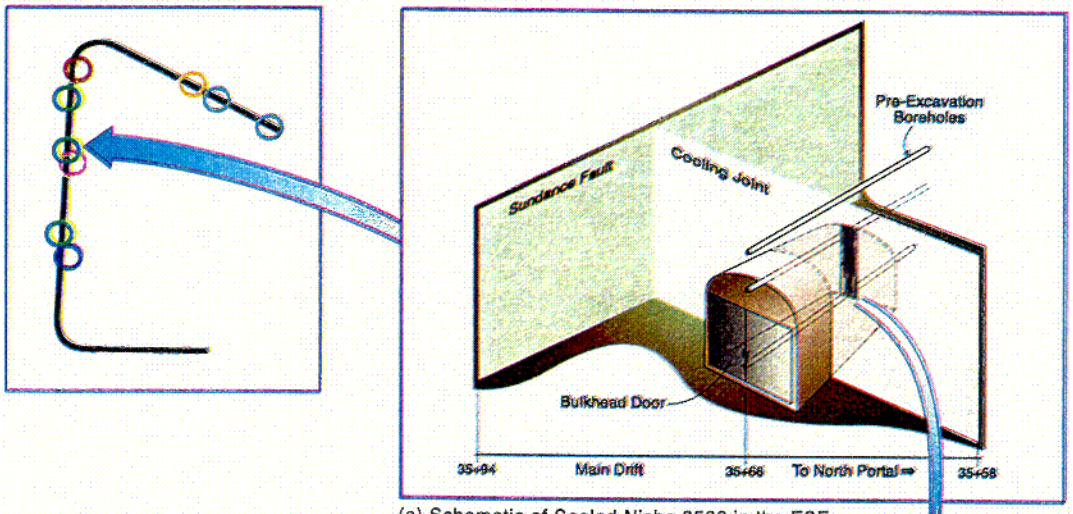

(a) Schematic of Sealed Niche 3566 in the ESF

Objectives:

- Characterize the hydrologic setting of a site with bomb-pulse ^{36}Cl signals, the Sundance fault and its first cooling joint.
- Quantify seepage processes.

Approaches:

- Mine the niche without spreading water to the ceiling during excavation.
- Close the bulkhead to prevent moisture removal by ventilation.
- Monitor the rock and drift over long time periods.

Results:

- One damp feature observed after dry excavation at end of the niche. It dried up before bulkhead installation and did not rewet after long-term monitoring over two years.

(b) Photograph of a Damp Feature in the Brecciated Zone at the Back of Niche 3566

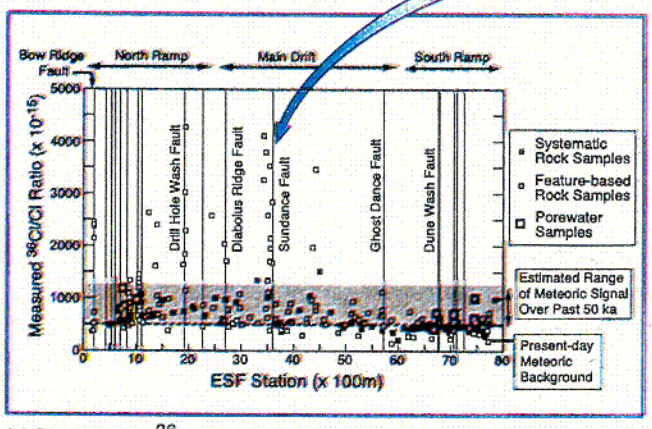

(c) Distribution of $^{36}Cl/Cl$ in the ESF

Figure 2.2-4. Damp Feature Observed during Dry Excavation of Niche 3566 and Bomb-Pulse $^{36}Cl/Cl$ Signals along the ESF (Wang et al. 1999, pp. 331–332; CRWMS M&O 2000, U0085, Section 6.6)

C010

Drift Seepage Test at ECRB Cross Drift Niche 1620

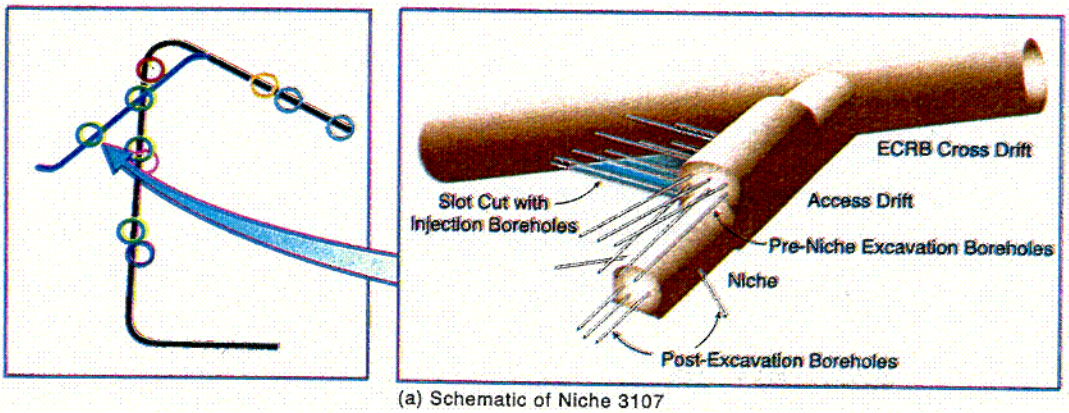

(a) Schematic of Niche 3107

Objectives:

- Quantify seepage into drift in the lower lithophysal unit at a cavity-rich zone.
- Characterize the pneumatic and liquid flows in the presence of lithophysal cavities and porous tuff.
- Determine the differences between lower lithophysal unit and middle non-lithophysal unit of the potential repository rock.
- Quantify fracture-matrix interaction at lower lithophysal unit.

Approaches:

- Observe flow paths during dry excavation, use air-injection tests to characterize liquid release intervals, and conduct drift seepage tests with liquid releases at different rates.
- Adopt, improve, and extend the methodologies used in tests conducted in the middle non-lithophysal niches and test beds.

Results:

- Pre-excavation air-injection test results suggest that lower lithophysal unit has higher permeability than middle non-lithophysal unit.
- Access drift has been excavated with an Alpine Miner.
- Seepage tests are prepared to be conducted after niche excavations.

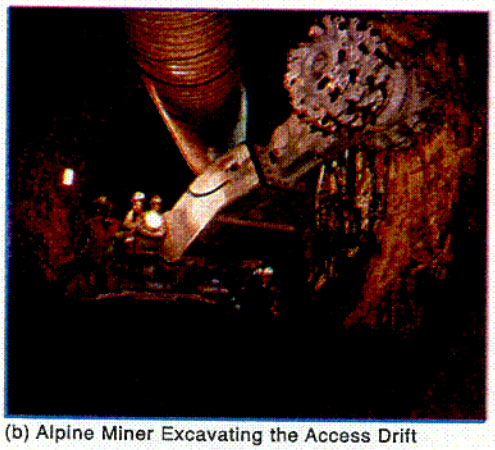

(b) Alpine Miner Excavating the Access Drift

(c) Example of a Cavity in the Lower Lithophysal Tuff Unit

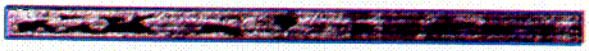

(d) Scanner Image along Borehole AK-1 at Niche1620

Figure 2.2-5. Lower Lithophysal Seepage Test at ECRB Cross Drift Niche 1620

C011

Fracture-Matrix Interaction Test at Alcove 6

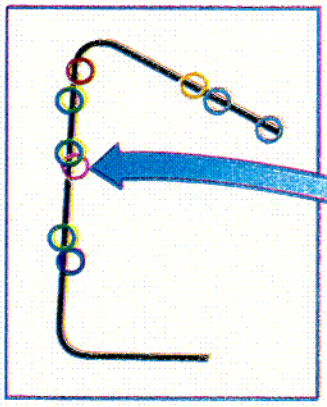

(a) Photograph of Alcove 6 Test Bed

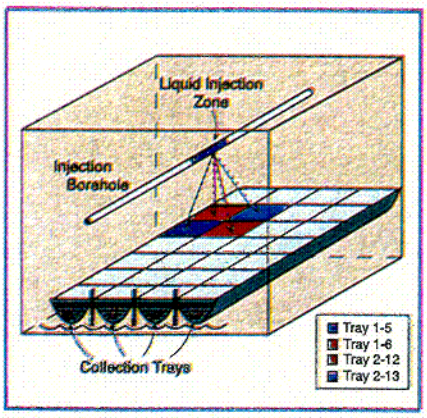

(c) Schematic of Liquid Release Test

(b) Close-up of Trays on the Slot

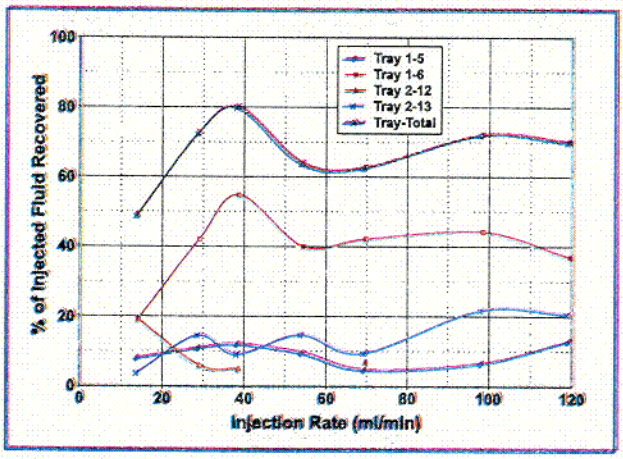

(d) Water Collected in the Slot

Objectives:

- Quantify fracture-matrix interaction and the fraction of fracture flow.

Approaches:

- Use a slot below boreholes to capture fracture flows.
- Estimate the fracture/matrix flow partitioning by mass balance.
- Use borehole sensors to detect wetting front arrivals.

Results:

- A maximum of 80% of injected water was recovered for high-rate injection tests (i.e. 80% fracture flow).
- Out flows occurred in step increments which could be related to water stored in fracture flow paths.

Figure 2.2-6. Fracture-Matrix Interaction Test at Alcove 6 (CRWMS M&O 2000, U0015, Section 6.6)

C012

Fault Flow Damping Test at Alcove 4

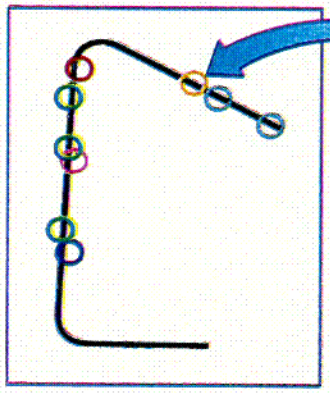

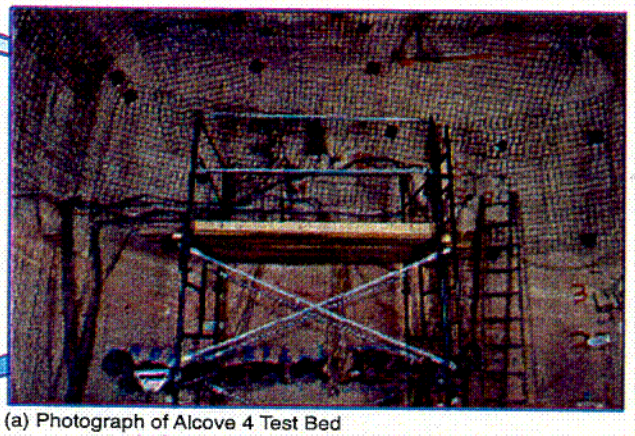

(a) Photograph of Alcove 4 Test Bed

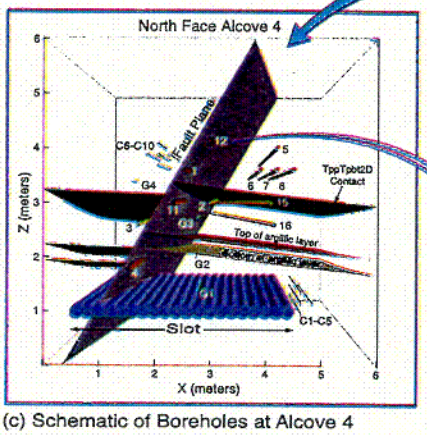

(c) Schematic of Boreholes at Alcove 4

(b) Close-up of Tray on the Left-Hand Side of the Slot

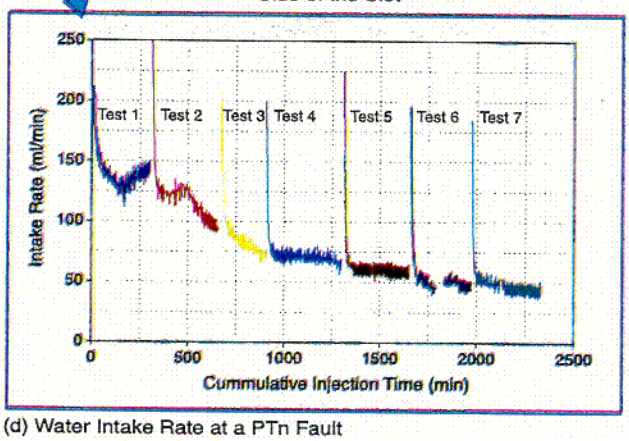

(d) Water Intake Rate at a PTn Fault

Objectives:

- Evaluate flow mechanism in the Paintbrush nonwelded tuff unit.
- Quantify the damping and lateral diversion processes along a fault and along bedded tuff interfaces.

Approaches:

- Select a test bed containing bedded tuff layers (including an argillic layer), a fault, and a fracture.
- Release water under constant-head conditions to determine the intake rates.
- Monitor wetting front arrivals and measure potential changes in boreholes.

Results:

- Water intake rate in the fault decreased as more water was introduced into the release zone.
- Clay swelling is one mechanism proposed to interpret the field data.
- Detection of down-gradient increases in saturation occurred over shorter time intervals with each liquid release test.

Figure 2.2-7. Paintbrush Fault and Porous Matrix Test at Alcove 4 (CRWMS M&O 2000, U0015, Section 6.7)

C013

El Niño Infiltration Test at Alcove 1

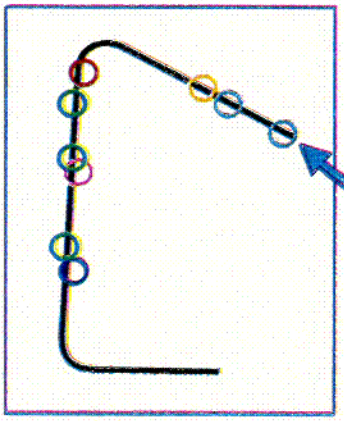

(a) Photography of ESF North Portal and Infiltration Plot (Blue Cover)

Objectives:

- Quantify large-scale infiltration and seepage processes in the bedrock.
- Evaluate matrix diffusion mechanism in long-term flow and transport tests.

Approaches:

- Water applied on the surface 30 m directly above the alcove.
- Tests conducted in two phases: March - August 1998 and May 1999 - present, with Phase 1 focusing on flow and Phase 2 focusing on tracer transport.

Results:

- Over 100,000 liters infiltrated in Phase 1, with observed seepage rates of up to 300 liter/day.
- First seepage was observed 58 days after Phase 1 test initiation. Pressure/flow response of the system was observed to be ~2 days once a nearly steady-state system had developed.
- High concentrations of LiBr were used in Phase 2 tracer test.
- First tracer breakthrough in Phase 2 observed in 28 days with a nearly steady-state flow system using a conservative tracer.
- Tracer recovery data were used to compare with model predictions and to evaluate the importance of matrix diffusion.

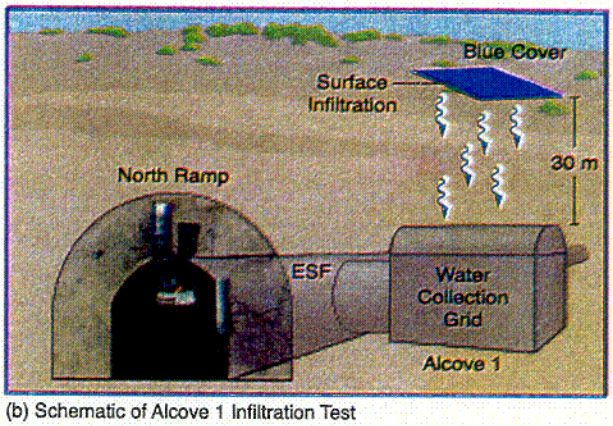

(b) Schematic of Alcove 1 Infiltration Test

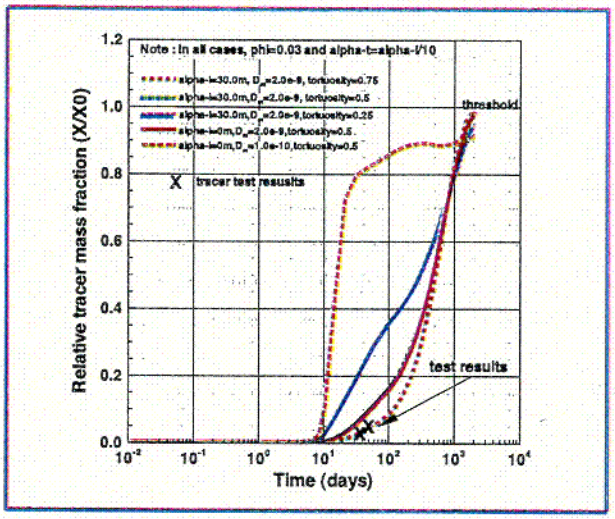

(c) Tracer Breakthoughs Test Results and Model Predictions with Matrix Diffusion

Figure 2.2-8. El Niño Infiltration and Seepage Test at Alcove 1

C014

Alcove 8-Niche 3107 Cross-Drift Test

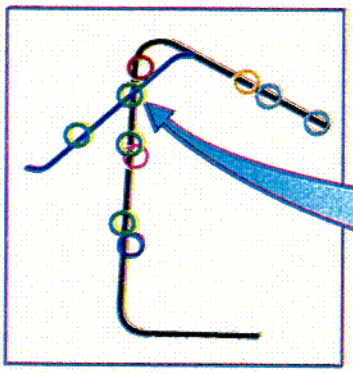

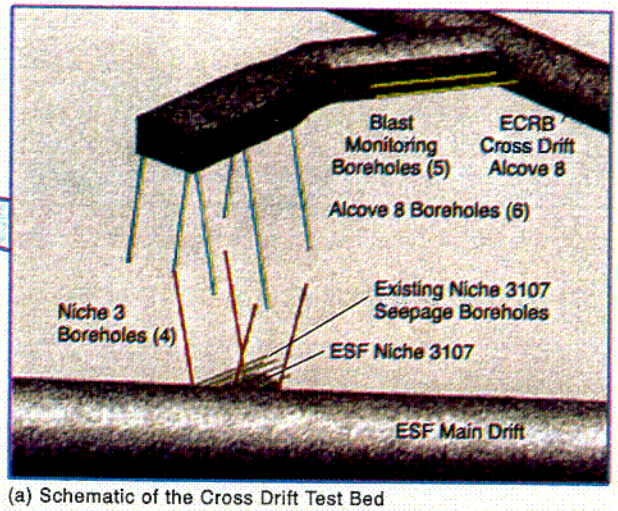

(a) Schematic of the Cross Drift Test Bed

Objectives:

- Quantify large-scale infiltration and seepage processes in the potential repository horizon.
- Evaluate matrix diffusion mechanism in long-term flow and transport tests across an lithophysal-nonlithophysal interface.

Approaches:

- Water releases are in Alcove 8 and seepage collections are in Niche 3107.
- Niche 3107 is instrumented with seepage collectors and wetting front sensors.
- Geophysical tomographs are conducted in vertically slanted boreholes.

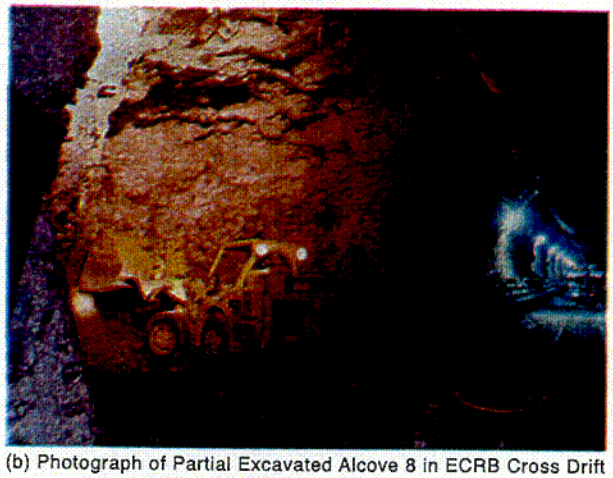

(b) Photograph of Partial Excavated Alcove 8 in ECRB Cross Drift

Status:

- Drill-and-blast phase of Alcove 8 excavation was completed in 1999.
- Tests are prepared to be conducted after alcove excavation.

Supporting Results:

- Seepage tests at Niche 3107 behind bulkhead demonstrate the existence of seepage threshold under high humidity conditions.
- During ECRB Cross Drift construction, no water was observed to seep into the ESF Main Drift 20 m below.

(c) Photograph of Water Collection Trays on the Ceiling of the ESF Main Drift

Figure 2.2-9. Cross-Drift Test between ECRB Cross Drift Alcove 8 and ESF Main Drift Niche 3107 (CRWMS M&O 2000, U0015, Section 6.9)

C015

Geochemical Measurements on Borehole and ESF Samples

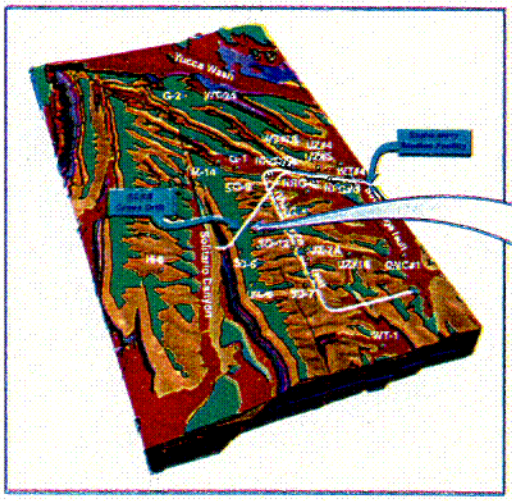

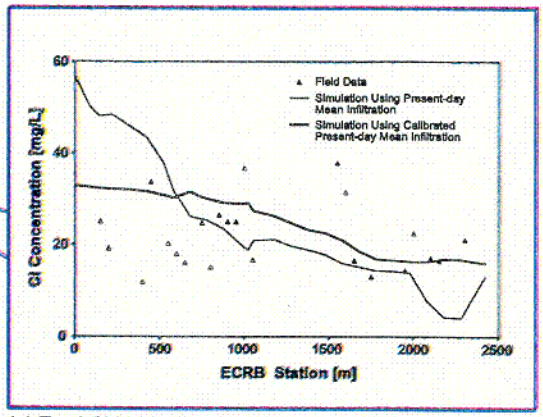

(a) Total Chloride Contents Along the ECRB Cross Drift

Objectives:

- Provide data to define geochemical evolution of water in the UZ.
- Provide data to estimate percolation flux at depth.

Approaches:

- Collect gas and perched water samples by pumping.
- Extract pore water by compression, ultracentrifuge, or vacuum distillation.
- Determine major ion concentrations by chemical analyses.

Results:

- Total dissolved solid and chloride are used to estimate infiltration rates and percolation fluxes.
- Pore waters are related to soil-zone processes: evapotranspiration, dissolution and precipitation of pedogenic calcite and amorphous silica.
- Deep pore waters are used to evaluate restricted water-rock interactions and significant lateral movement within Calico Hills unit.

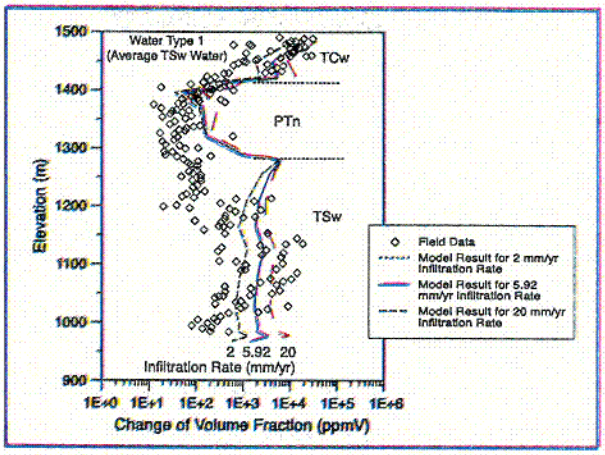

(b) Calcite Distributions Used for Infiltration and Percolation Evaluations

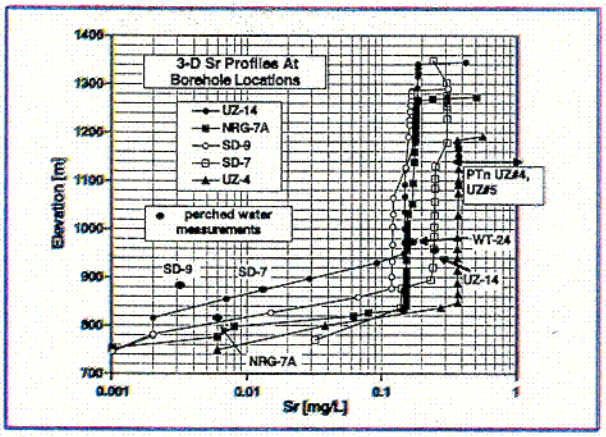

(c) Strontium Profiles Used for Zeolite Quantification

Figure 2.2-10. Geochemical Studies of Tuff Samples (CRWMS M&O 2000, U0050, Section 6.5; Sonnenthal and Bodvarsson 1999, p. 146)

CD16

Isotopic Measurements on Fracture Minerals and Perched Waters

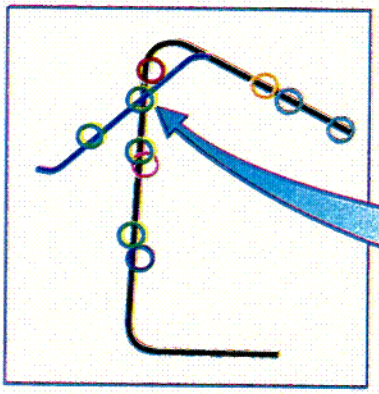

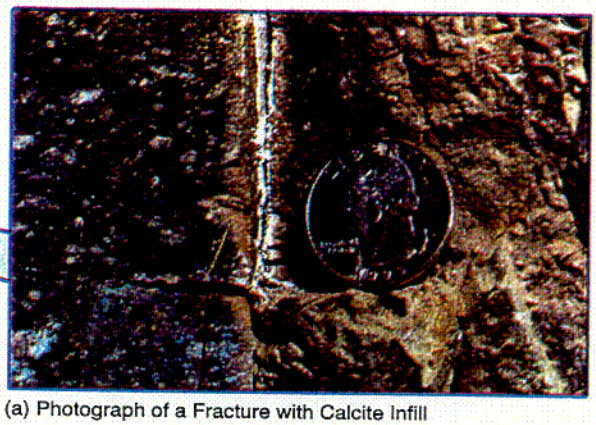

(a) Photograph of a Fracture with Calcite Infill

Objectives:

- Provide isotopic data to define age evolution of water in the UZ.
- Provide data to delineate flow paths over geological time scales.

Approaches:

- Leach salts from UZ cores or cutting for ^{36}Cl and Sr isotopic analyses.
- Extract water for tritium, hydrogen and oxygen stable isotopes, and carbon isotopic analyses.
- Digest mineral samples for analyses of Sr isotope ratios and of U series nuclides.

Results:

- Bomb-pulse $^{36}Cl/Cl$ signals are present in the vicinity of some fault zones in the ESF.
- Detectable levels of tritium are present in ~6% of pore waters sampled.
- Bomb-pulse $^{36}Cl/Cl$ and tritium signals are not present in perched waters.
- Age of perched waters, mixing between fast and slow flows, climate of recharge are estimated by carbon and stable isotope analyses.
- $^{234}U/^{238}U$ activity ratios indicate recharge through fractures and minimal exchange between pore water and fracture water.

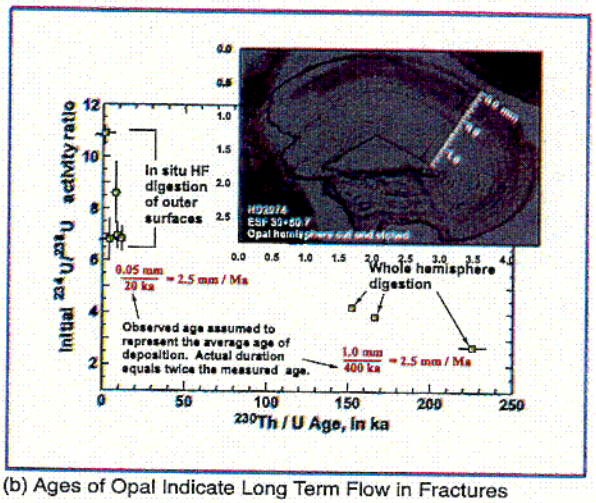

(b) Ages of Opal Indicate Long Term Flow in Fractures

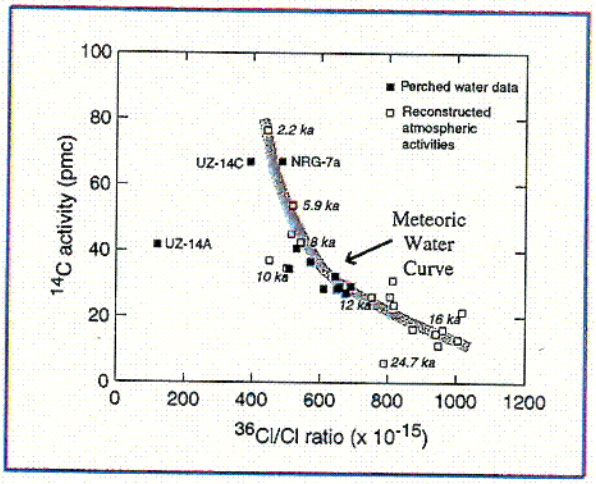

(c) Perched Water Ages Determined by ^{14}C and $^{36}Cl/Cl$ Data

Figure 2.2-11. Isotopic Studies of Tuff Samples (CRWMS M&O 2000, U0085, Section 6.6)

C017

UZ Transport Test at Busted Butte

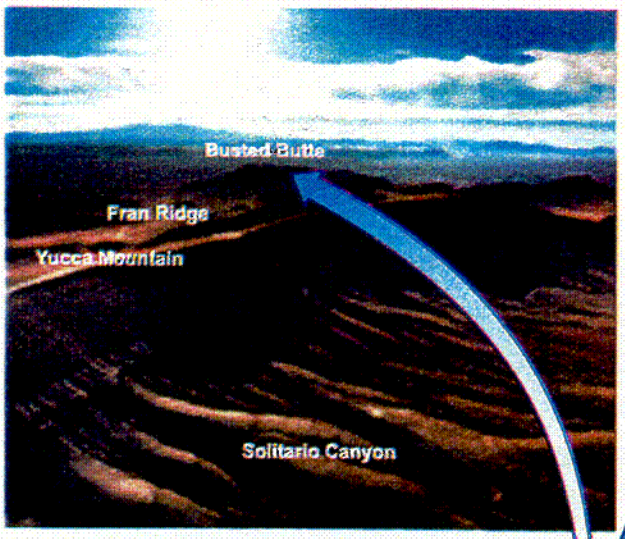

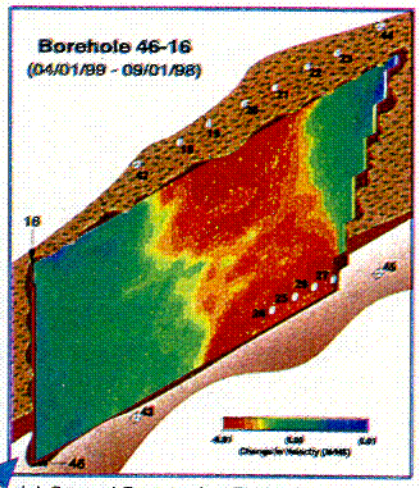

(a) Ground Penetrating Radar Tomograph of Injected Plume (Phase 2)

Objectives:

- Quantify UZ transport processes in Calico Hills nonwelded unit.
- Measure retardation coefficients in the field to compare with laboratory measured values.

Approaches:

- A test bed was excavated 70 m below the surface in mainly vitric CHn underlying the vitrophyre.
- A mixture of conservative and sorbing tracers is used in tracer injection tests.
- Absorbent pads are used to sample periodically the tracer distributions below injections.
- Ground-penetrating radar tomography, together with electrical resistivity tomography and neutron logging, are used to track plume migrations.

Results:

- Phase 1A was conducted with single point injections from April 1998 to mineback in 1999. Capillary driven flow mechanism is confirmed.
- Phase 2 tests with areal injections are on-going with breakthroughs and plume migrations monitored.

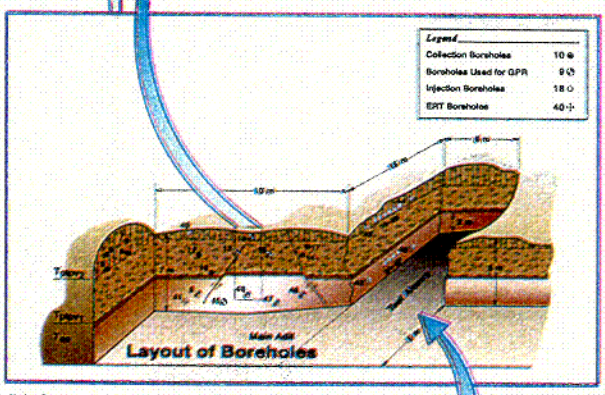

(b) Schematic of Busted Butte Test Area

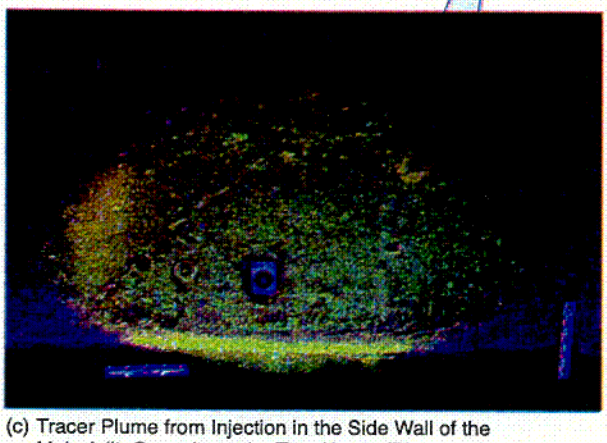

(c) Tracer Plume from Injection in the Side Wall of the Main Adit, Opposite to the Test Alcove (Phase 1A)

Figure 2.2-12. UZ Transport Test at Busted Butte (CRWMS M&O 2000, U0100, Section 6.8)

C018

Single Heater Test at Alcove 5

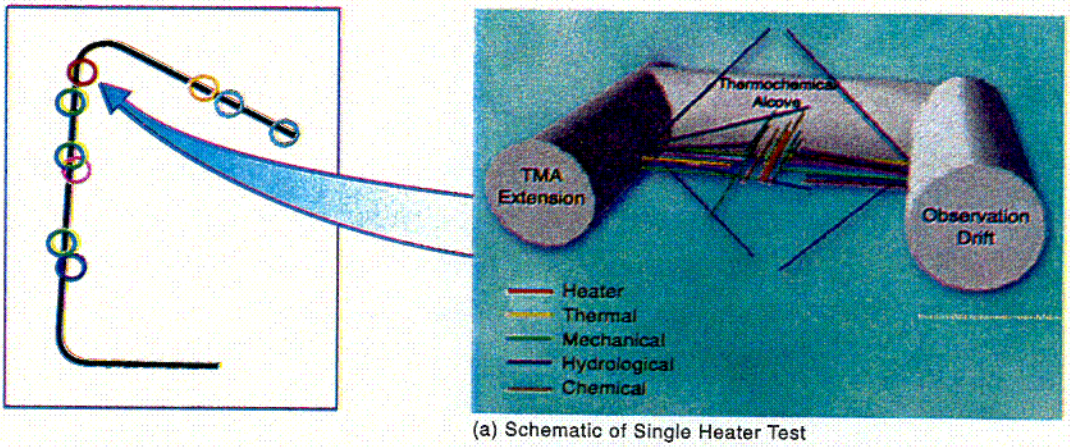

(a) Schematic of Single Heater Test

Objectives:

- Evaluate THMC coupled processes around a line heater source in fractured tuff.
- Develop testing methodologies and modeling approaches for high temperature conditions.

Approaches:

- Heating with a 5-m long 4-kW heater lasted 9 months in 1996 and 1997.
- Borehole sensing and cross-hole testing were used before, during, and after heating period.

Results:

- Extent of dry-out of about 1 m around the heater hole was measured with geophysical techniques (ERT, GRP and neutron).
- Condensate zone below the heater was measured to be larger than above the heater horizon.
- Chemical composition of water collected during heating in packed borehole intervals was analyzed.
- Characterization data by air-injection tests and mechanical displacement measurements located high-k flow paths.

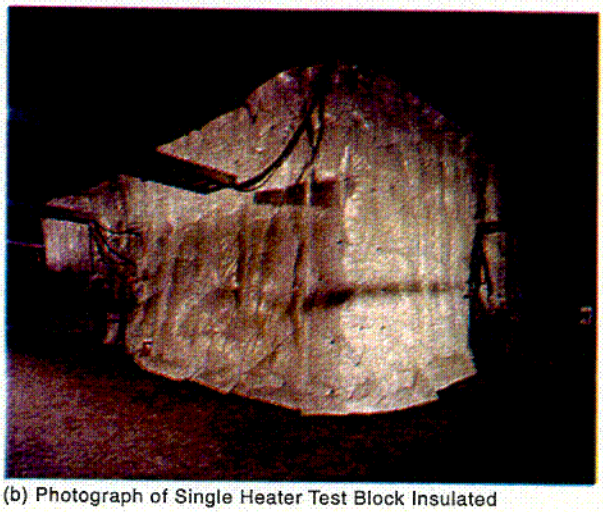

(b) Photograph of Single Heater Test Block Insulated

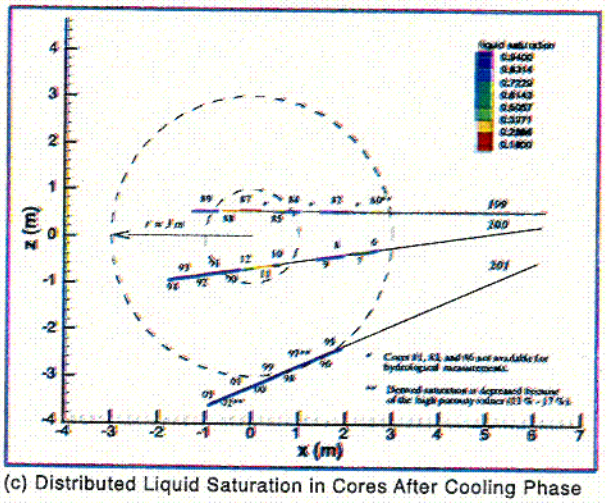

(c) Distributed Liquid Saturation in Cores After Cooling Phase

Figure 2.2-13. Single Heater Test at Alcove 5 (Tsang and Birkholzer 1999, pp. 411-415)

C019

Drift Scale Test at Alcove 5

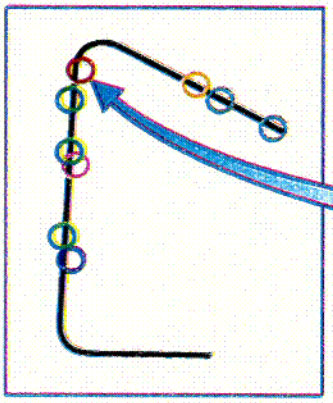

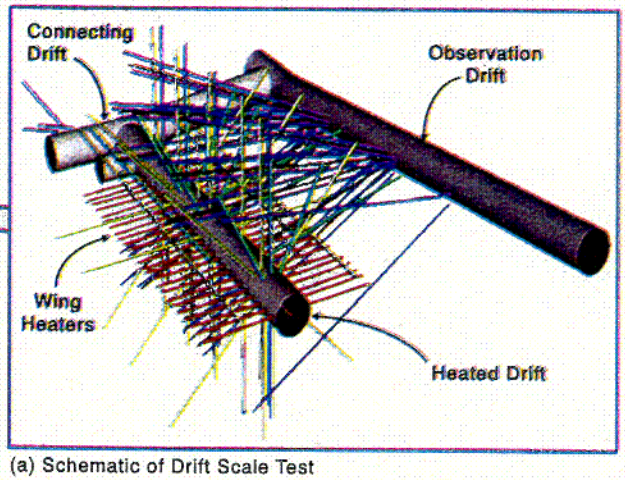

(a) Schematic of Drift Scale Test

Objectives:

- Evaluate THCM coupled processes in emplacement drift scale with full-scale heaters.
- Evaluate multi-drift heating effects with wing heaters to simulate multi-drift test conditions in fractured tuff.

Approaches:

- Install extensive borehole sensor arrays for monitoring of heating responses.
- Perform periodic geophysical imaging, pneumatic testing, and fluid sampling to measure the thermally induced coupled effects.

Results:

- Drift wall temperature reached ~190°C after 2 years of heating (since December 1997 at 187 kW).
- Condensate accumulated mainly below the wing heaters at early times.
- Wetting and drying zones were identified by periodic air-injection tests and geophysical methods.
- Gas phase CO_2 concentration increased strongly in large region around the heaters.
- Interactions of calcite and silicate minerals were indicated by chemical analyses of water collected.

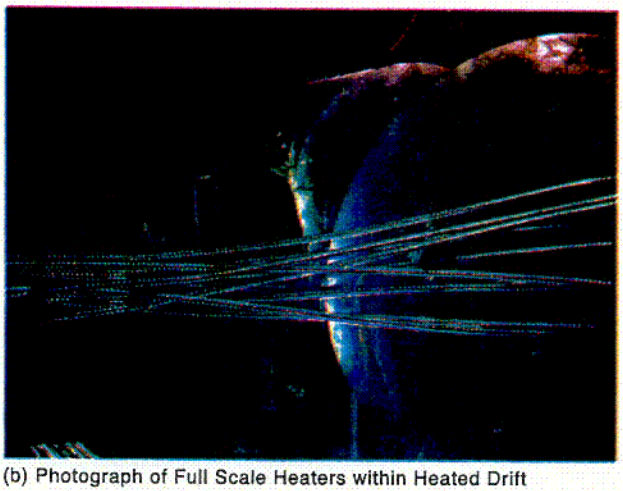

(b) Photograph of Full Scale Heaters within Heated Drift

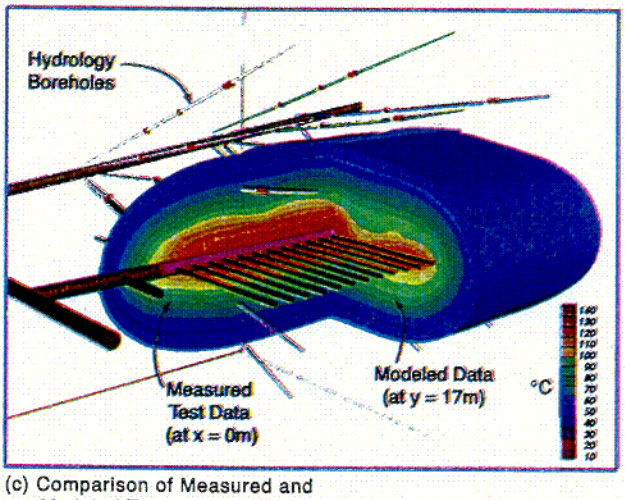

(c) Comparison of Measured and Modeled Temperature Distributions

Figure 2.2-14. Drift Scale Test at Alcove 5 (CWRMS M&O 2000, U0110/N0120, Section 6.2)

C20

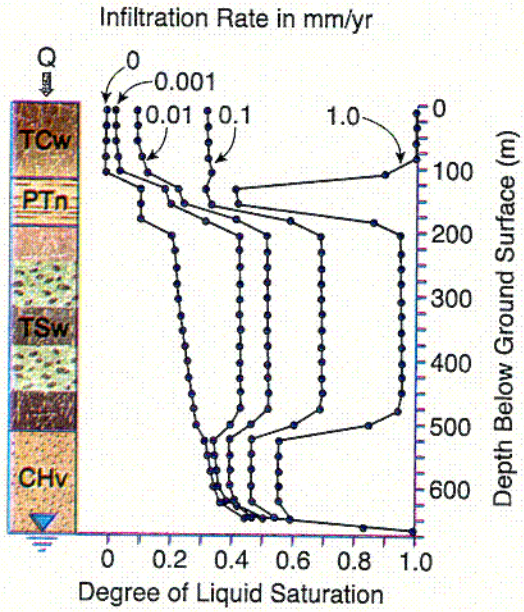

(a) 1-D Model of ambient saturation conditions for different percolation flux values UZ Flow – 1986

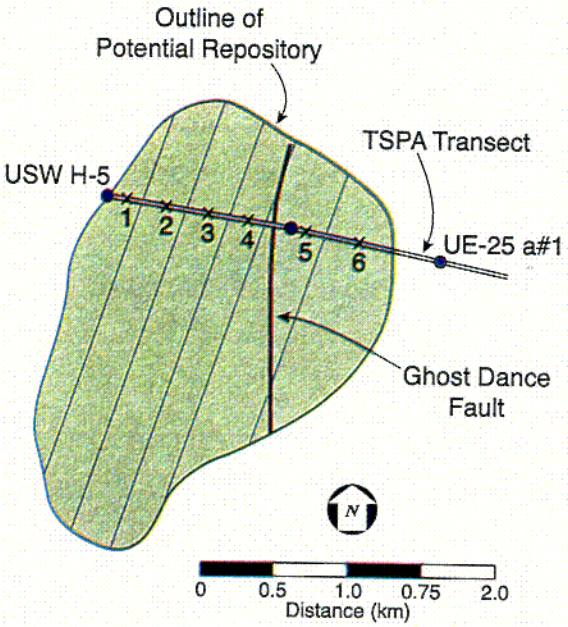

(b) 6 1-D Columns in 1 transect with 1mm/yr infiltration, composite-porosity and weep models TSPA – 1991

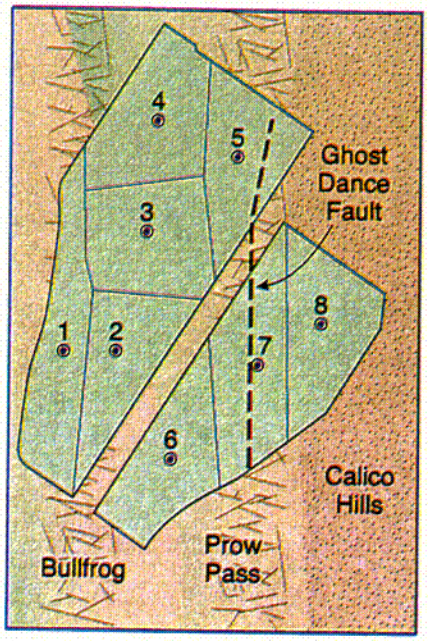

(c) 8 1-D Columns from different areas, 0-5 mm/yr infiltration during dry periods and 10 mm/yr during wet periods TSPA – 1993

Figure 2.4-1. One-Dimensional Column Simulations with the UZ-1986, the TSPA-1991, and the TSPA-1993 Models (Rulon et al. 1986, Barnard et al. 1992, and Wilson et al. 1994)

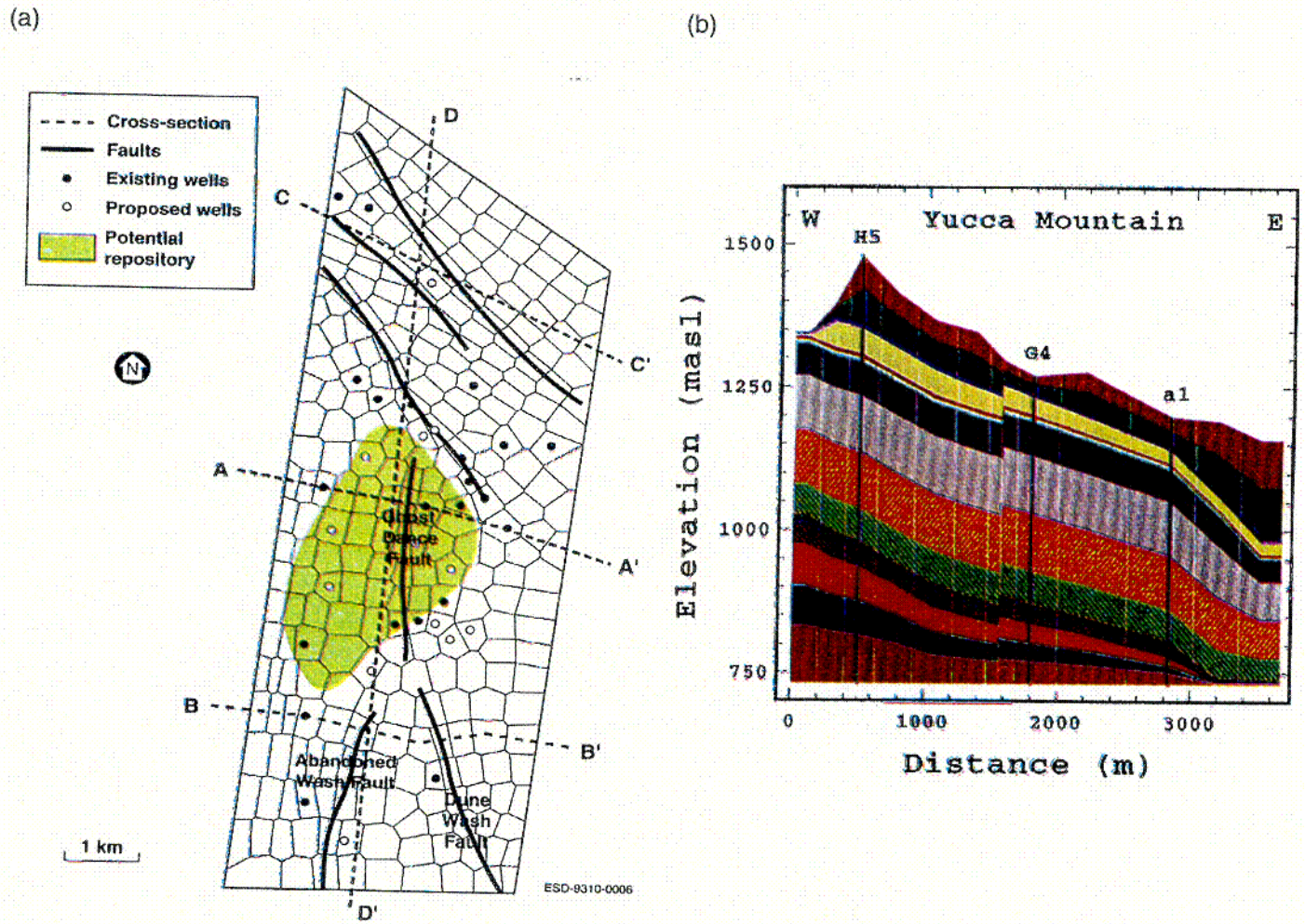

Figure 2.4-2. The Mesh and Approximations Used in the UZ-1995 Model (Wittwer et al. 1995, pp. 46-47)

C022

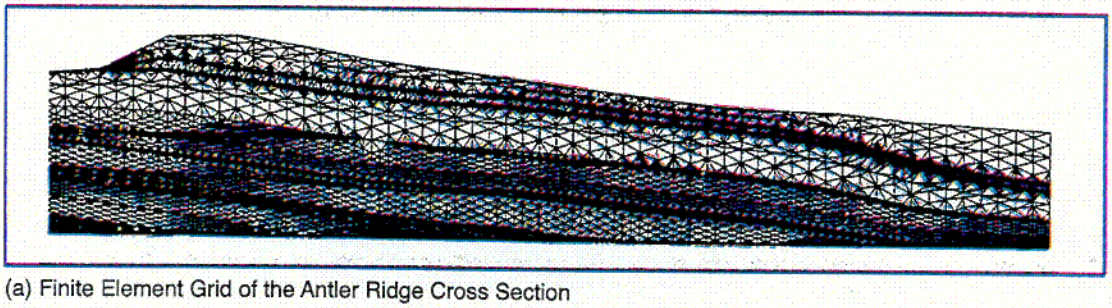

(a) Finite Element Grid of the Antler Ridge Cross Section

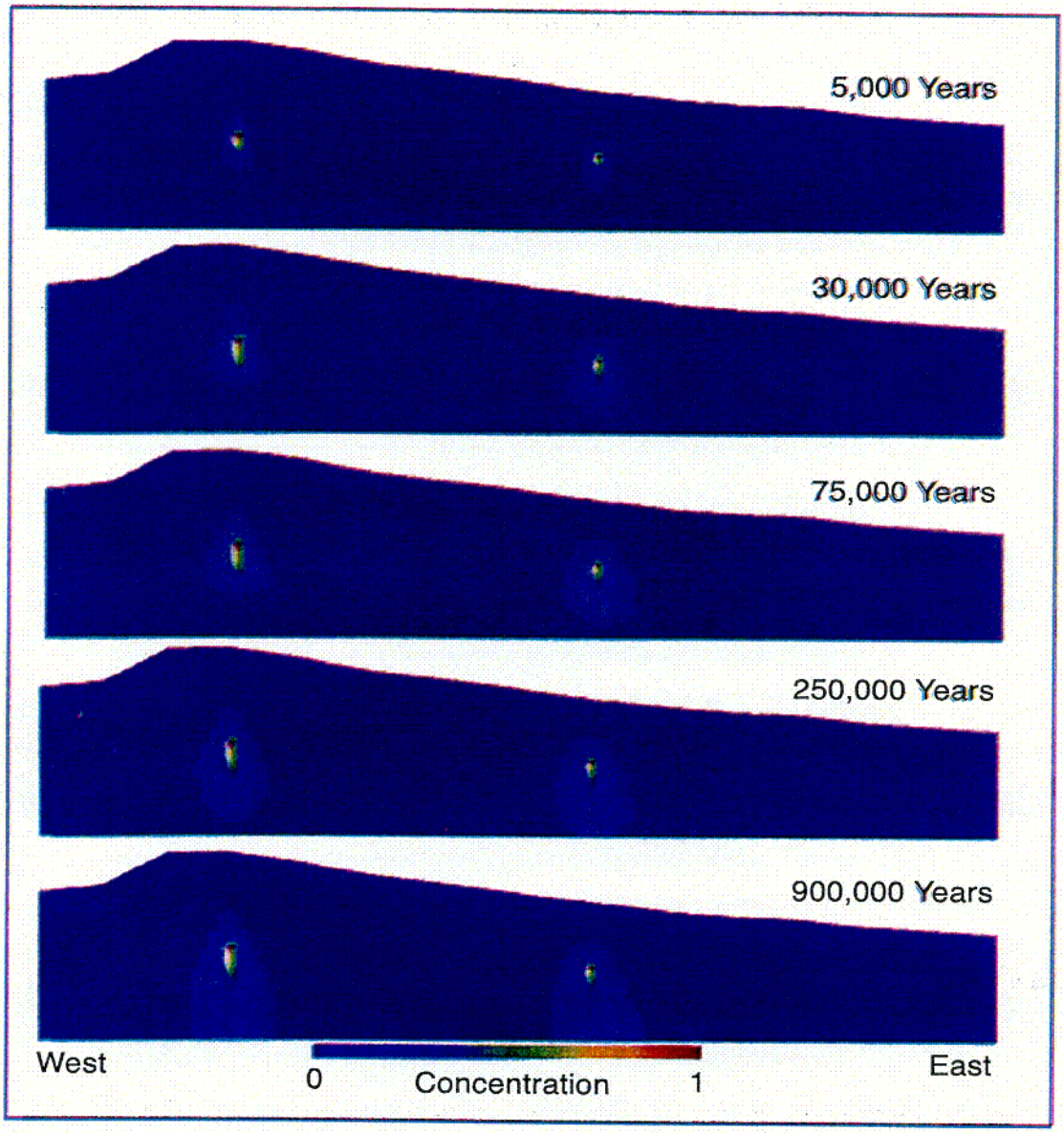

(b) Simulations of Transport of ^{237}Np from the Potential Repository

Figure 2.4-3. Simulations of ^{237}Np Transport by the UZ Transport-1995 Model (Robinson et al. 1995, p. 61, p. 125)

C023

(a) Areal Grid

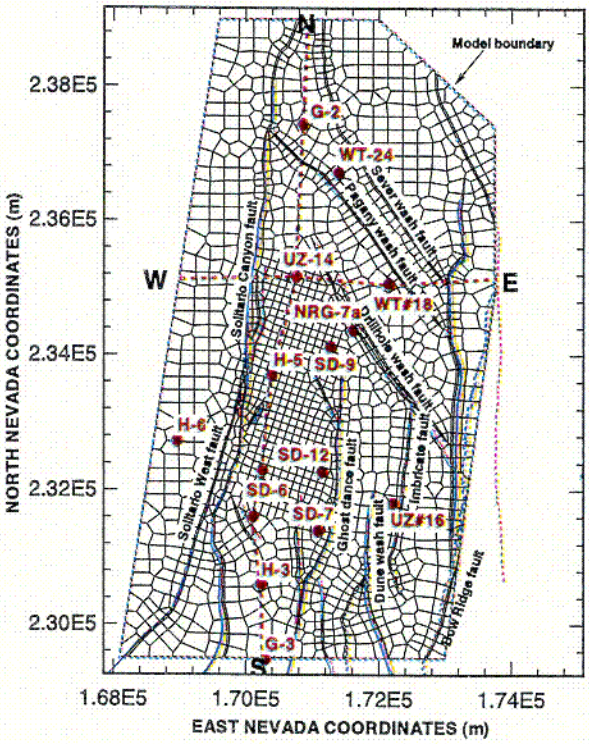

(b) Vertical Grid

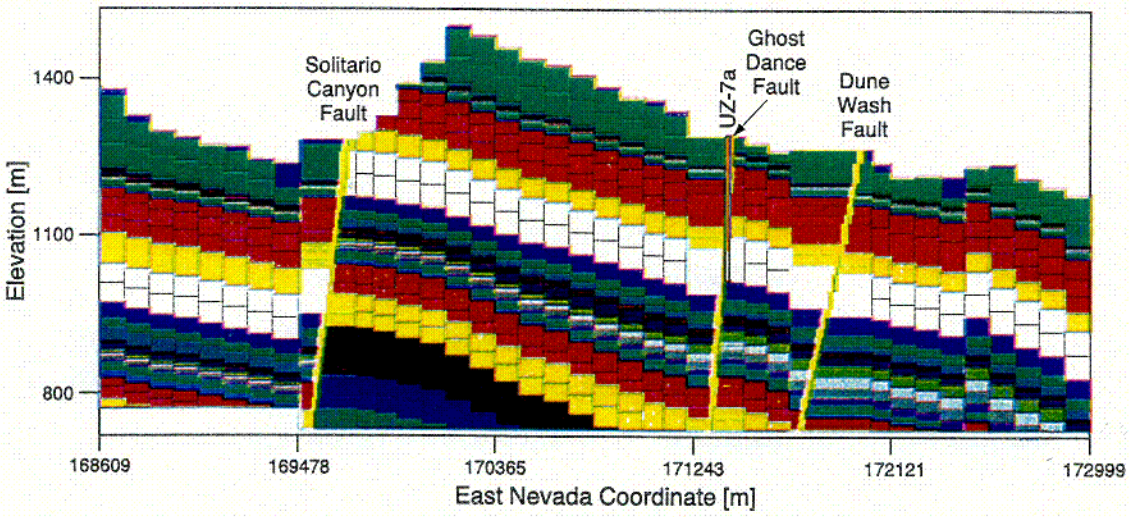

Figure 2.4-4. The Mesh and the Approximations Used in the UZ-1997 Model for TSPA-VA (adapted from Wu et al. 1999b, pp. 190-193)

C024

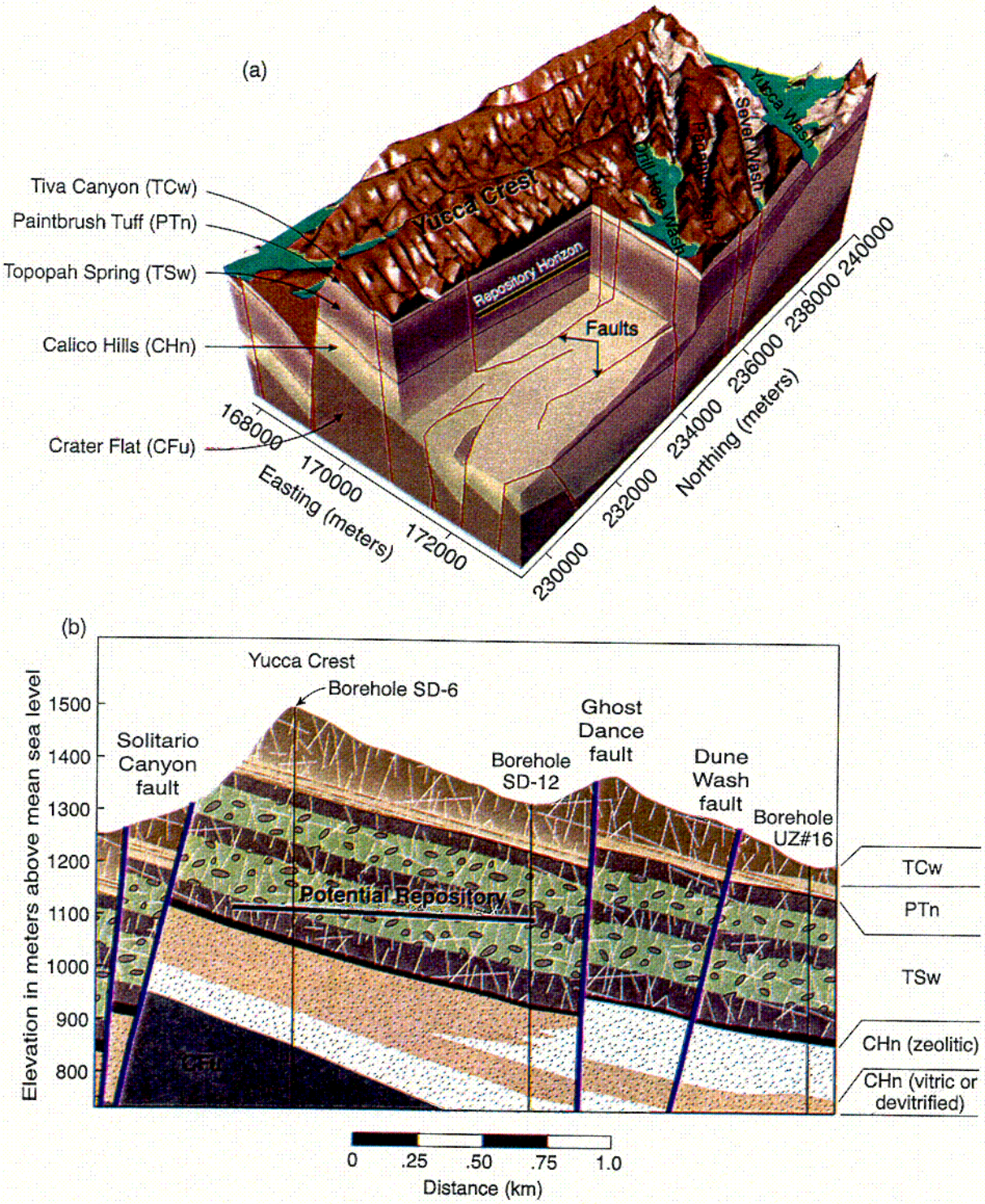

Figure 3.2-1. Yucca Mountain Site-Scale Geology: (a) in 3-D Perspective and (b) along an East-West Cross Section (adapted from GFM3.1 data, CRWMS M&O 2000, I0035)

C025

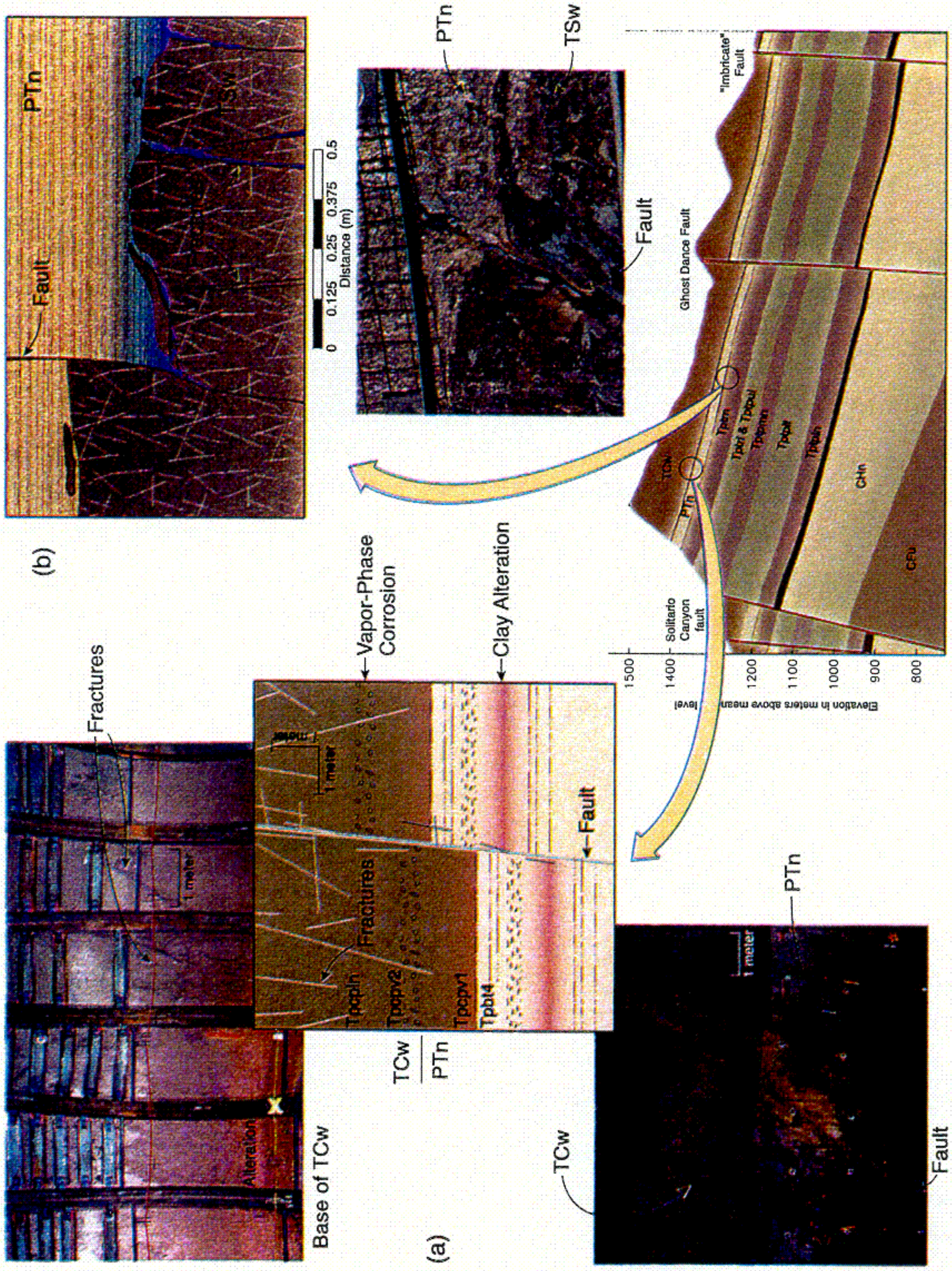

Figure 3.2-2. Lithostratigraphic Transitions at the Upper and Lower Margins of the PTn Hydrogeological Unit. (a) Photos and schematic at the TCw-PTn interface, where tuffs grade downward from densely welded to nonwelded, accompanied by an increase in matrix porosity and a decrease in fracture frequency. (b) Photo and schematic at the PTn-TSw interface, where tuffs grade downward from nonwelded to densely welded, accompanied by a decrease in matrix porosity and an increase in fracture frequency.

C026

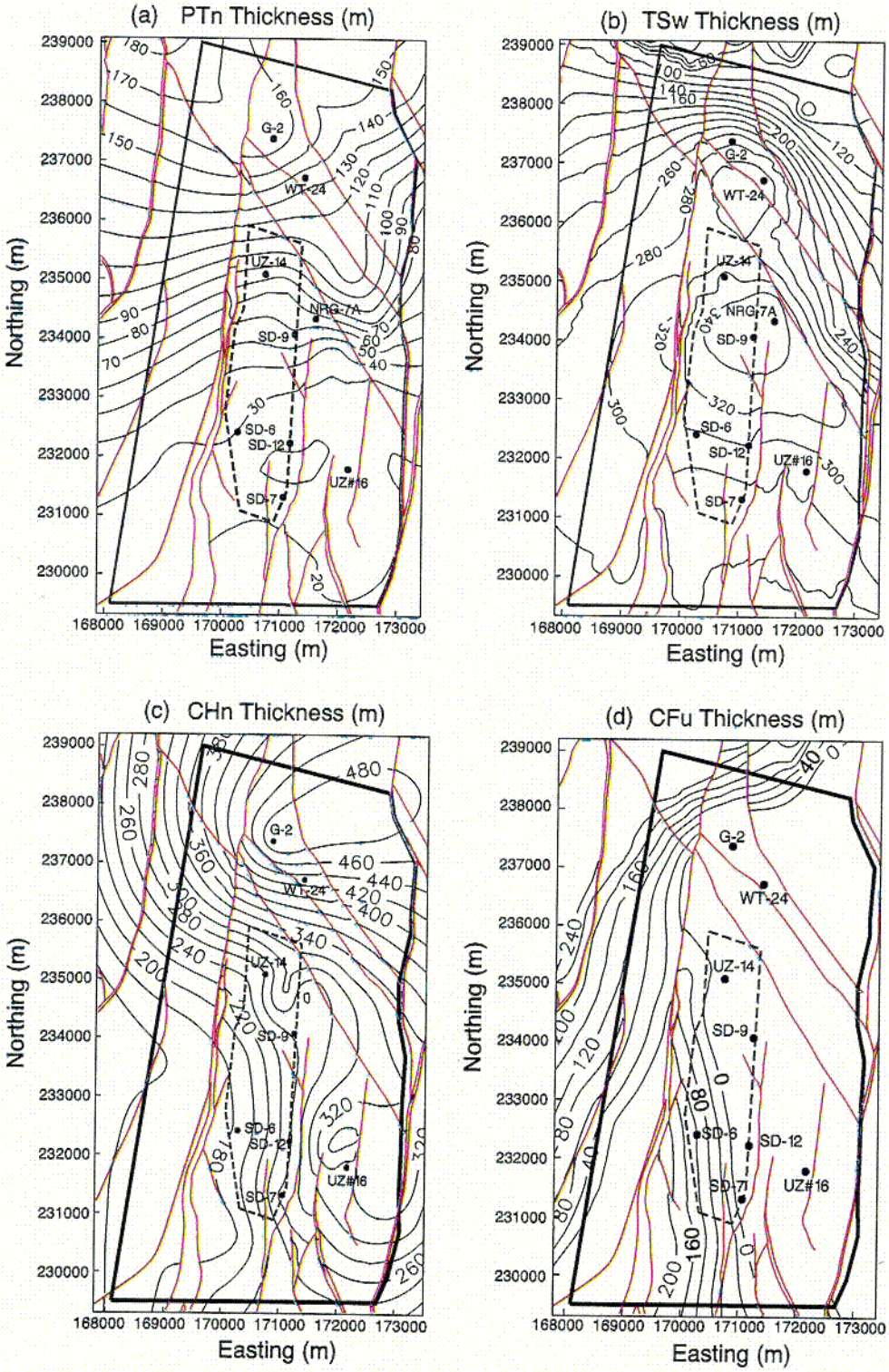

Figure 3.2-3. Thickness Contour Plots of the (a) PTn, (b) TSw, (c) CHn, and (d) CFu Hydrogeological Units (Adapted from DTN: MO9901MWDGFM31.000). Contours are in meters.

C027

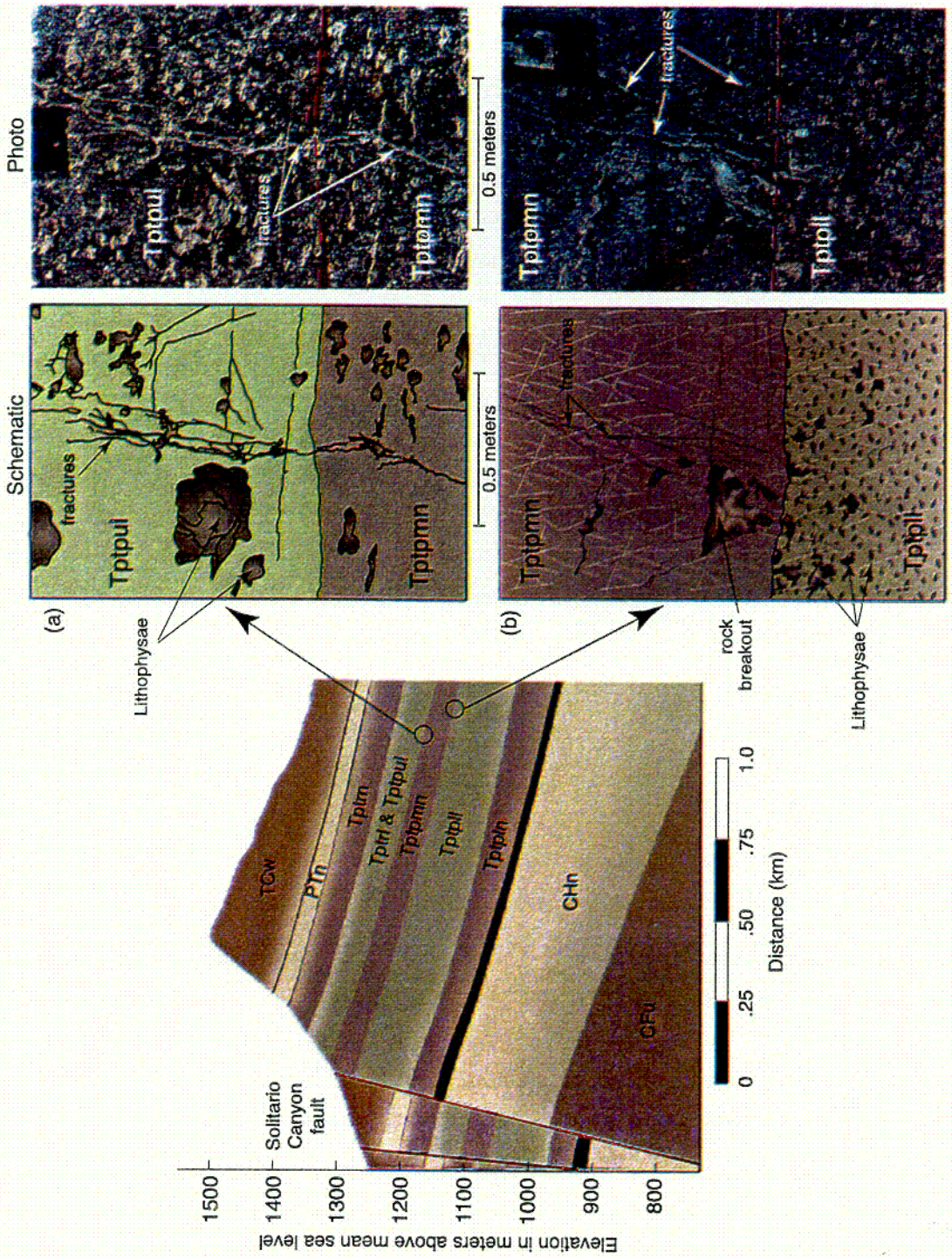

Figure 3.2-4. Lithophysal Transitions within the TSw Unit. (a) Photo and schematic of the contact between the upper nonlithophysal (Tptpul) and the middle nonlithophysal (Tptpmn) zones showing a downward decrease in lithophysal volume. (b) Photo and schematic of the contact between the middle nonlithophysal (Tptpmn) and lower lithophysal (Tptpll) zones showing a downward increase in lithophysal volume. Fractures in the nonlithophysal unit are generally smoother, more planar, and more continuous than fractures in the lithophysal units.

C028

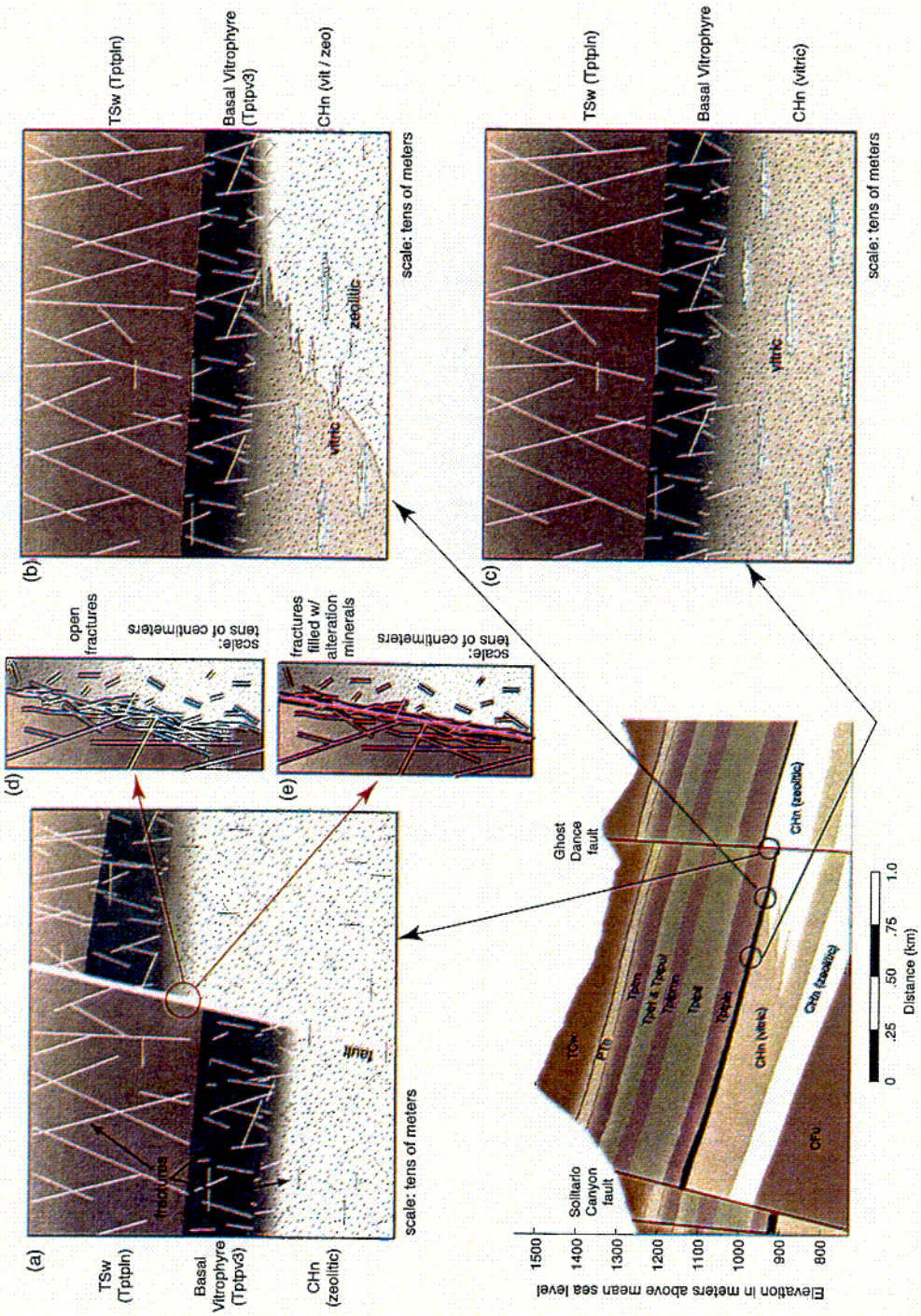

Figure 3.2-5. Lithostratigraphic Transitions at the TSw-CHn Interface. (a) Schematic with prevalent alteration at the TSw-CHn contact. (b) Schematic with variable alteration at the TSw-CHn contact. (c) Schematic with minimal alteration at the TSw-CHn contact. (d) Schematic representation of a fault zone as a well-connected fracture network that may represent a fast flow pathway. (e) Schematic representation of a fault zone showing alteration within the fracture network that creates a flow barrier.

C029

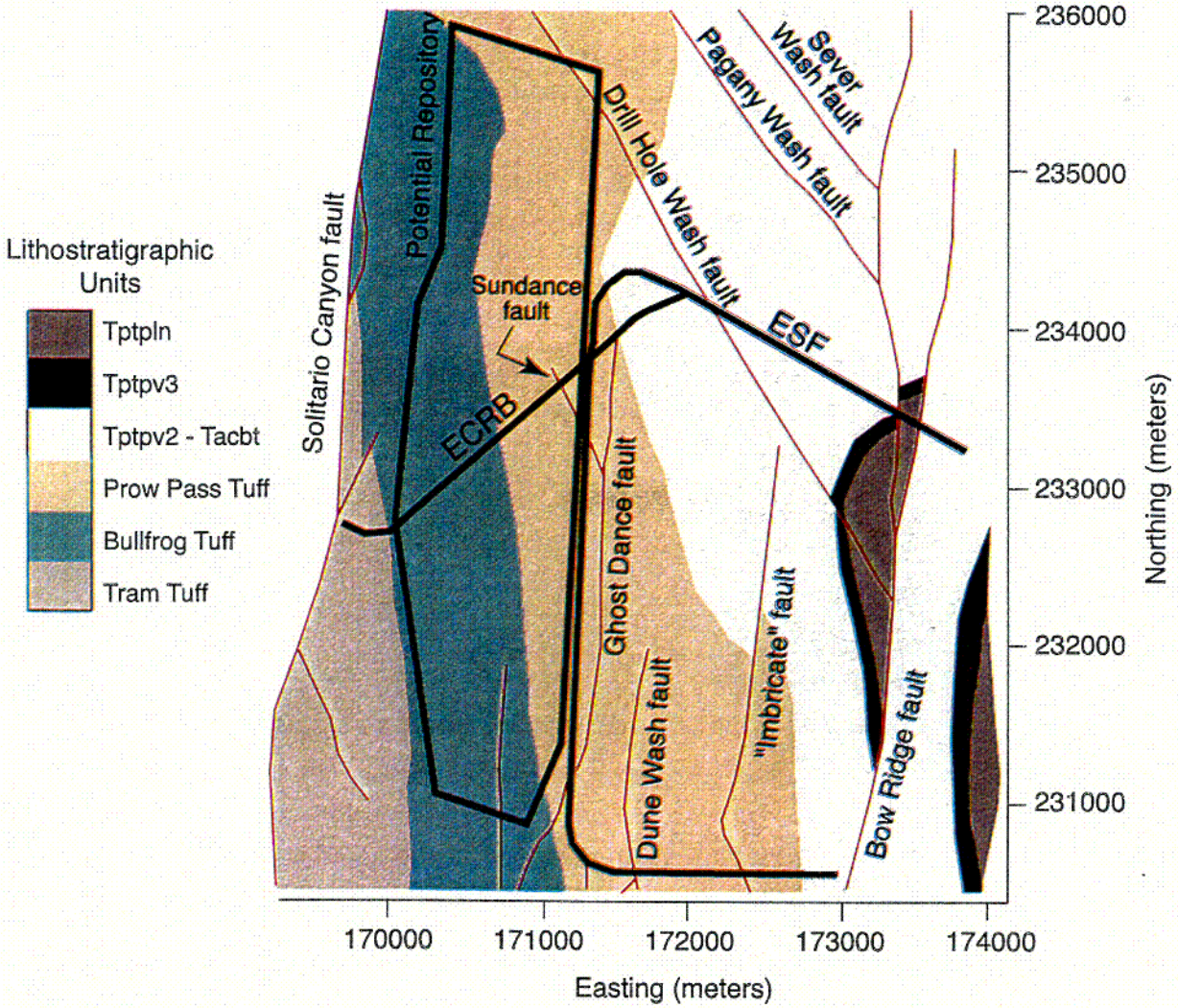

Figure 3.2-6. Occurrence of Lithostratigraphic Units at the Water Table (730 meters above sea level) (Adapted from DTN: MO9901MWDGFM31.000)

C030

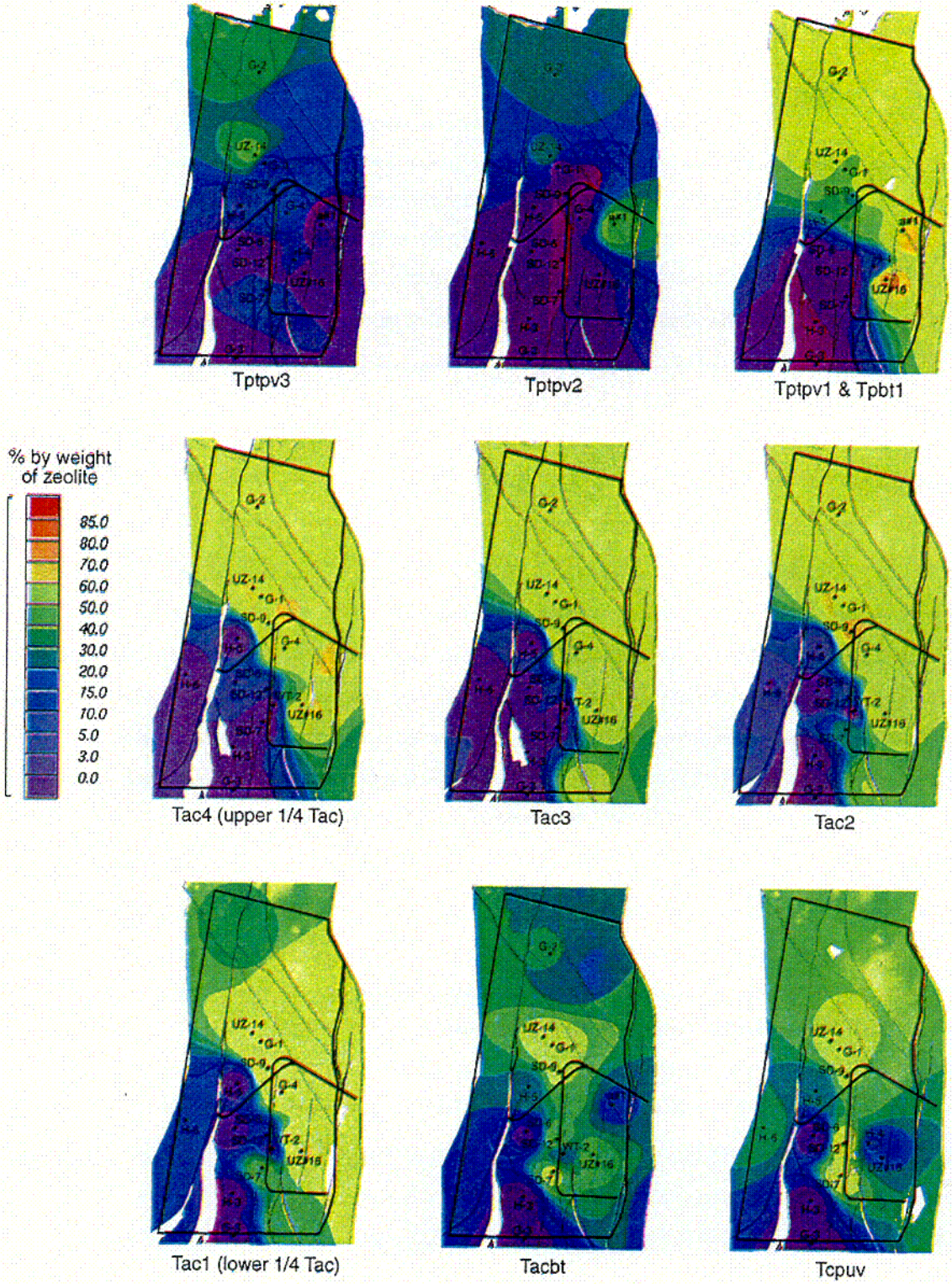

Figure 3.2-7. Distribution of Zeolites in Certain Layers below the Potential Repository Horizon. (CRWMS M&O 2000, I0045, Section 6.3.2; DTN: MO9910MWDISMMM.003). Areas with less than or equal to 3% zeolite are considered vitric, or unaltered.

C031

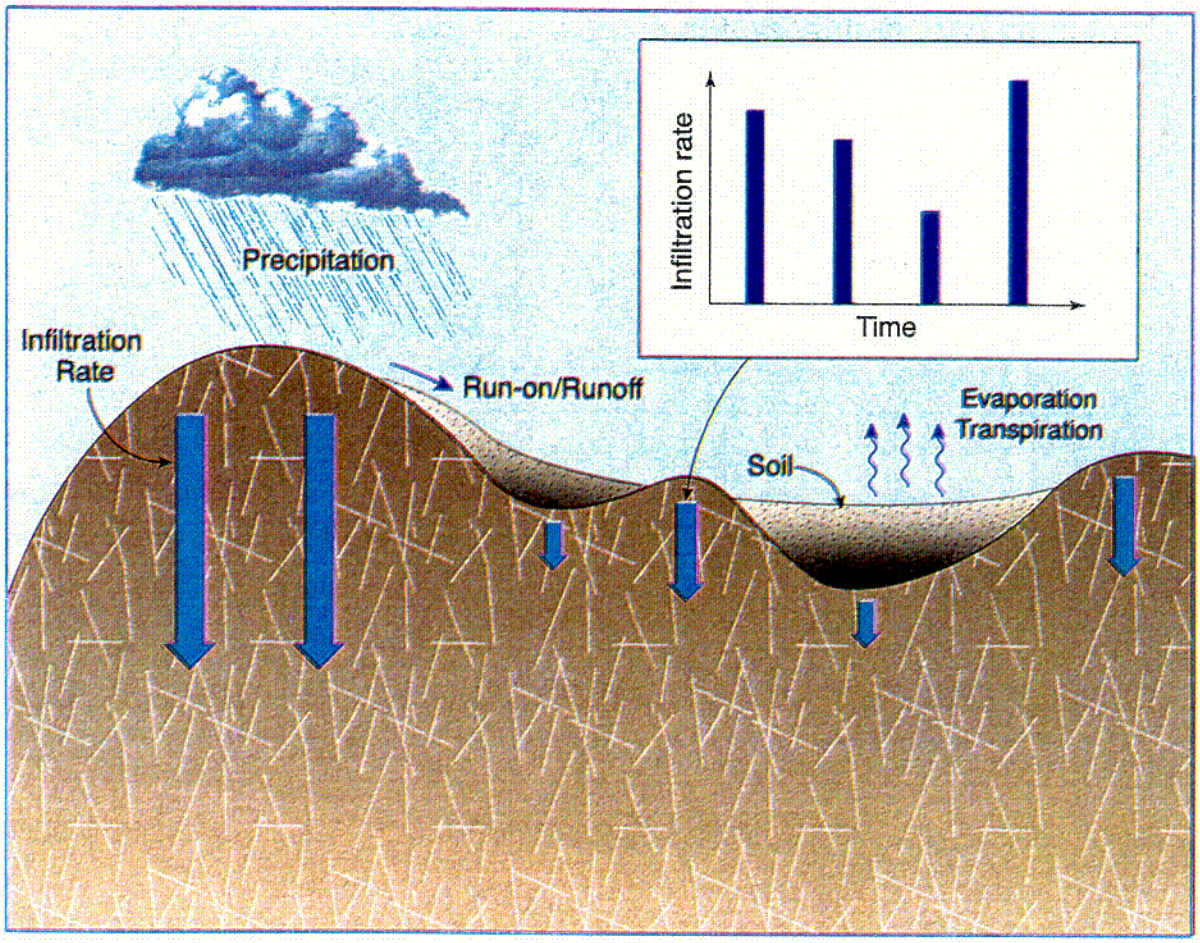

Figure 3.3-1. Schematic Showing Temporal and Spatial Variabilities of Net Infiltration Rates Resulting From the Nature of the Storm Events and Variation in Soil Cover and Topography. The size of the arrow indicates the relative magnitude of infiltration rates.

C032

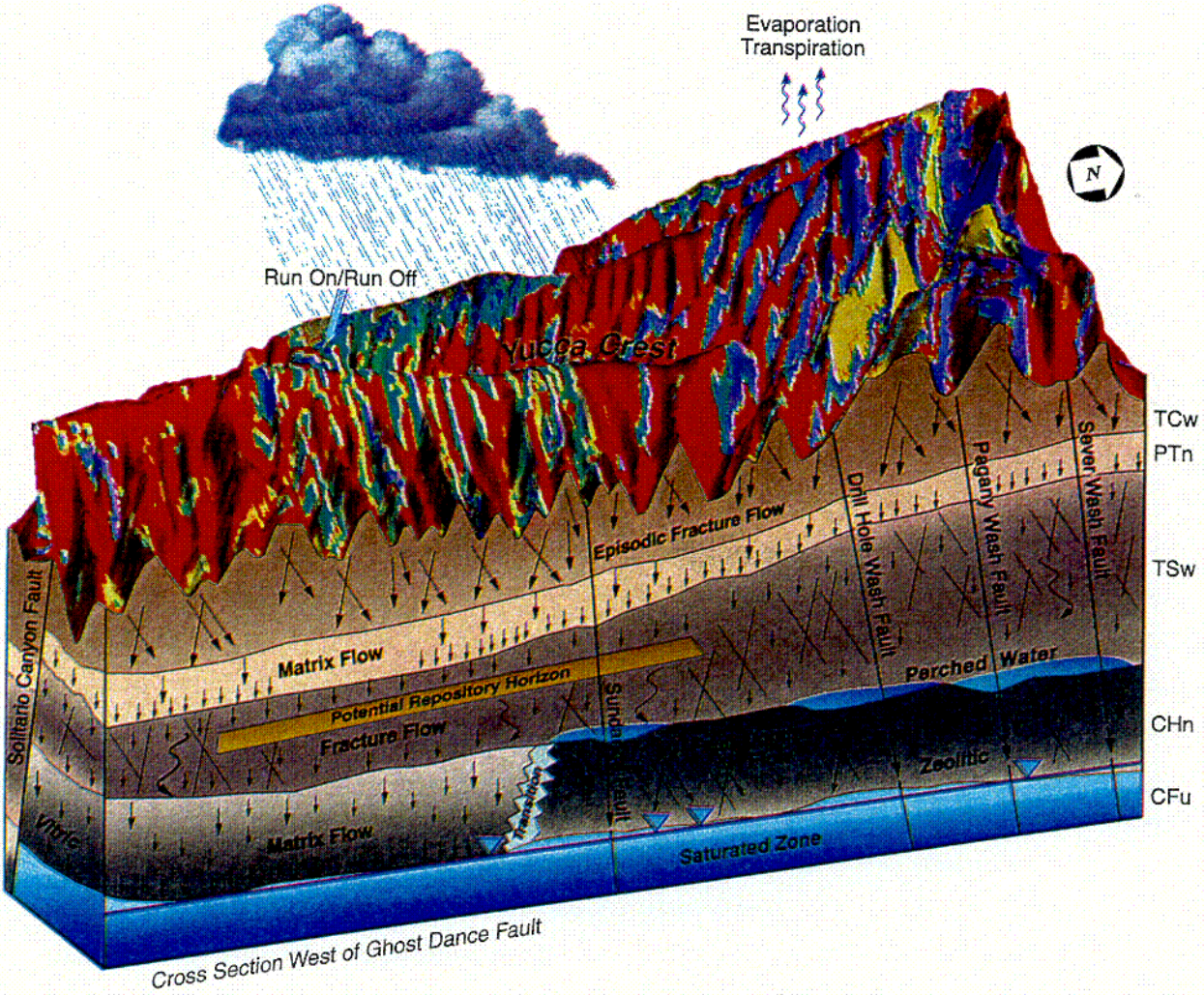

Figure 3.3-2. Schematic Showing Overall Water Flow Behavior in the UZ Including the Relative Importance of Fracture and Matrix Flow Components in the Different Hydrogeologic Units. The blue and red colors on the land surface correspond to high and low infiltration rates, respectively, while the other colors correspond to intermediate infiltration rates (CRWMS M&O 2000, U0030, Figure 1).

C033

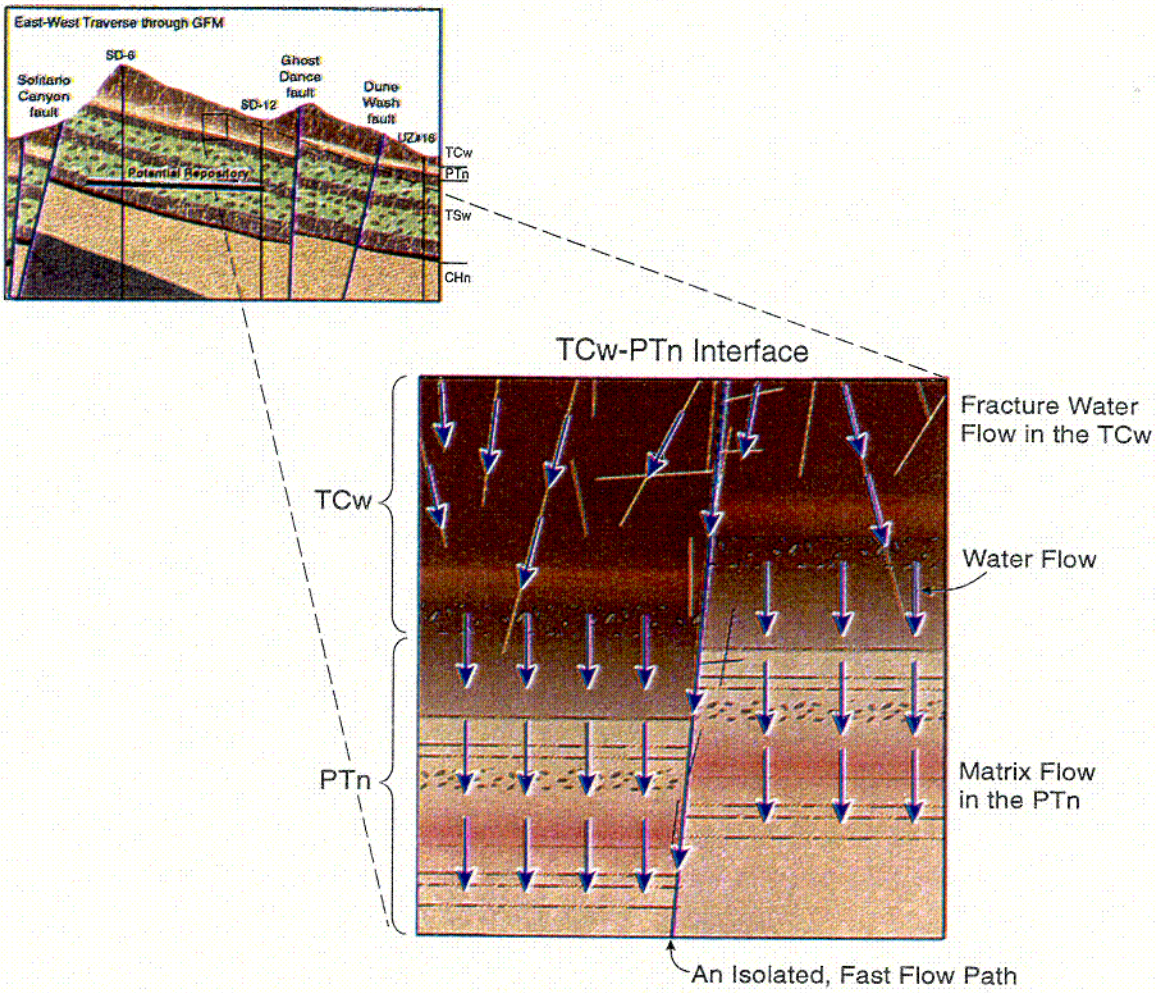

Figure 3.3-3. Schematic Showing Water Flow Behavior within the PTn Characterized by Dominant Matrix Flow and a Few Fast Flow Paths

C034

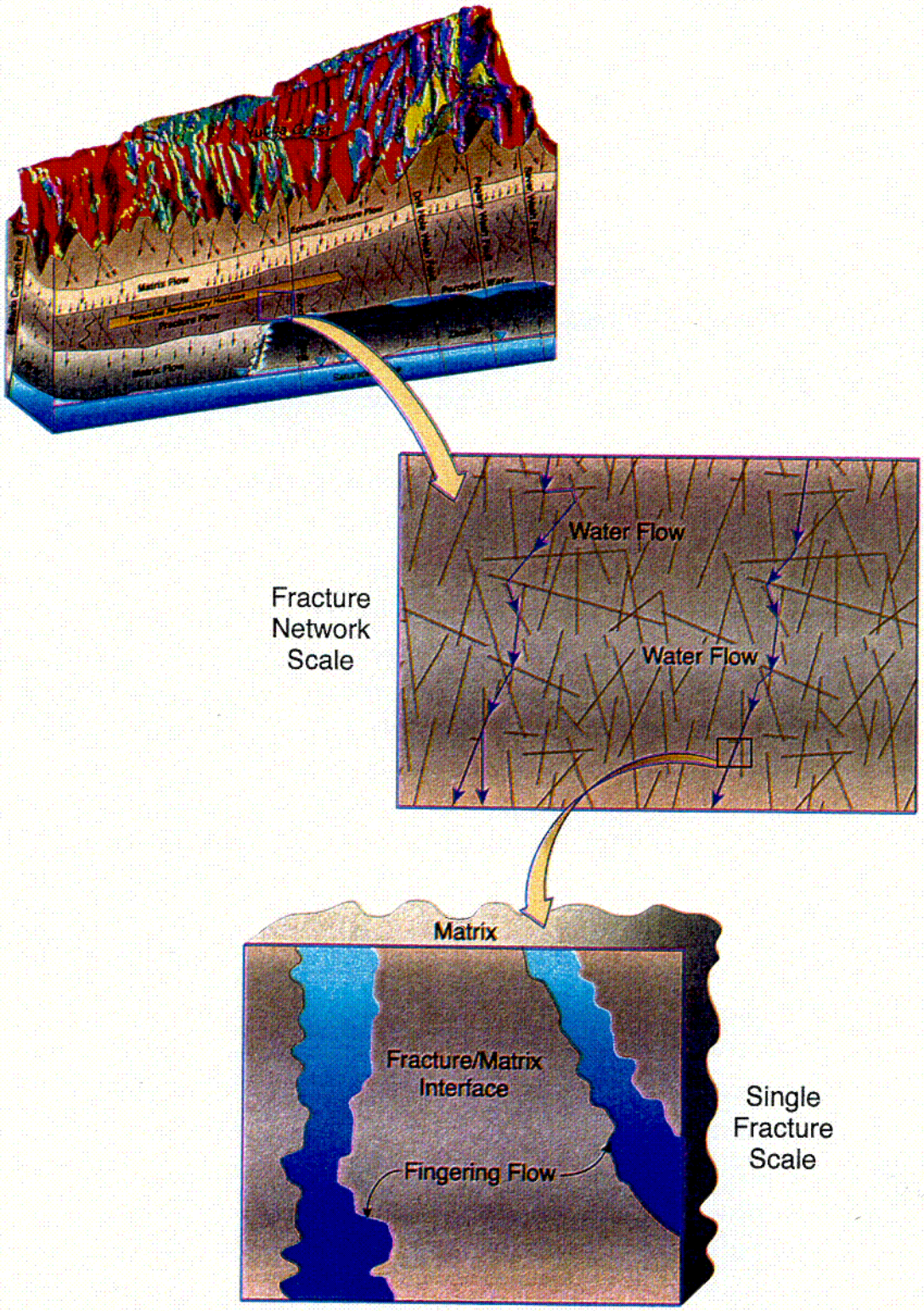

Figure 3.3-4. Water Flow in Fractures Characterized by Fingering Flow at Different Scales

C035

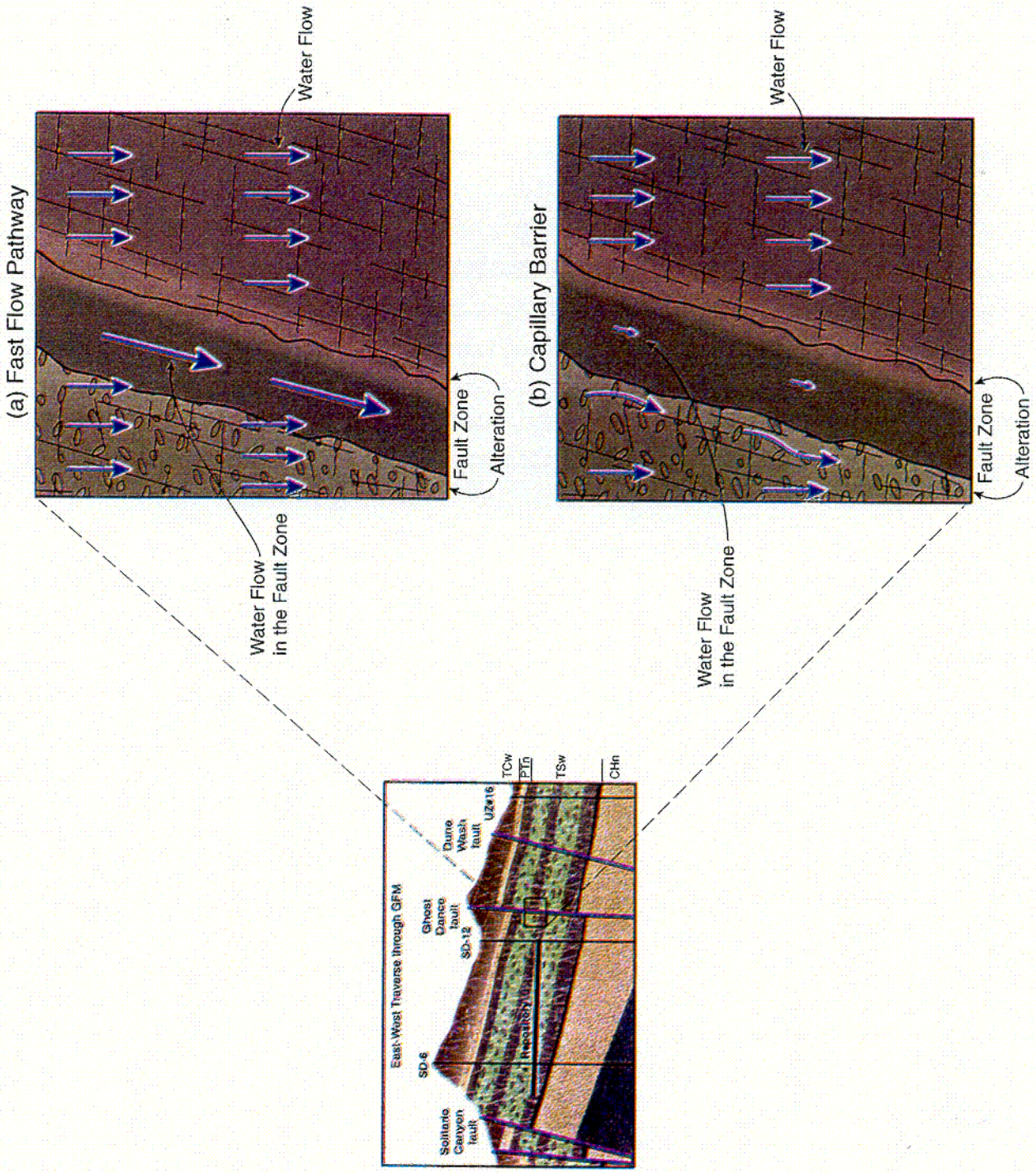

Figure 3.3-5. Major Faults Can Act as Fast-Flow Conduits or Capillary Barriers. The size of the arrows in (a) and (b) indicates the relative magnitude of flow.

C036

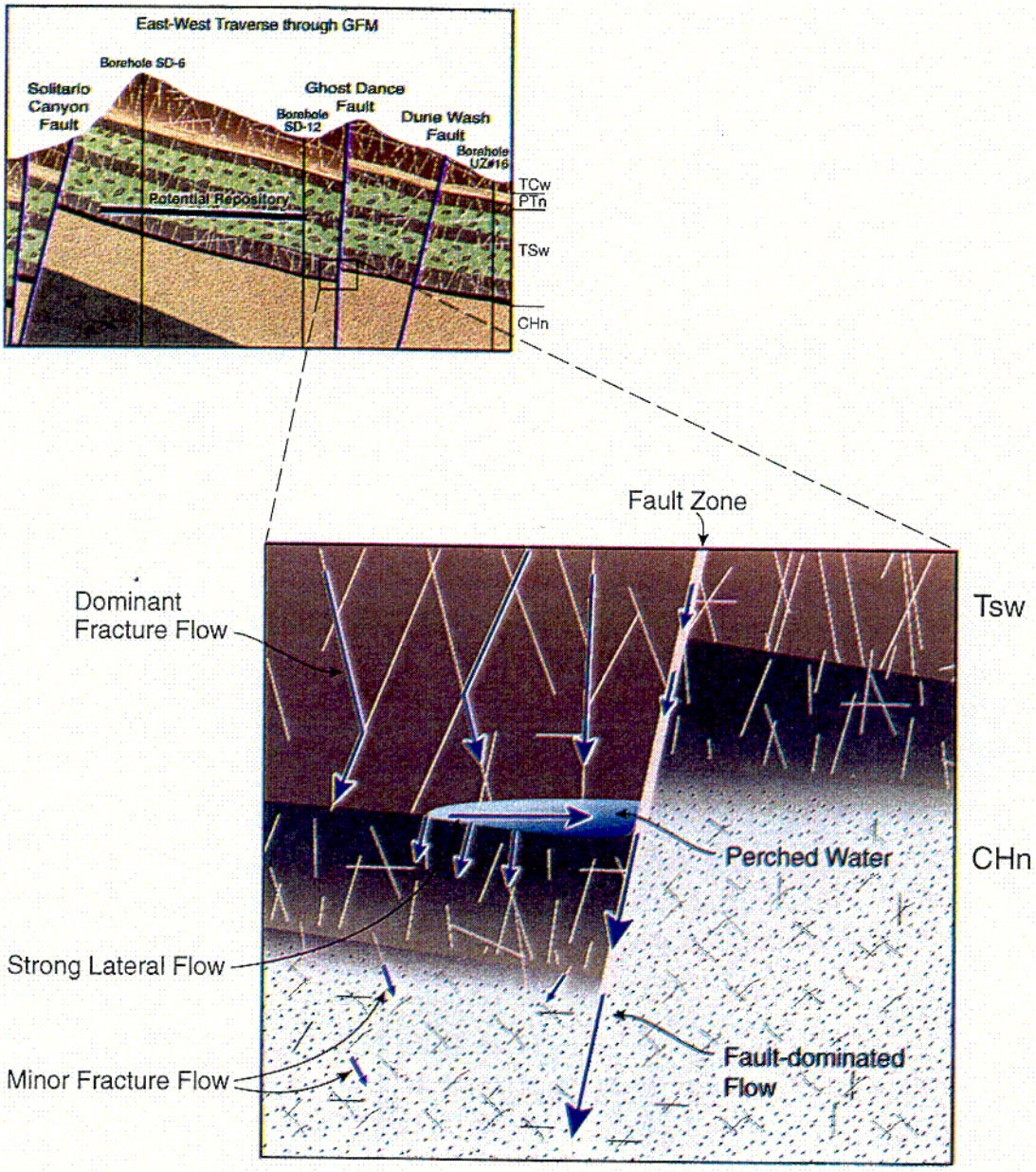

Figure 3.3-6. Schematic Showing Flow Patterns within and near a Perched Water Body Characterized by Strong Lateral Flow within the Perched Water Body and the Associated Fault-Dominated Flow

C037

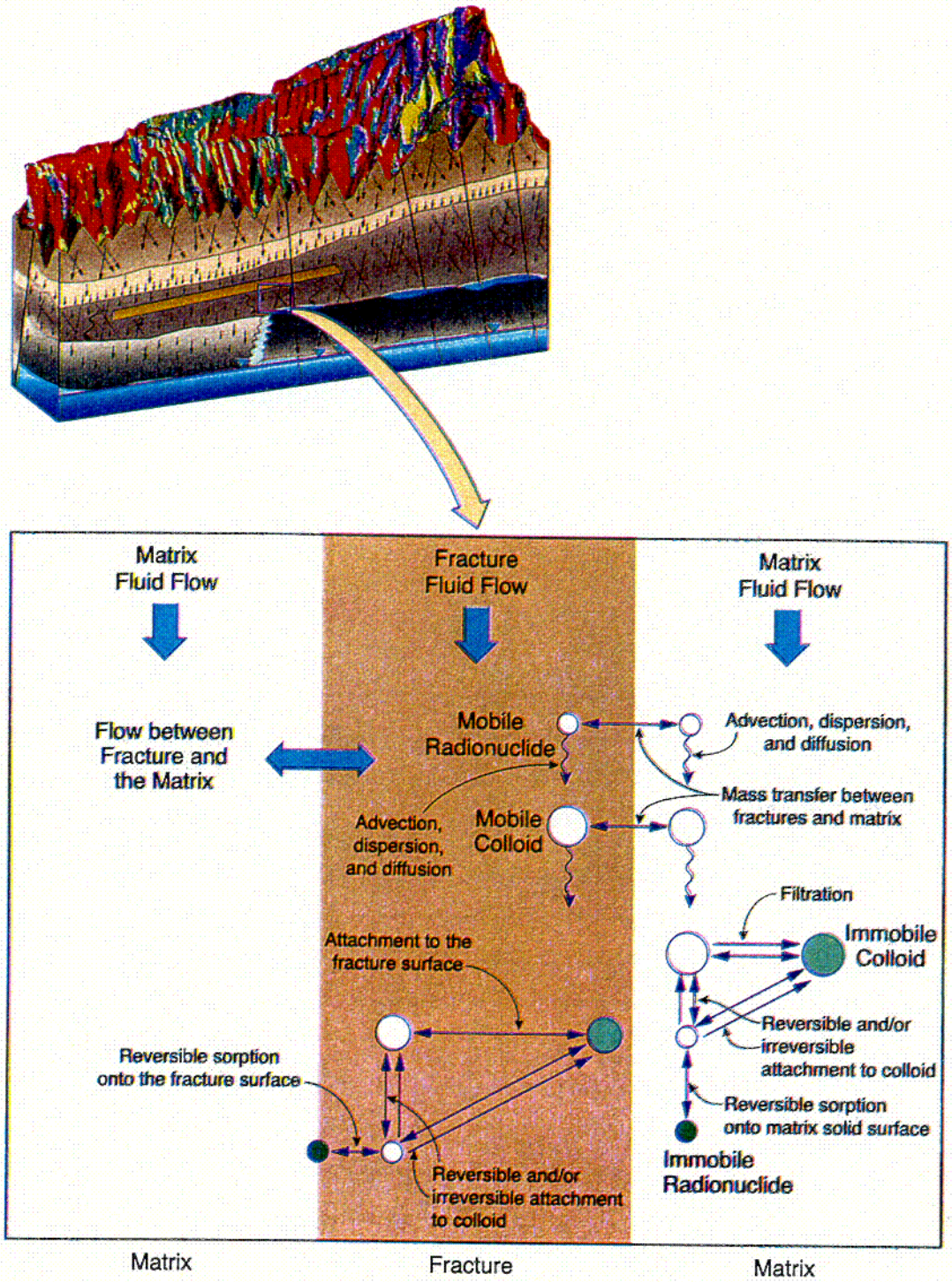

Figure 3.3-7. Important Radionuclide Transport Processes. (Note that the radionuclides also undergo radioactive decay, but this is not shown in the schematic.)

C038

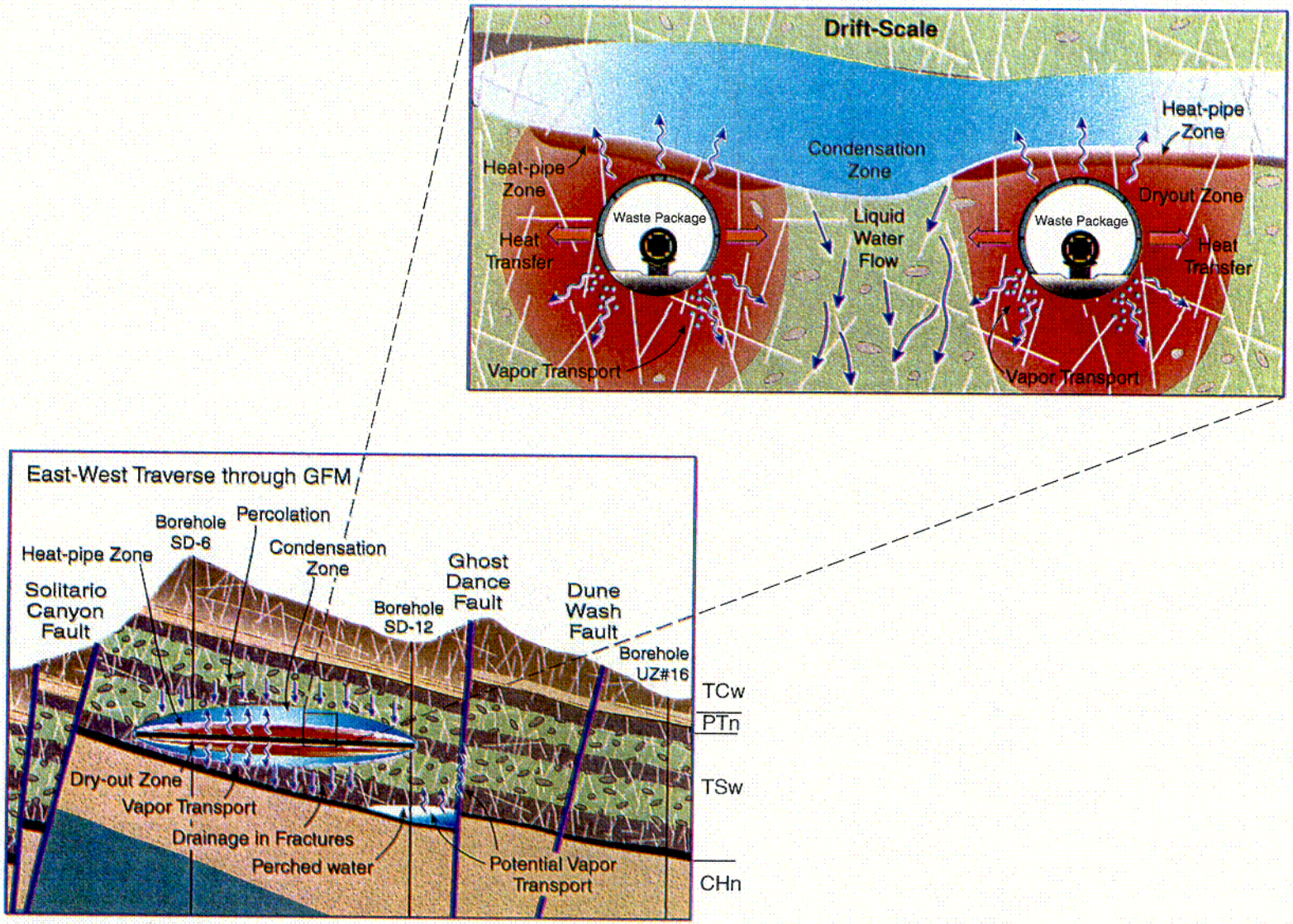

Figure 3.3-8. TH Processes at Mountain and Drift Scales

C039

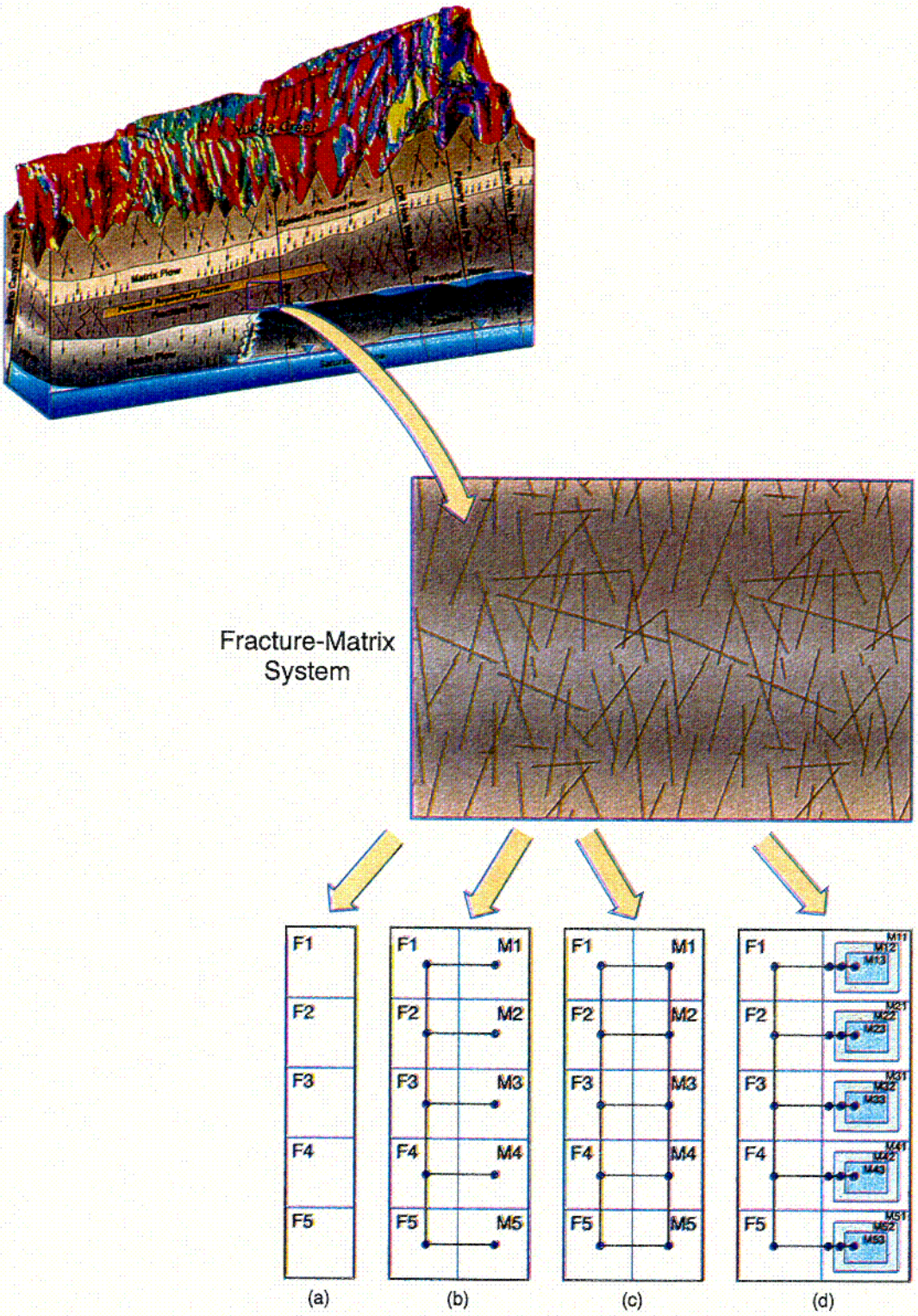

Figure 3.4-1. Schematic Demonstrating (a) ECM, (b) Dual-Porosity with One Matrix Gridblock, (c) Dual-Permeability with One Matrix Gridblock per Fracture Gridblock, and (d) MINC with Three Matrix Gridblocks per Fracture Gridblock

C040

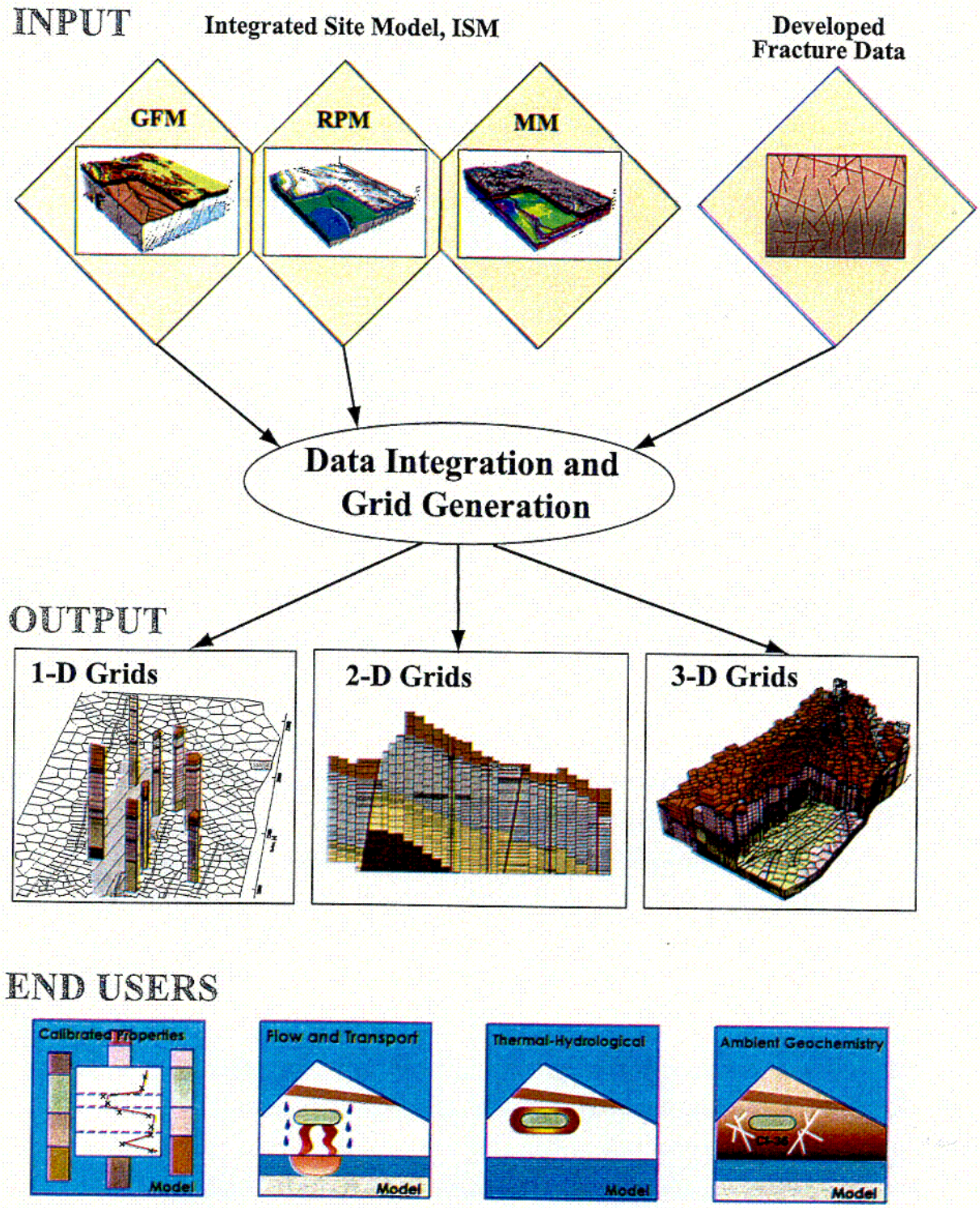

Figure 3.4-2. Flow Diagram Showing Key Input Data Used in Numerical Grid Development, the Types of Grids Generated, and their End Users

C041

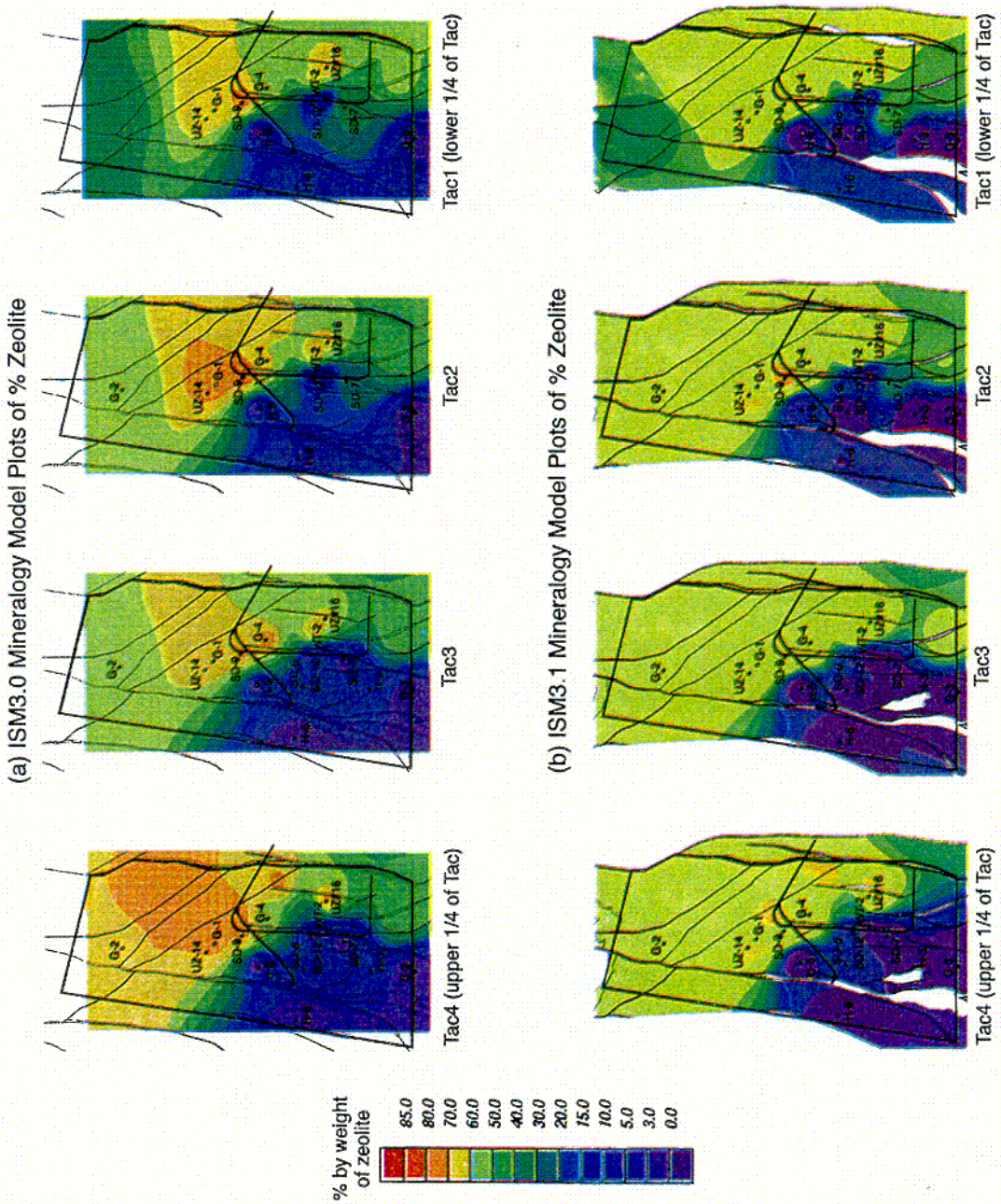

Figure 3.4-3. Distribution of Percent Zeolite Mineral Abundance in the Calico Hills Formation (lithostratigraphic unit Tac): (a) MM2.0, (b) MM3.0. (DTNs: MO9901MWDISMMM.000, MO9910MWDISMMM.003, respectively). Areas with less than or equal to 3% zeolite by weight are considered vitric, or unaltered.

C042

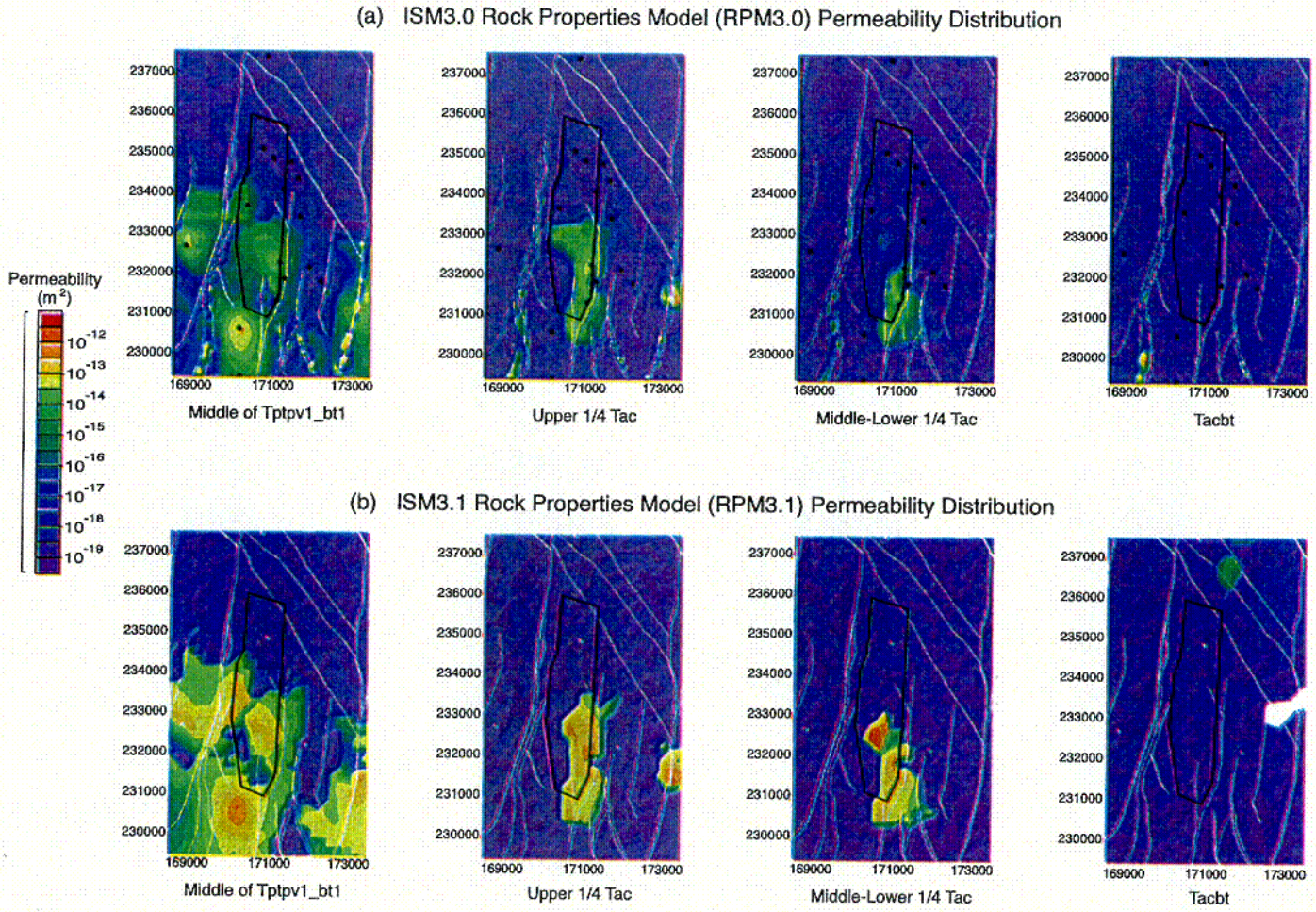

Figure 3.4-4. Distribution of Matrix Permeability (m^2) in Select Layers of the CHn Hydrogeologic Unit: (a) RPM3.0, (b) RPM3.1. (DTNs: MO9901MWDISMRP.000, MO9910MWDISMRP.002, respectively). In order to maintain consistent parameters within the UZ Flow and Transport Model PMR, saturated hydraulic conductivity (K_{sat}, m/s) from the RPM was converted to permeability (m^2) by multiplying K_{sat} values by 10^{-7}.

C043

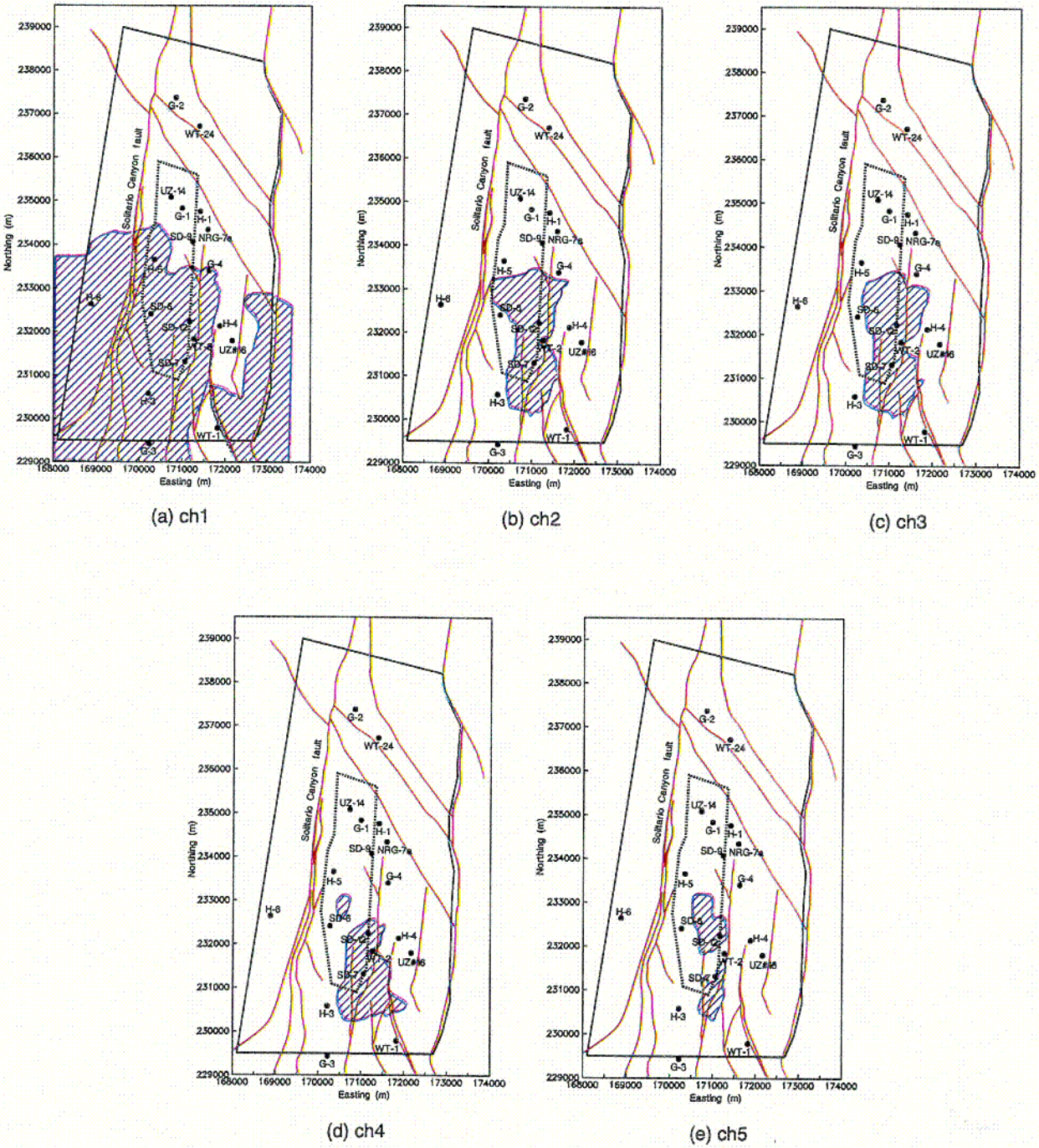

Figure 3.4-5. Extent of Vitric Region (Indicated by Pattern of Diagonal Lines) in Model Layers (a) ch1, (b) ch2, (c) ch3, (d) ch4, and (e) ch5. White areas indicate prevalent zeolitization (from CRWMS M&O 2000, U0000, Figure 5).

C044

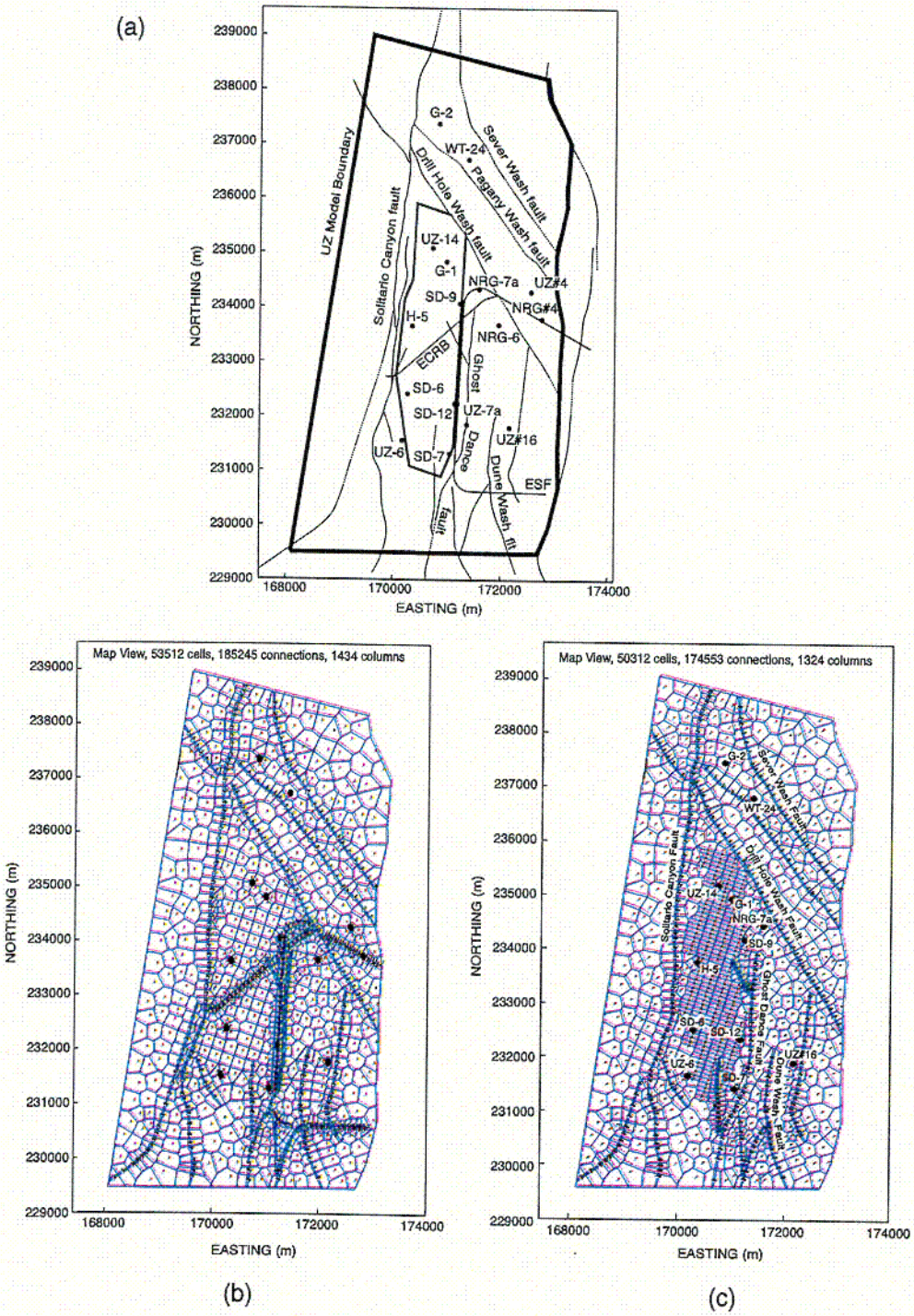

Figure 3.4-6. Plan-View (a) Schematic Showing the UZ Model Boundary, the Repository Outline, Major Fault Locations Adapted from GFM3.1, Select Boreholes, the ESF, and the ECRB, (b) Numerical Grid Design for the Mountain-Scale Model Used for UZ Calibration (adapted from Figure V-1 of CRWMS M&O 2000, U0000), and (c) Numerical Grid Design for the Mountain-Scale Model Used for PA Calculations (Adapted from CRWMS M&O 2000, U0000, Figure VI-1).

C045

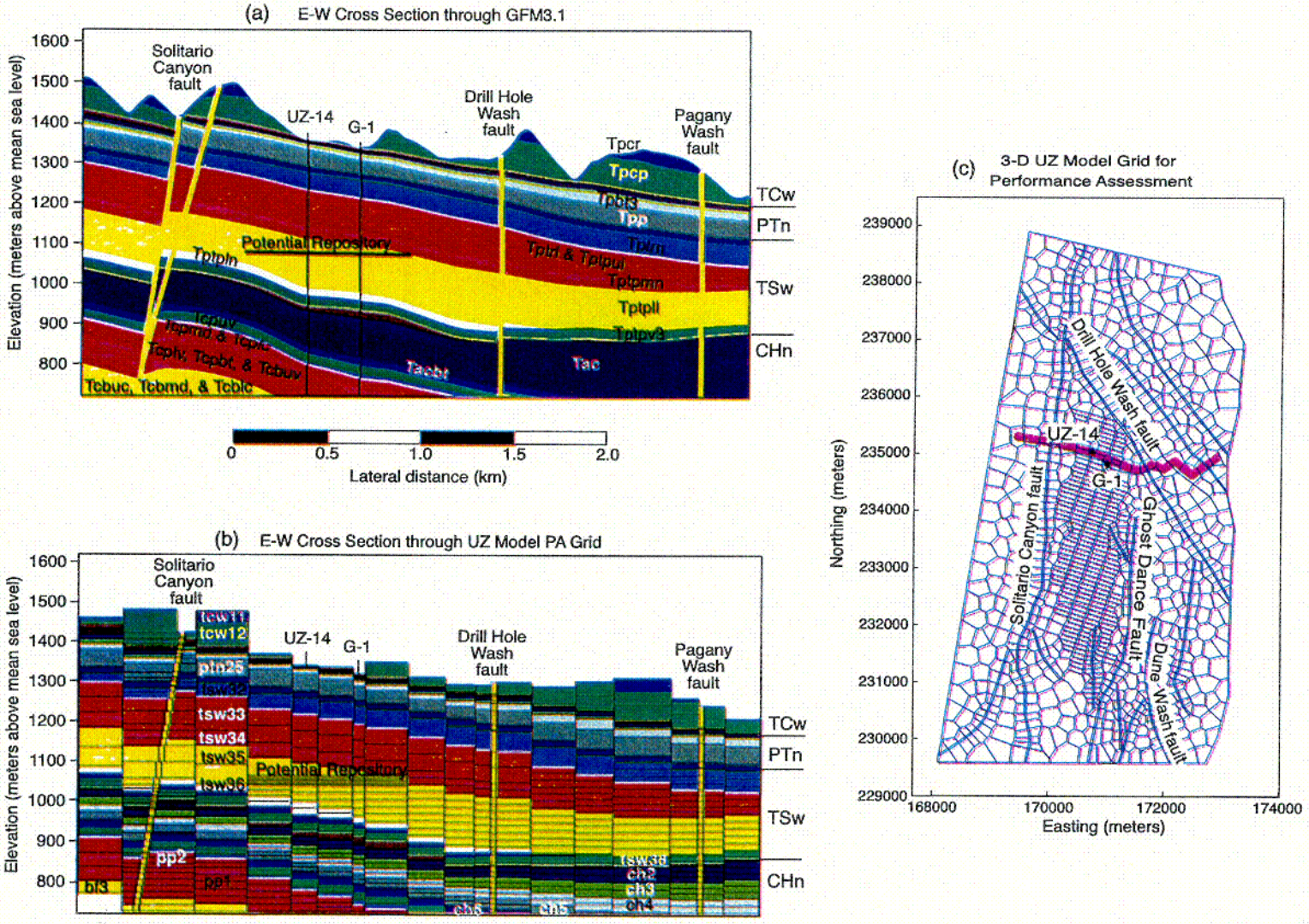

Figure 3.4-7. East-West Cross-Section through Borehole UZ-14: (a) Adapted from Data Contained in CRWMS M&O (2000, I0035) (b) from the 3-D UZ Model Numerical Grid for PA (Adapted from CRWMS M&O 1999a, Figure VI-2). The 3-D UZ Model Grid in plan view (c) shows the location of the cross section. Bottom elevation along cross sections is 730 m above mean sea level.

C046

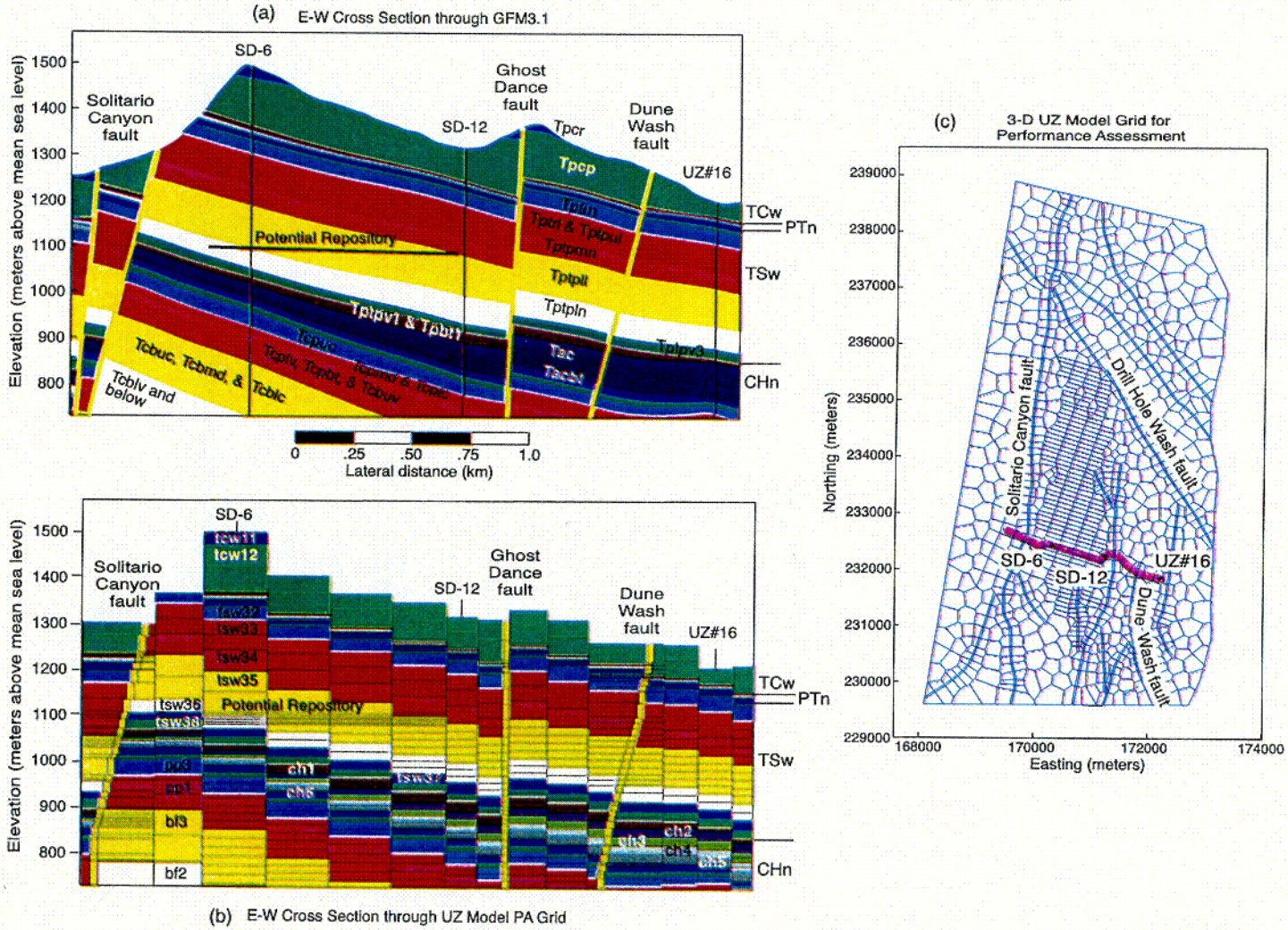

Figure 3.4-8. East-West Cross-Section through Boreholes SD-6, SD-12, UZ#16: (a) Adapted from Data Contained in CRWMS M&O (2000, I0035) (b) from the 3-D UZ Model Numerical Grid for PA (Adapted from CRWMS M&O 1999a, Figure VI-3). The 3-D UZ Model Grid in plan view (c) shows the location of the cross section. Bottom elevation along cross sections is 730 m above mean sea level.

C047

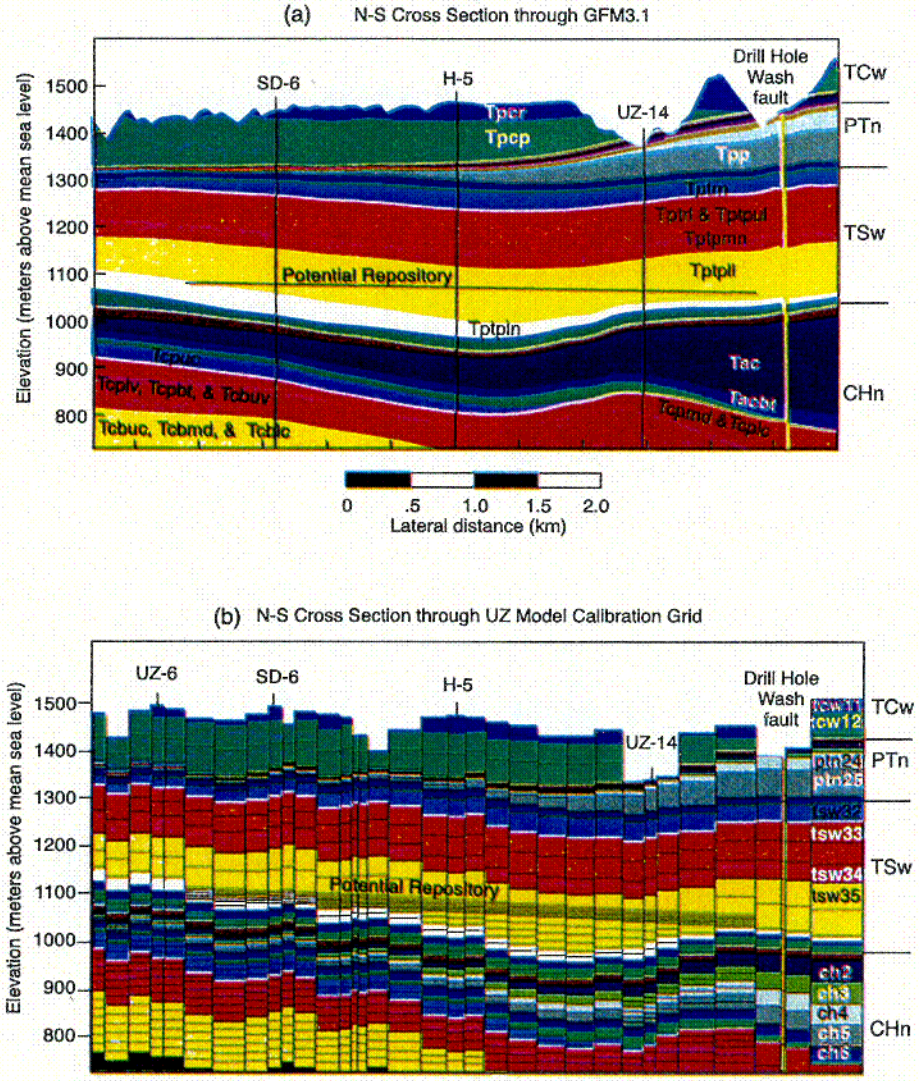

Figure 3.4-9. North-South Cross-Section through Boreholes UZ-14, H-5, and SD-6: (a) Adapted from Data Contained in CRWMS M&O (2000, I0035) (b) from the 3-D UZ Model Calibration Grid (Adapted from CRWMS M&O 1999a, Figure V-4). The 3-D UZ Model Calibration Grid in plan view (c) shows the location of the cross sections. Bottom elevation along cross sections is 730 m above mean sea level.

C048

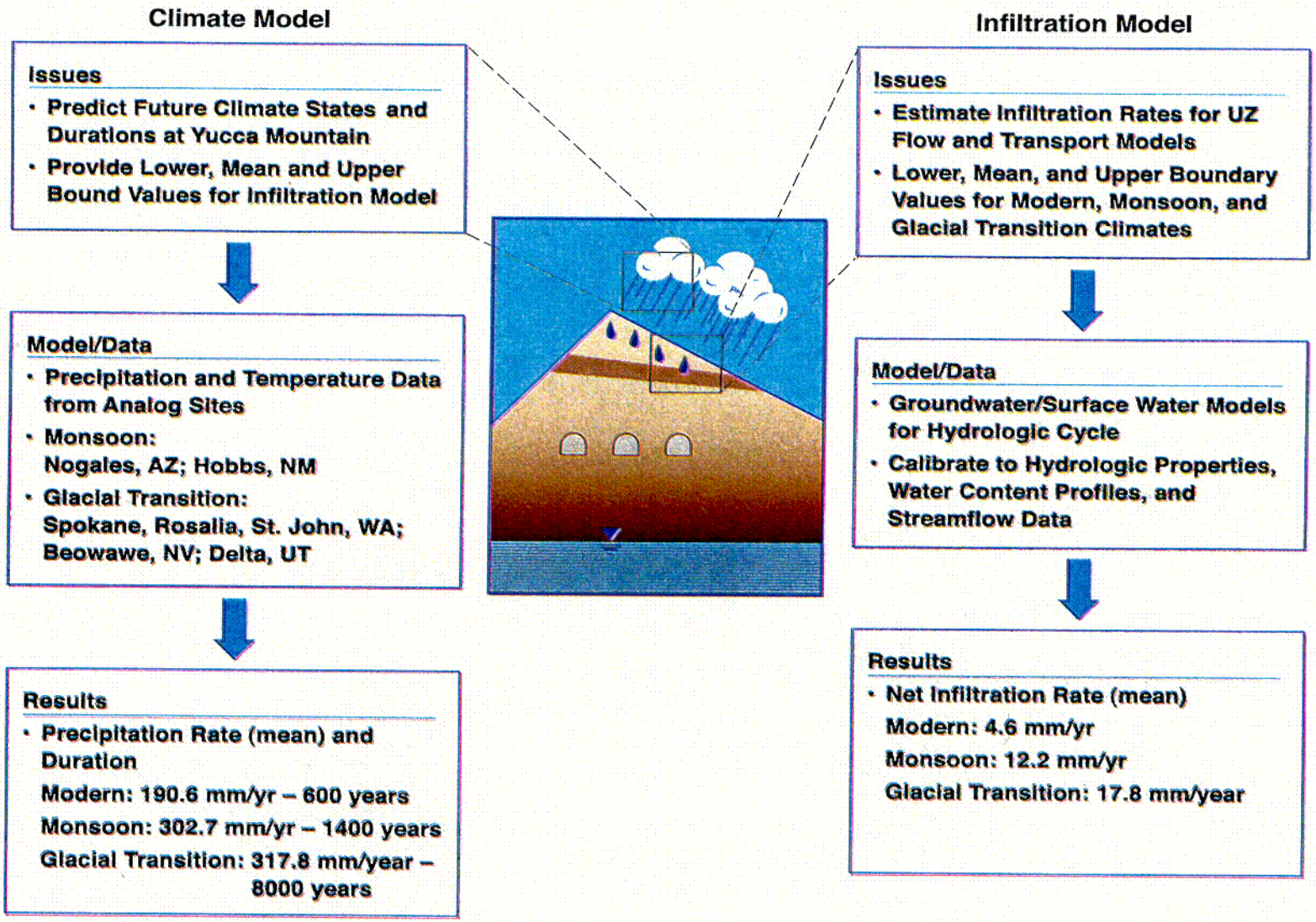

Figure 3.5-1. Summary of Issues, Modeling Methodology, Data, and Results for both the Climate and Infiltration Models

C049

(a)

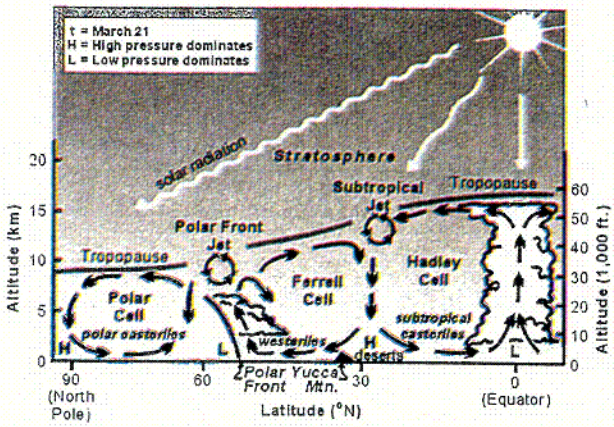

(b)

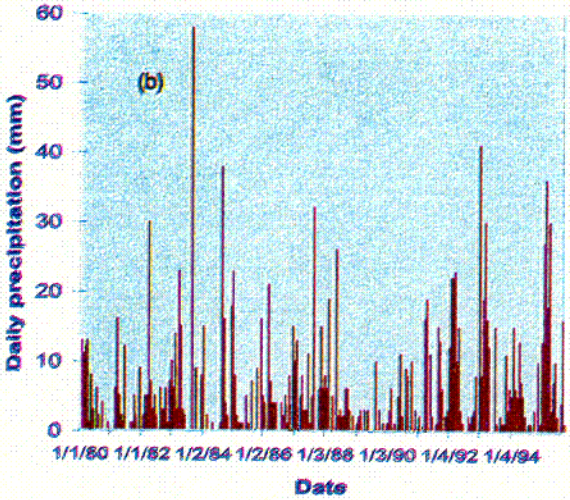

(c)

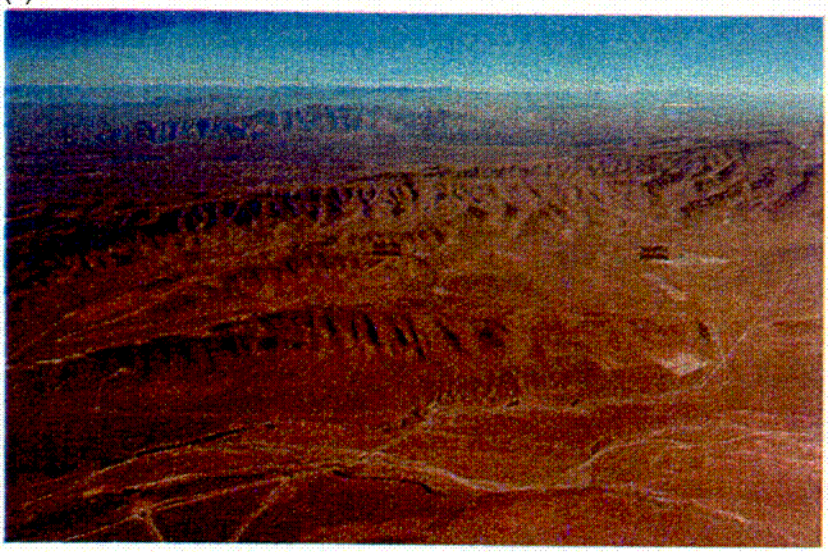

Figure 3.5-2. (a) Generalized View of Present-Day Atmospheric Circulation (USGS 2000, U0005, Figure 2) and (b) Daily Precipitation Record Between 1980 and 1995 at Yucca Mountain (USGS 2000, U0010, Figure 6-18) with (c) an Aerial View of the Arid Conditions at the Yucca Mountain Site

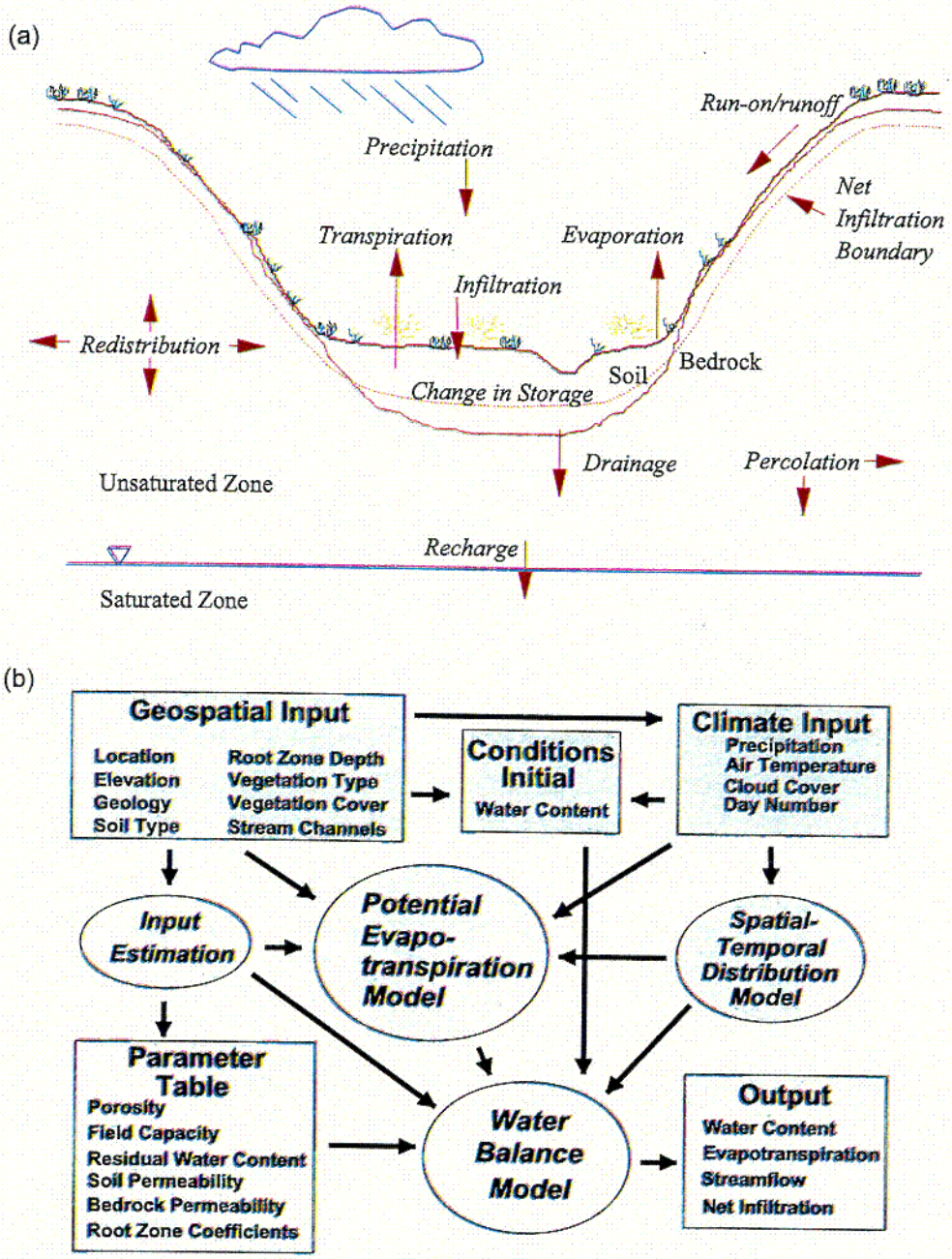

Figure 3.5-3. (a) Field-Scale Water Balance and Processes Controlling Net Infiltration (USGS 2000, U0010, Figure 5-1) and (b) Major Components of the Net Infiltration Modeling Process (USGS 2000, U0010, Figure 6-1)

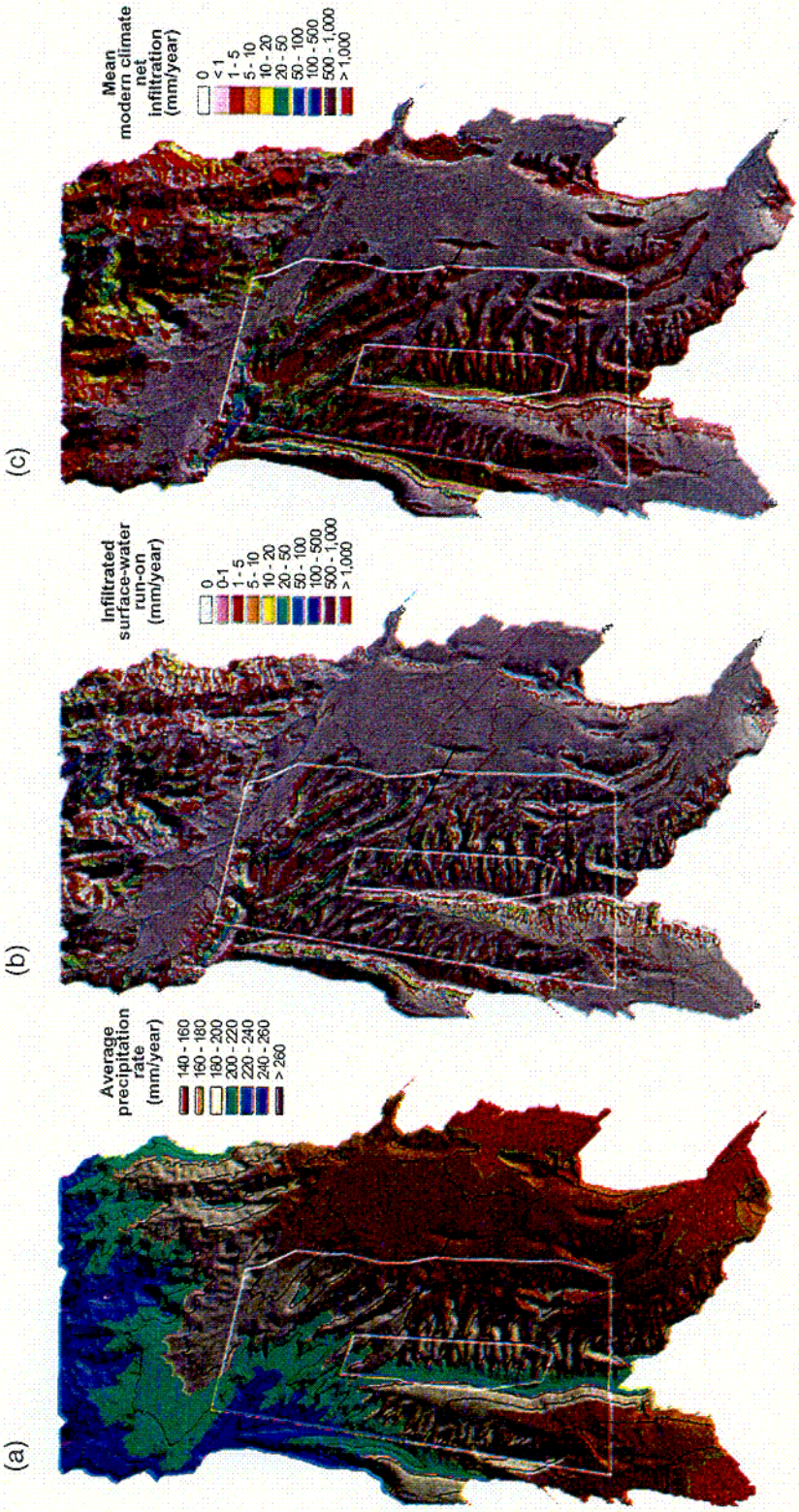

Figure 3.5-4. (a) Precipitation (USGS 2000, U0010, Figure 7-1), (b) Surface Run-On (USGS 2000, U0010, Figure 7-3) and (c) Net-Infiltration Rates (USGS 2000, U0010, Figure 7-4) for the Mean Modern Climate Scenario

CD52

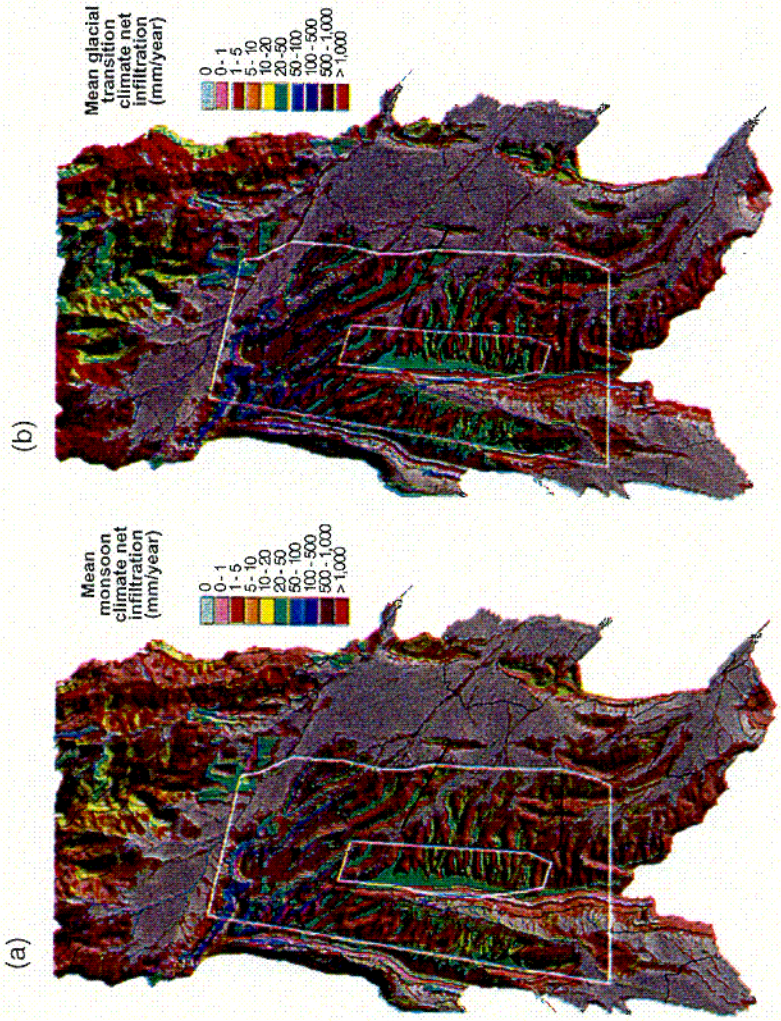

Figure 3.5-5. Net-Infiltration Rates for (a) Mean Monsoon (USGS 2000, U0010, Figure 7-7) and (b) Mean Glacial-Transition (USGS 2000, U0010, Figure 7-14) Climates

C053

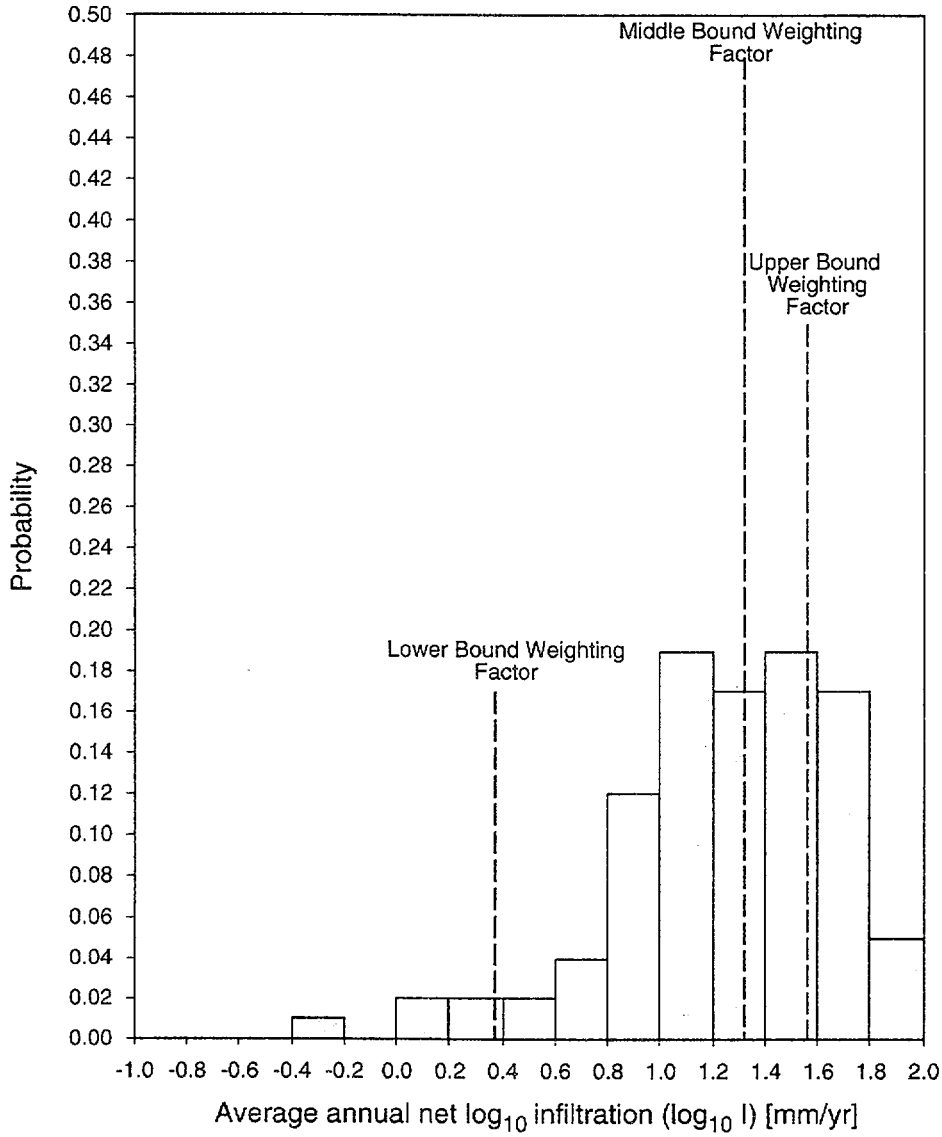

Figure 3.5-6. Histogram of Log of Potential Repository-Average Infiltration for Glacial-Transition Climate (adapted from CRWMS M&O 2000, U0095, Figure 6-2)

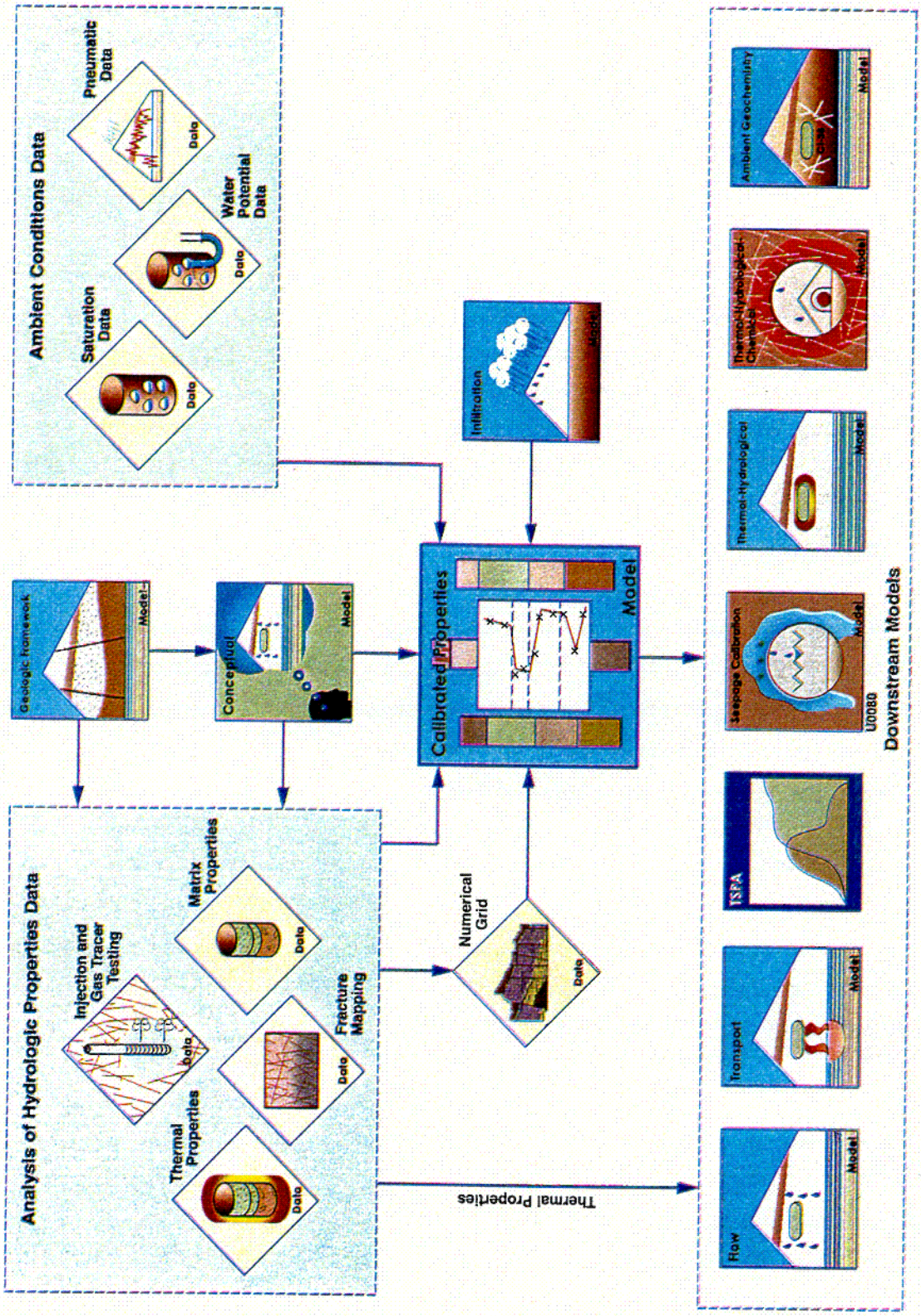

Figure 3.6-1. Relationship of the Analysis of Hydrologic Properties Data and the Calibrated Properties Model to Input Data and Models and to Analyses and Models that use the Developed UZ Properties

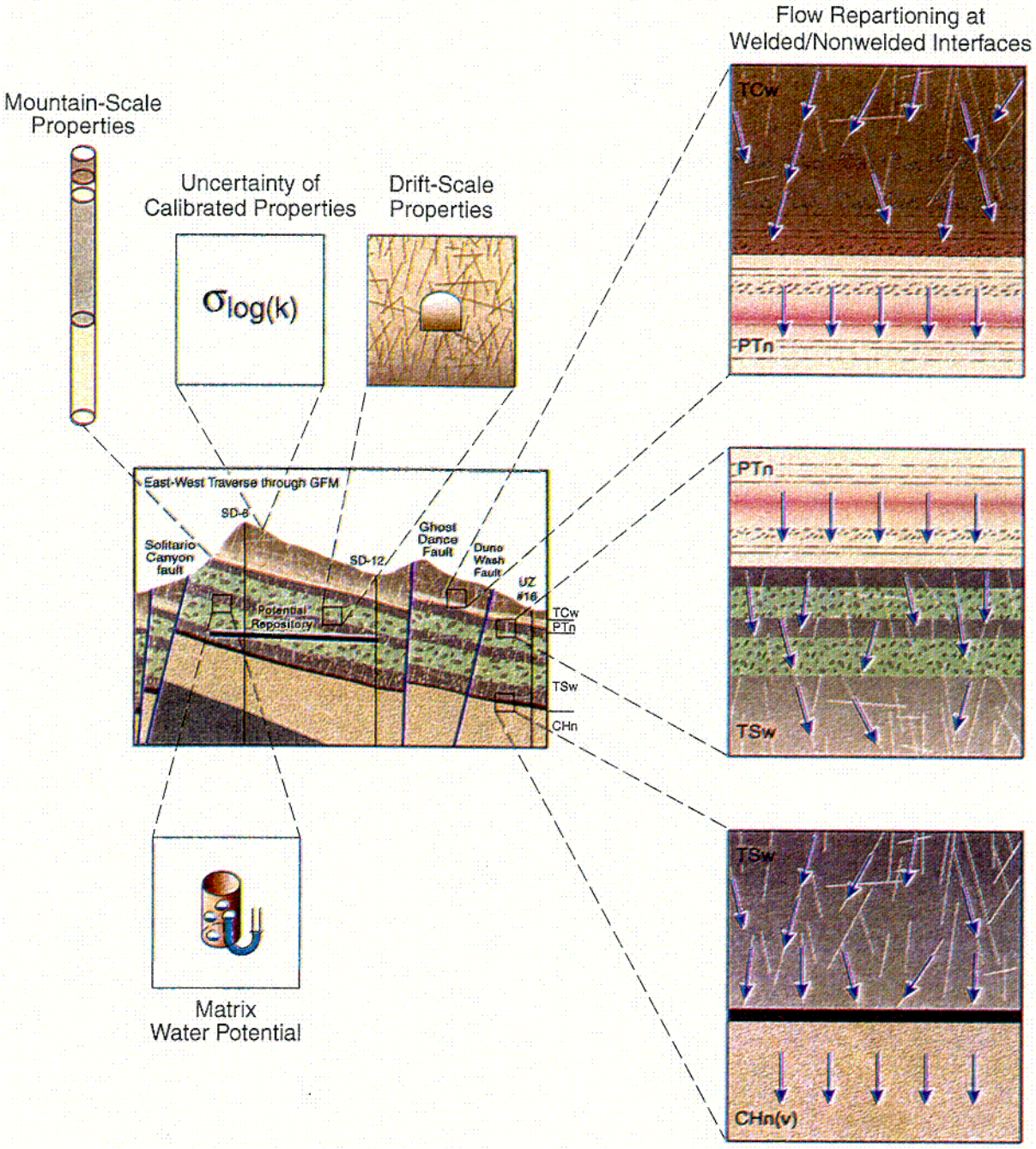

Figure 3.6-2. Issues for Development of UZ Properties

C055

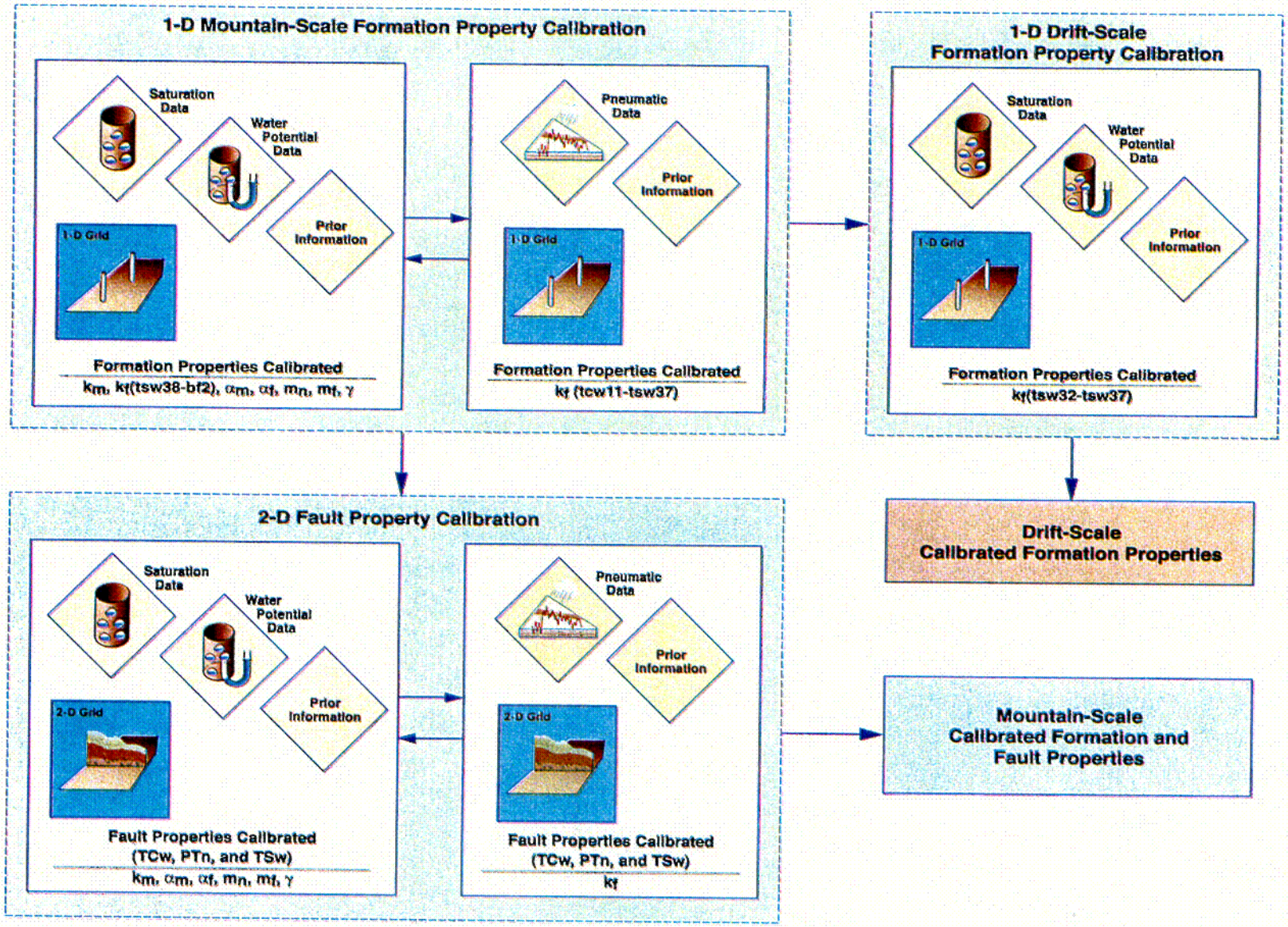

Figure 3.6-3. Calibrated Property Development

C056

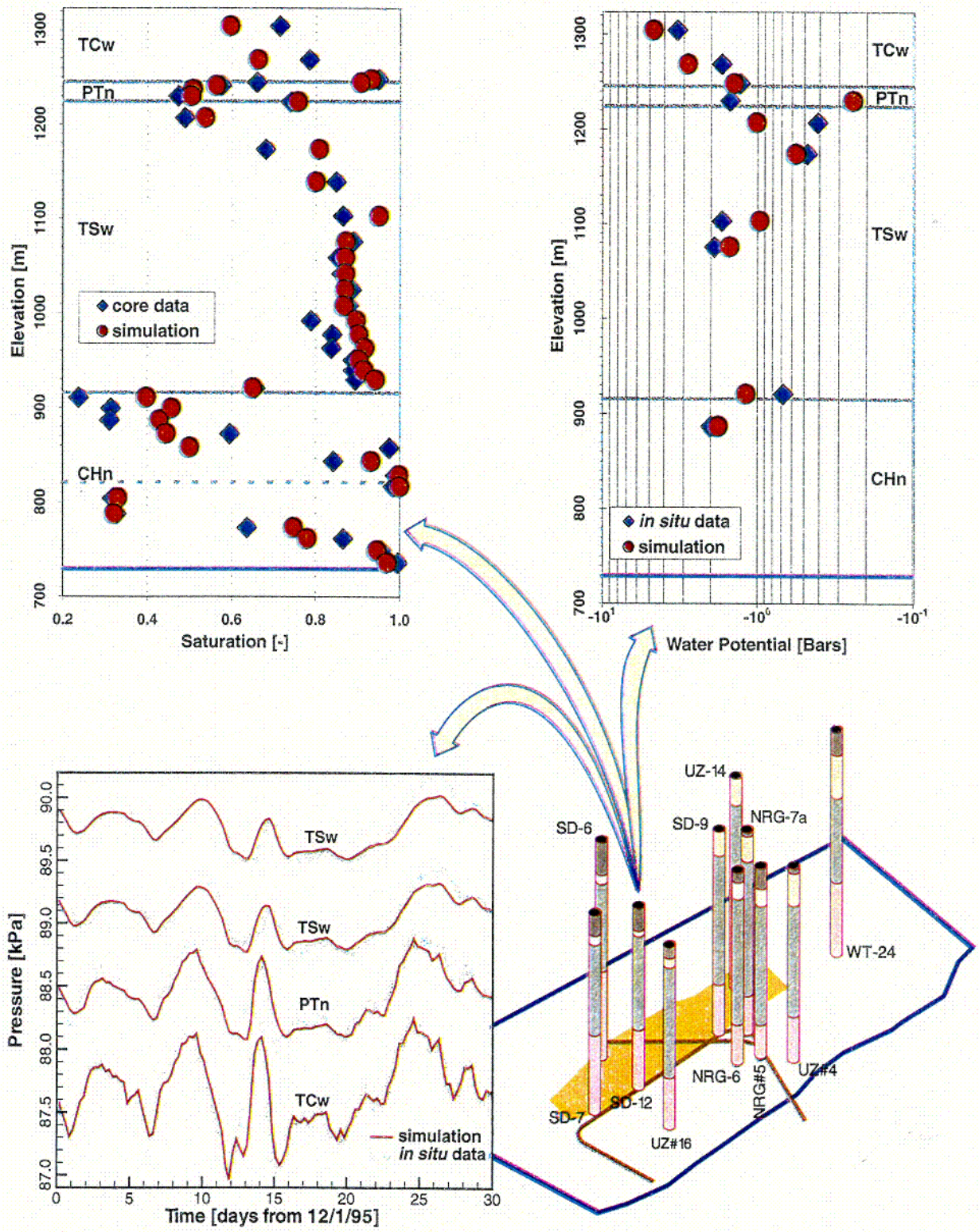

Figure 3.6-4. Calibrated 1-D Simulation Match to Saturation, Water Potential, and Pneumatic Data. Data from Borehole USW SD-12 for the Base Case Infiltration Scenario (adapted from CRWMS M&O 2000, U0035, Figures 2, 3, and 4)

C057

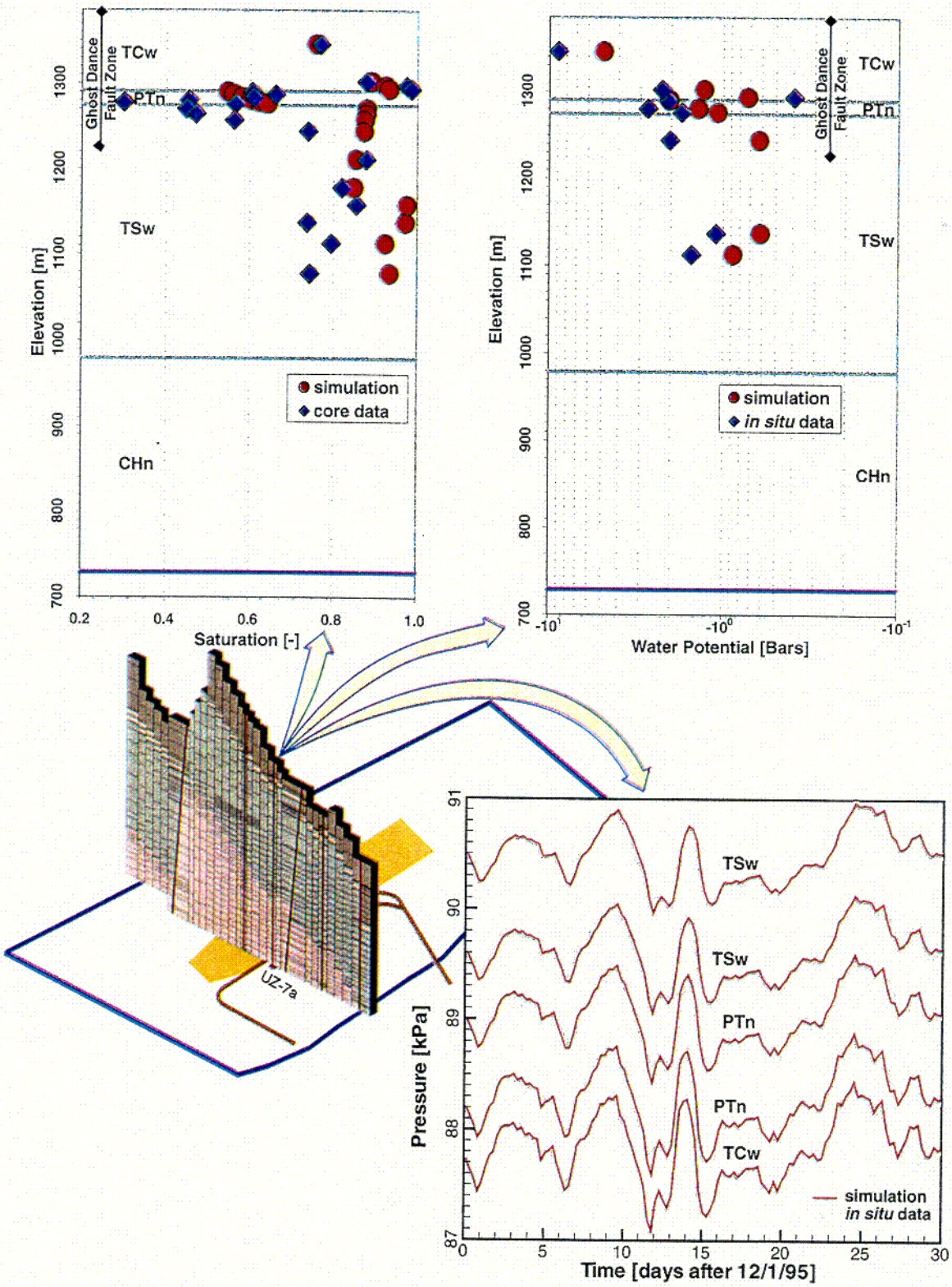

Figure 3.6-5. Calibrated 2-D Simulation Match to Saturation, Water Potential, and Pneumatic Data from Borehole USW UZ-7a Base Case Infiltration Scenario (adapted from CRWMS M&O 2000, U0035, Figures 9, 10, and 11)

C058

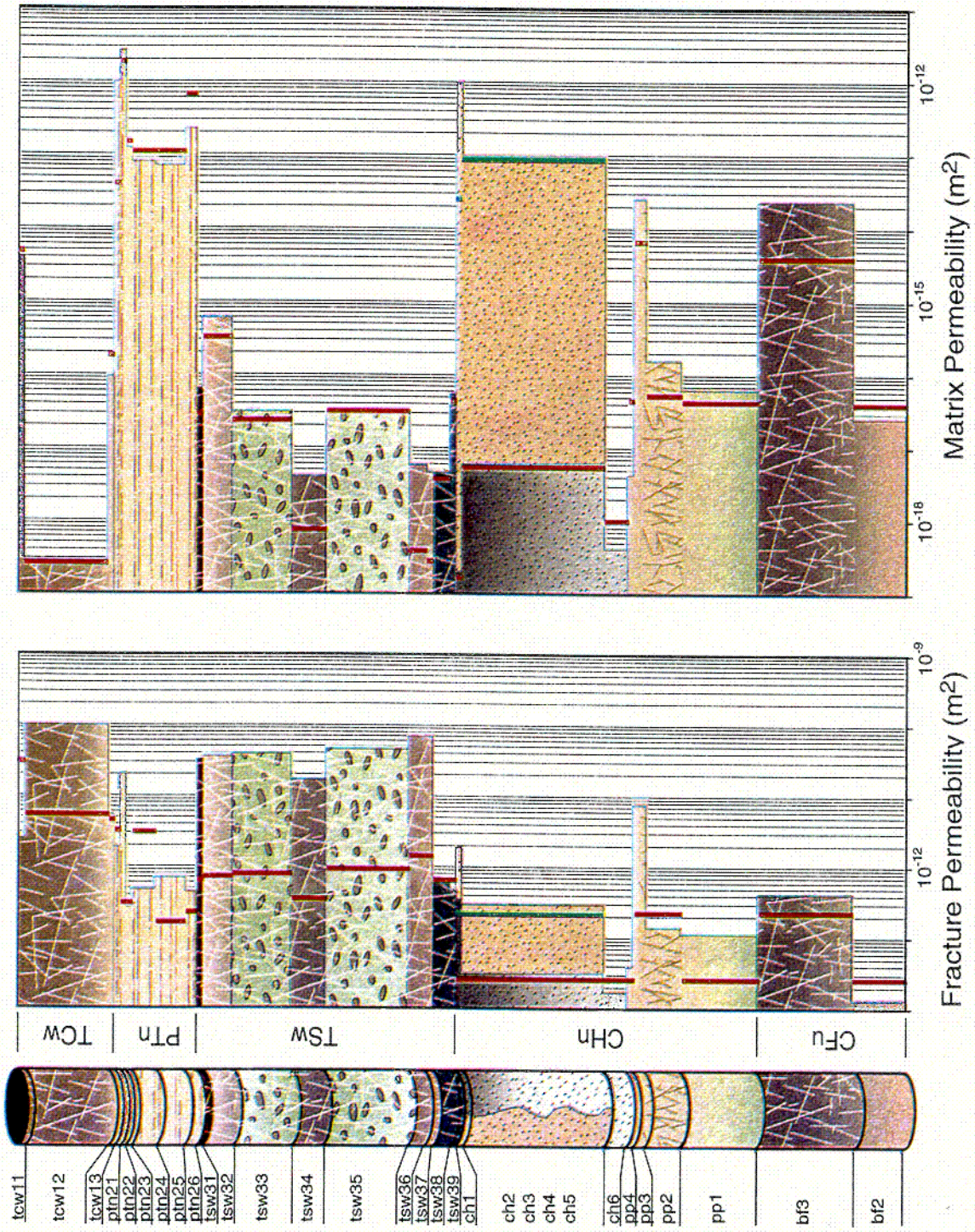

Figure 3.6-6. Initial Estimate of and Calibrated Fracture and Matrix Permeability for the Base Case, Present-Day Infiltration Scenario (adapted from data in CRWMS M&O 2000, U0035, Table 13). The calibrated values for the vitric ch1 through ch5 layers are shown in a lighter color than the zeolitic. The prior information (initial estimate) is shown as a red line (green for the vitric ch1 through ch5).

C059

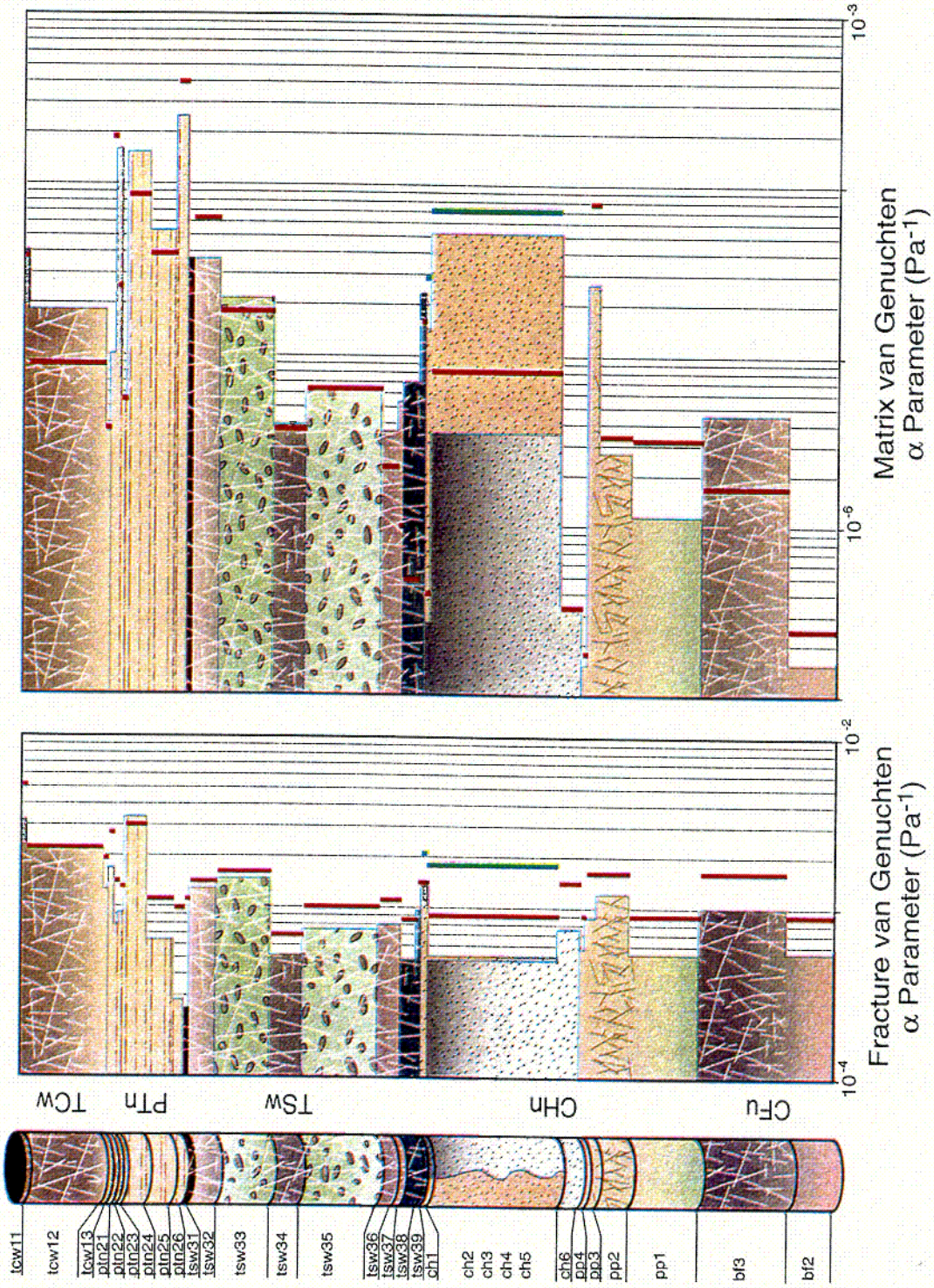

Figure 3.6-7. Initial Estimate of and Calibrated Fracture and Matrix van Genuchten α Parameter for the Base Case, Present-Day Infiltration Scenario (adapted from data in CRWMS M&O 2000, U0035, Table 13). The calibrated values for the vitric ch1 through ch5 layers are shown in a lighter color than the zeolitic. The prior information (initial estimate) is shown as a red line (green for the vitric ch1 through ch5).

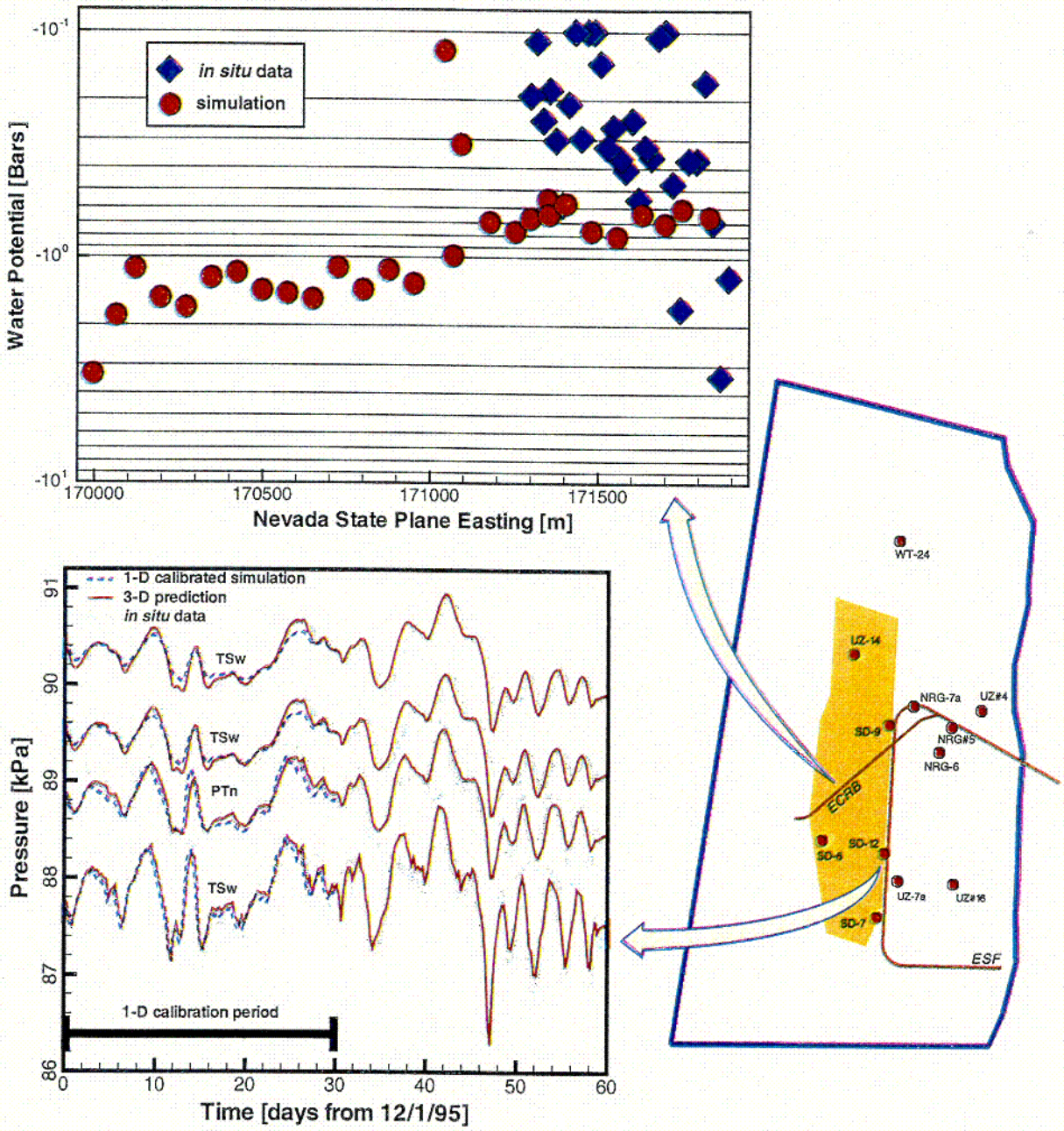

Figure 3.6-8. Comparison of Predictions from the 3-D Model with In Situ Water Potential Data from the ECRB Cross Drift and Pneumatic Pressure Data from Borehole USW SD-12 (adapted from CRWMS M&O 2000, U0050, Figures 6-69 and 6-70)

C061

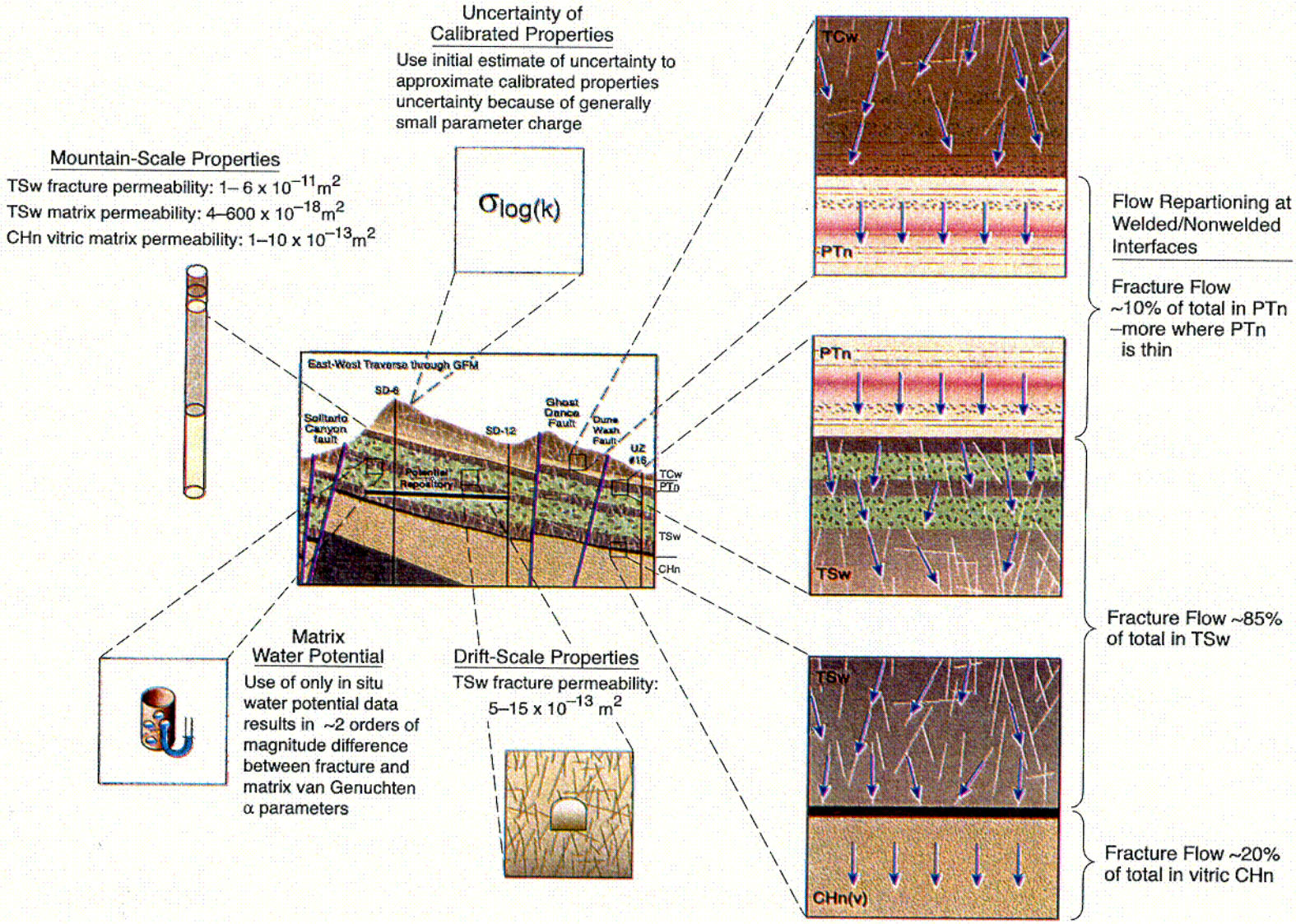

Figure 3.6-9. Important Results of Analysis of Hydrologic Properties Data and Calibrated Properties Model

C062

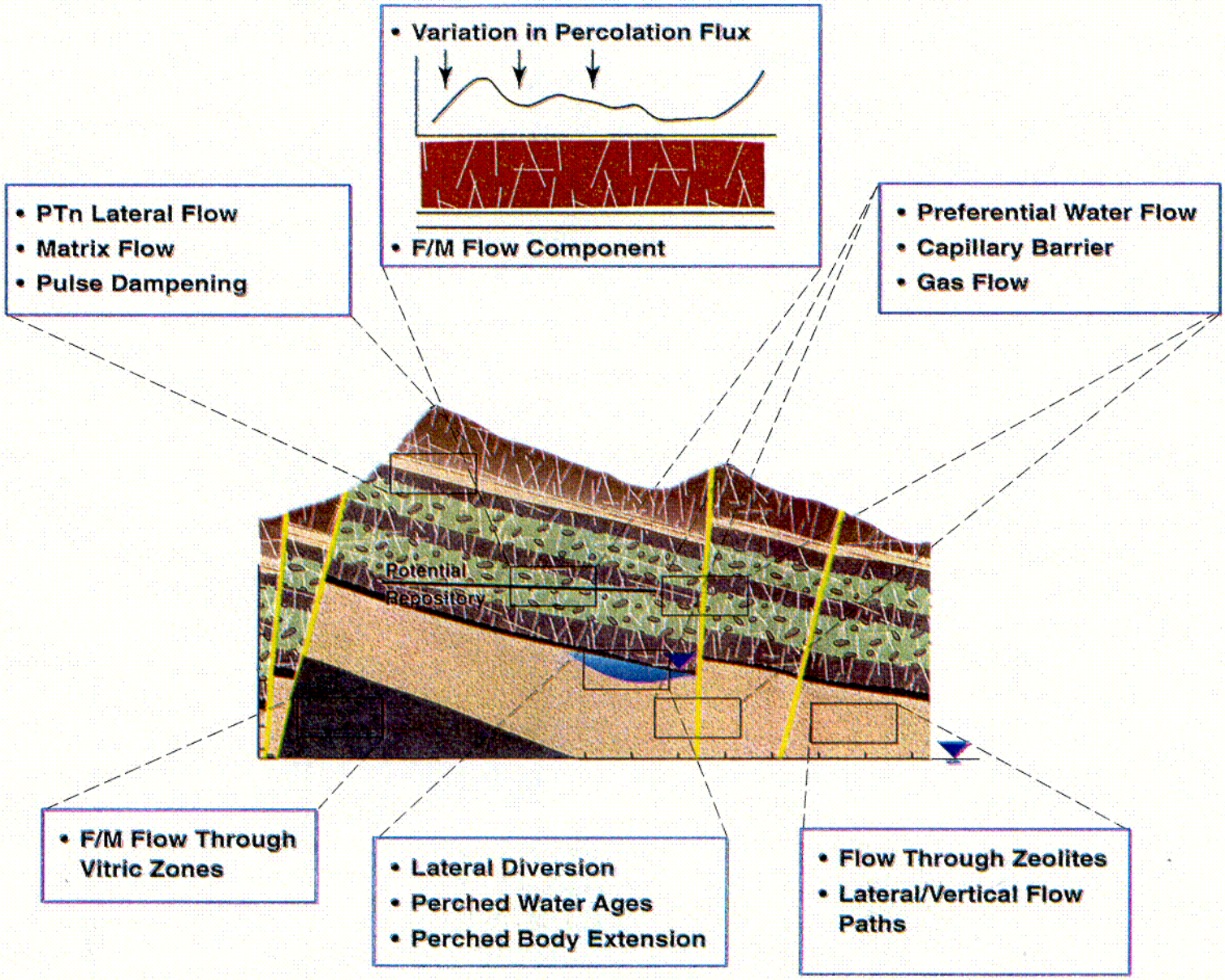

Figure 3.7-1. Diagram Showing the Important UZ Flow and Transport Issues, Addressed by the Flow Model and Its Submodels

C063

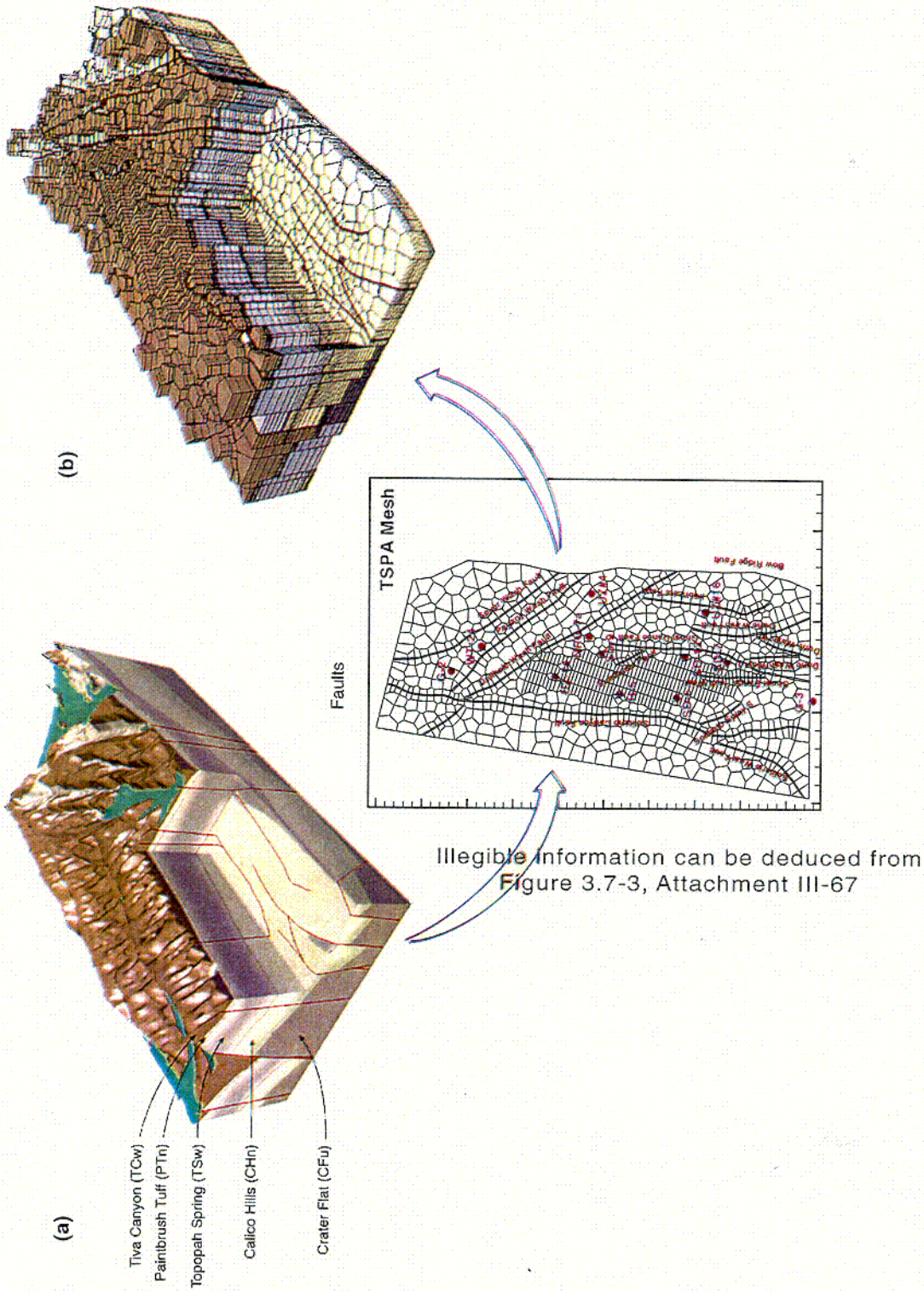

Illegible information can be deduced from Figure 3.7-3, Attachment III-67

Figure 3.7-2. Perspective View of the UZ Model Domain of Yucca Mountain, Showing the Hydrogeological Units and Layers and Major Faults: (a) Geological Model and (b) Numerical Grid

C064

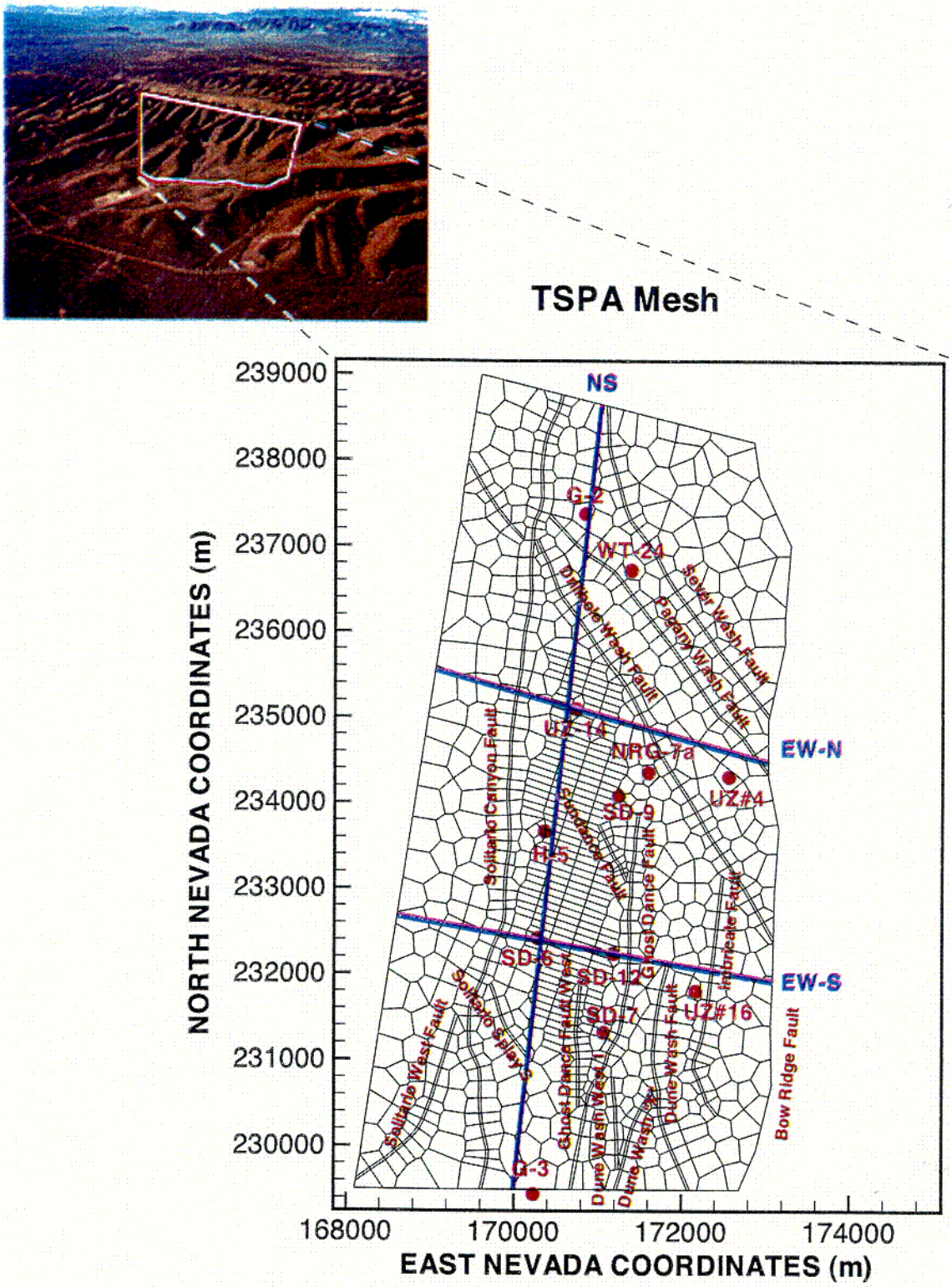

Figure 3.7-3. Plan View of the 3-D UZ TSPA Model Grid, Showing the Model Domain at Yucca Mountain, Faults Incorporated and Borehole Locations (Adapted from CRWMS M&O, 2000, U0000, Figure VI-1)

C065

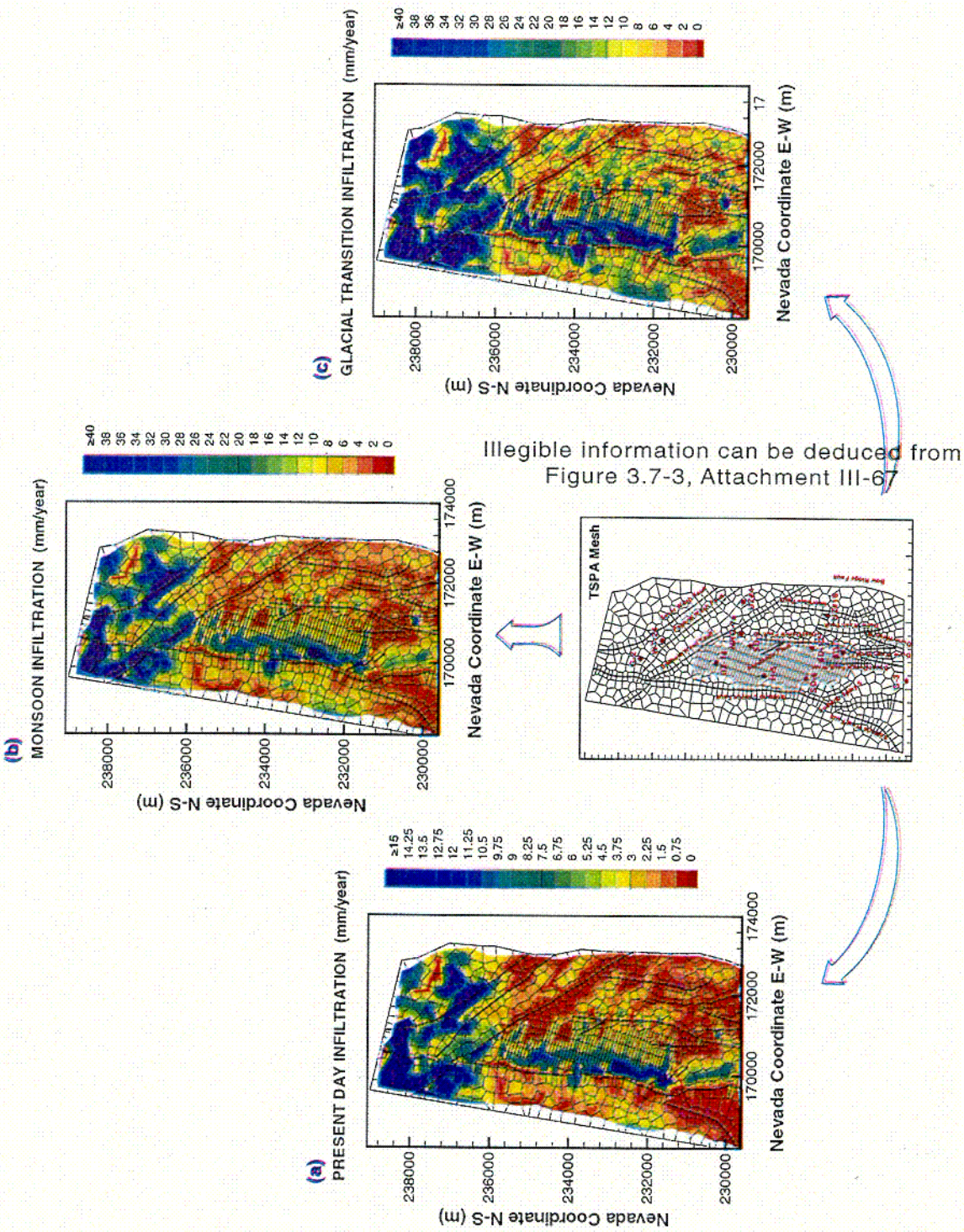

Illegible information can be deduced from Figure 3.7-3, Attachment III-67

Figure 3.7-4. Three Base-Case Maps of Mean Surface Infiltration over the Flow Model Domain for (a) Present-Day Climate, (b) Monsoon Climate, (c) Glacial-Transition Climate (Adapted from CRWMS M&O, 2000, U0050, Figures 6-3, 6-4 and 6-5)

C066

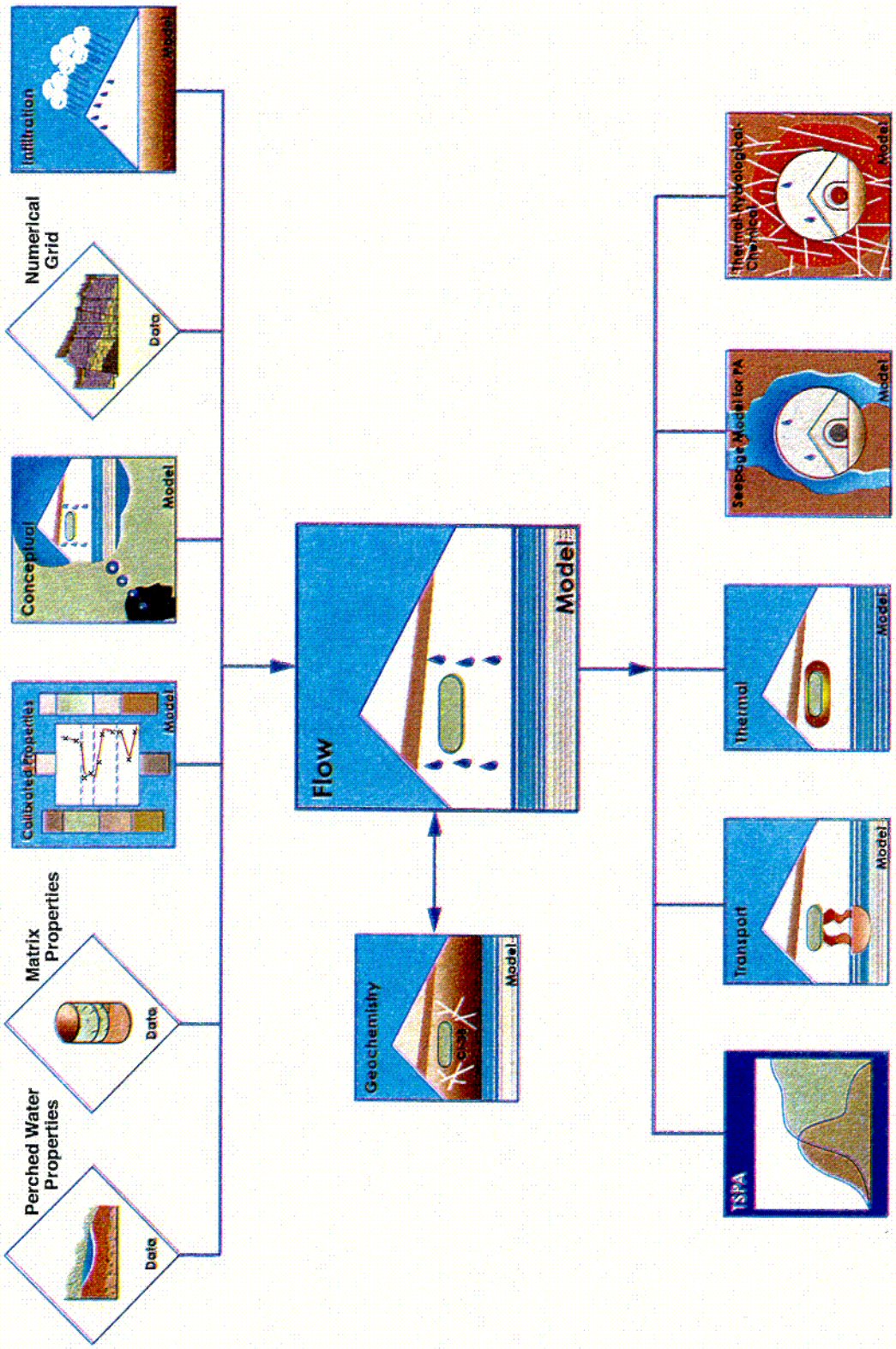

Figure 3.7-5. Schematic of the Major Input Data to, and Output Models from, the UZ Flow Model

C067

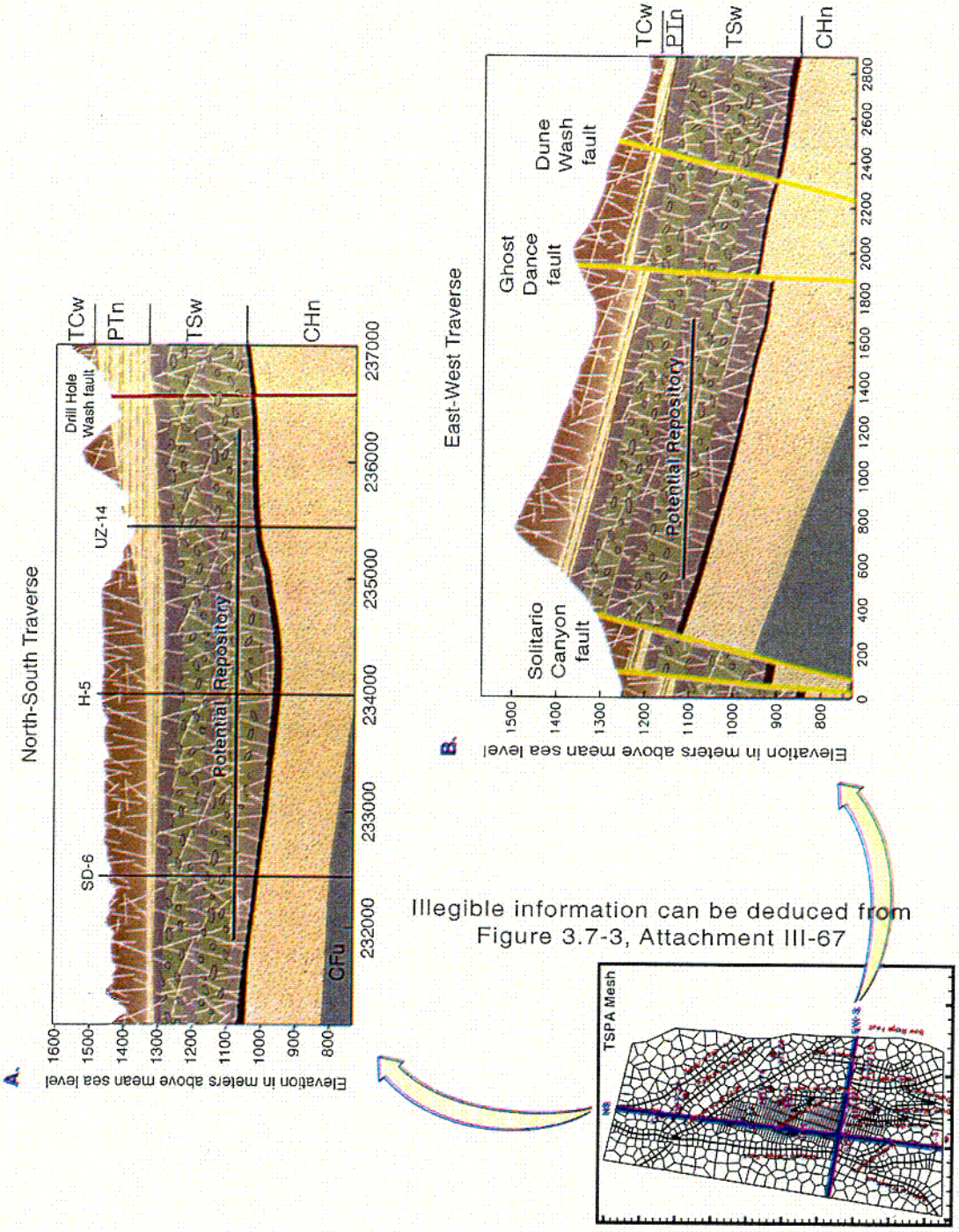

Figure 3.7-6. Geological Profiles in Cross Sections Crossing the Model Domain, (a) North-South Transect at Yucca Mountain, Showing Thickness of the Hydrogeologic Units (b) East-West Transect at Yucca Mountain, Showing Incorporated Faults and Displacements as well as Hydrogeologic Units.

C068

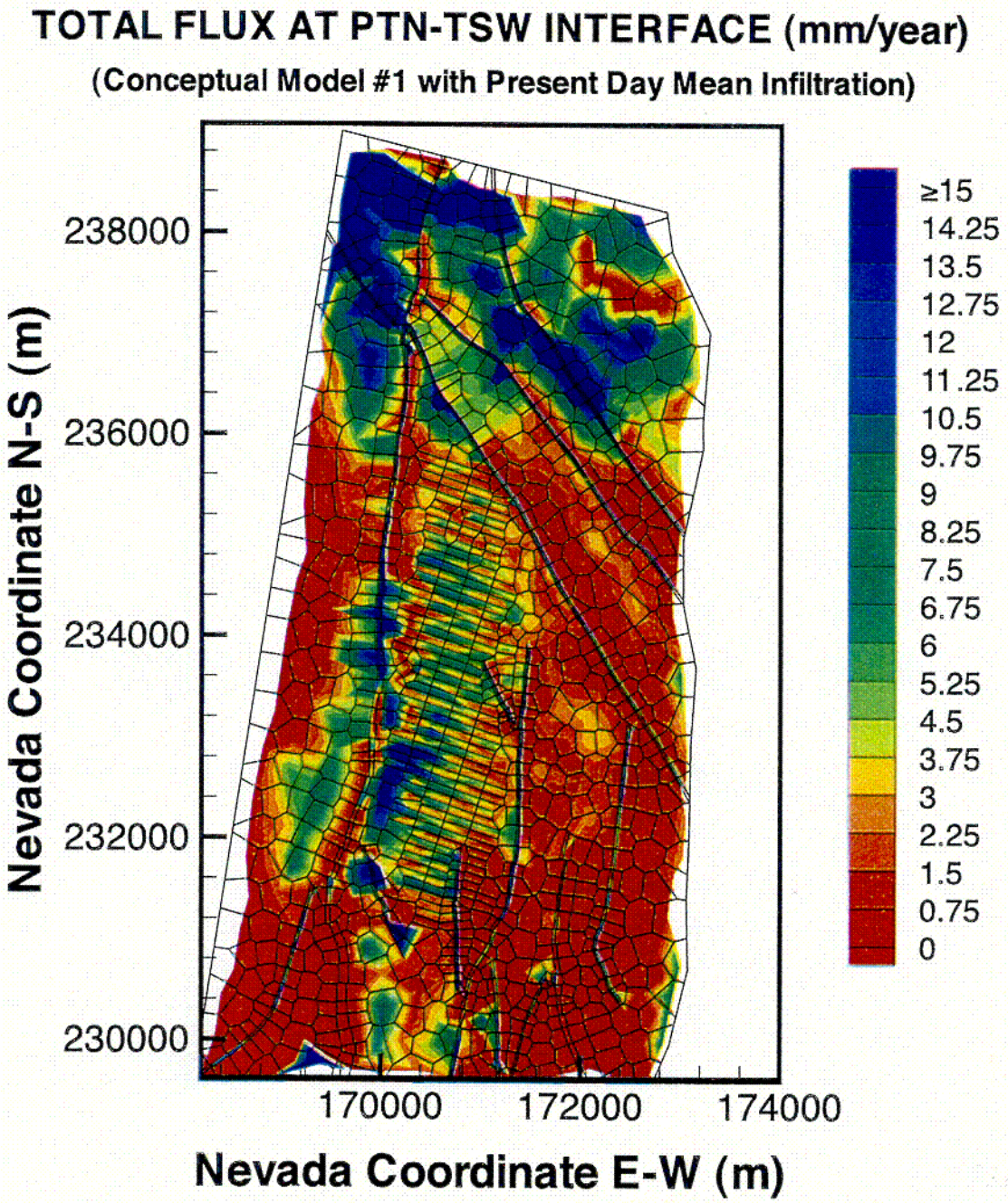

Figure 3.7-7. Simulated Vertical Percolation Fluxes at the PTn-TSw Interface with the Present-Day, Mean Infiltration Map (Data from CRWMS M&O, 2000, U0050, Section 6.6.3)

C069

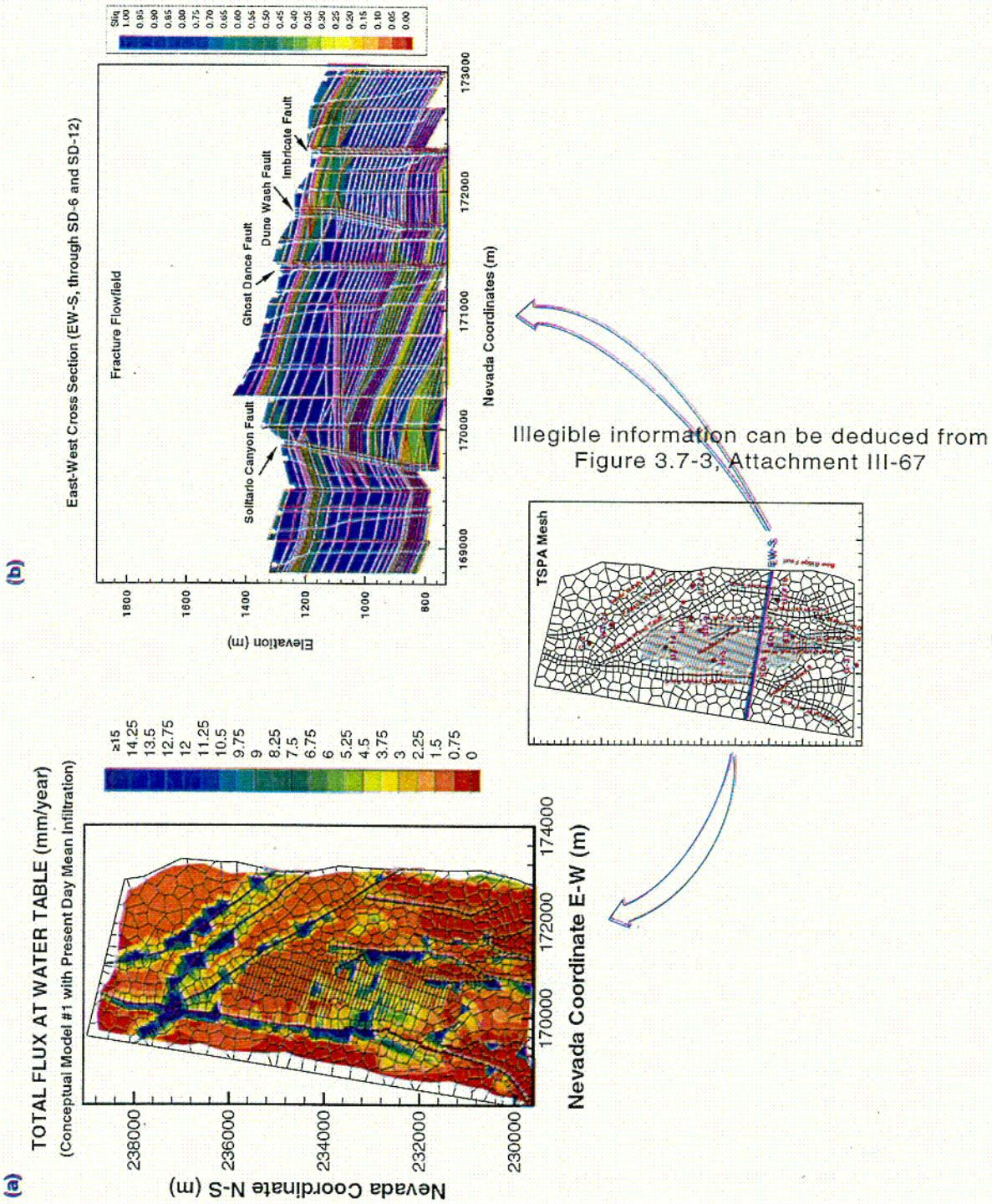

Figure 3.7-8. Effects of Faults on UZ Flow for the Present-Day, Mean Infiltration Rate; (a) Simulated Vertical Percolation Fluxes at the Water Table, (b) Simulated Groundwater Flow paths along the West-East Cross Section within Fracture-Fracture Flow Fields (Data from CRWMS M&O, 2000, U0050, Section 6.6.3)

C070

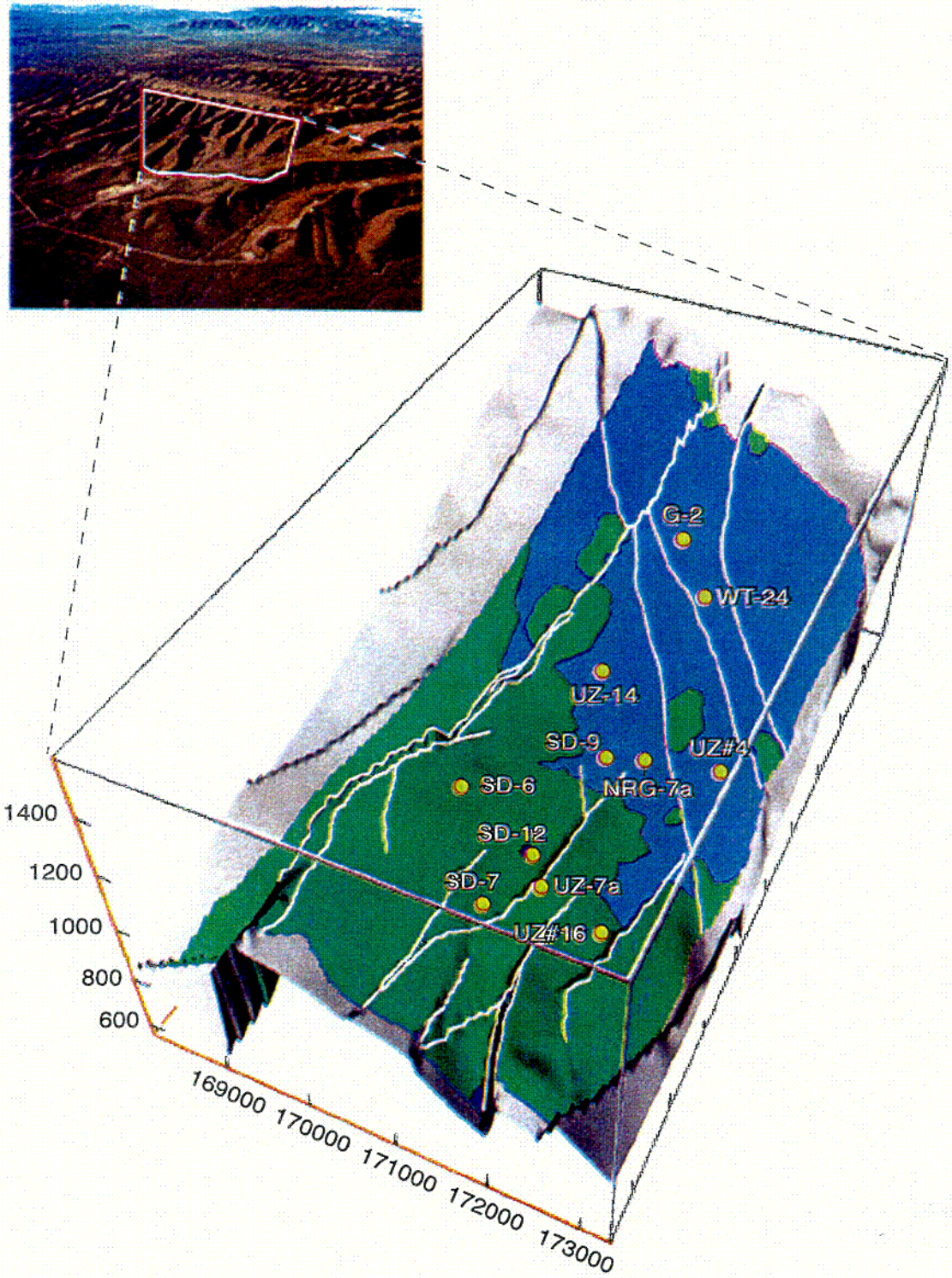

Figure 3.7-9. Simulated 3-D View of Perched Water Bodies along the Base of the TSw, Using the Simulation Results of Conceptual Model #1 with Present-Day, Mean Infiltration Rate (the blue contours denote the domain with 100% water saturation and the green for the areas with less than 100% water saturation) (CRWMS M&O, 2000, U0050, Figure 6.9)

C071

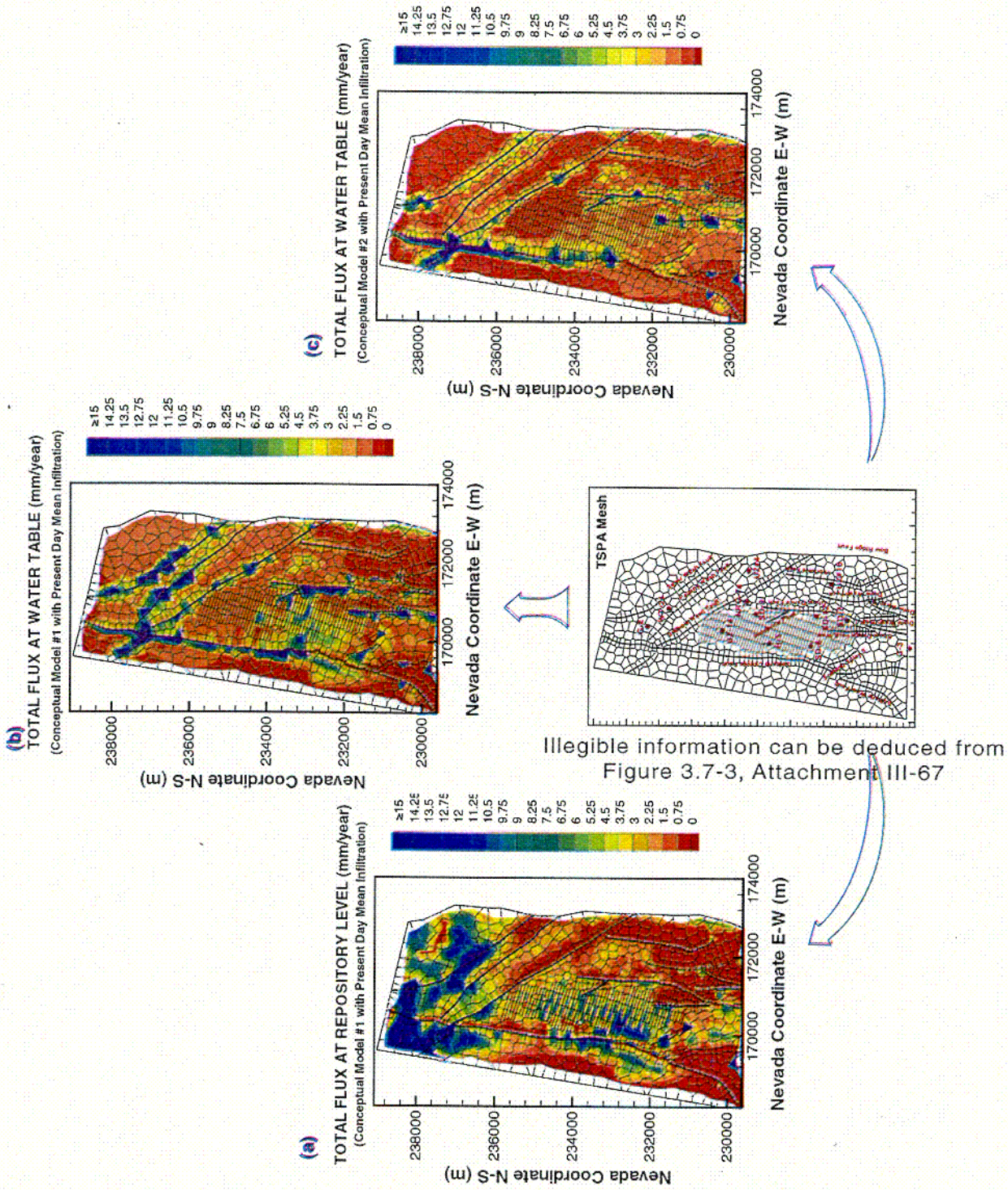

Figure 3.7-10. Comparison between Percolation Flux (mm/yr) Contours Simulated: (a) at the Potential Repository Horizon; (b) at the Water Table with Conceptual Model #1; and (c) at the Water Table with Conceptual Model #2, under the Present-Day, Mean Infiltration Rate (Data from CRWMS M&O, 2000, U0050, Section 6.6.3)

C072

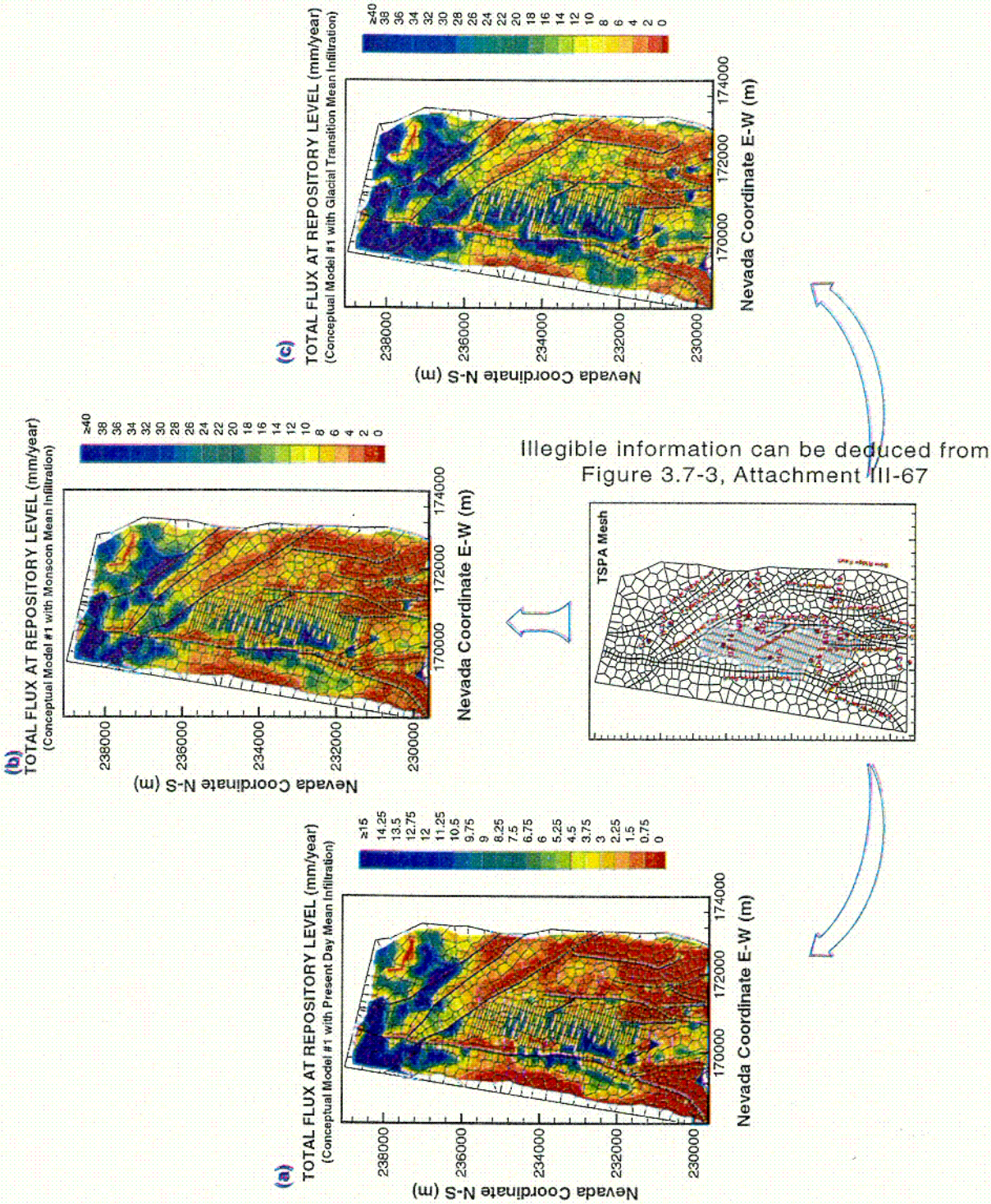

Figure 3.7-11. Simulated Percolation Fluxes at the Potential repository Under Three Mean Infiltration Rates: (a) Present-Day; (b) Monsoon; and (c) Glacial-Transition (Data from CRWMS M&O, 2000, U0050, Section 6.6.3)

C073

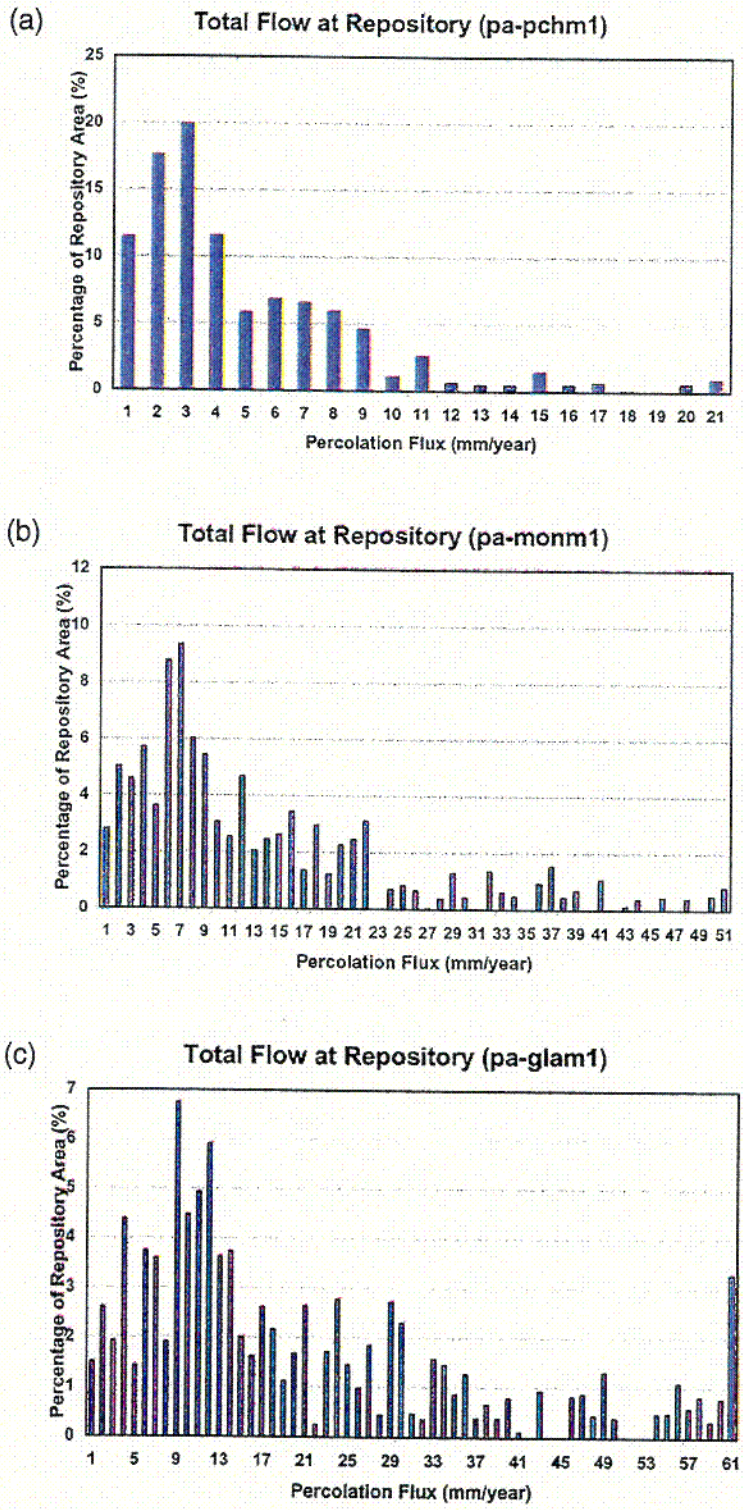

Figure 3.7-12. Areal Frequency and Distribution of Simulated Percolation Fluxes within the Potential Repository Horizon Under Three Mean Infiltration Rates: (a) Present Day; (b) Monsoon; and (c) Glacial Transition (Data from CRWMS M&O, 2000, U0050, Section 6.6.3)

C074

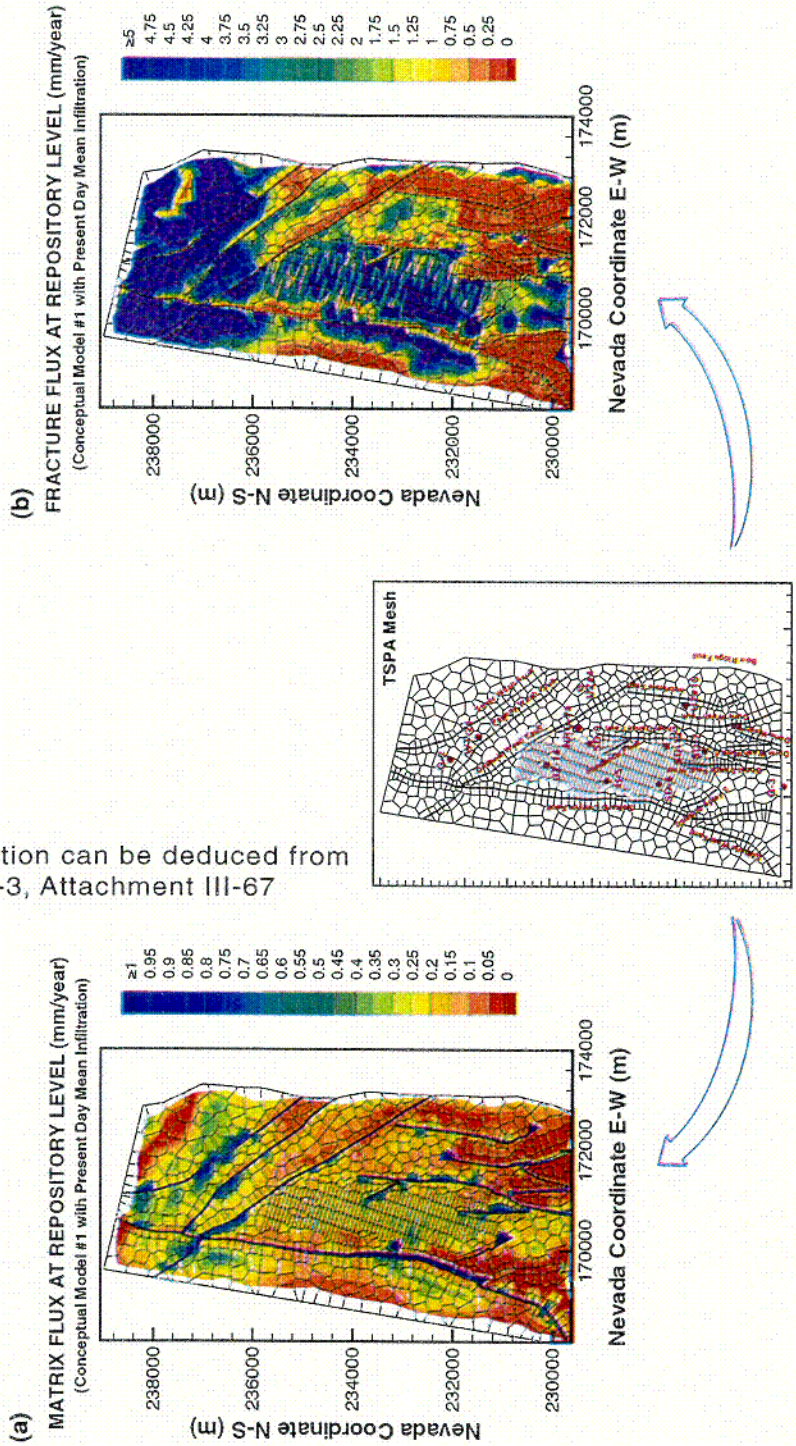

Illegible information can be deduced from Figure 3.7-3, Attachment III-67

Figure 3.7-13. (a) Matrix Flow (mm/yr) and (b) Fracture Flow at Potential Repository Horizon, Simulated Using the Present-Day, Mean Infiltration Rate. Data from CRWMS M&O, 2000, U0050, Section 6.6.3.

C075

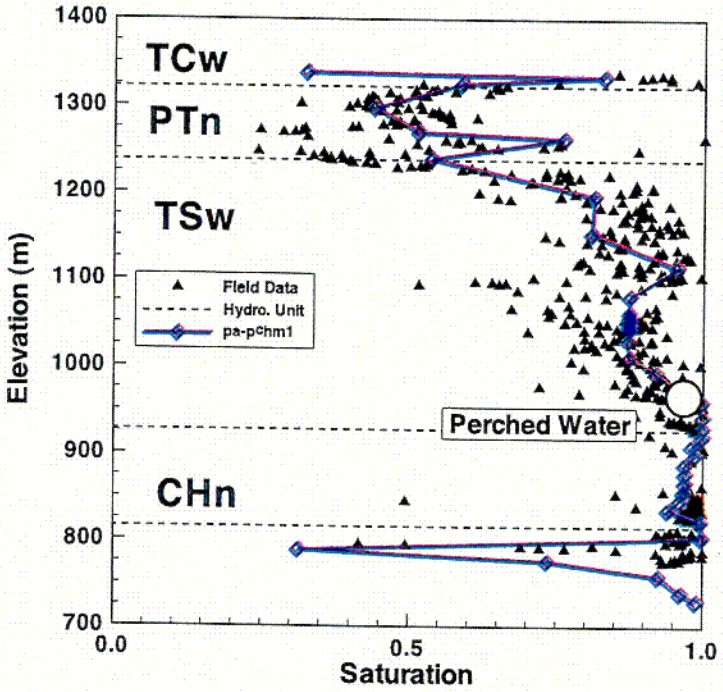

Figure 3.7-14. Comparison to the Simulated and Observed Matrix Liquid Saturations and Perched Water Elevations for Borehole UZ-14, Using the Simulation Results for the Mean Infiltration Rates of the Three Climates Scenarios (Data from CRWMS M&O, 2000, U0050, Section 6.6.3, Figure 6-41)

C076

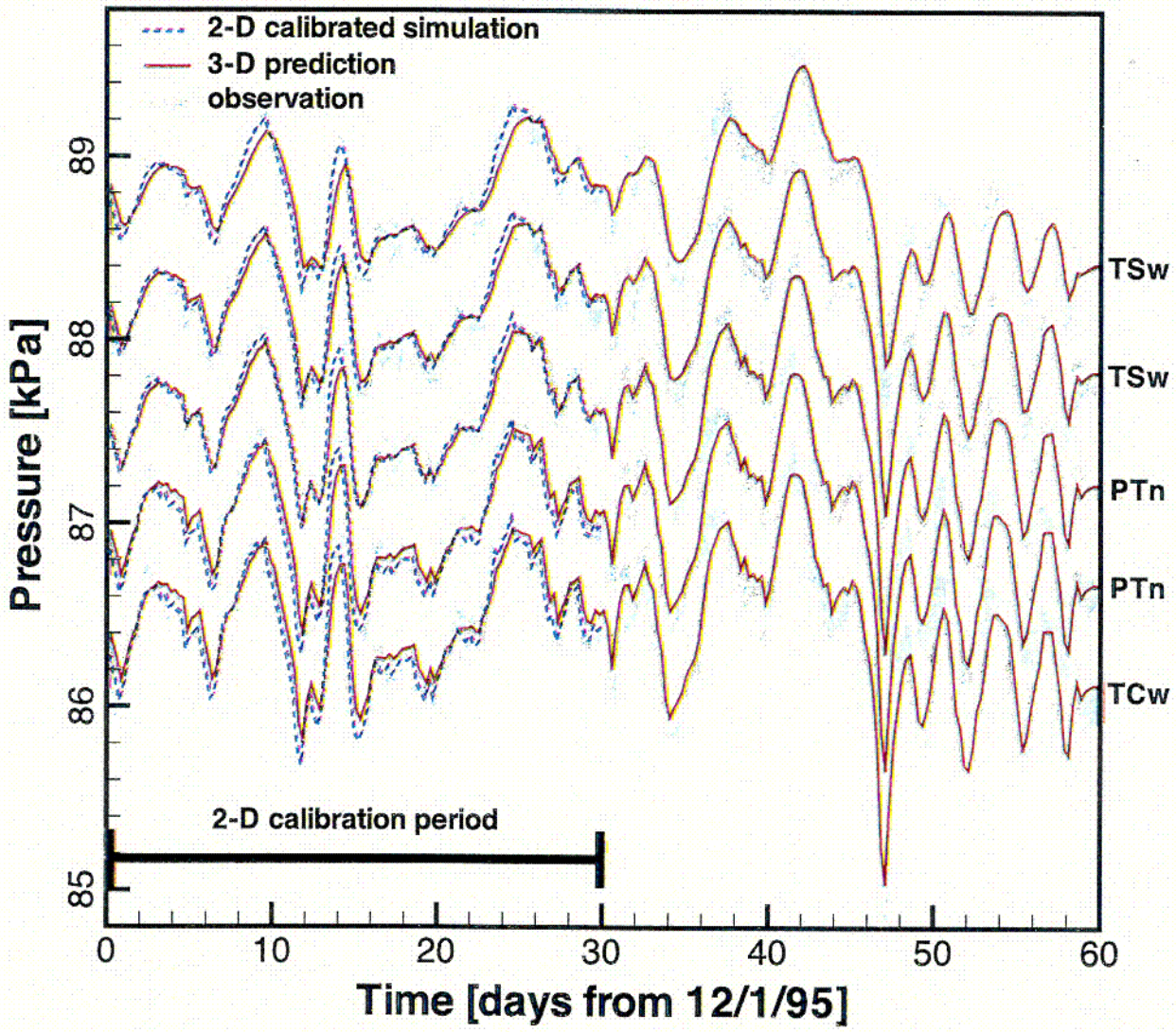

Figure 3.7-15. Comparison of 3-D Pneumatic Prediction to Data from Borehole UZ-7a (CRWMS M&O 2000, U0050, Figure 6-70)

C077

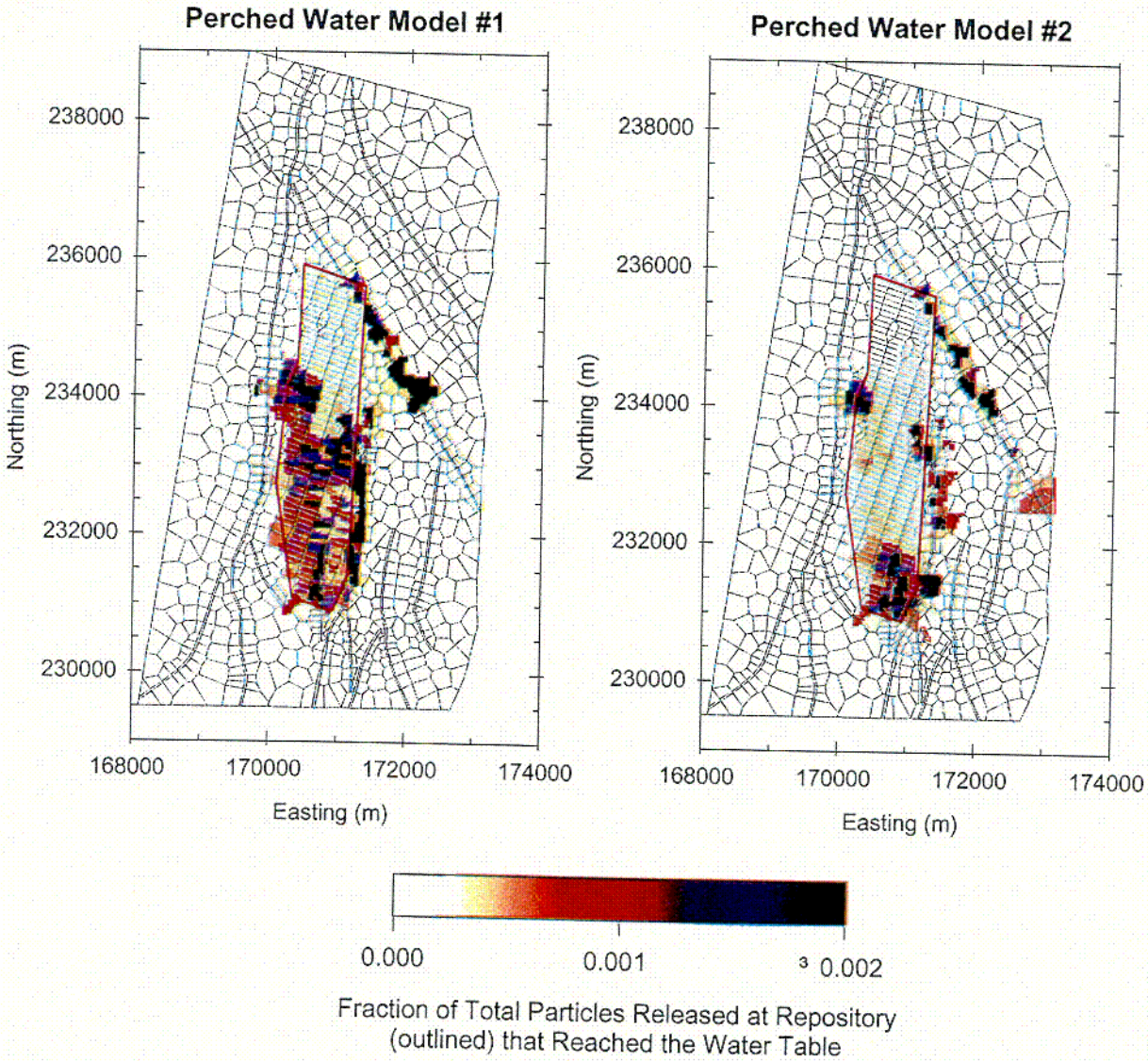

Figure 3.7-16. Locations of Particle Breakthrough at the Water Table for the Mean Infiltration, Glacial-Transition Climate Using Two Perched Water Models (CRWMS M&O 2000, U0160, Figure 3)

C078

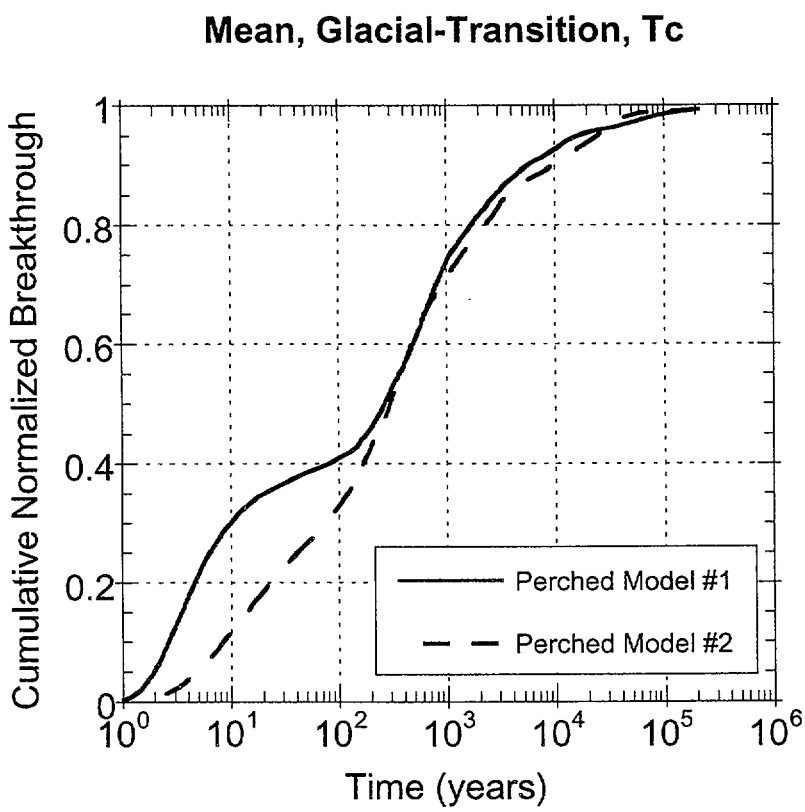

Figure 3.7-17. Comparison of Cumulative Normalized Breakthrough Curves at the Water Table Using Perched Water Model #1 and #2 with a Non-Sorbing Tracer (Tc) for Mean-Infiltration, Glacial-Transition Climate (CRWMS M&O 2000, U0160, Figure 8. The data shown in this figure are based on a model that is appropriately conservative for TSPA analysis and consequently should not be used to evaluate expected breakthrough curves of radionuclides at the water table.)

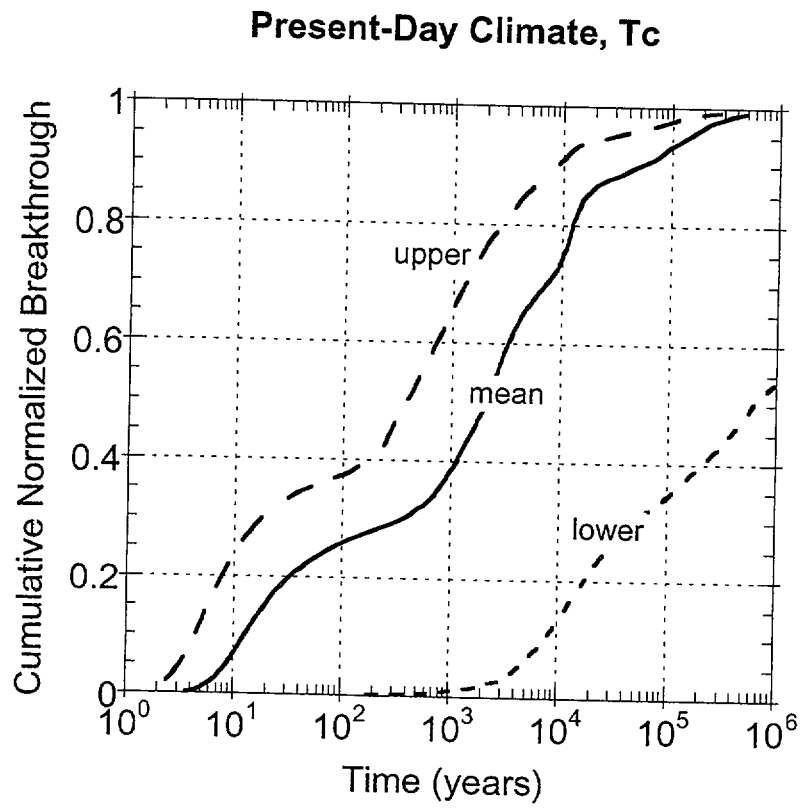

Figure 3.7-18. Effect of Infiltration (lower, mean, and upper) on Cumulative Normalized Breakthrough Curves at the Water Table for a NonSorbing Tracer (Tc) Using FEHM V2.0 (STN: 10031-2.00-00) with Present-Day Climate (CRWMS M&O 2000, U0160, Figure 12. The data shown in this figure are based on a model that is appropriately conservative for TSPA analysis and consequently should not be used to evaluate expected breakthrough curves of radionuclides at the water table.)

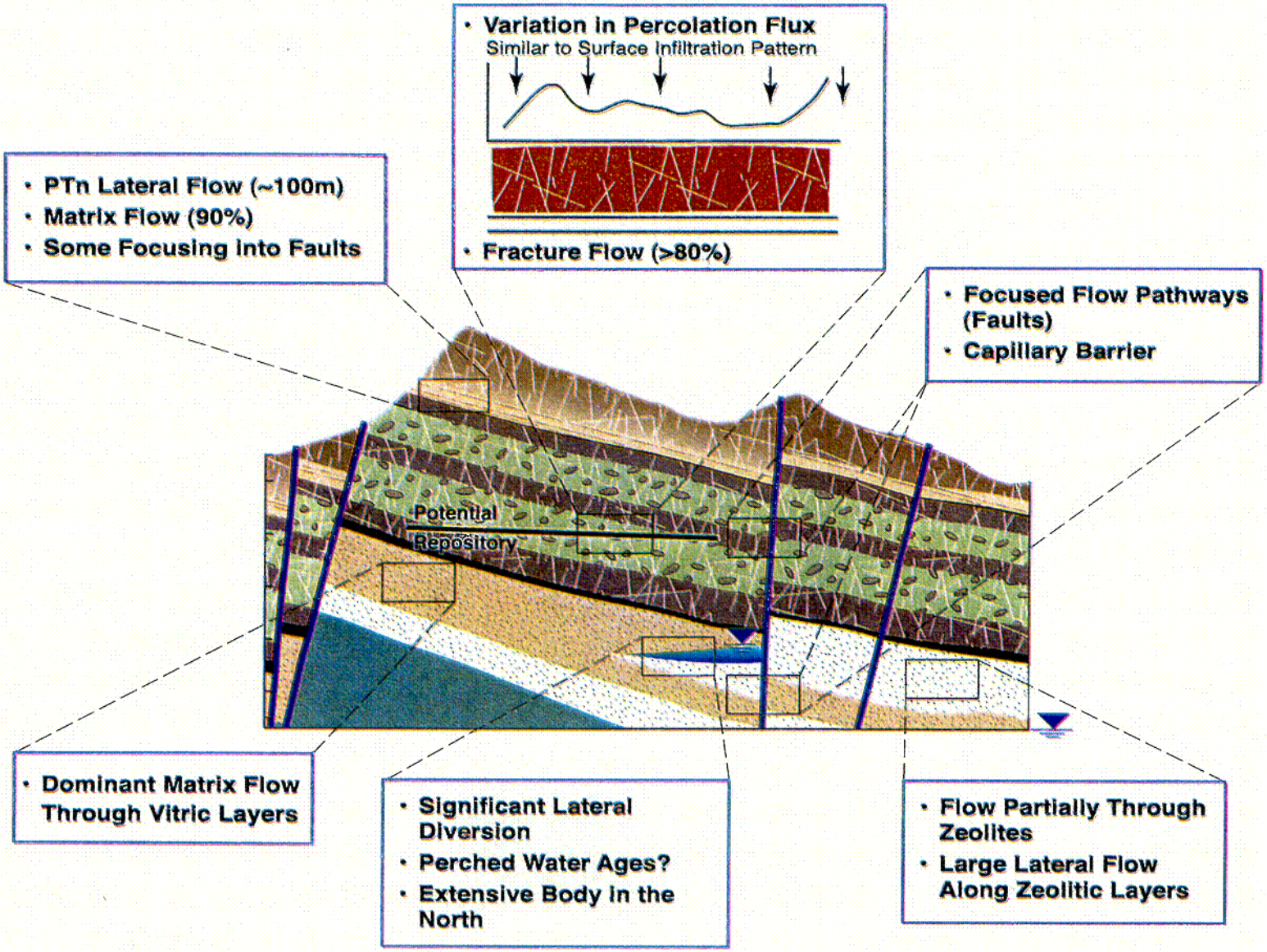

Figure 3.7-19. Summary of the UZ Flow Model Results and Issues to be Resolved

C079

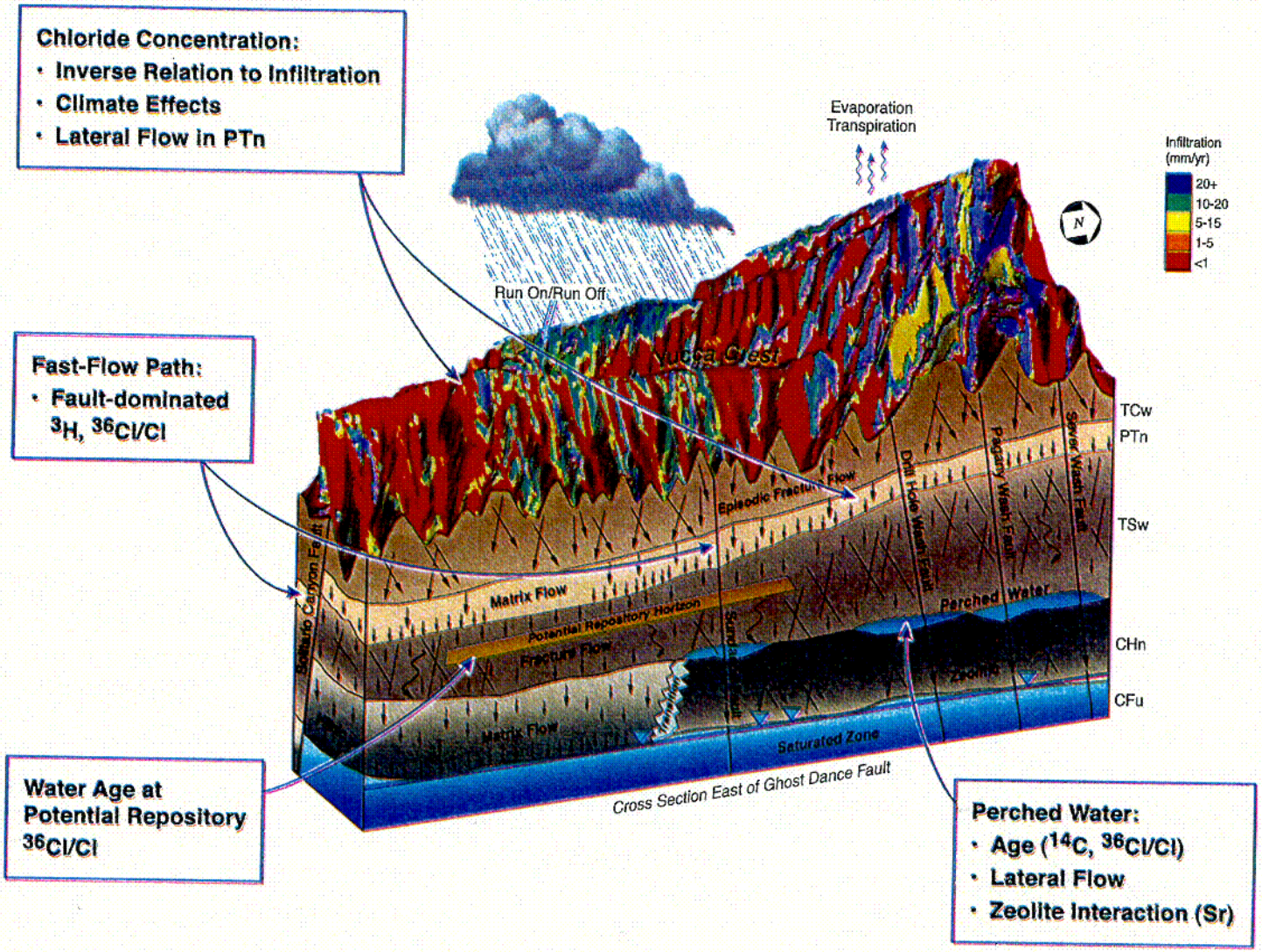

Figure 3.8-1. Conceptual Model of Yucca Mountain Showing Major Processes Affecting Cl and $^{36}Cl/Cl$ Distributions and Important Issues for Performance

C080

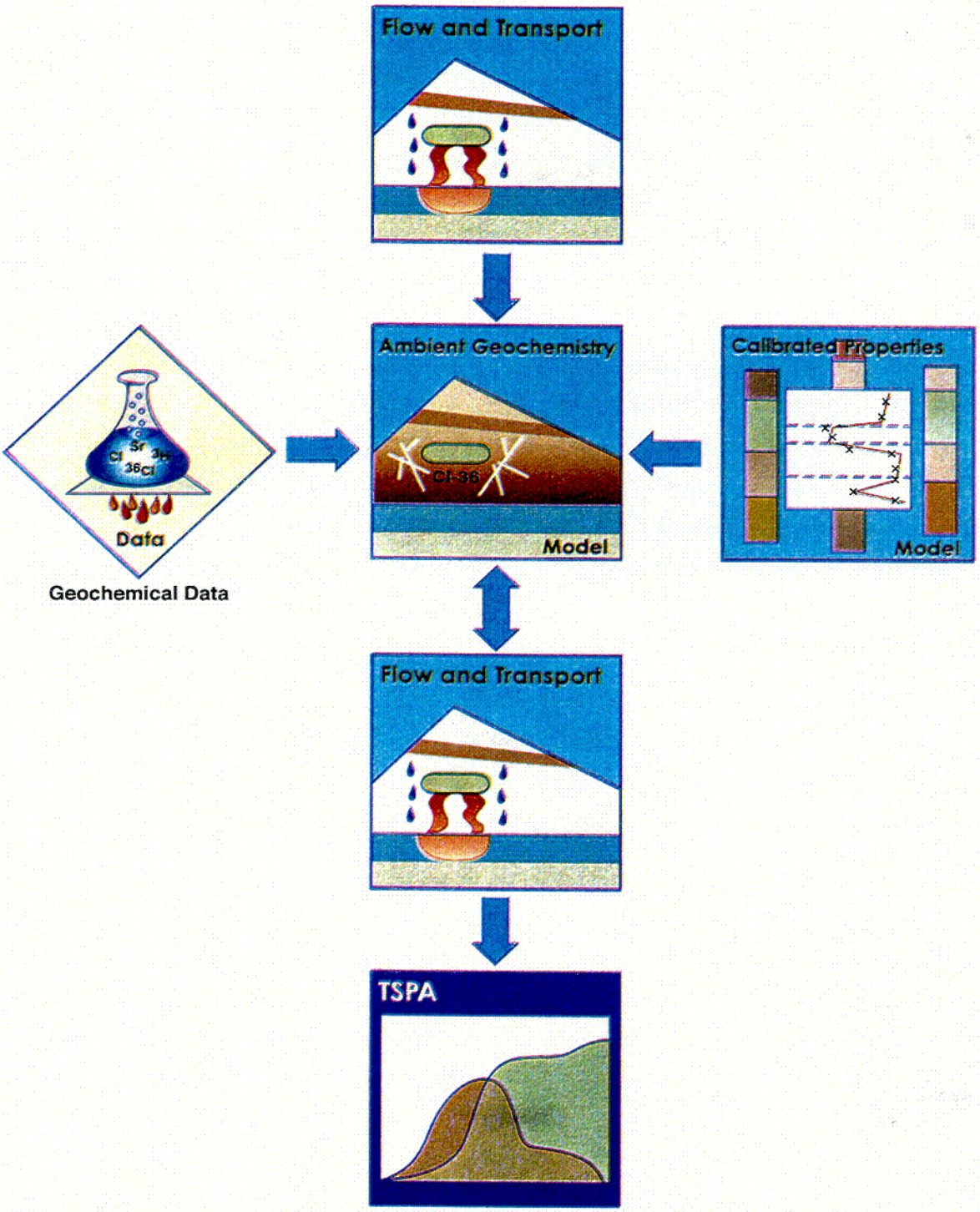

Figure 3.8-2. Model Diagram Showing Inputs and Outputs for Ambient Geochemistry Model. Icons are described in the text.

C081

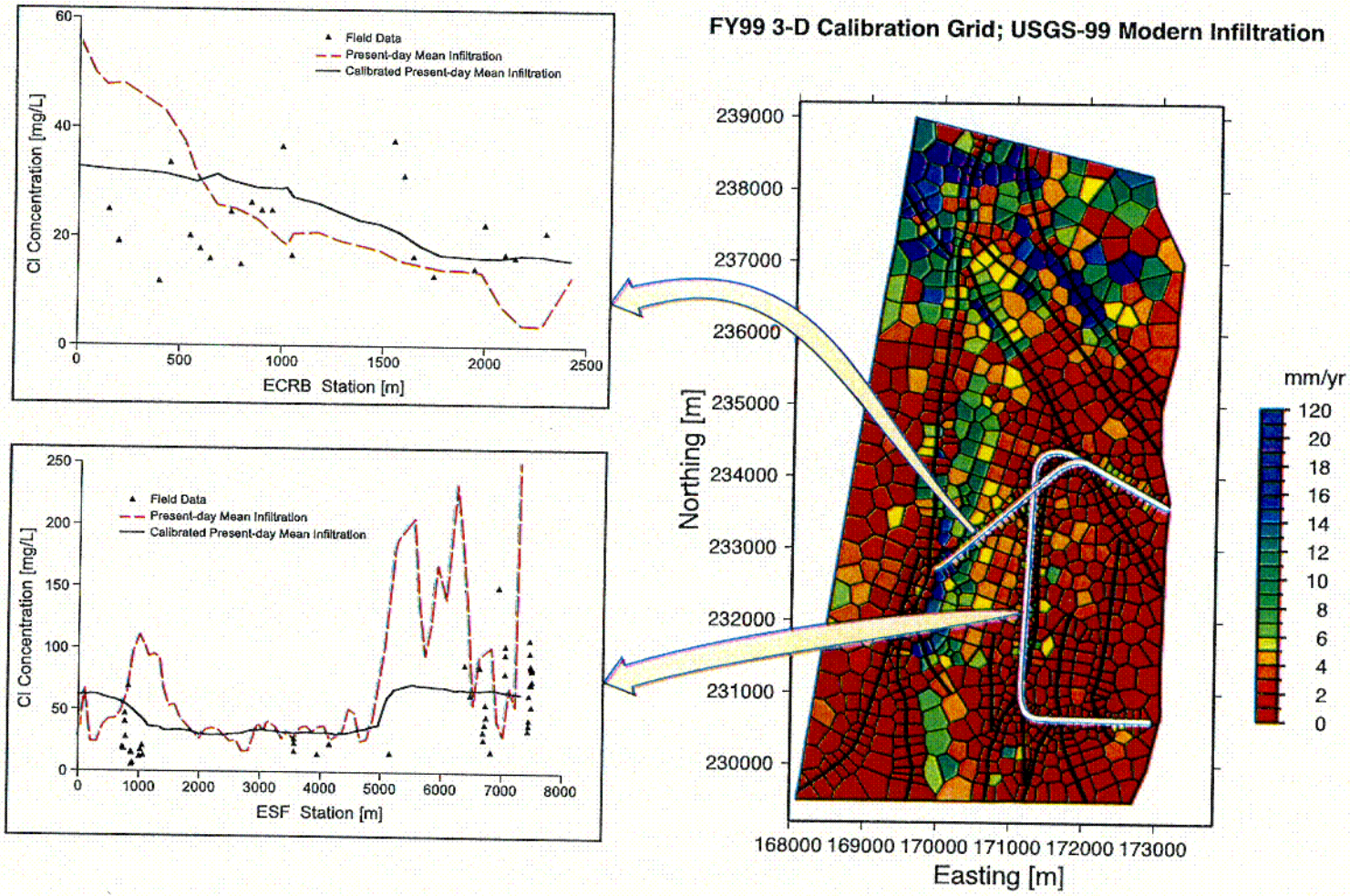

Figure 3.8-3. Infiltration Rates (USGS 2000, U0010) Plotted on UZ 3-D Calibration Grid. Simulated (using base-case infiltration rates), calibrated, and measured Cl concentrations in the ESF and the ECRB (Adapted from CRWMS M&O 2000, U0050, Figure 6-18).

C082

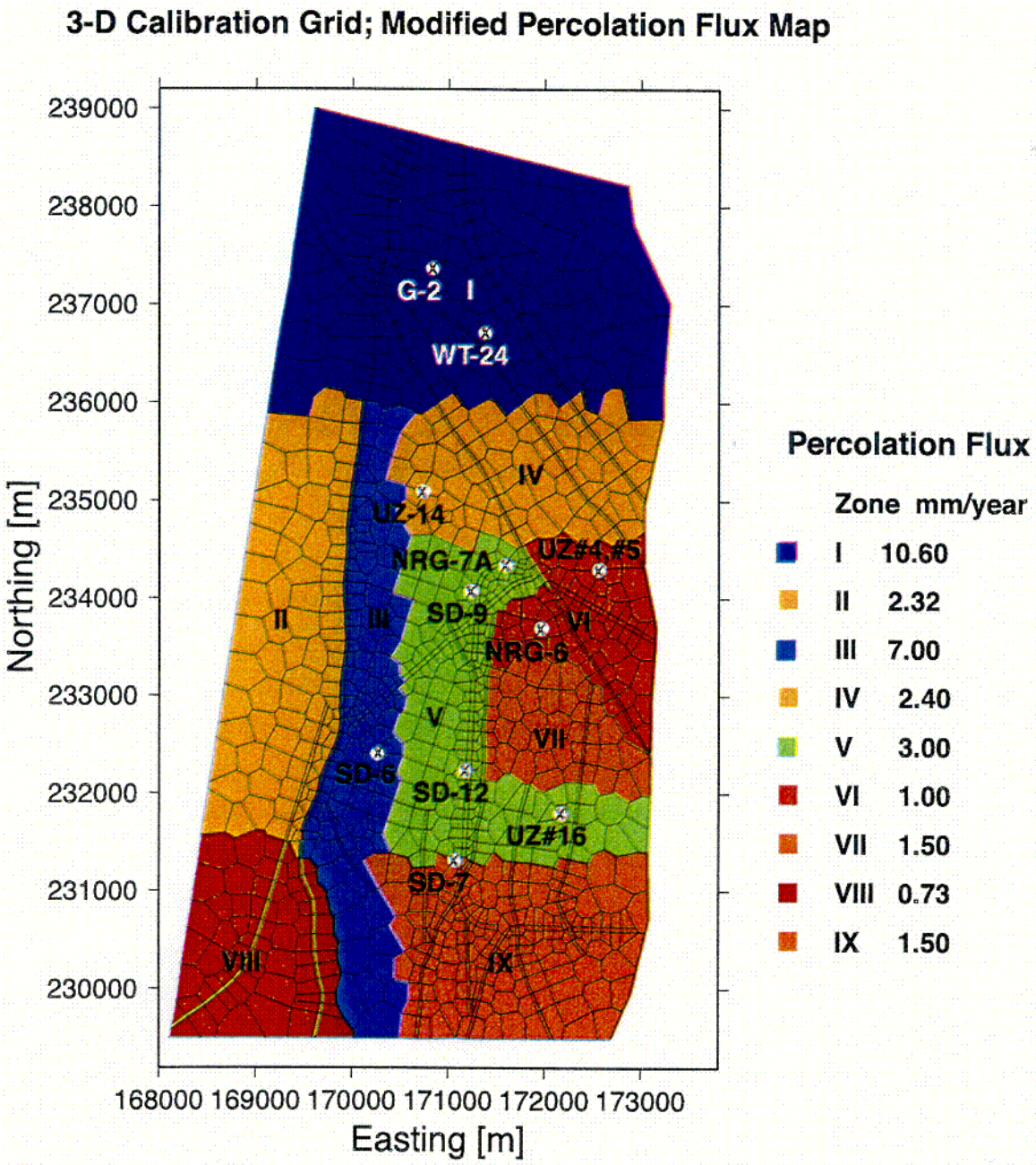

Figure 3.8-4. Percolation Flux Map for 3-D Calibration Grid (Adapted from CRWMS M&O 2000, U0050, Figure 6-24)

C083

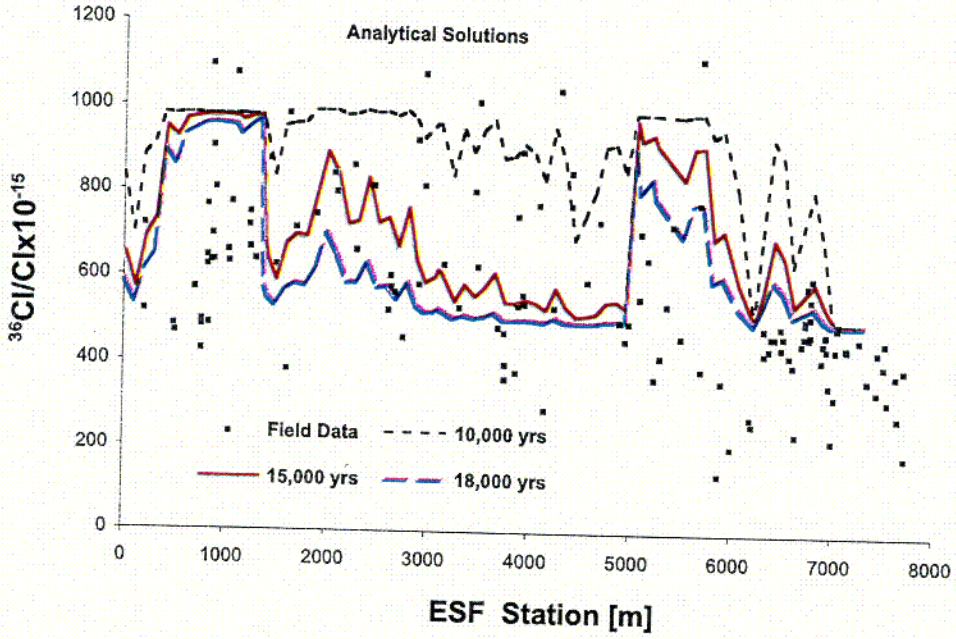

Figure 3.8-5. Analytical Results of ^{36}Cl/Cl Along ESF (Using Calibrated Infiltration) for Transient Changes in Initial Ratios, Compared to Measured Ratios (CRWMS M&O 2000, U0050, Figure 6-31)

C084

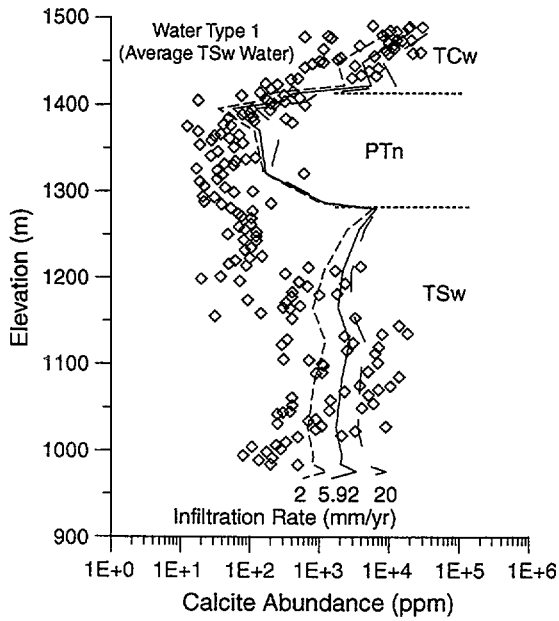

Figure 3.8-6. Simulated Calcite Abundance (Lines) with Infiltration Rate After 10 Million Years in the WT-24 Column Together with Measured Calcite Mass Abundances (Diamond Symbols) (Data from CRWMS M&O 2000, U0085, Section 6.10, Figure 53; CRWMS M&O 2000, U0050, Figure 6-36)

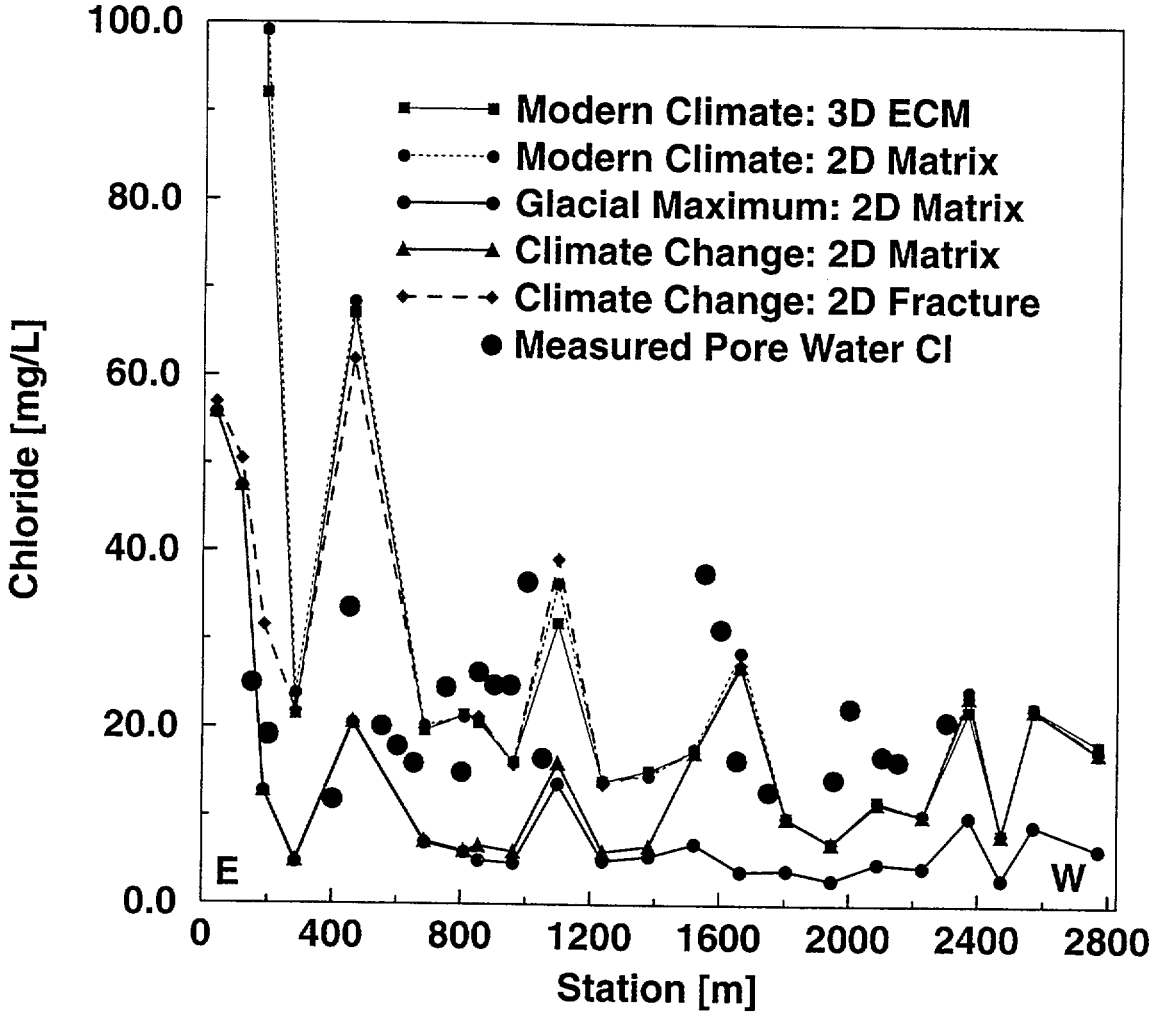

Figure 3.8-7. Prediction of Cl Concentrations in Pore Waters Made Prior to Excavation of the ECRB Compared to Data Collected Subsequently (Adapted from Sonnenthal and Bodvarsson (1999, Figure 14) and CRWMS M&O 2000, U0050, Figure 6-23)

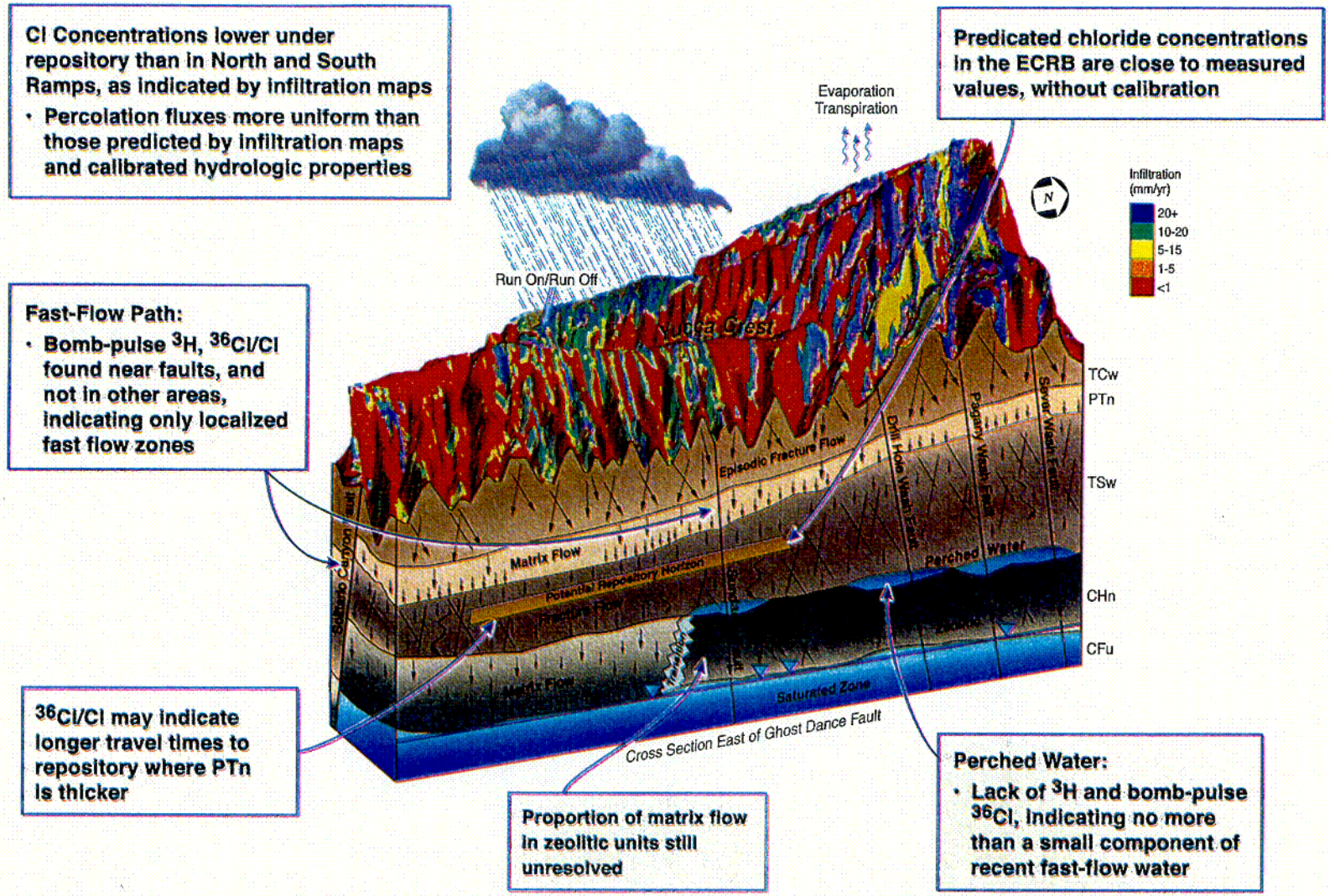

Figure 3.8-8. Conceptual Model of UZ Flow and Transport at Yucca Mountain, Showing Results Gained from Analysis of Geochemical Data and Modeling

C085

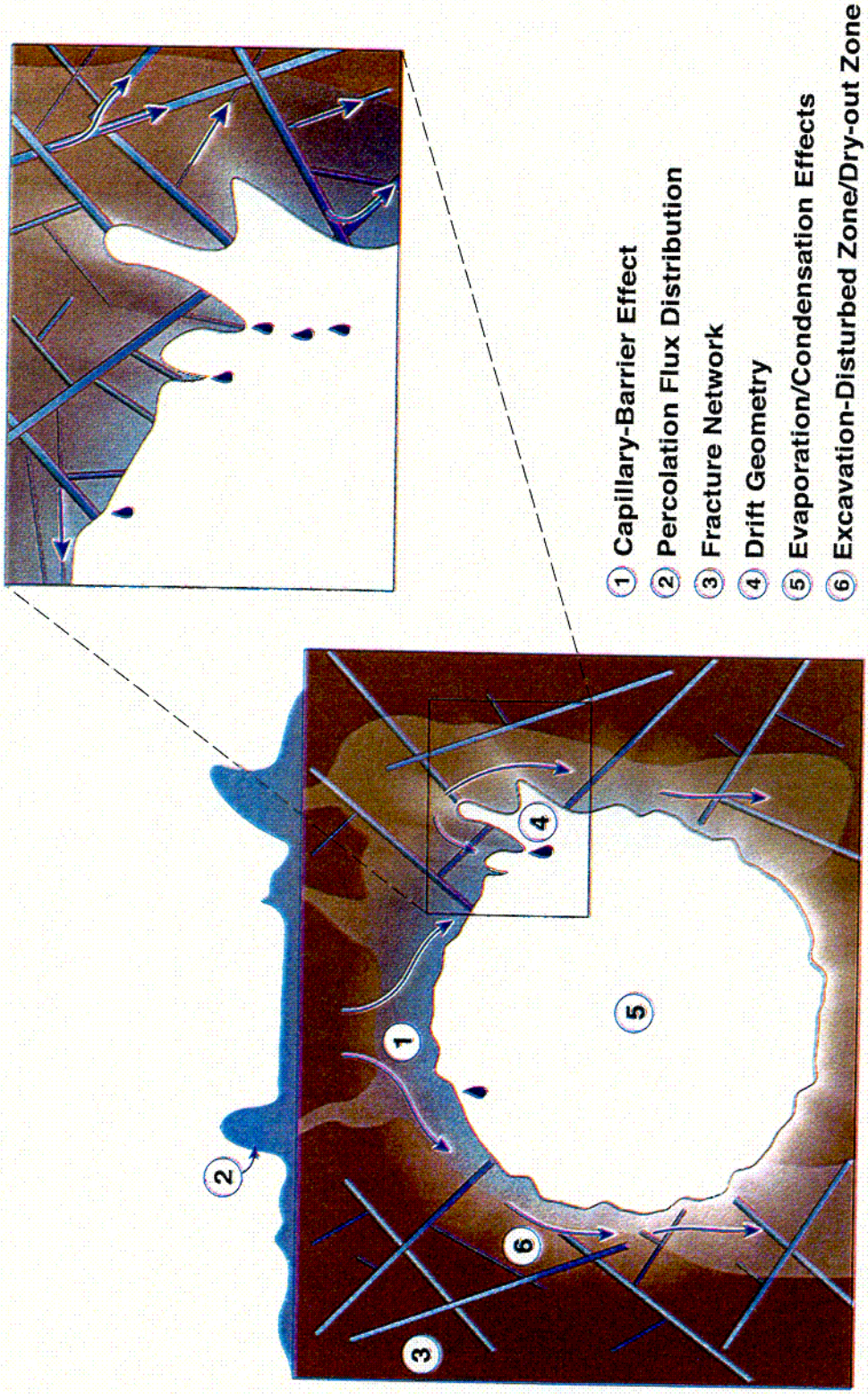

Figure 3.9-1. Schematic of Phenomena and Processes Affecting Drift Seepage. Numerals refer to list items in text.

C086

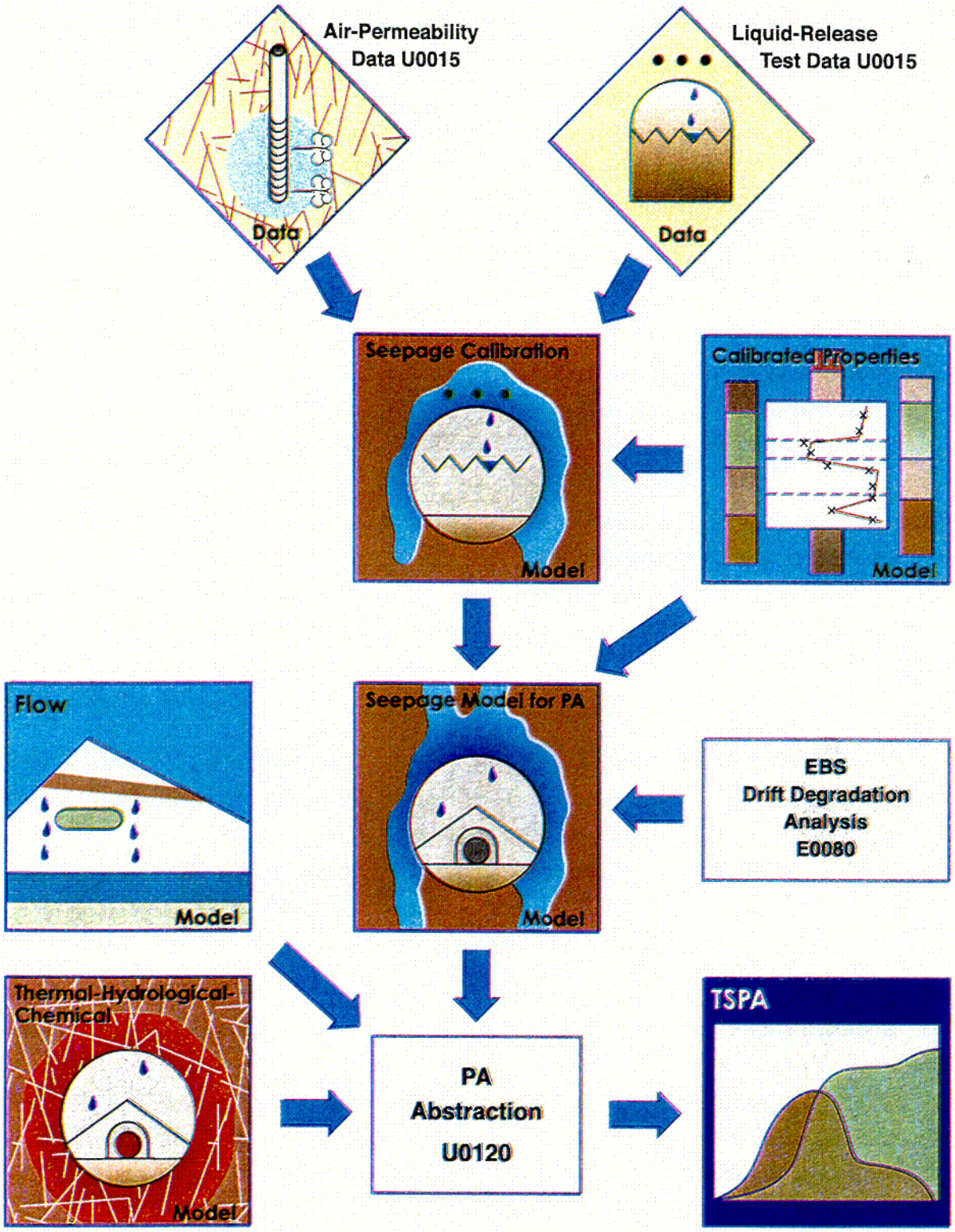

Figure 3.9-2. Schematic Showing Data Flow and Series of Models Supporting Evaluation of Drift Seepage

C087

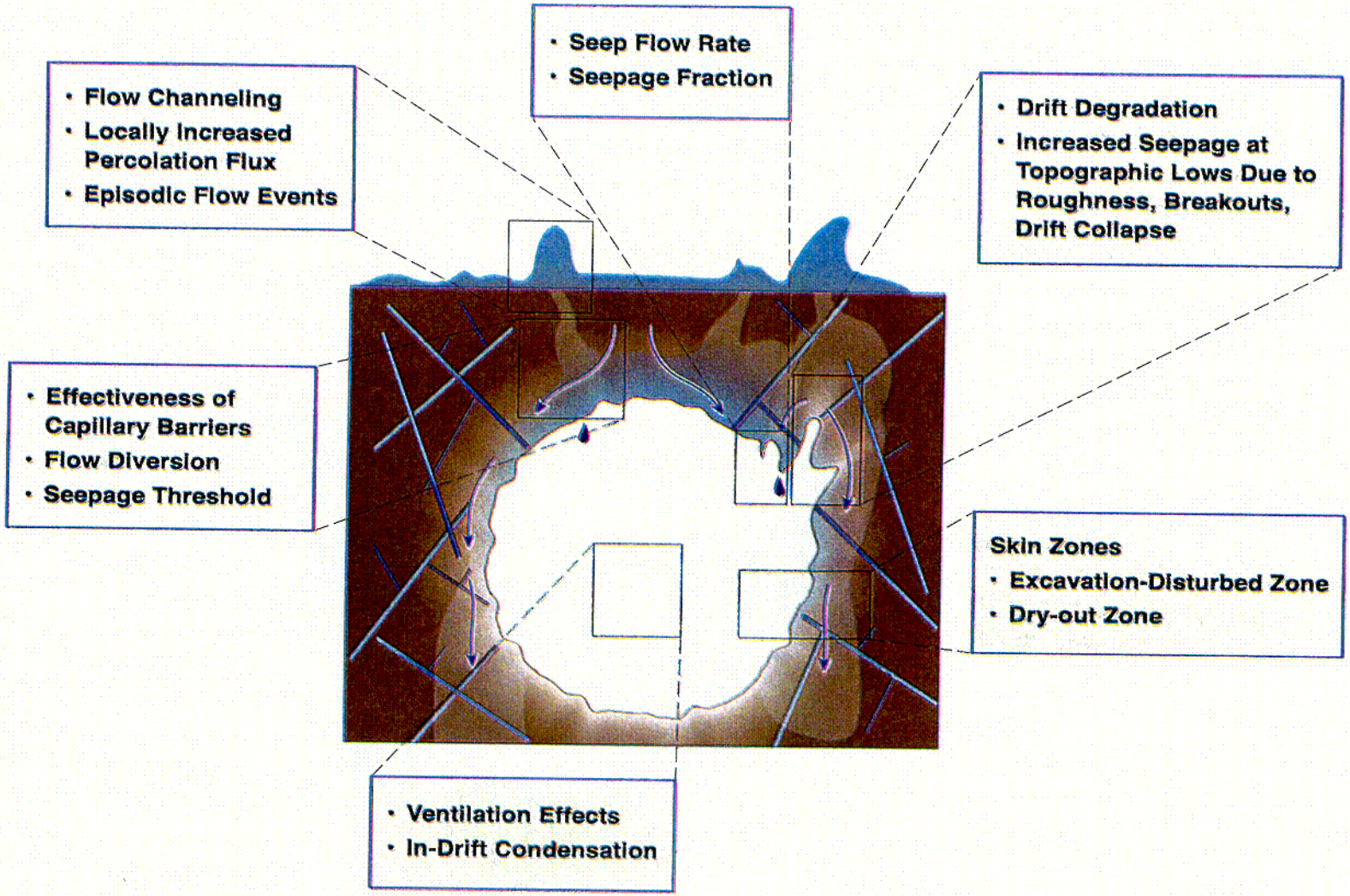

Figure 3.9-3. Seepage Issues

C088

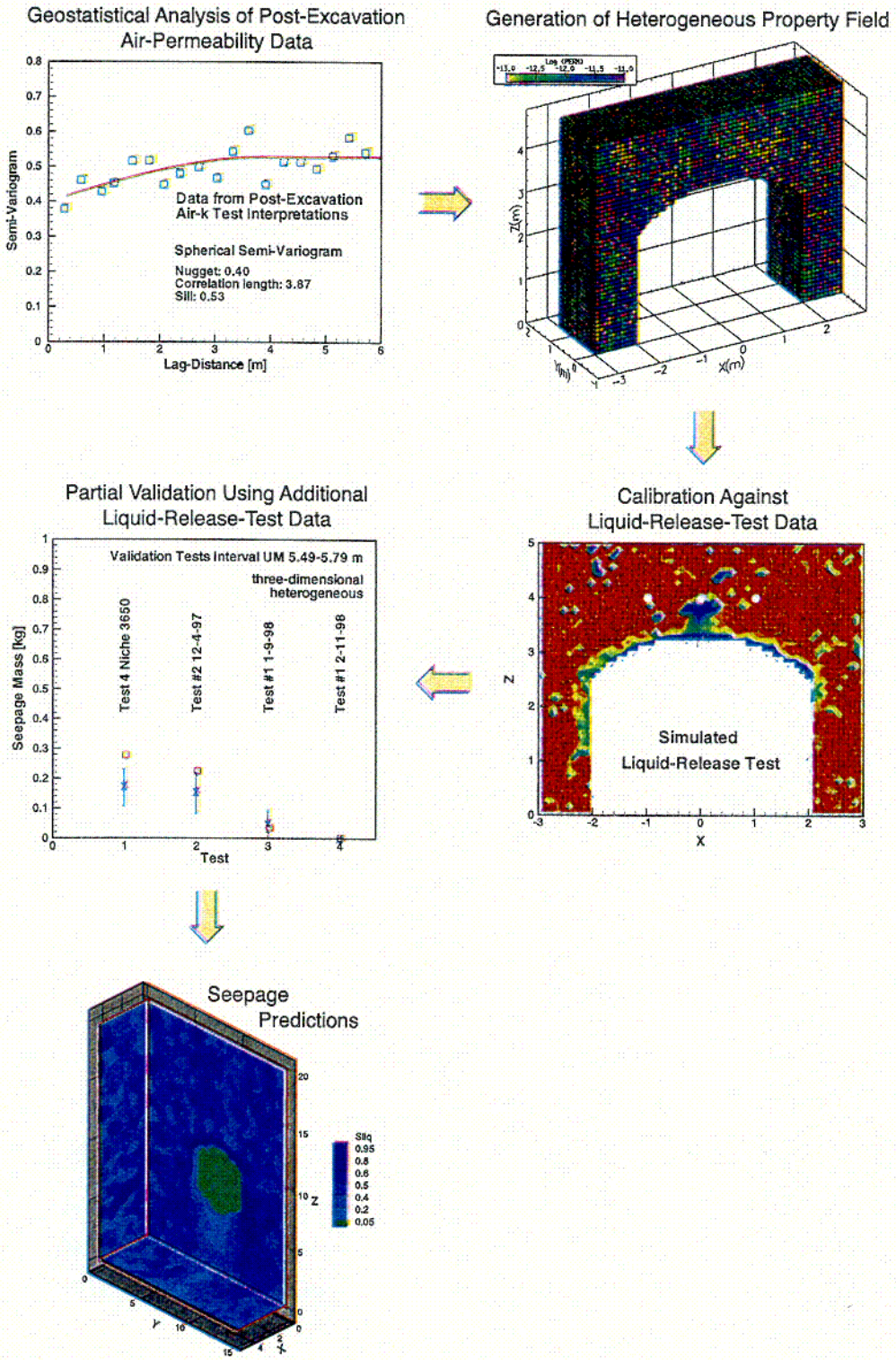

Figure 3.9-4. Schematic Showing General Approach for the Development of the Seepage Calibration Model (Adapted from CRWMS M&O 2000, U0080, Section 6)

C089

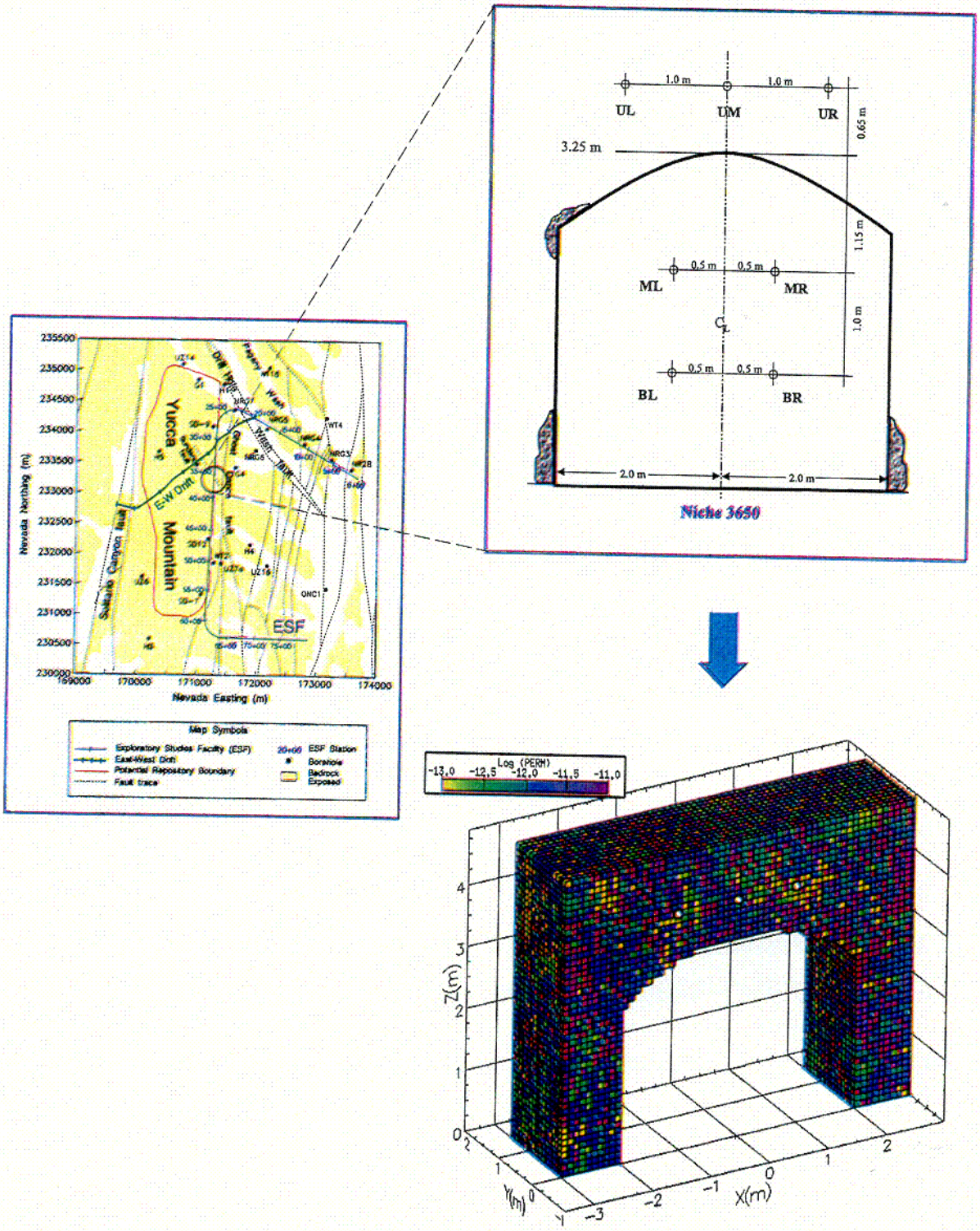

Figure 3.9-5. Schematic Showing Location and Layout of Niche 3650 as well as Log-Permeability Field of the Three-Dimensional Seepage Calibration Model (Adapted from CRWMS M&O 2000, U0080, Figures 12, 13, and 18)

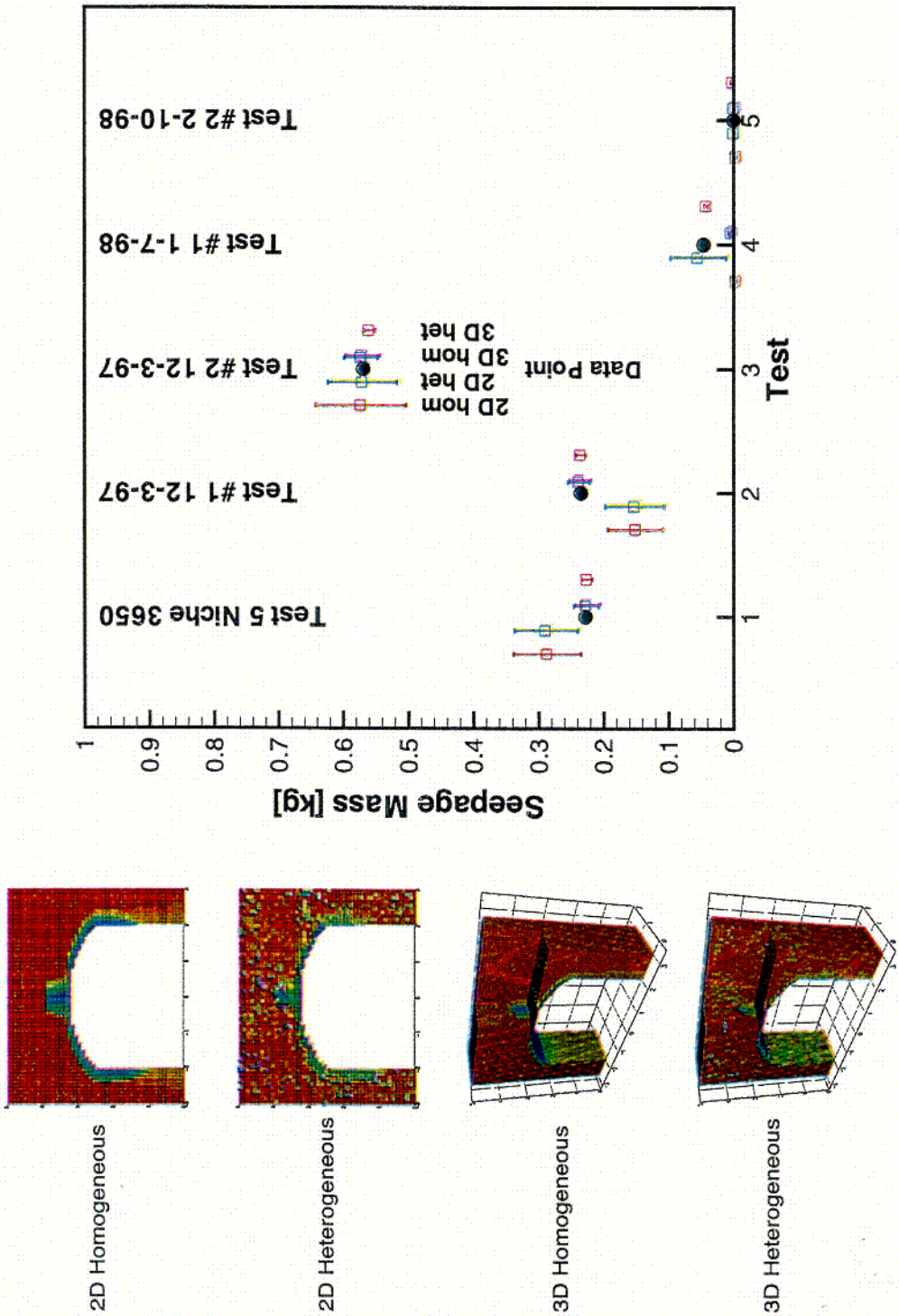

Figure 3.9-6. Comparison between the Measured Seepage Mass (Circles) and That Calculated with Two- and Three-Dimensional, Homogeneous and Heterogeneous Models (Squares). The four models are visualized on the left. The uncertainty of the model predictions is shown as error bars on the 95% confidence level. The three-dimensional heterogeneous Seepage Calibration Model matches the data best (Adapted from CRWMS M&O 2000, U0080, Figure 19).

C091

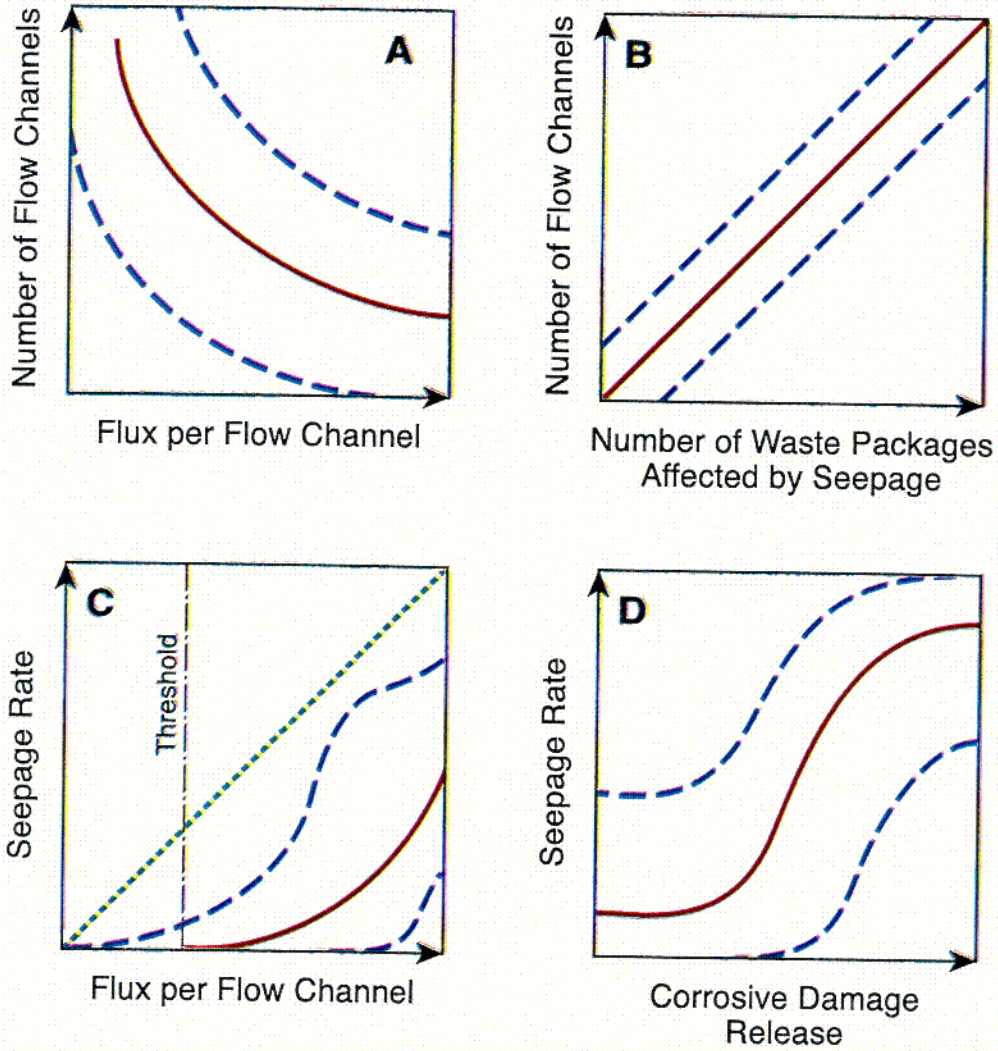

Figure 3.9-7. Schematic Showing Relationships between Seepage-Relevant Factors. The red solid lines schematically indicate the expected behavior; uncertainty is schematically shown as blue dashed lines; the green dotted line shows the conservative assumption that no capillary-barrier effect exists.

C092

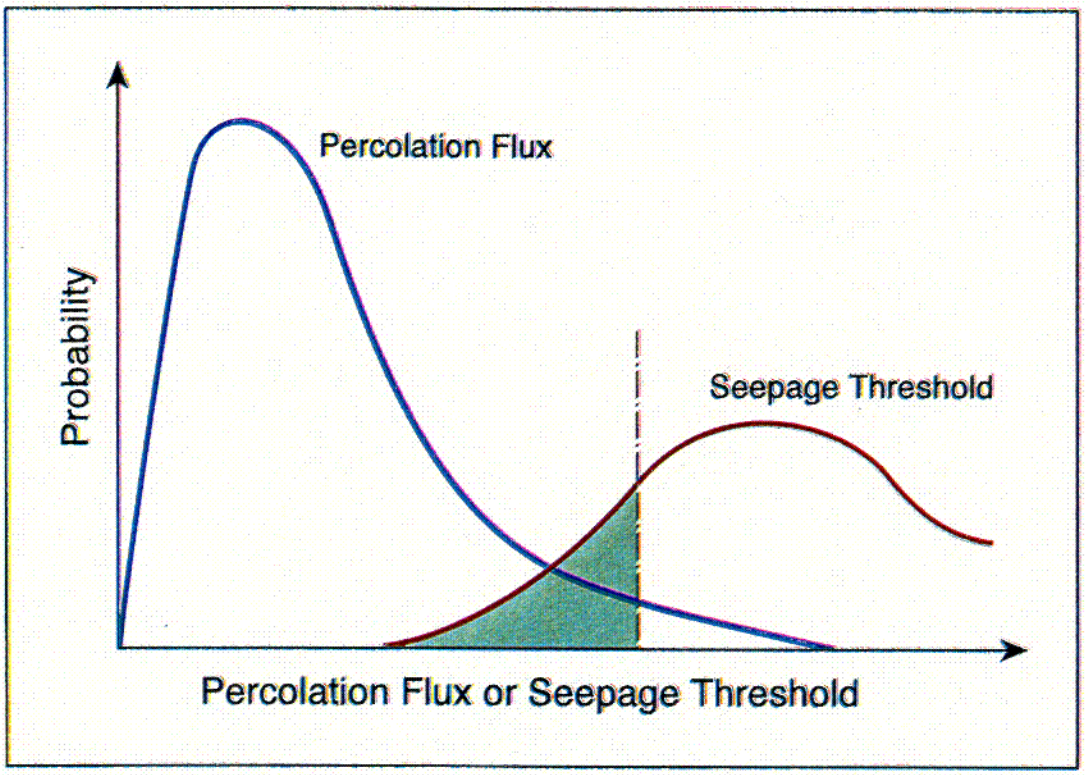

Figure 3.9-8. Schematic Showing Percolation-Flux and Seepage-Threshold Distributions, Which Determine the Seepage-Fraction Probability

C093

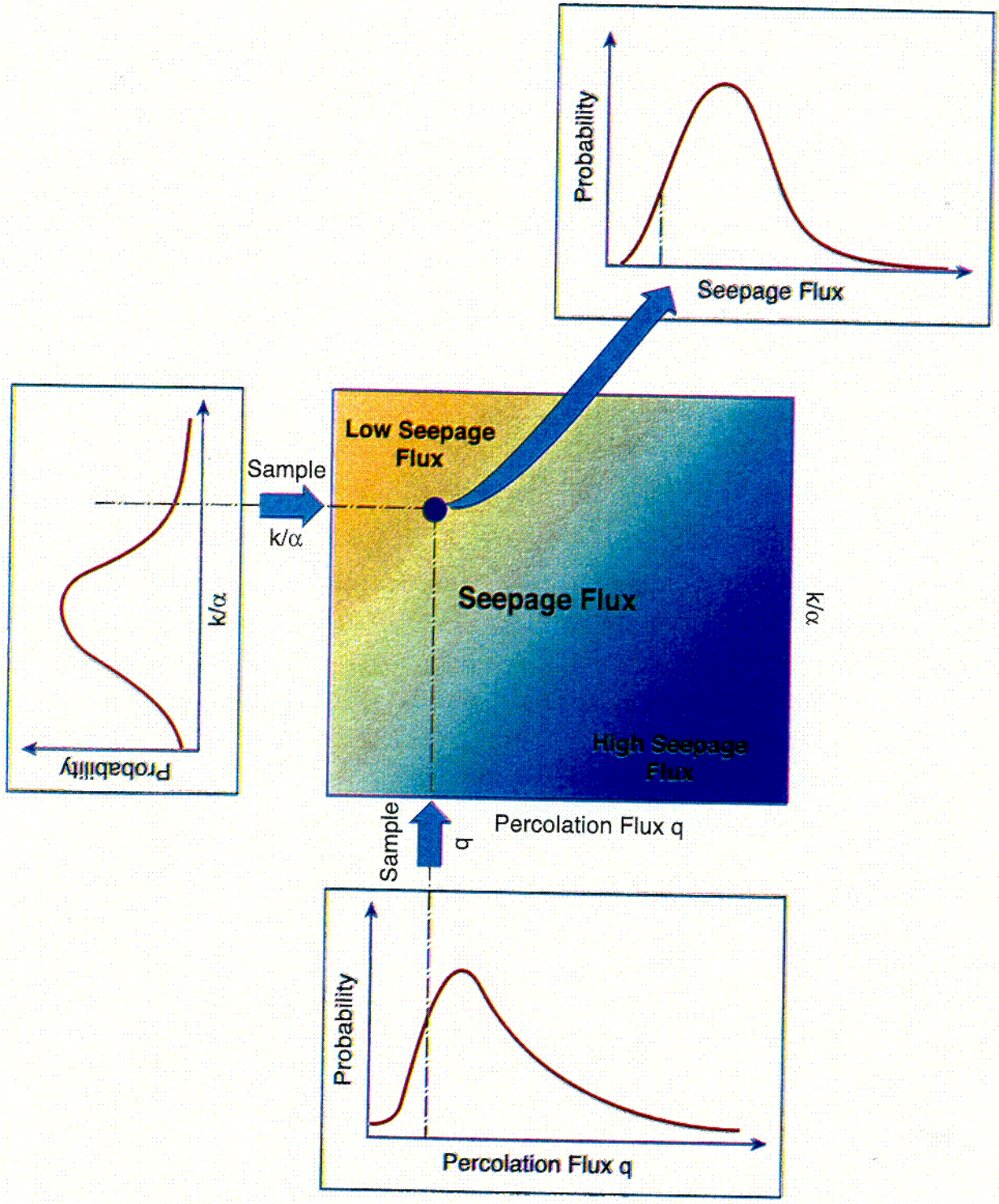

Figure 3.9-9. Schematic Illustrating Monte Carlo Sampling Approach for Seepage TSPA Calculations

C094

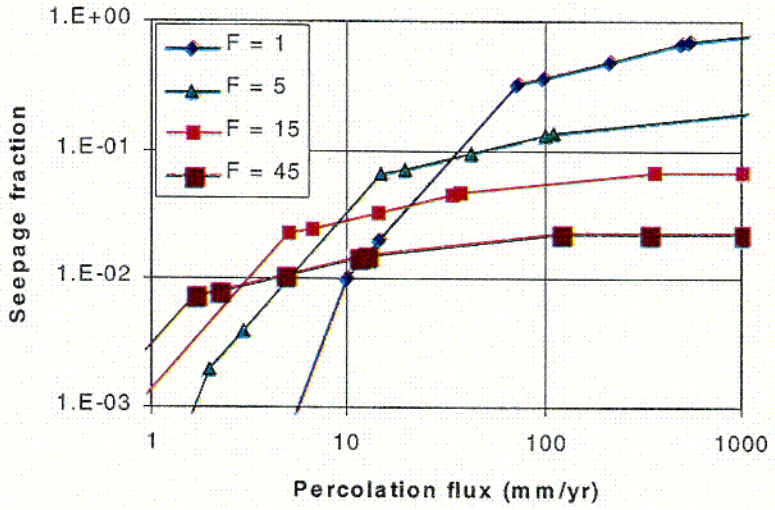

Figure 3.9-10. Effect of Flow Focusing on Seepage Fraction (CRWMS M&O 2000, U0120, Figure 5)

C095

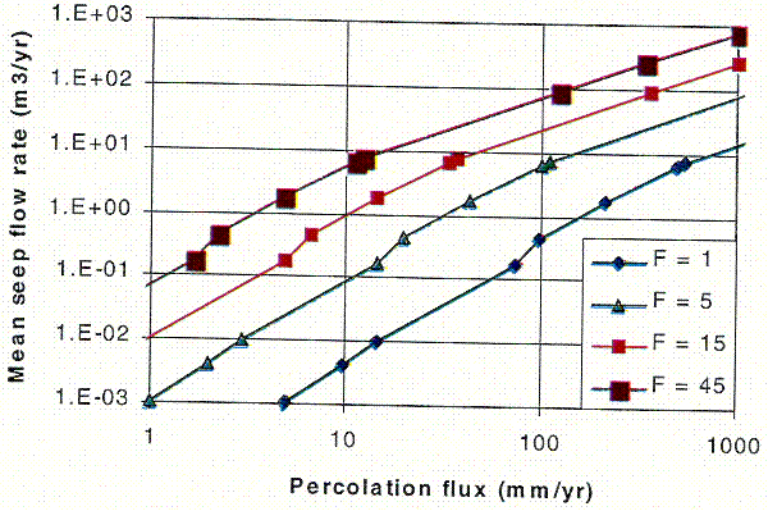

Figure 3.9-11. Effect of Flow Focusing on Mean Seep Flow Rate (CRWMS M&O 2000, U0120, Figure 6)

C096

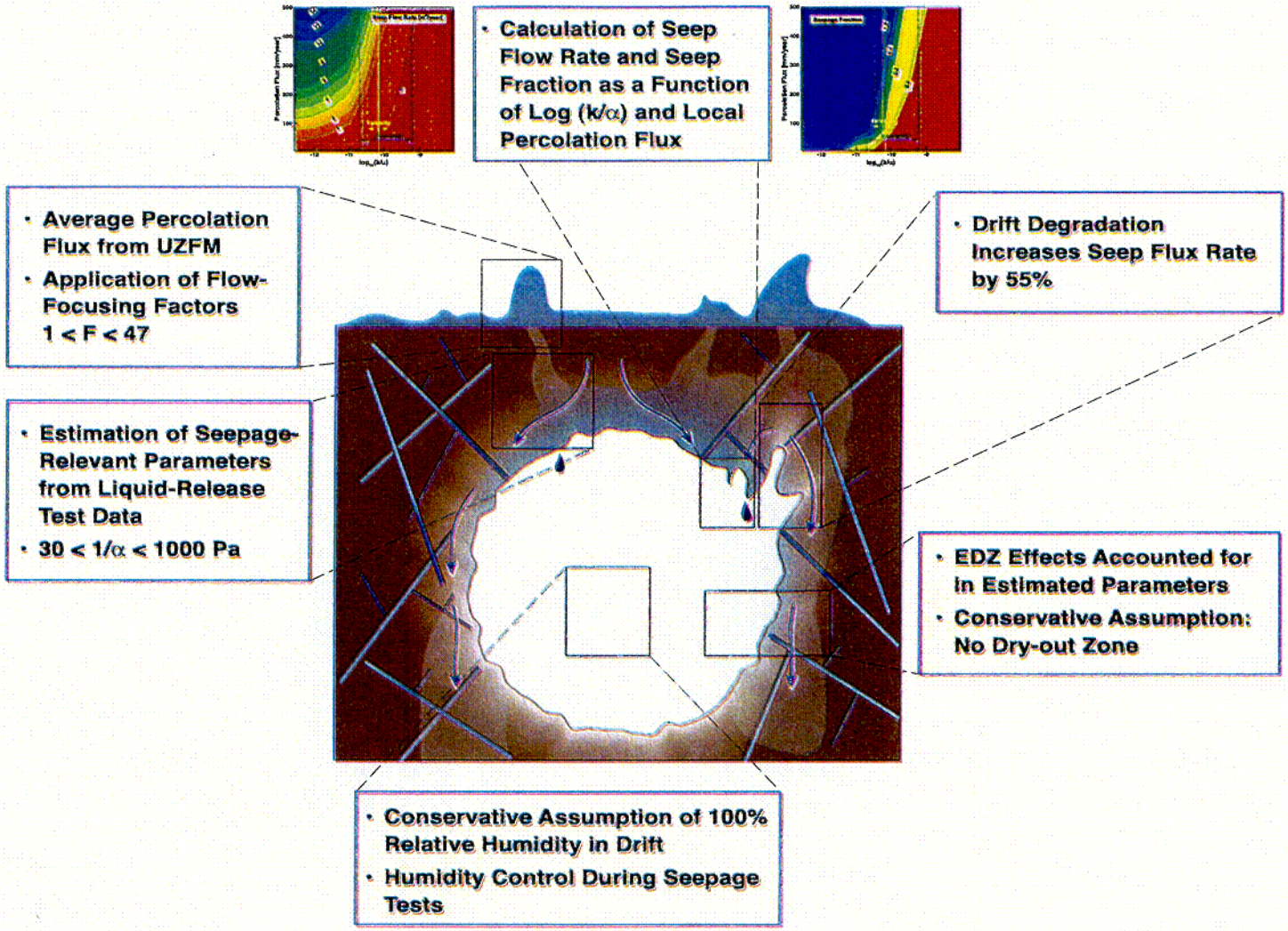

Figure 3.9-12. Summary of Results

C097

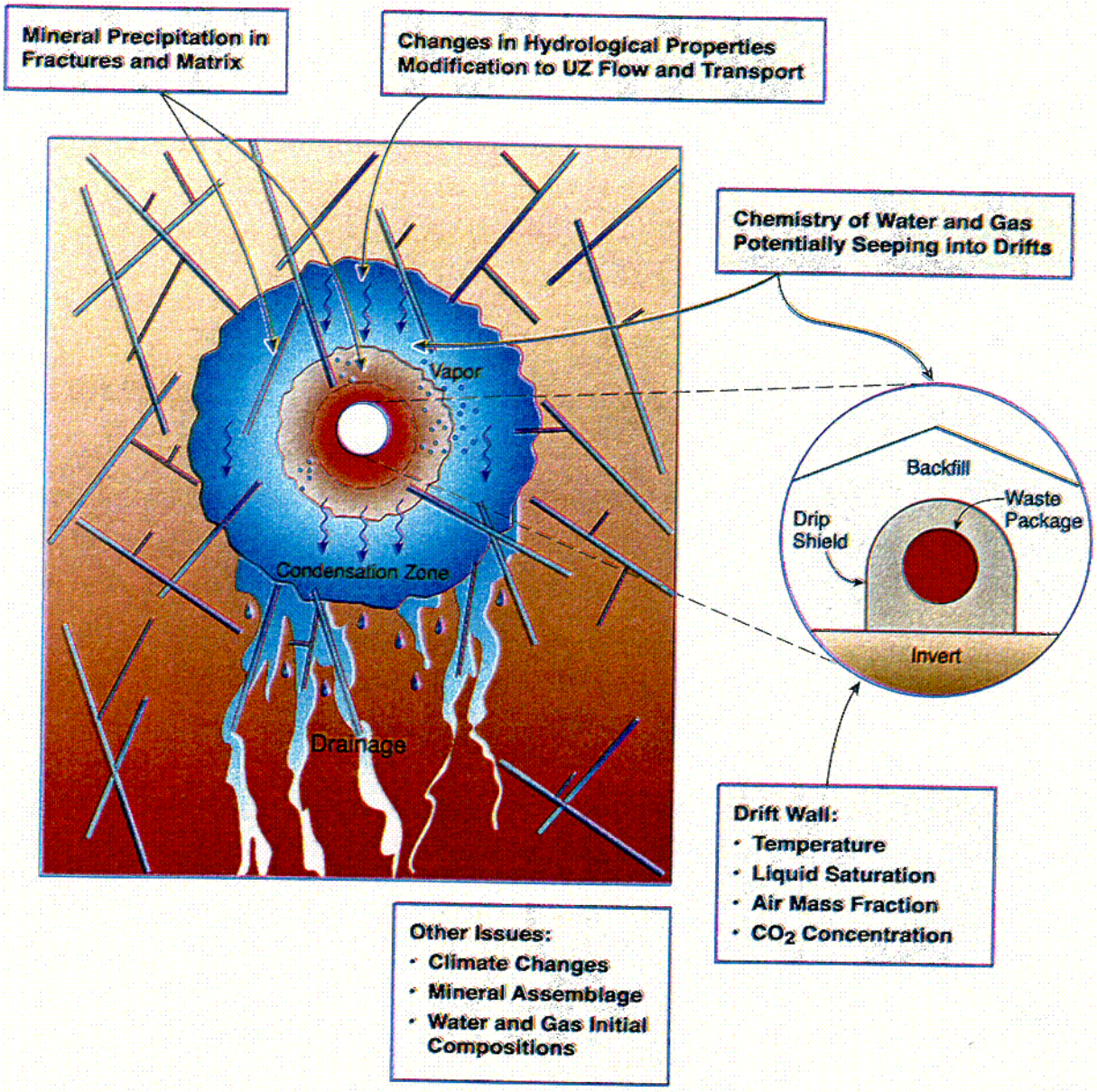

Figure 3.10-1. Schematic Diagram of THC Processes Around a Heated Drift

C098

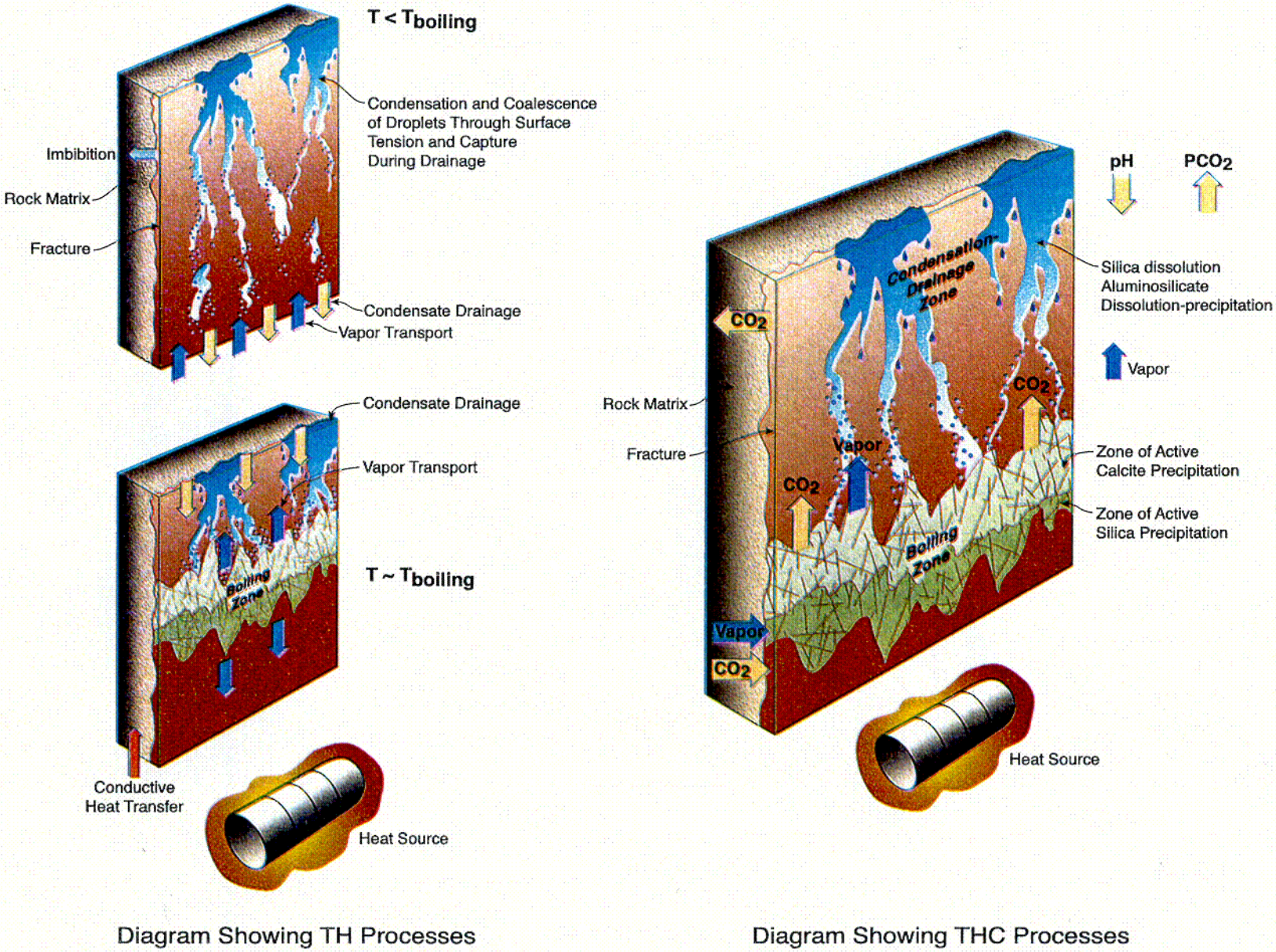

Figure 3.10-2. Schematic Diagram Showing Relation Between TH Processes and Geochemical Processes

0099

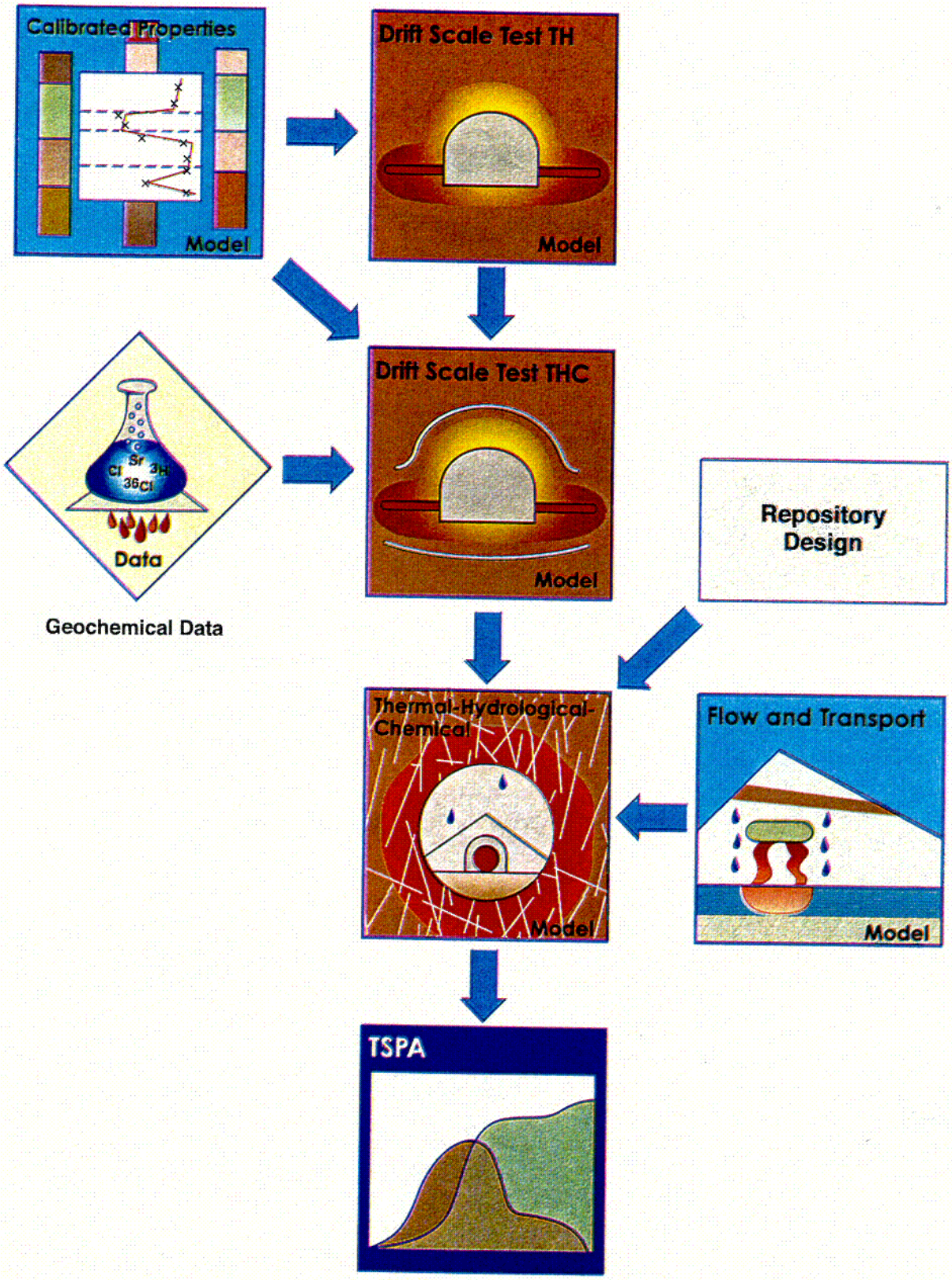

Figure 3.10-3. Model Diagram Relating Inputs and Outputs for the THC Seepage Model and Drift Scale Test THC Model

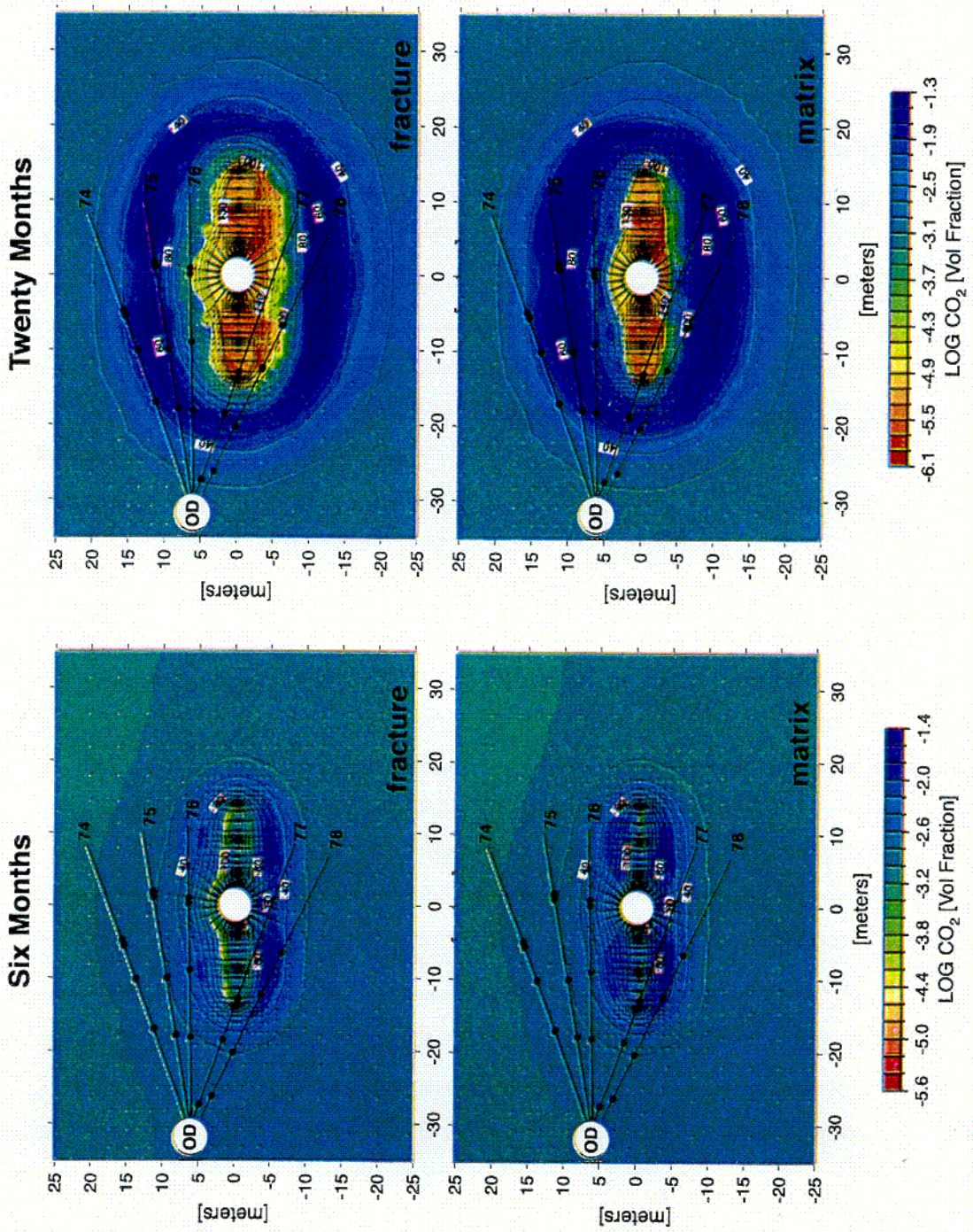

Figure 3.10-4. Simulated CO_2 Volume Fractions in Fractures and Matrix After 6 (a&b) and 20 (c&d) Months of Heating During the Drift Scale Test (adapted from CRWMS M&O 2000, N0120/U0110, Figures 5 and 6). Temperature contours are superimposed. "OD" refers to the Observation Drift.

C101

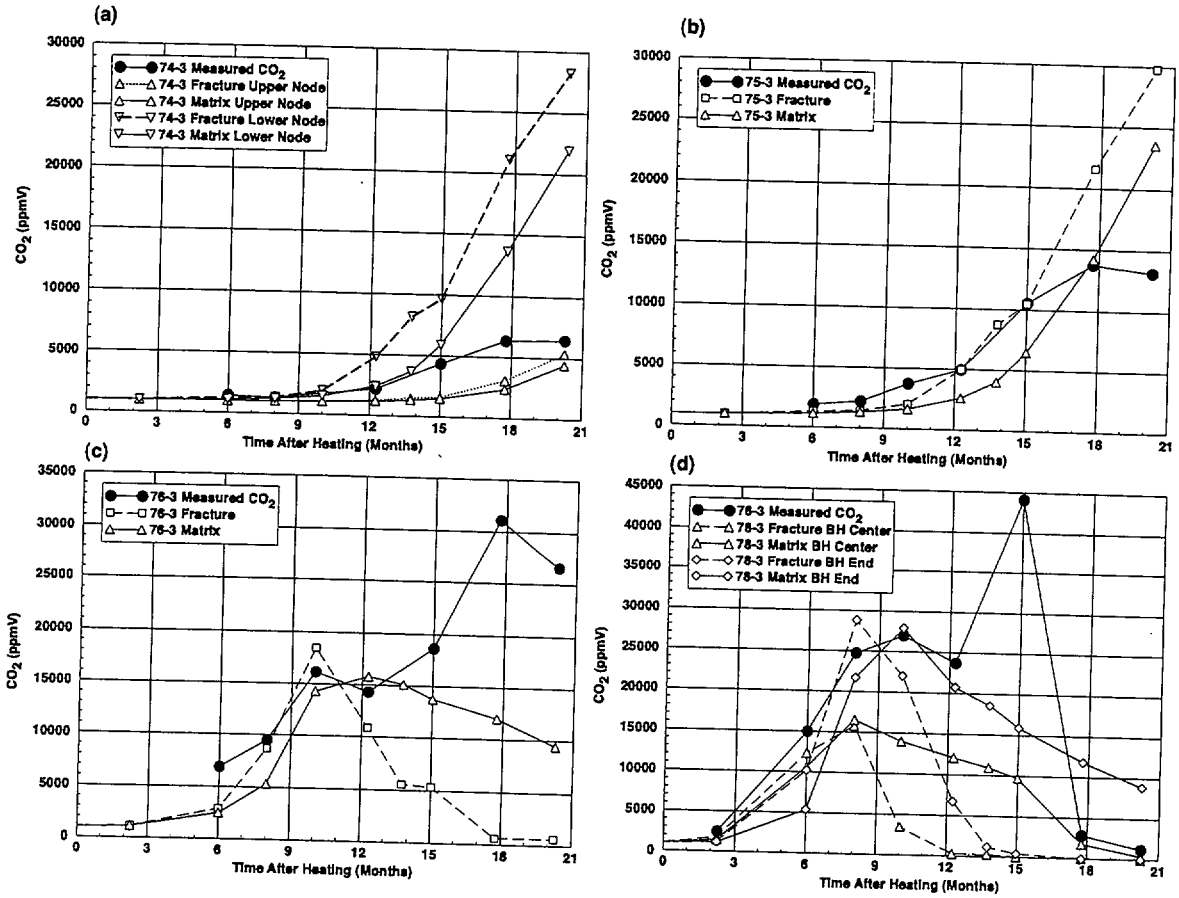

Figure 3.10-5. Simulated CO_2 Volume Fractions at Grid Nodes near Borehole (BH) Intervals Where Gas-Phase CO_2 Measurements were Made (CRWMS M&O 2000, N0120/U0110, Figure 10). Filled circles are measured CO_2 concentrations in the gas phase. Modeled data come from locations in 2-D grid close to center of borehole interval.

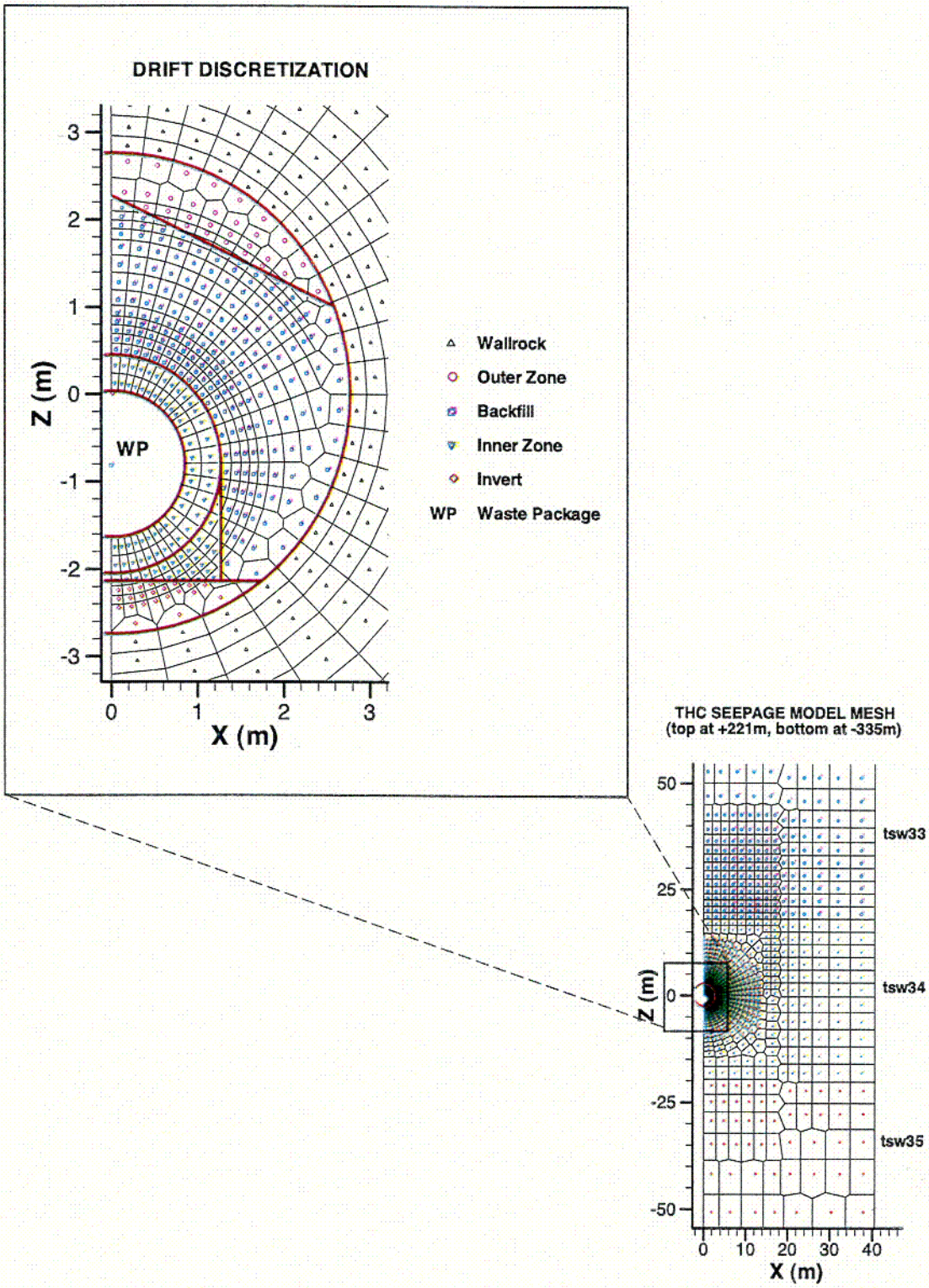

Figure 3.10-6. THC Seepage Model Mesh Showing Hydrogeologic Units in Proximity of the Drift: Topopah Spring Tuff Upper Lithophysal (tsw33), Middle Nonlithophysal (tsw34), and Lower Lithophysal (tsw35) Units, and Blowup Showing Discretization of In-Drift Design Components (adapted from CRWMS M&O 2000, N0120/U0110, Figures 18 and 19)

C102

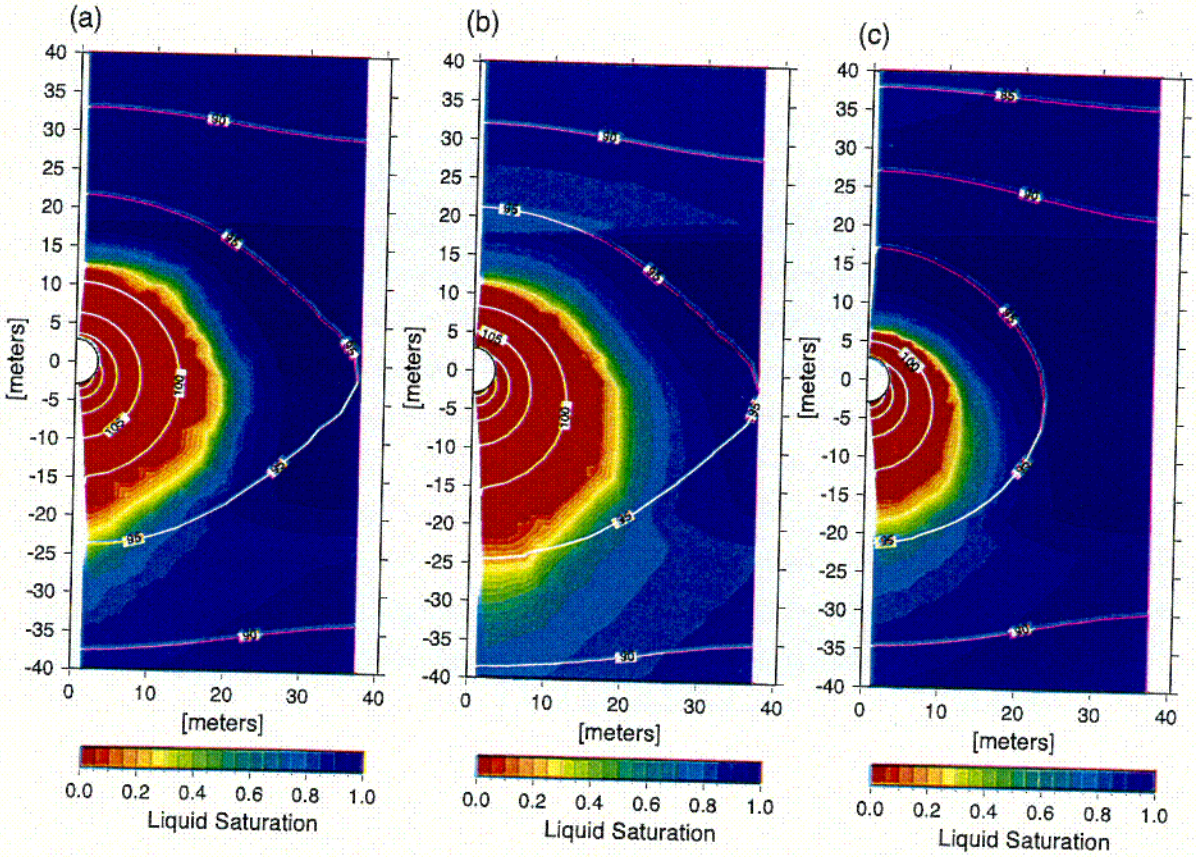

Figure 3.10-7. Contour Plot of Modeled Liquid Saturations and Temperatures (Labeled Contour Lines) in the Matrix at 600 Years (Near Maximum Dryout) for Three Climate Change Scenarios: (a) Lower Bound, (b) Mean, and (c) Upper Bound (Calcite-Silica-Gypsum System) (CRWMS M&O 2000, N0120/U0110, Figure 26)

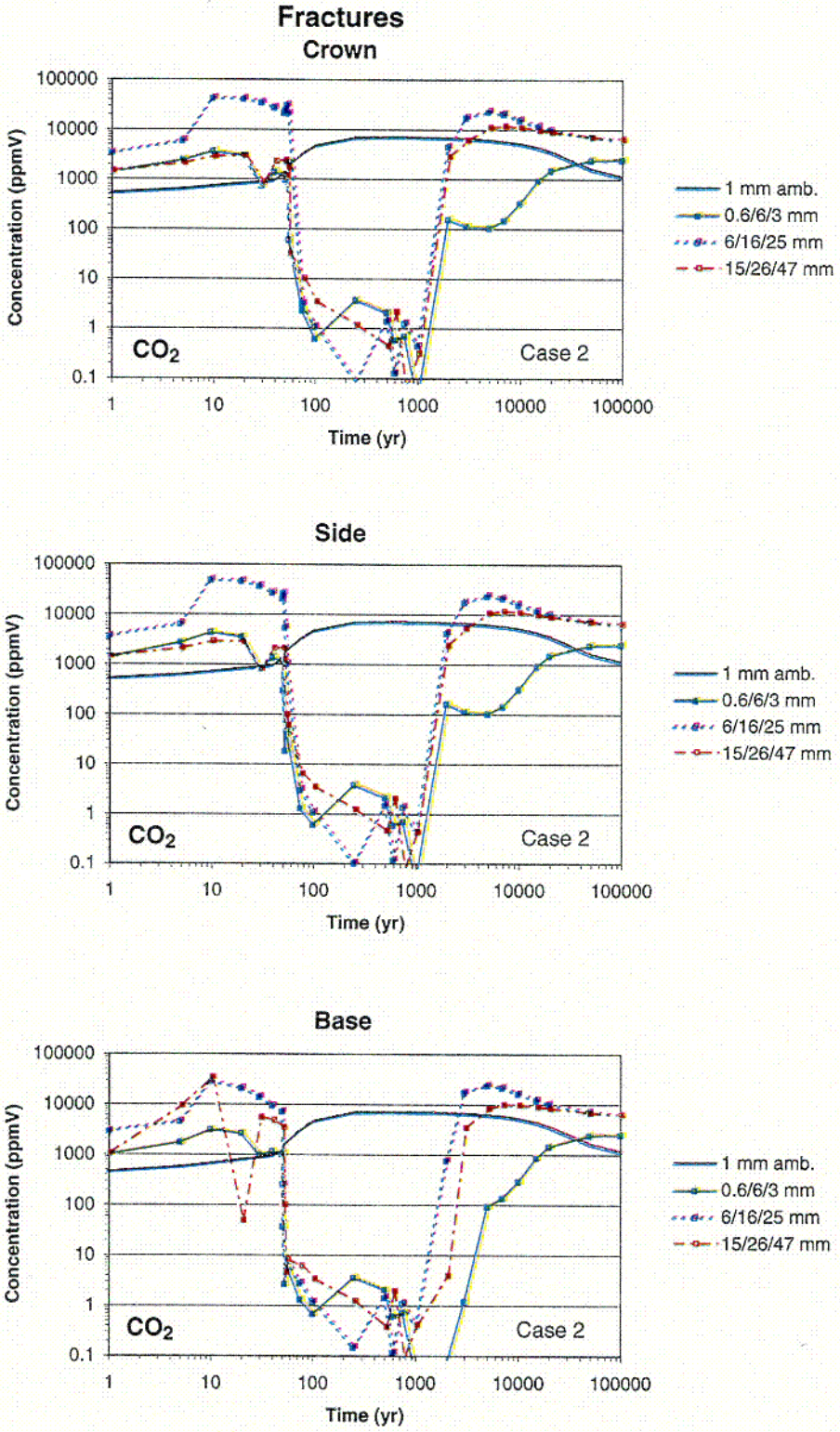

Figure 3.10-8. Time Profiles of Modeled CO_2 Concentrations in the Gas Phase in Fractures at Three Drift Wall Locations for Different Climate Change Scenarios (Calcite-Silica-Gypsum System) (CRWMS M&O 2000, N0120/U0110, Figure 29)

C104

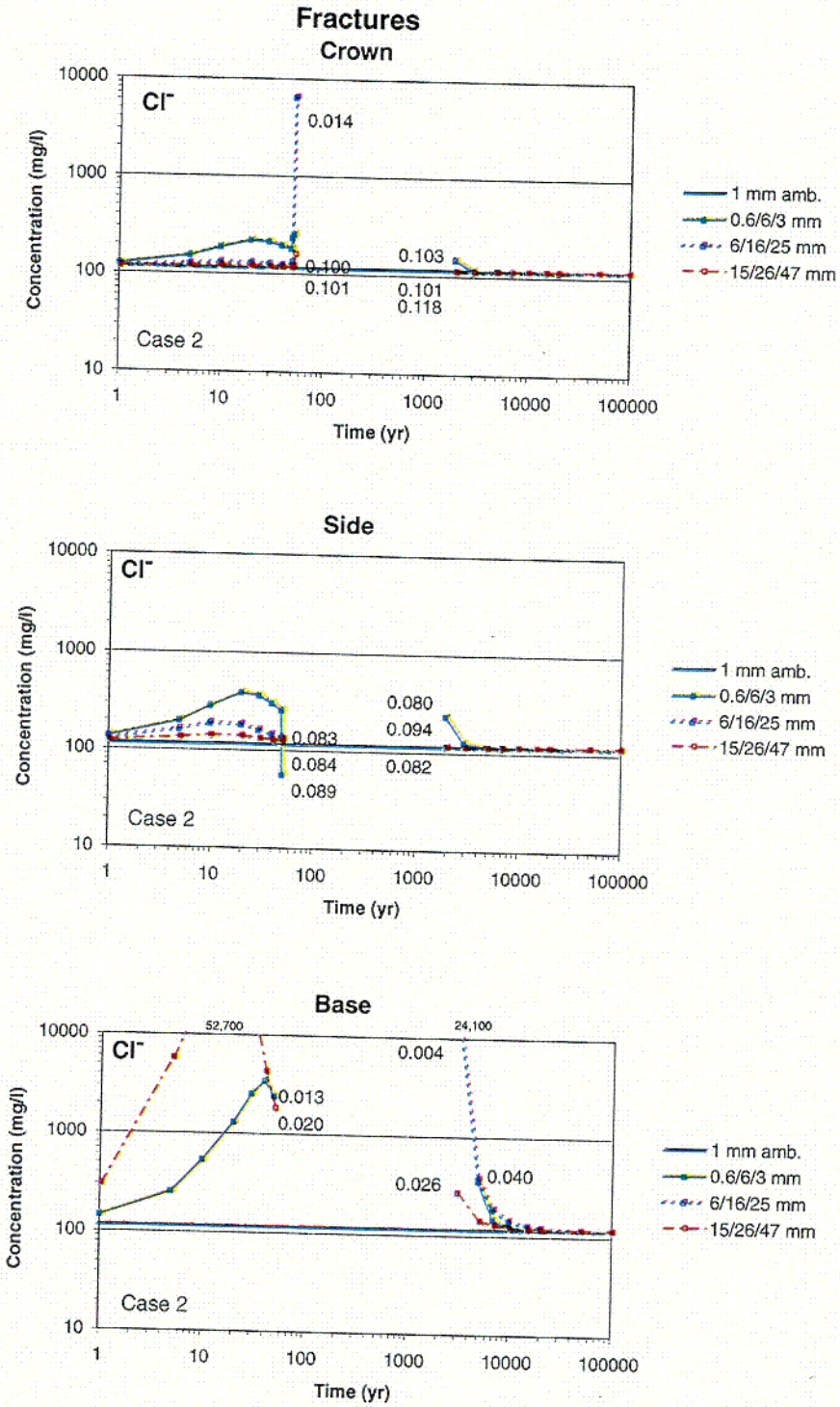

Figure 3.10-9. Time Profiles of Modeled Total Aqueous Chloride Concentrations in Fracture Water at Three Drift Wall Locations for Different Climate Change Scenarios (Case 2). The dryout period is left blank. Numbers by each curve indicate the last output liquid saturation before dryout and the first output liquid saturation during rewetting (CRWMS M&O 2000, N0120/U0110, Figure 38).

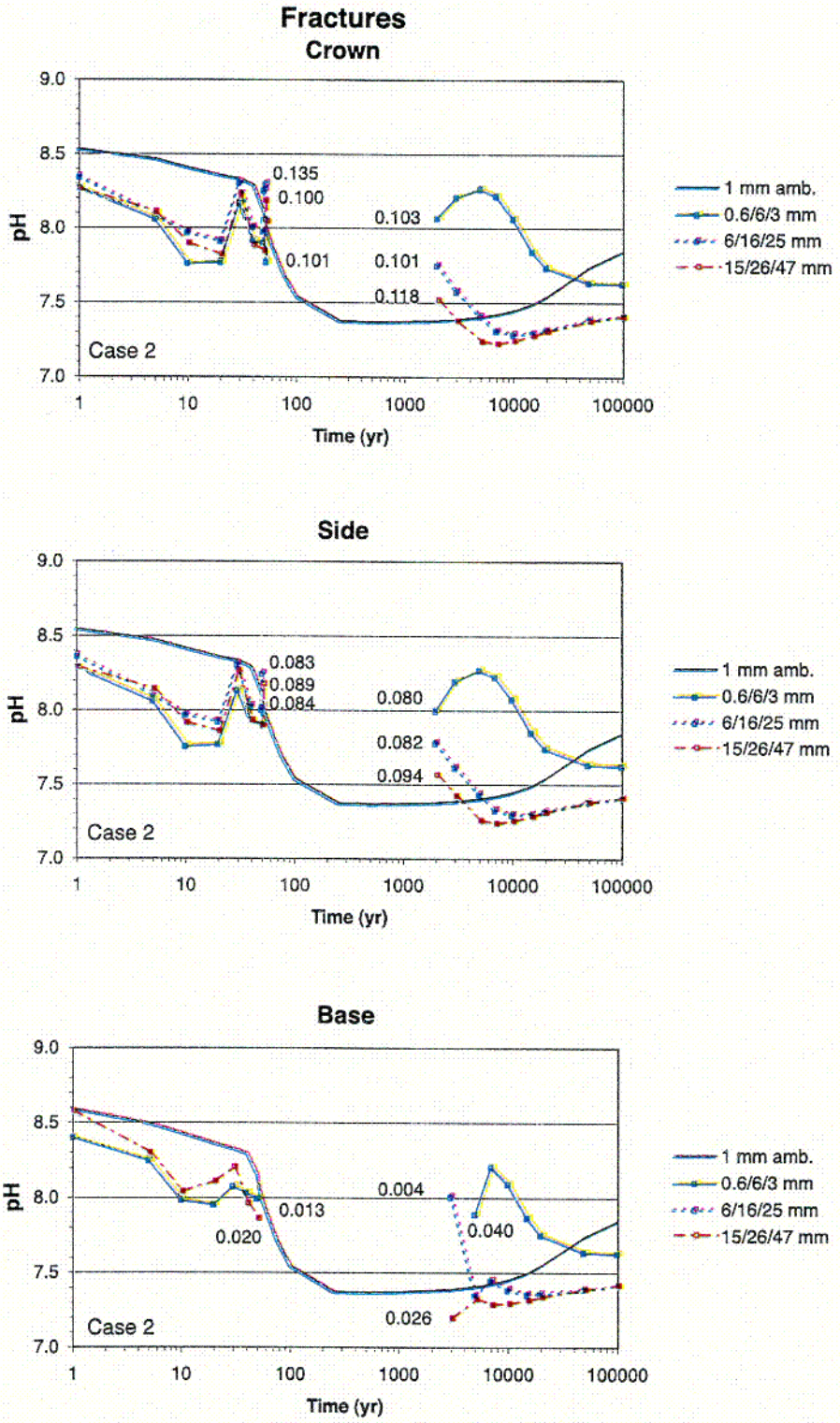

Figure 3.10-10. Time Profiles of the Modeled pH of Fracture Water at Drift Wall Locations for Different Climate Change Scenarios (Case 2 Calcite-Silica-Gypsum System). The dryout period is left blank. The last output liquid saturation before dryout and the first output liquid saturation during rewetting are noted on each curve (CRWMS M&O 2000, N0120/U0110, Figure 31).

C106

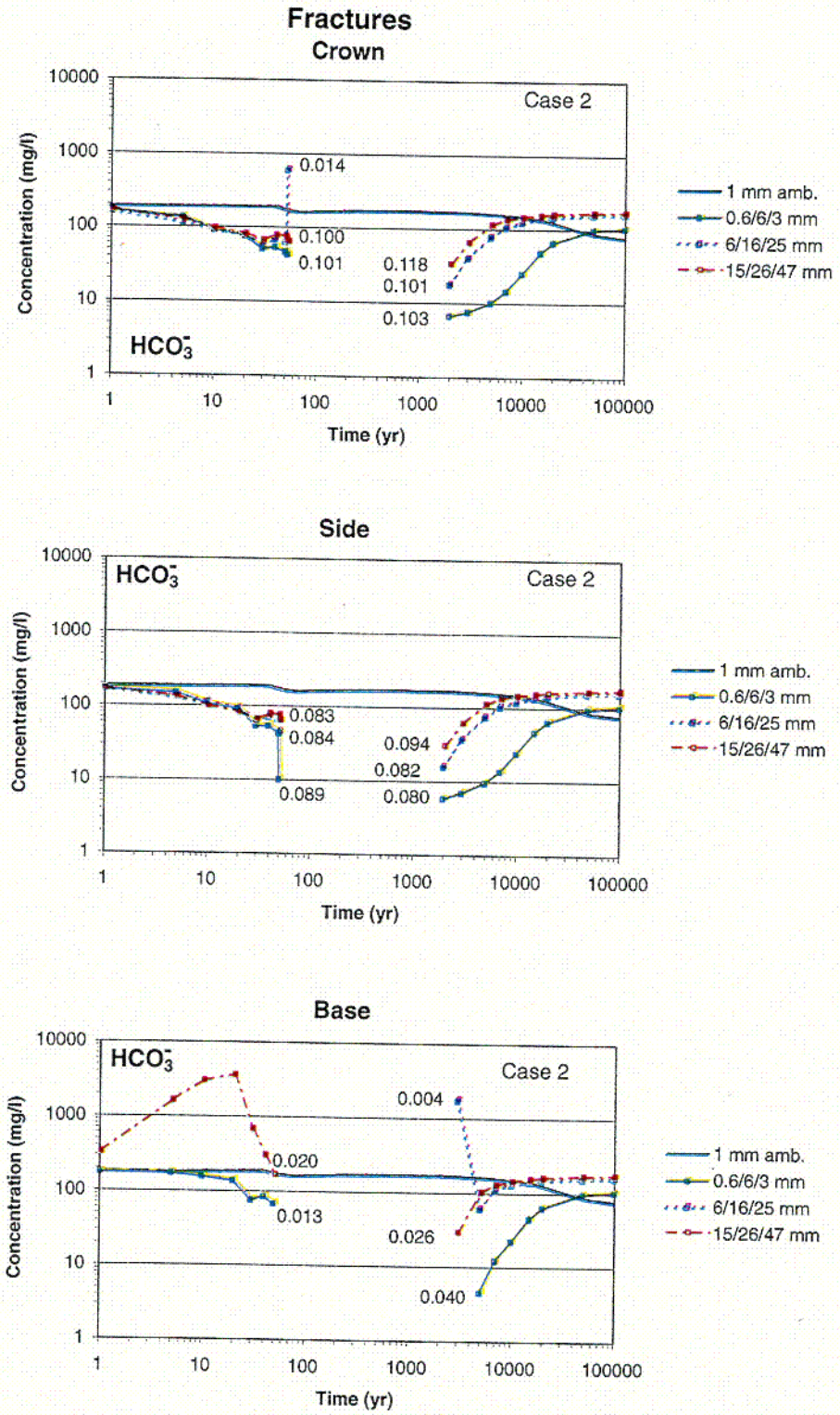

Figure 3.10-11. Time Profiles of Modeled Total Aqueous Carbonate Concentrations (as HCO_3^-) in Fracture Water at Drift Wall Locations for Different Climate Scenarios (Calcite-Silica-Gypsum System) (CRWMS M&O 2000, N0120/U0110, Figure 33)

C/07

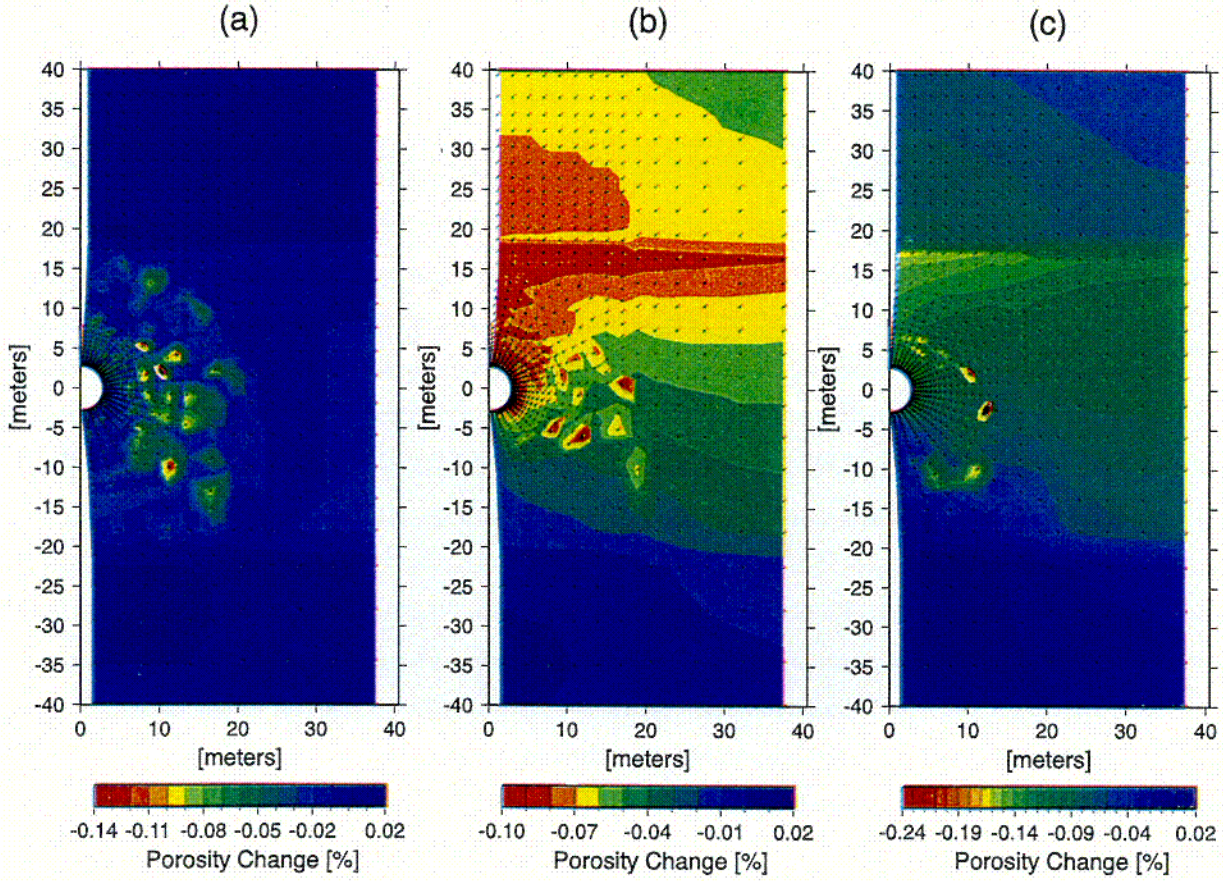

Figure 3.10-12. Contour Plot of Calculated Total Fracture Porosity Change at 10,000 Years for Three Climate Change Scenarios (Calcite-Silica-Gypsum System): (a) Lower Bound, (b) Mean, and (c) Upper Bound. Red areas indicate the maximum decrease in porosity as a result of mineral precipitation (CRWMS M&O 2000, N0120/U0110, Figure 42).

C108

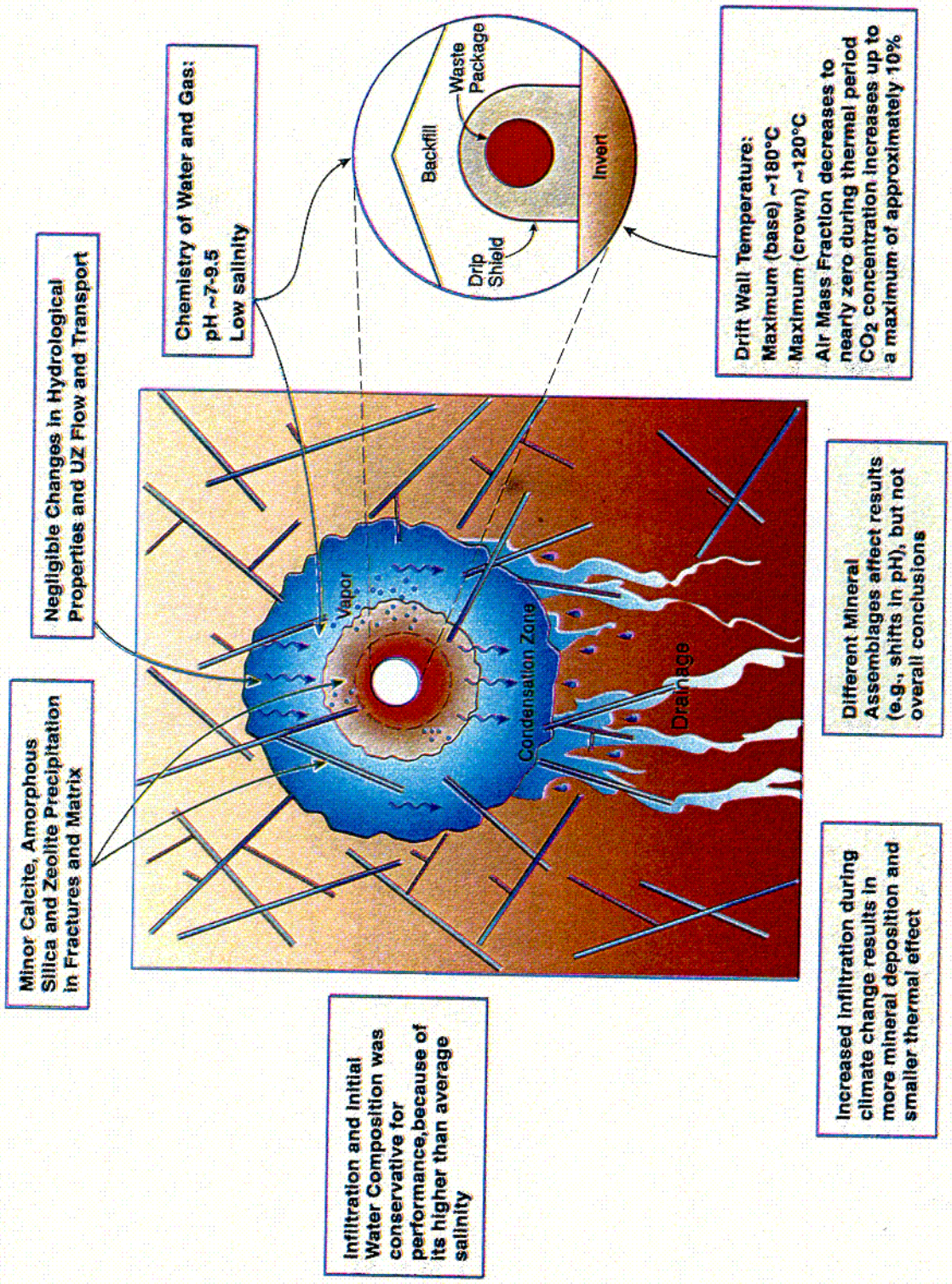

Figure 3.10-13. Conceptual Model of TH Processes Around a Heated Drift and Summaries of Important Results of Drift-Scale THC Simulations and Analyses

C109

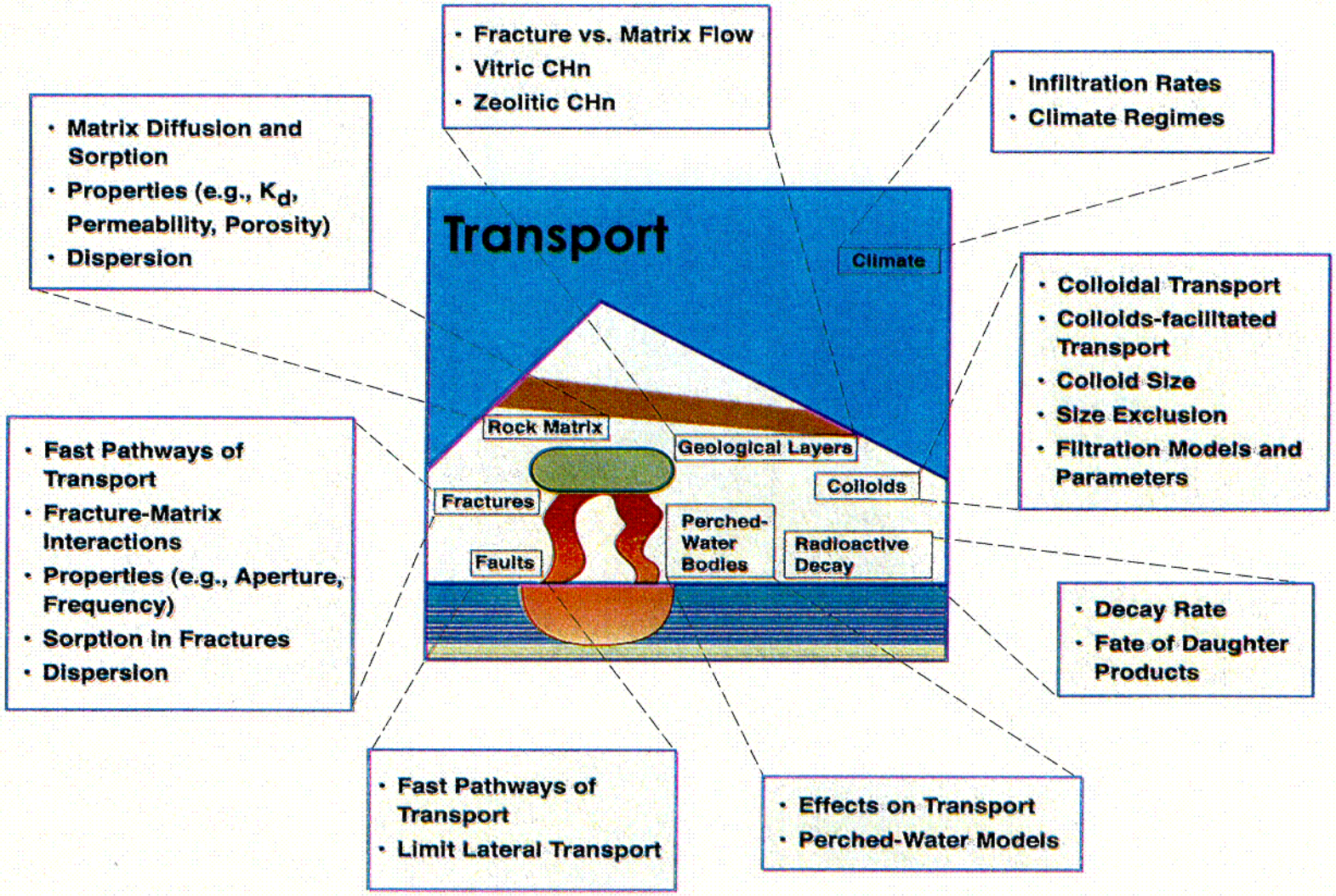

Figure 3.11-1. Key Issues Related to Potential Radionuclide Transport in the UZ

C110

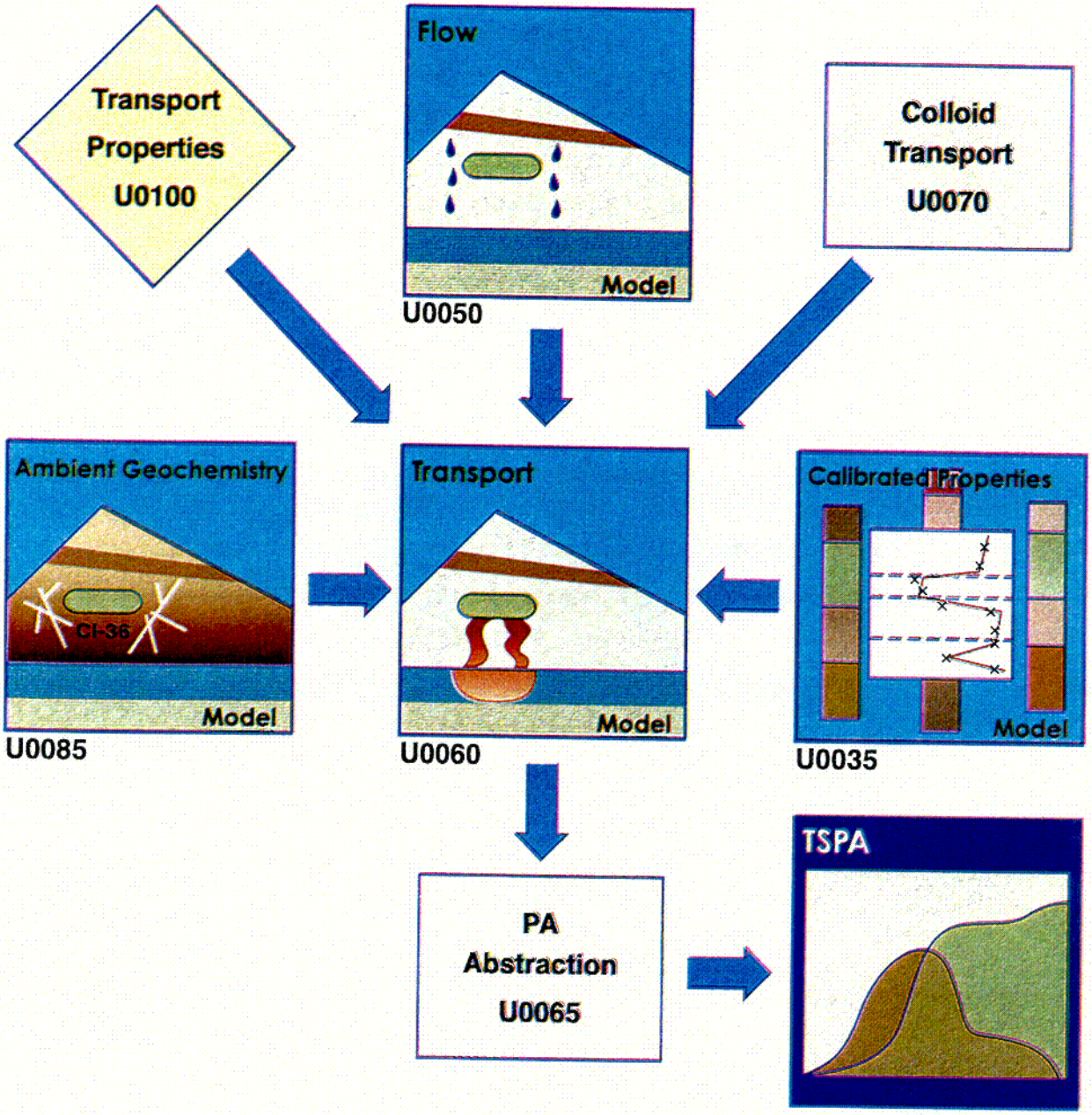

Figure 3.11-2. Relationships of Other Models and Data Feeds to the Transport Model

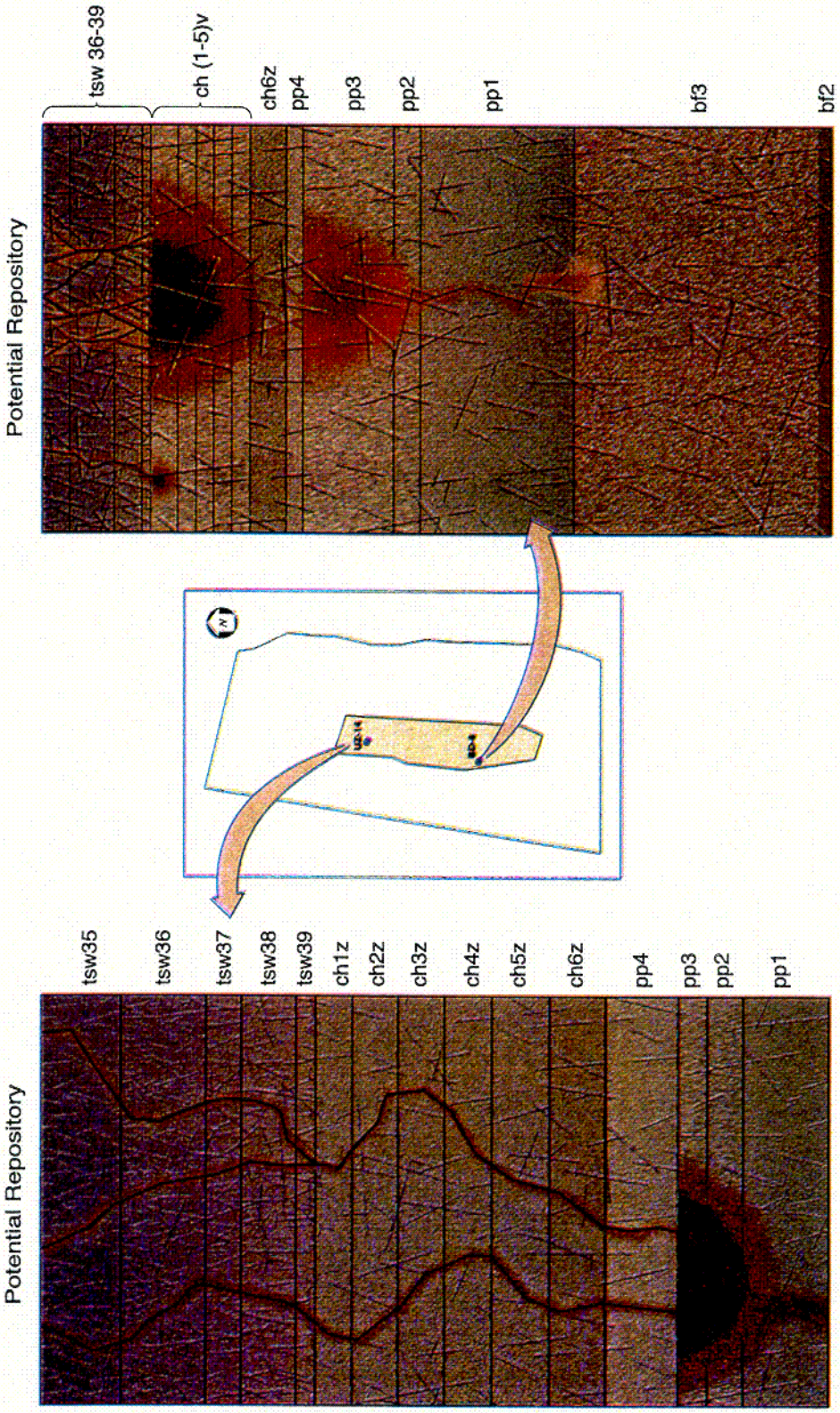

Figure 3.11-3. Schematic Illustration of Flow and Transport in the UZ Model Layers below the Potential Repository (Boreholes SD-6 and UZ-14)

C112

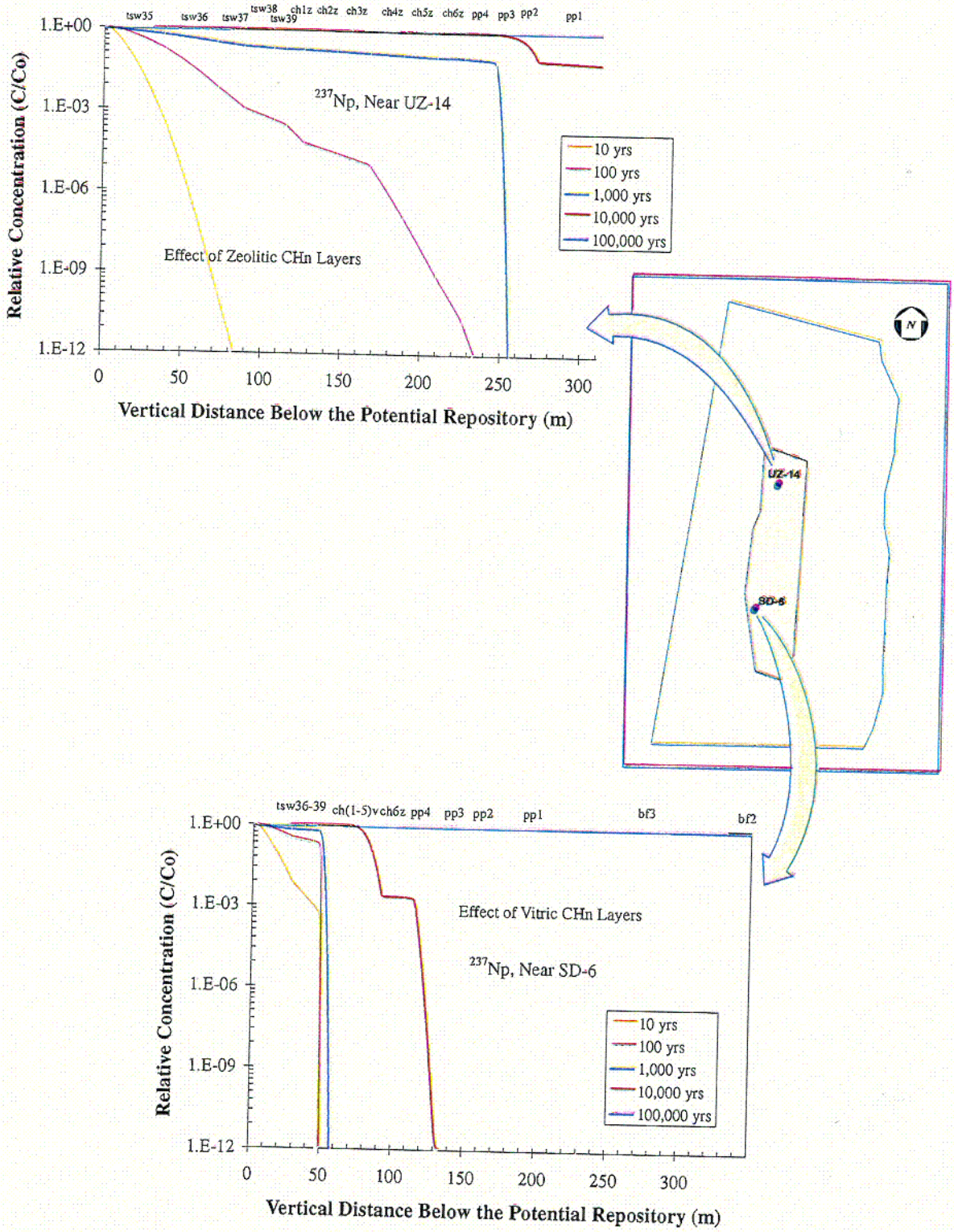

Figure 3.11-4. Concentration Profiles of ^{237}Np in 2-D Cross Sections of SD-6 and UZ-14 (Adapted from CRWMS M&O 2000, U0060, Figures V.2 and V.8)

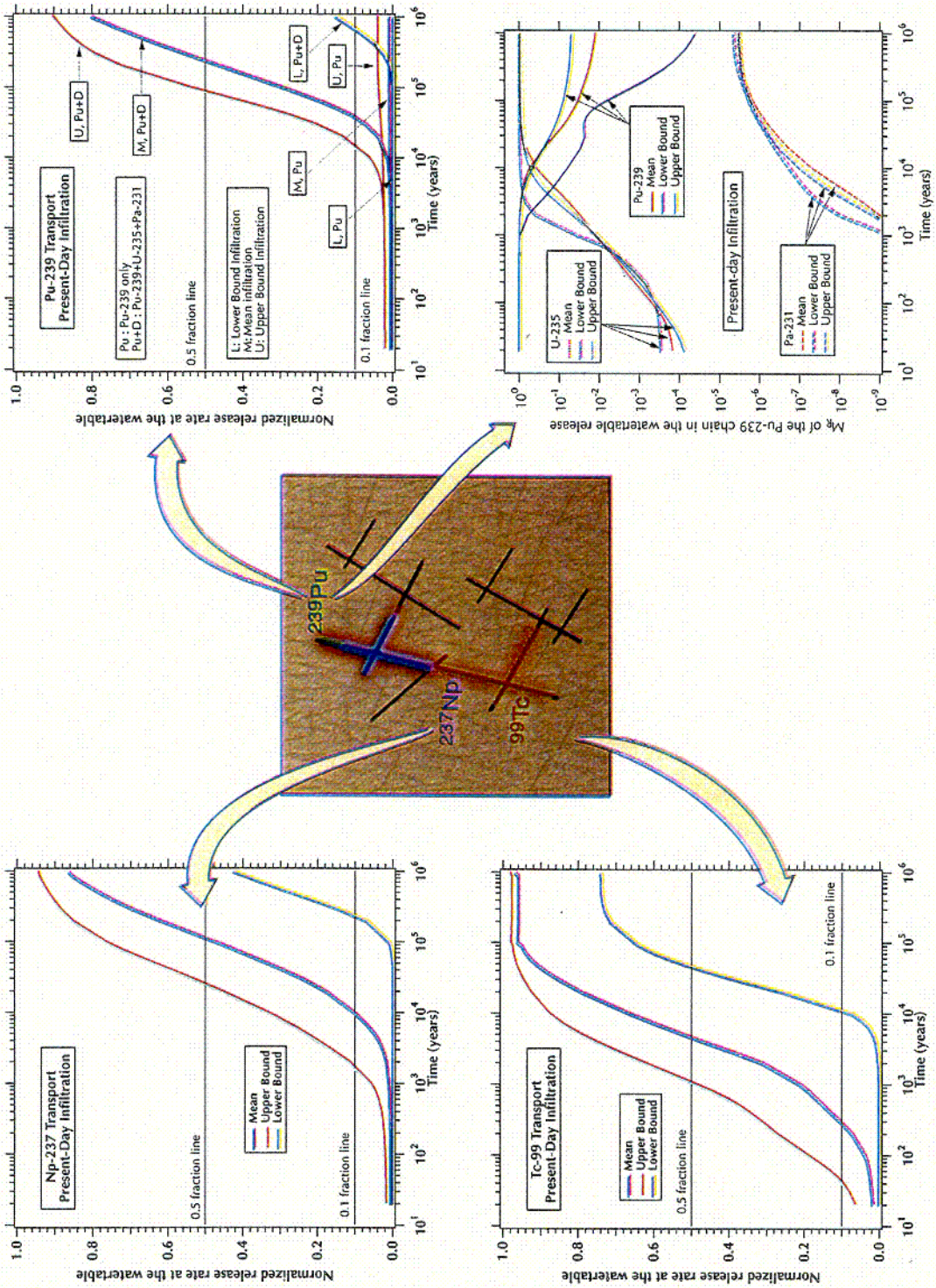

Figure 3.11-5. Concentration Profiles of ^{99}Tc, ^{237}Np, ^{239}Pu and its Daughters at the Water Table for Varying Present-day Climatic Scenarios (Adapted from CRWMS M&O 2000, U0060, Figures 6.12.1, 6.13.1, 6.14.1, and 6.14.2. The data shown in this figure are based on a model that is appropriately conservative for TSPA analysis and consequently should not be used to evaluate expected breakthrough curves of radionuclides at the water table.)

C114

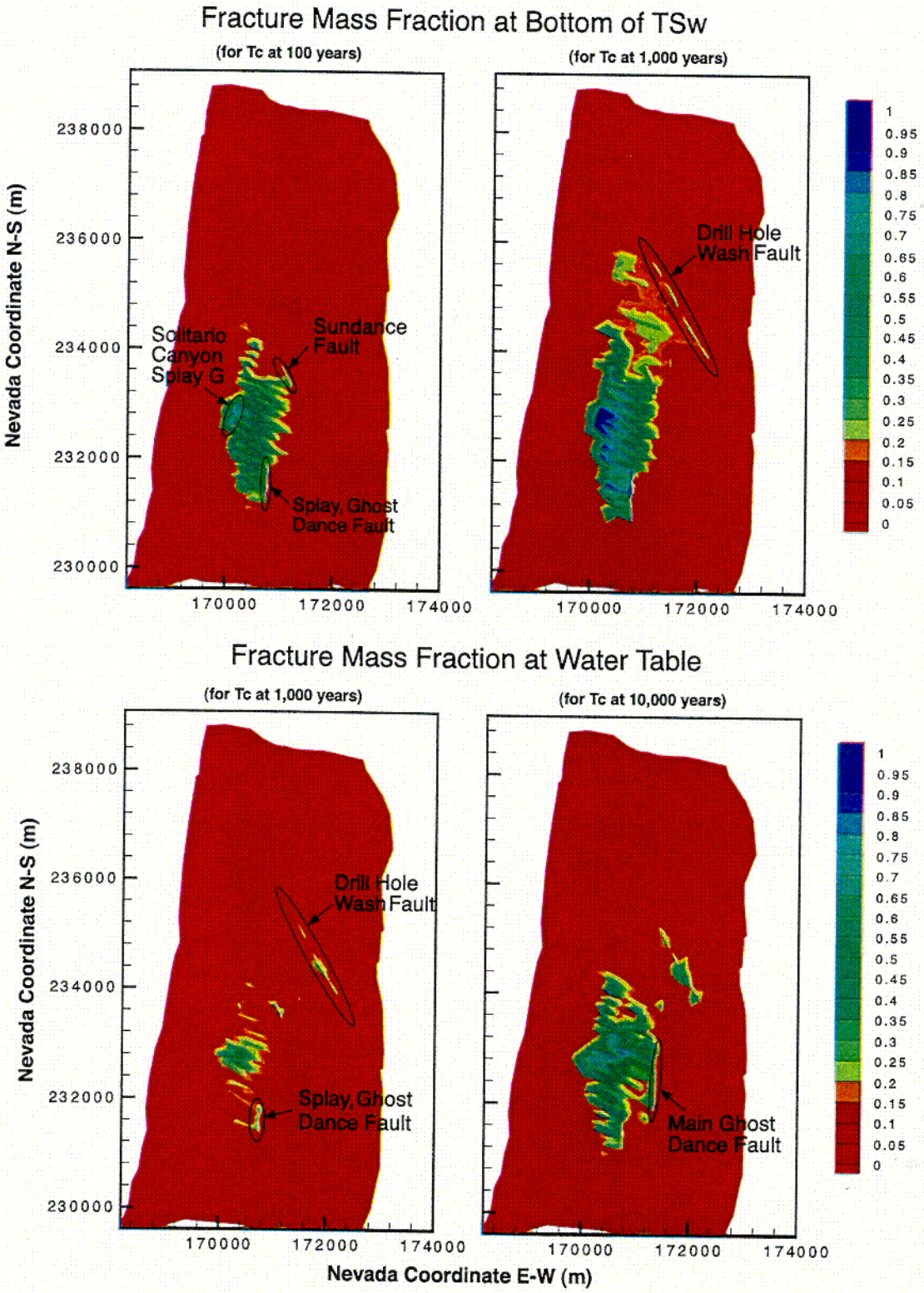

Figure 3.11-6. Normalized Mass Fraction Distribution of ^{99}Tc in the Fractures at the Bottom of the TSw and the Water Table (Adapted from CRWMS M&O 2000, U0060, Figures 6.12.2, 6.12.4, 6.12.12, and 6.12.14)

C115

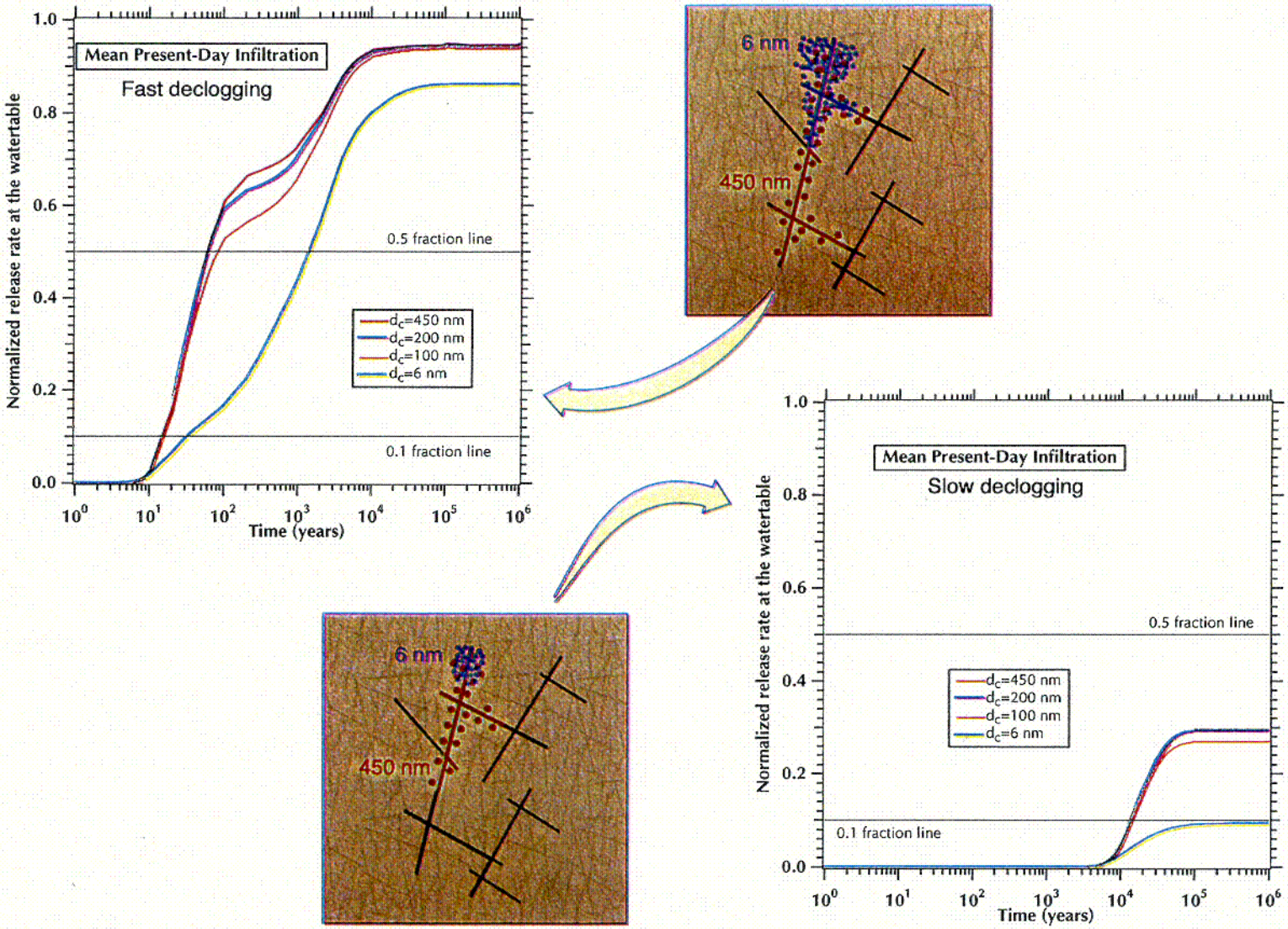

Figure 3.11-7. Influence of Colloid Size and Kinetic Model Parameters on Colloidal Transport (Adapted from CRWMS M&O 2000, U0060, Figures 6.16.1 and 6.16.2. The data shown in this figure are based on a model that is appropriately conservative for TSPA analysis and consequently should not be used to evaluate expected breakthrough curves of radionuclides at the water table.)

C116

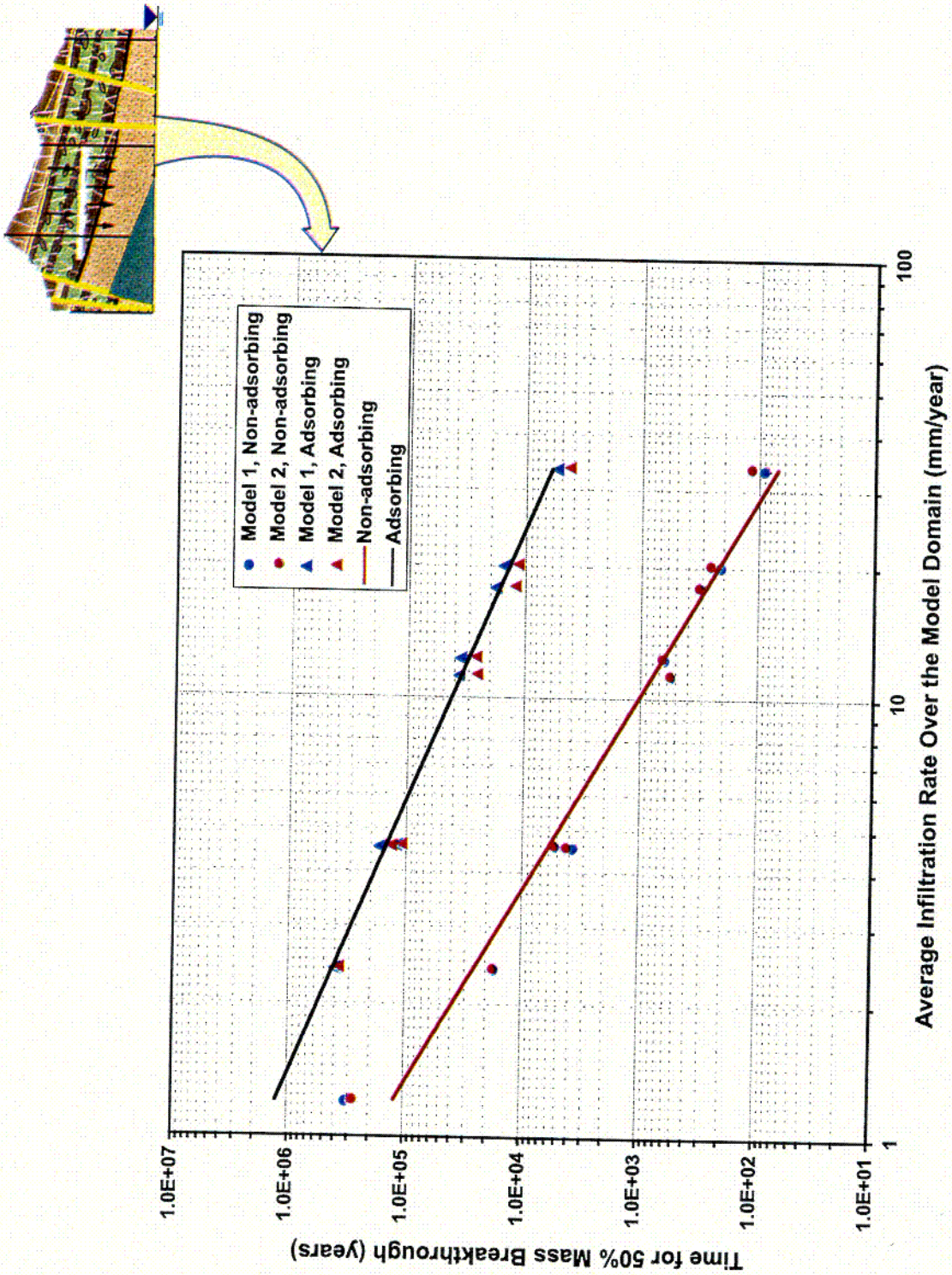

Figure 3.11-8. Correlations of Average Infiltration Rates and Tracer Transport Times at 50% Mass Breakthrough for 36 Simulation Scenarios (Data from CRWMS M&O, 2000, U0050, Section 6.7.3. The data shown in this figure are based on a model that is appropriately conservative for TSPA analysis and consequently should not be used to evaluate expected breakthrough curves of radionuclides at the water table.)

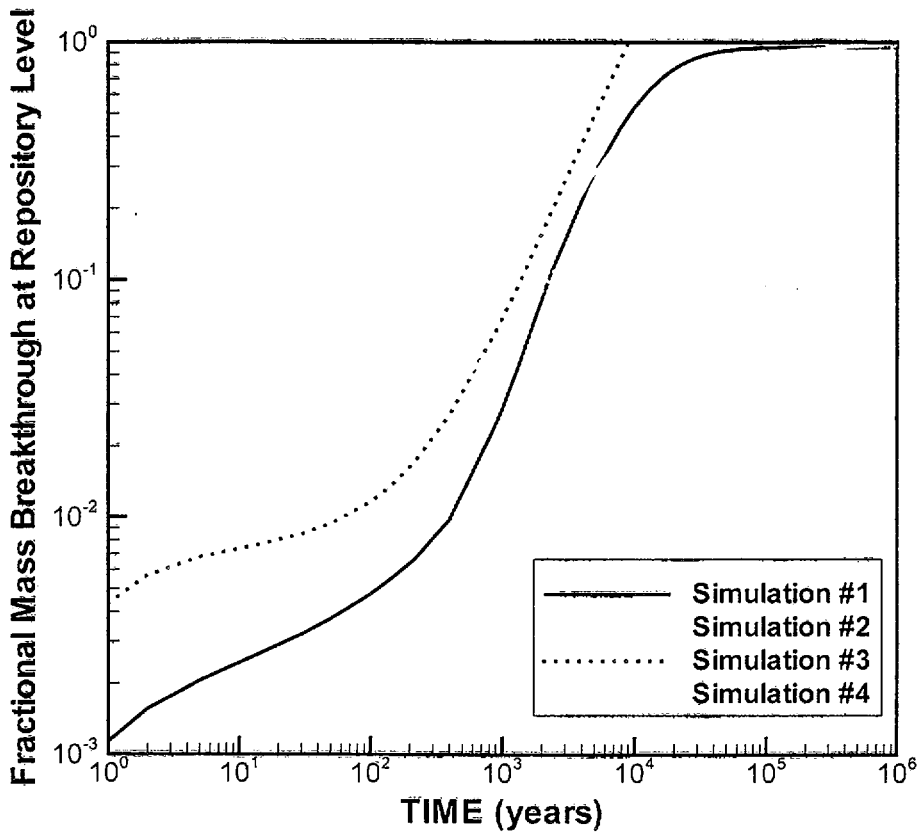

Figure 3.11-9. Simulated Breakthrough Curves of Cumulative Tracer (^{36}Cl) Mass Arriving at the Repository Level, Since Release from the Ground Surface, Using the Present-Day, Mean Infiltration and Four Simulation Scenarios (Data from CRWMS M&O, 2000, U0050, Section 6.7.3. The data shown in this figure are based on a model that is appropriately conservative for TSPA analysis and consequently should not be used to evaluate expected breakthrough curves of radionuclides at the water table.)

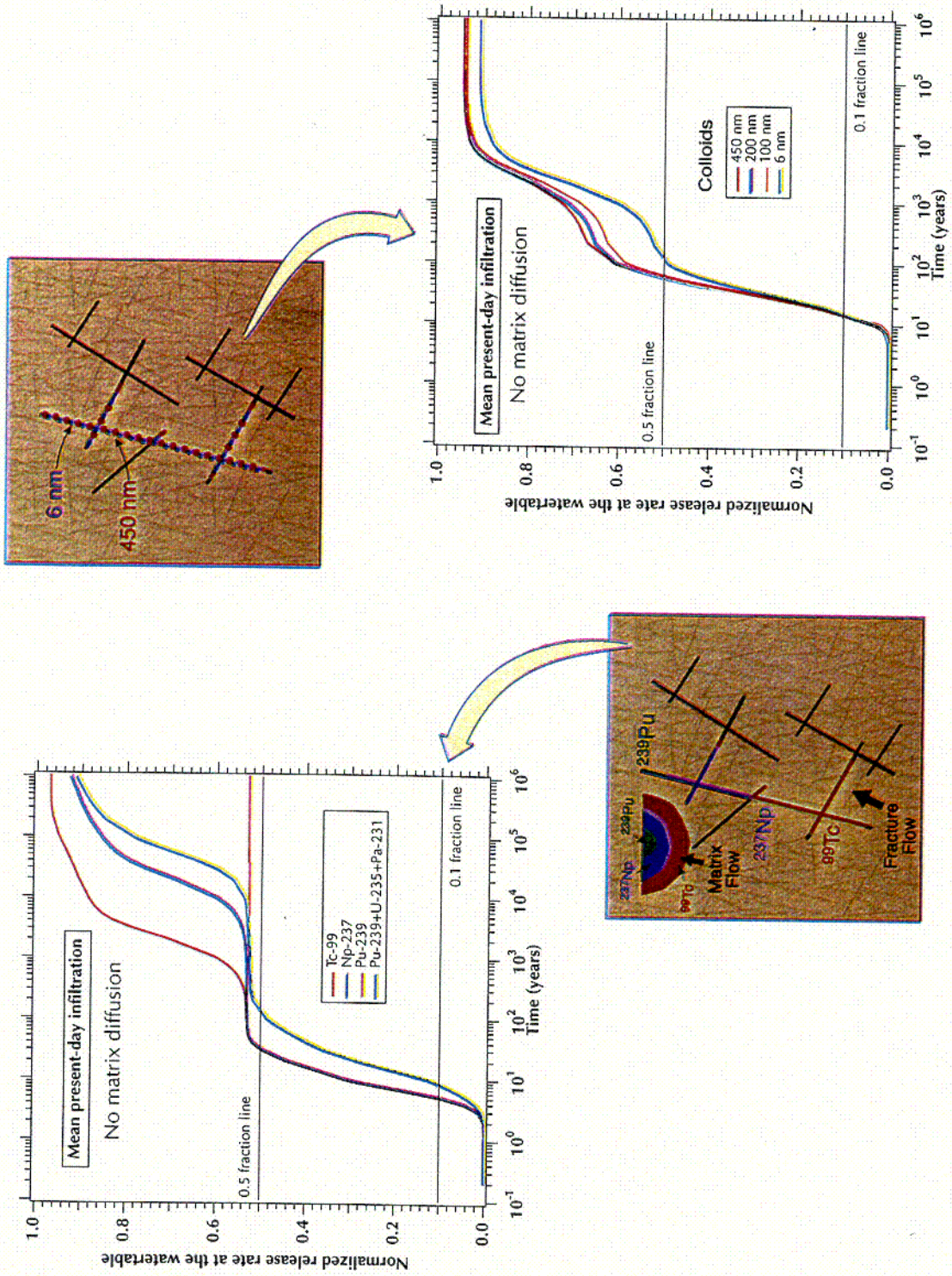

Figure 3.11-10. Effects of No Matrix Diffusion: Concentration of Radionuclides and Colloids at the Water Table for the No-diffusion Alternative Model (Adapted from CRWMS M&O 2000, U0060, Figures 6.17.1 and 6.17.2. The data shown in this figure are based on a model that is appropriately conservative for TSPA analysis and consequently should not be used to evaluate expected breakthrough curves of radionuclides at the water table.)

C118

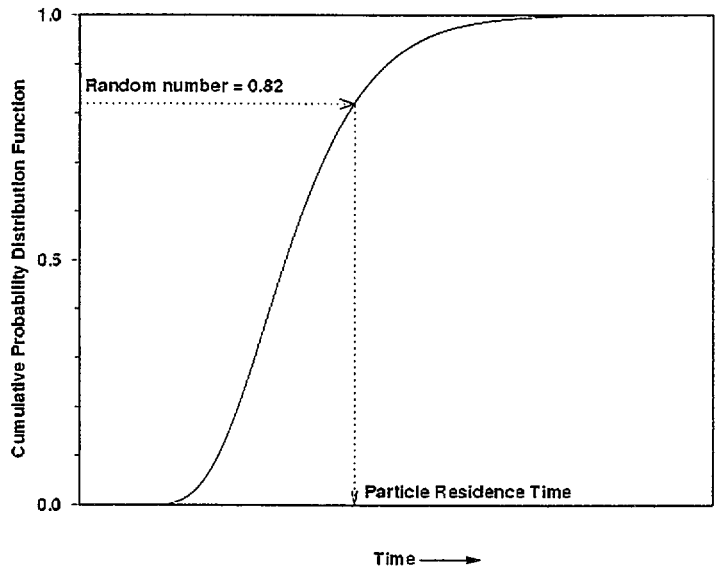

Figure 3.11-11. Schematic of the RTTF Technique for Determining Particle Residence Time in a Cell (CRWMS M&O 2000, U0065, Figure 2)

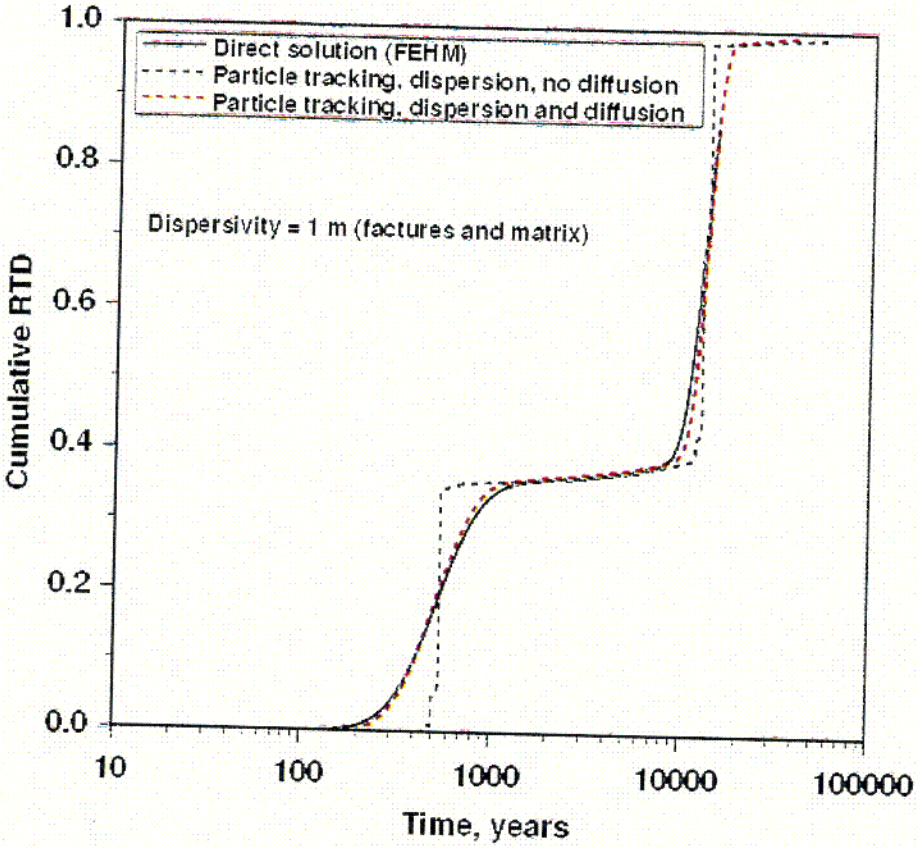

Figure 3.11-12. Comparison of the Particle-Tracking Solution and a Direct Finite-element Solution to the Transport (FEHM V2.10) for a 1-D, Dual-permeability Model (CRWMS M&O 2000, U0065, Figure 9. The data shown in this figure are based on a model that is appropriately conservative for TSPA analysis and consequently should not be used to evaluate expected breakthrough curves of radionuclides at the water table.)

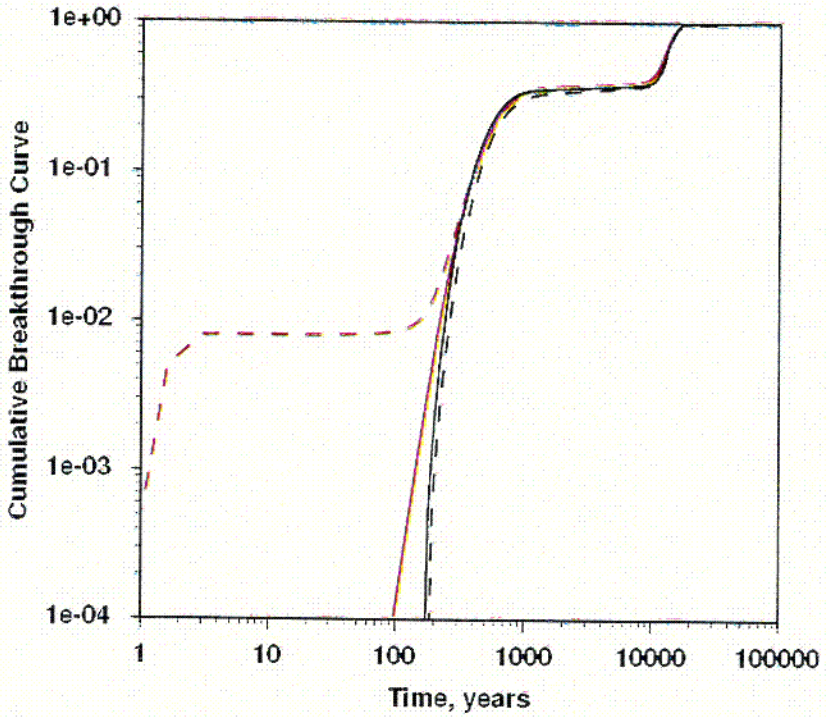

Figure 3.11-13. Comparison of the Particle-Tracking Solution and a Direct Finite-element Solution to the Transport for a 1-D, Dual-permeability Model. Red curves: finite element solution, black curves: particle tracking (solid - no diffusion, dashed - diffusion) (CRWMS M&O 2000, U0065, Figure 10. The data shown in this figure are based on a model that is appropriately conservative for TSPA analysis and consequently should not be used to evaluate expected breakthrough curves of radionuclides at the water table.)

C120

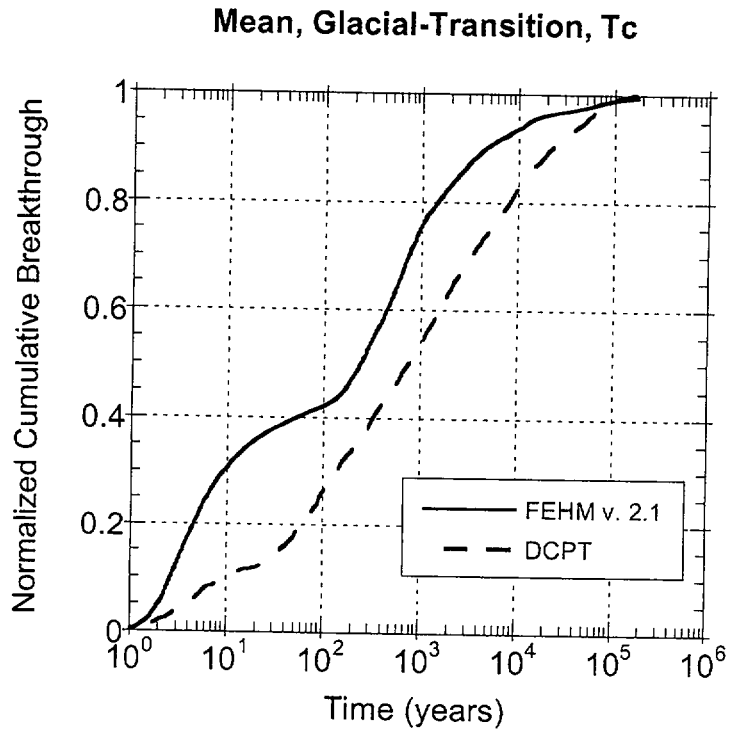

Figure 3.11-14. Comparison of Cumulative Normalized Breakthrough Curves at the Water Table Using FEHM V2.10 and DCPT V1.0 software with the Nonsorbing Tc for Mean-Infiltration, Glacial-Transition Climate (CRWMS M&O 2000, U0160, Figure 11. The data shown in this figure are based on a model that is appropriately conservative for TSPA analysis and consequently should not be used to evaluate expected breakthrough curves of radionuclides at the water table.)

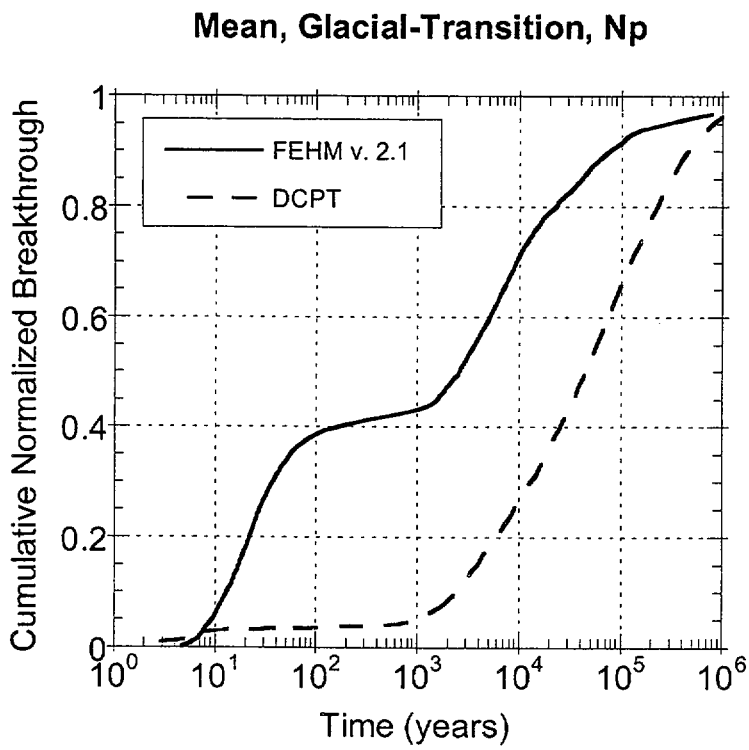

Figure 3.11-15. Comparison of Cumulative Normalized Breakthrough Curves at the Water Table Using FEHM V2.10 and DCPT V1.0 software with the Sorbing Np for Mean-Infiltration, Glacial-Transition Climate (CRWMS M&O 2000, U0160, Figure 11. The data shown in this figure are based on a model that is appropriately conservative for TSPA analysis and consequently should not be used to evaluate expected breakthrough curves of radionuclides at the water table.)

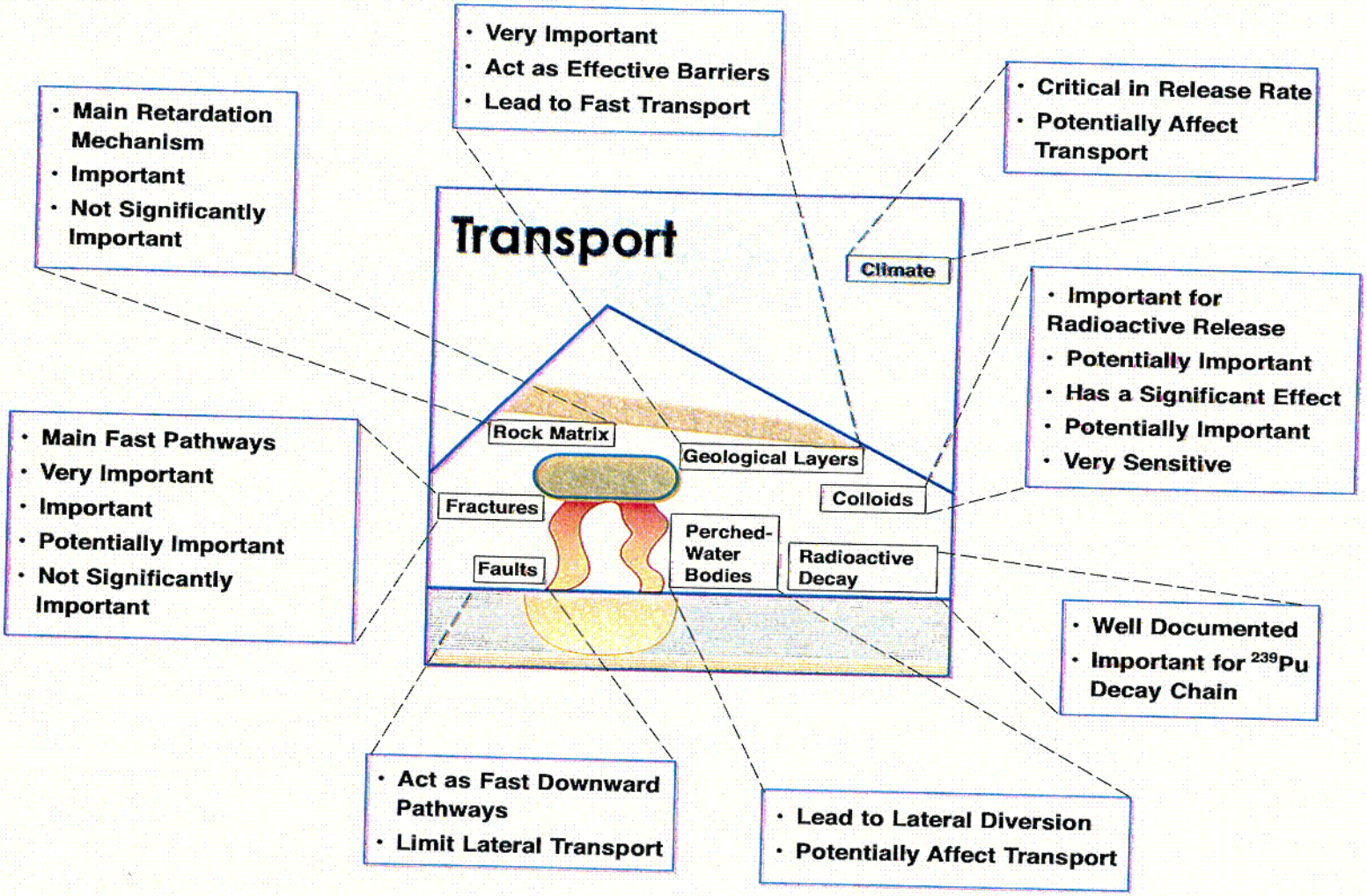

Figure 3.11-16. Results Related to Radionuclide Transport in the UZ

C/2/

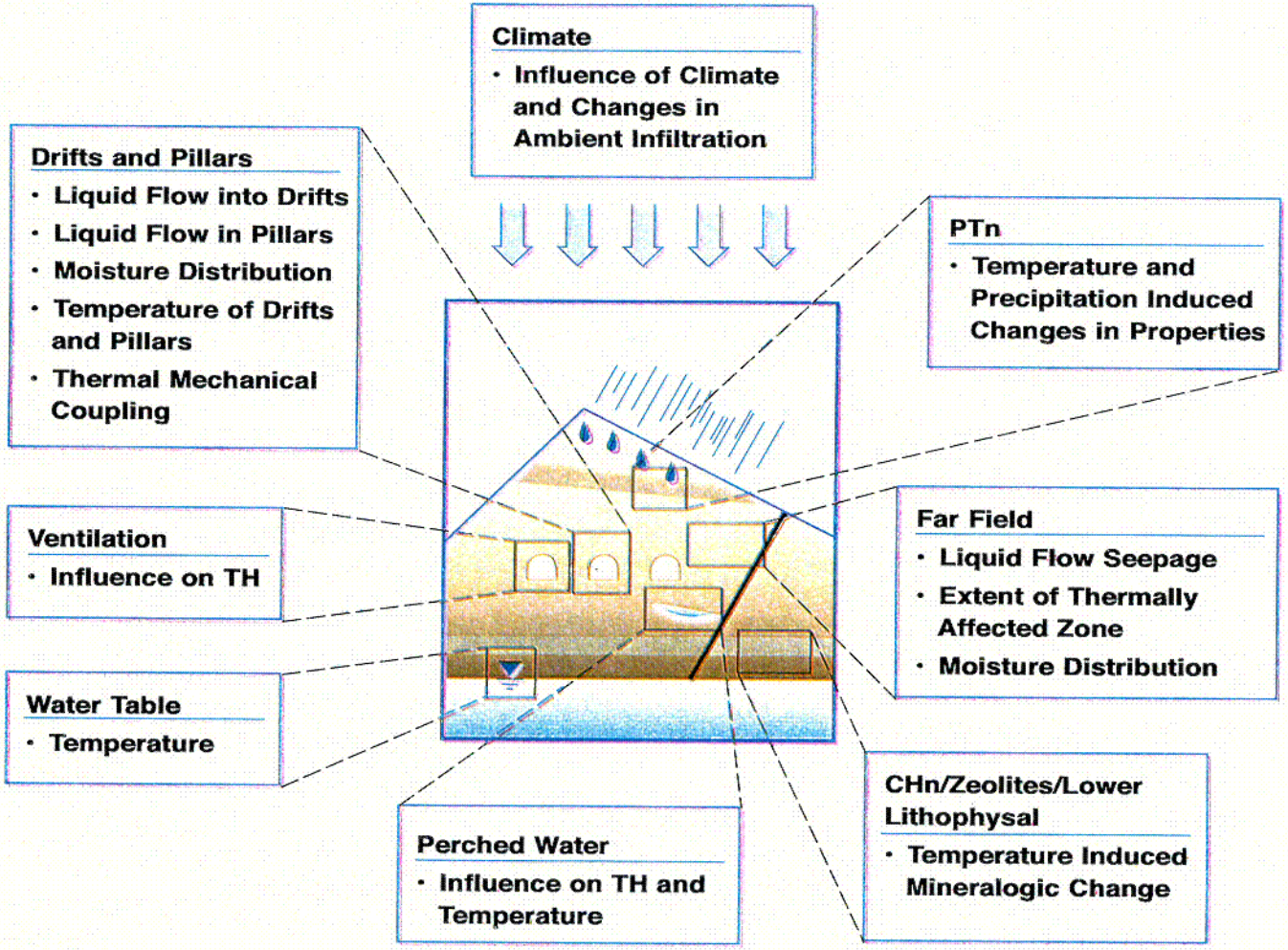

Figure 3.12-1. Schematic of the TH Modeling Issues

C/22

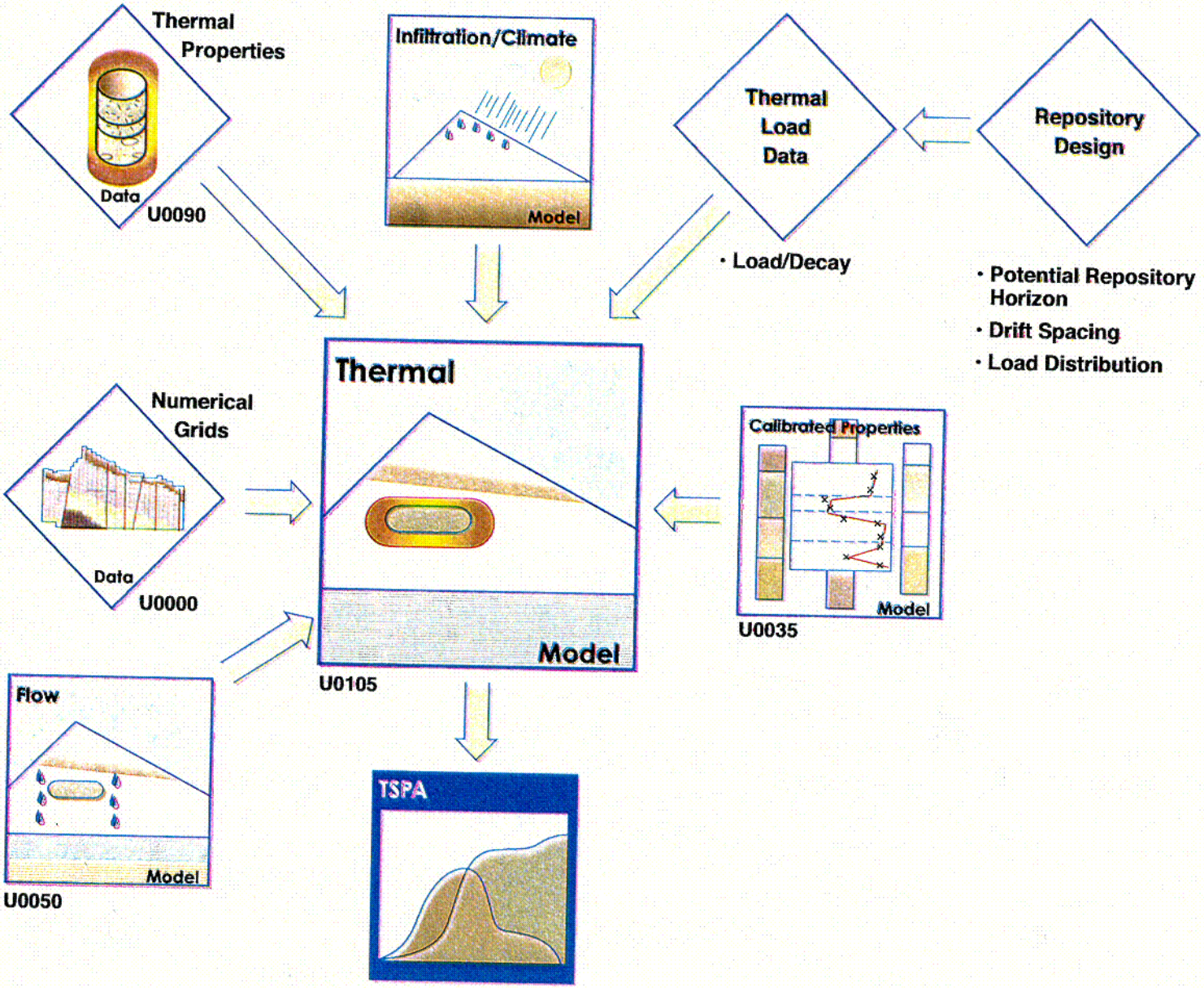

Figure 3.12-2. Schematic Showing Input Data and the UZ Models that Support the Development of the TH Model

C123

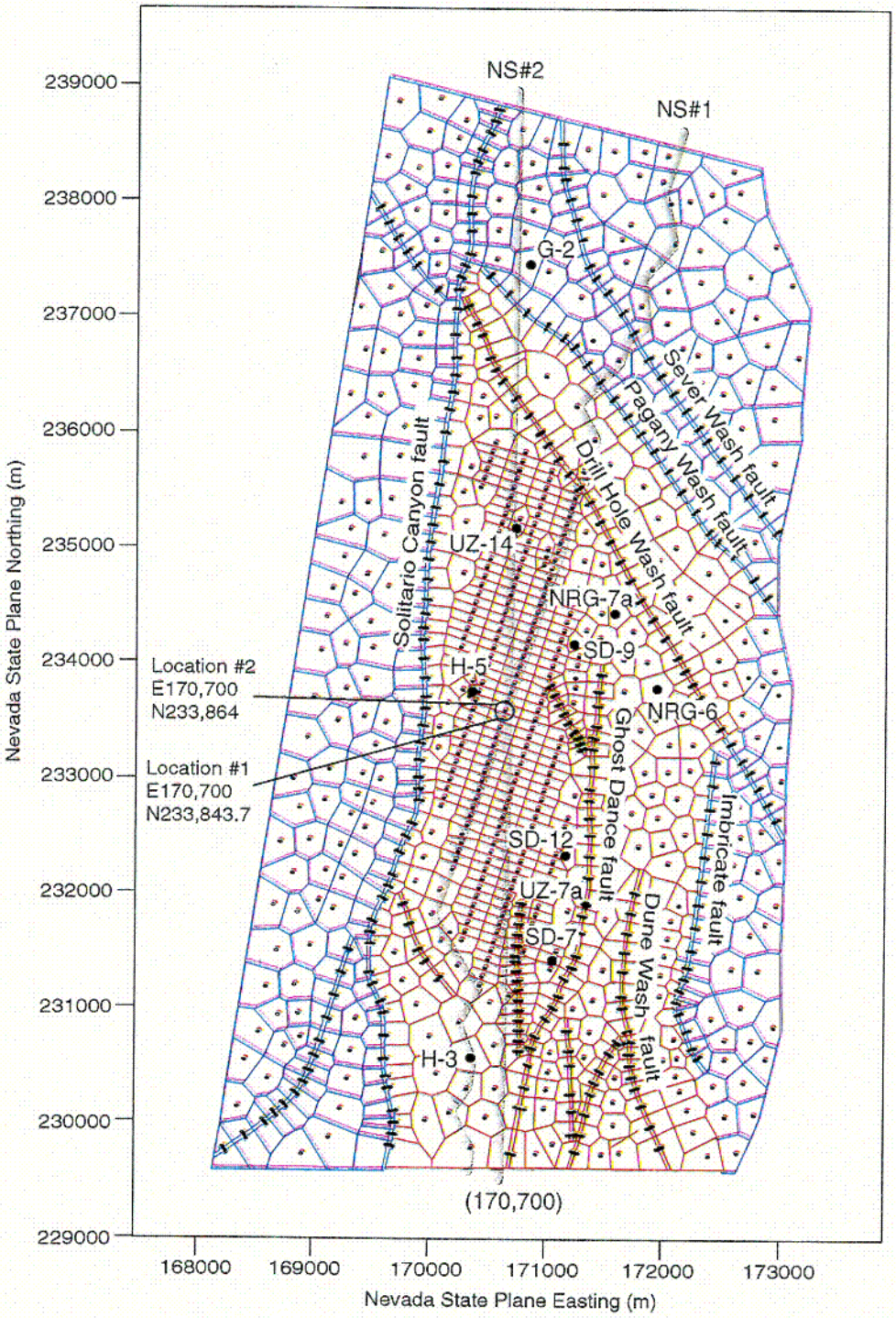

Figure 3.12-3. Plan View of the UZ TSPA Grid, Showing the Location of the Potential Repository Submodel Domain (in Red) and the Cross Sections, NS#1 and NS#2. Locations #1 and #2 are Used for Detail Plots. Large solid circles refer to boreholes; small circles refer to centers of grid columns (adapted from CRWMS M&O 2000, U0105, Figure 1).

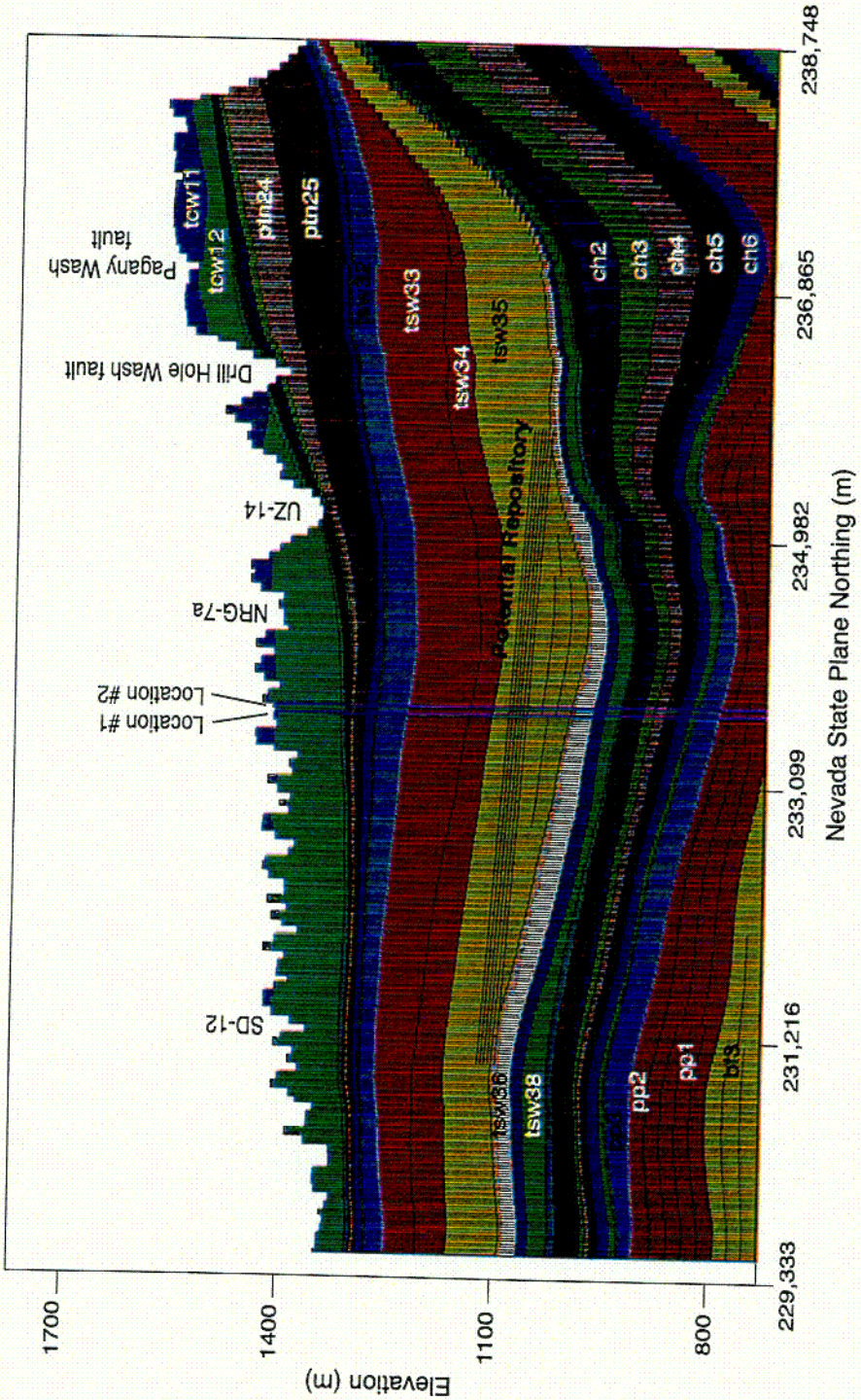

Figure 3.12-4. Lateral and Vertical Discretization at the NS#2 Cross-Section Based on the Refined Numerical Grid. Plot shows location of the potential repository and the hydrogeologic units layering (adapted from CRWMS M&O 2000, U0105, Figure 3).

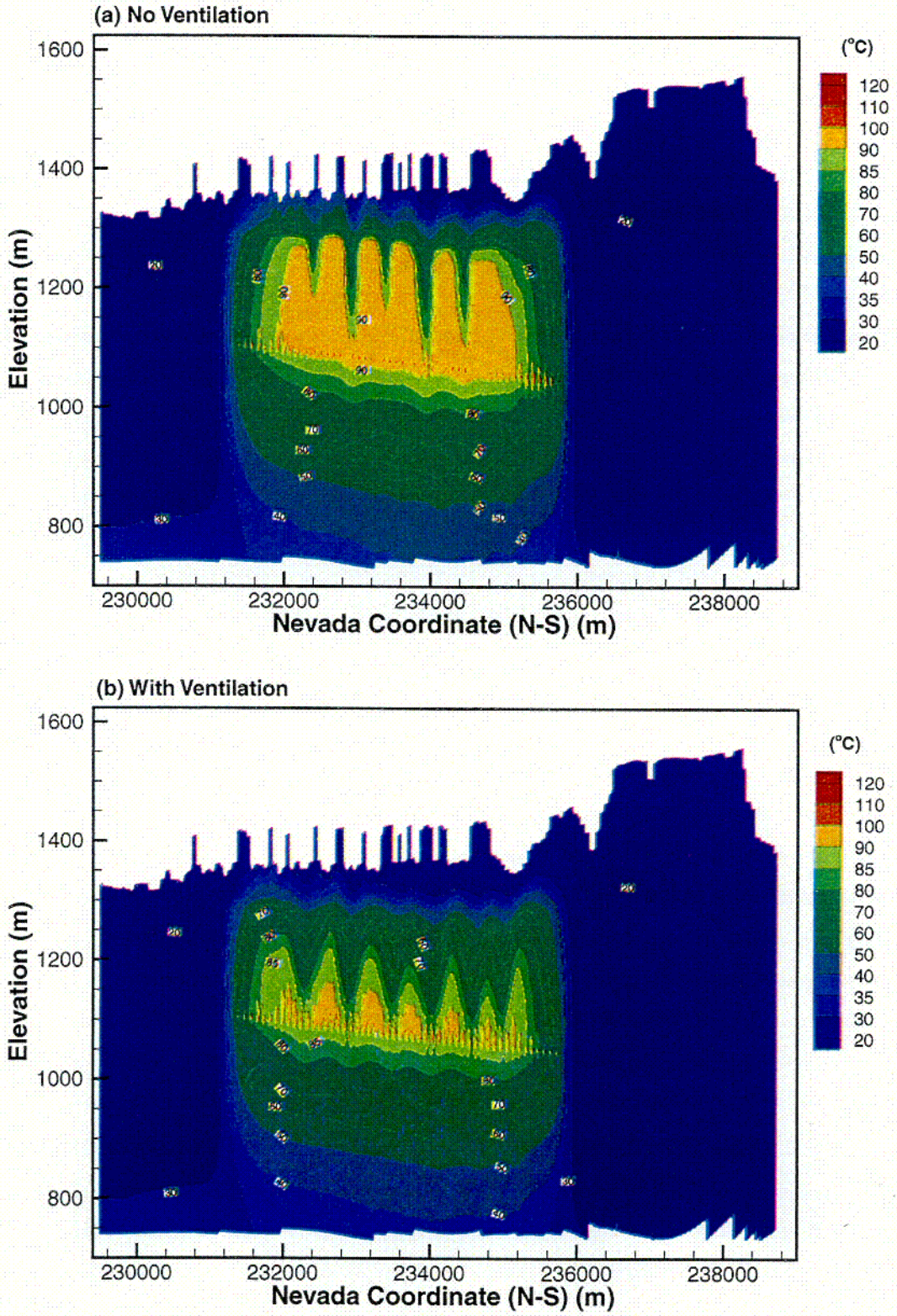

Figure 3.12-5. Temperature Distribution along NS#2 Cross-Section Grid at 1,000 Years (a) No Ventilation, (b) with Ventilation (Adapted from CRWMS M&O 2000, U0105, Figures 45 and 59).

C/26

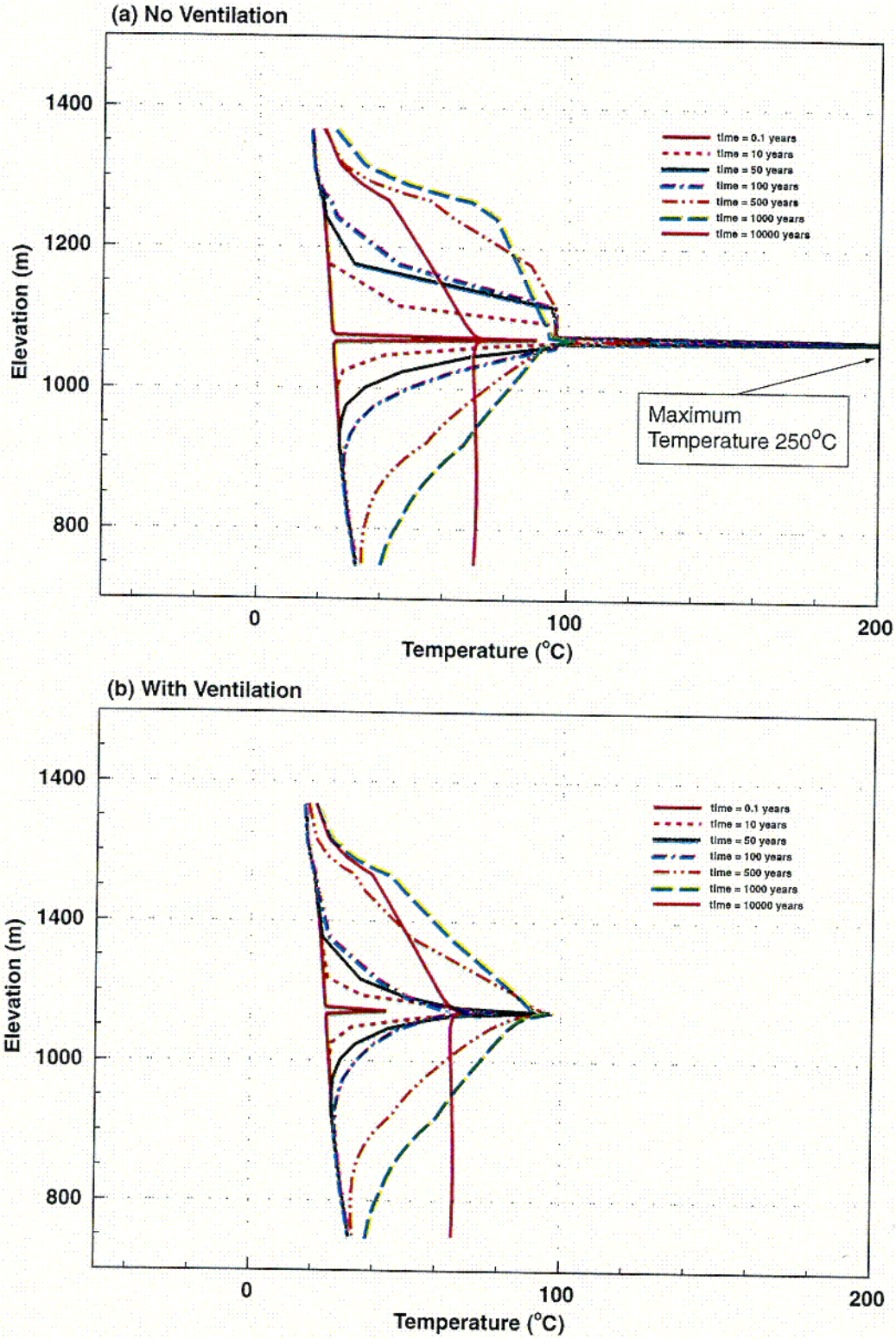

Figure 3.12-6. Temperature at Location #1, NS#2 Cross-Section Grid (a) No Ventilation (b) with Ventilation (Adapted from CRWMS M&O 2000, U0105, Figures 46 and 60).

C/27

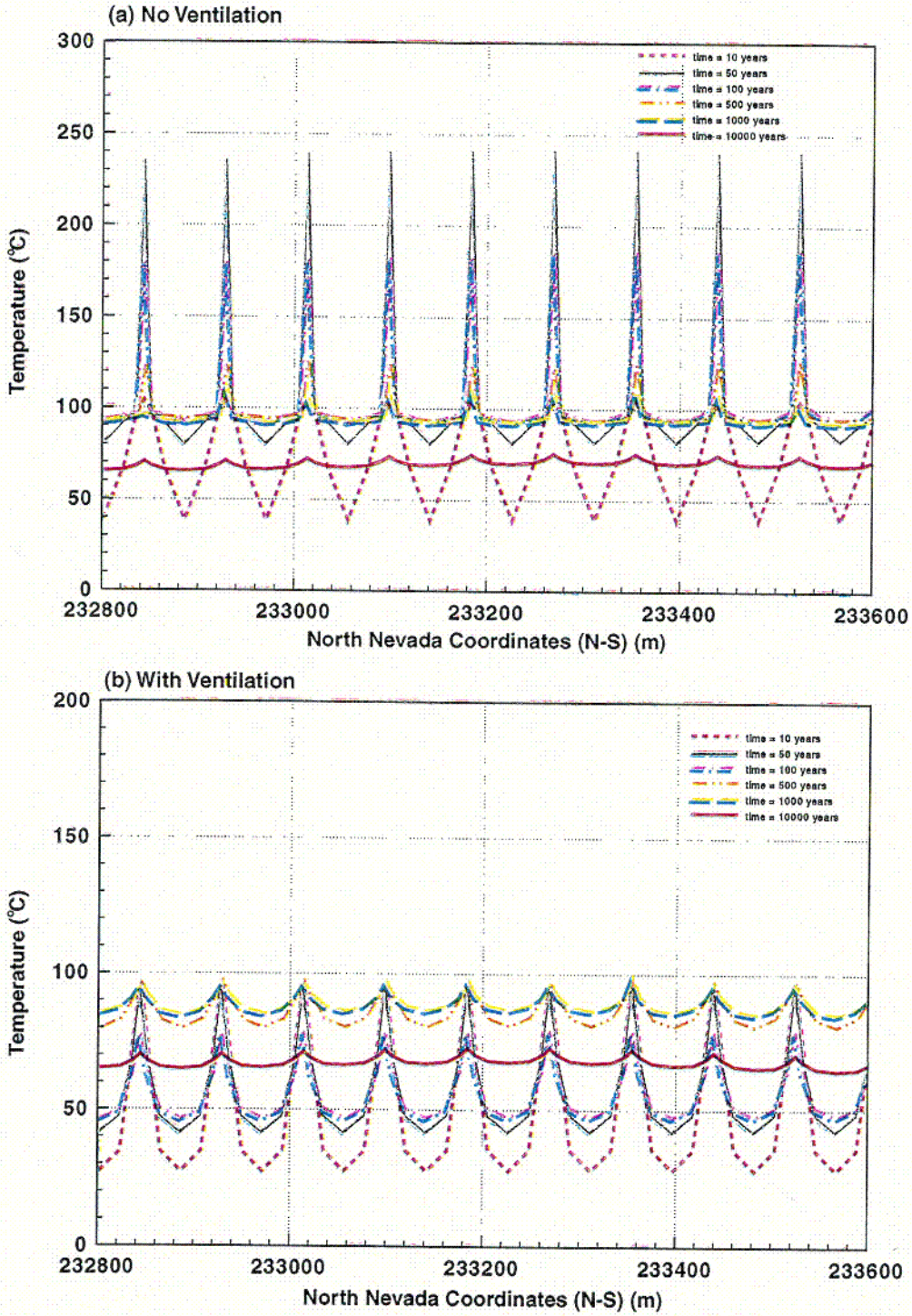

Figure 3.12-7. Temperature along a Section of the Potential Repository Horizon of the NS#2 Cross-Section Grid (a) No Ventilation, (b) with Ventilation (Adapted from CRWMS M&O 2000, U0105, Figures 48 and 62).

C128

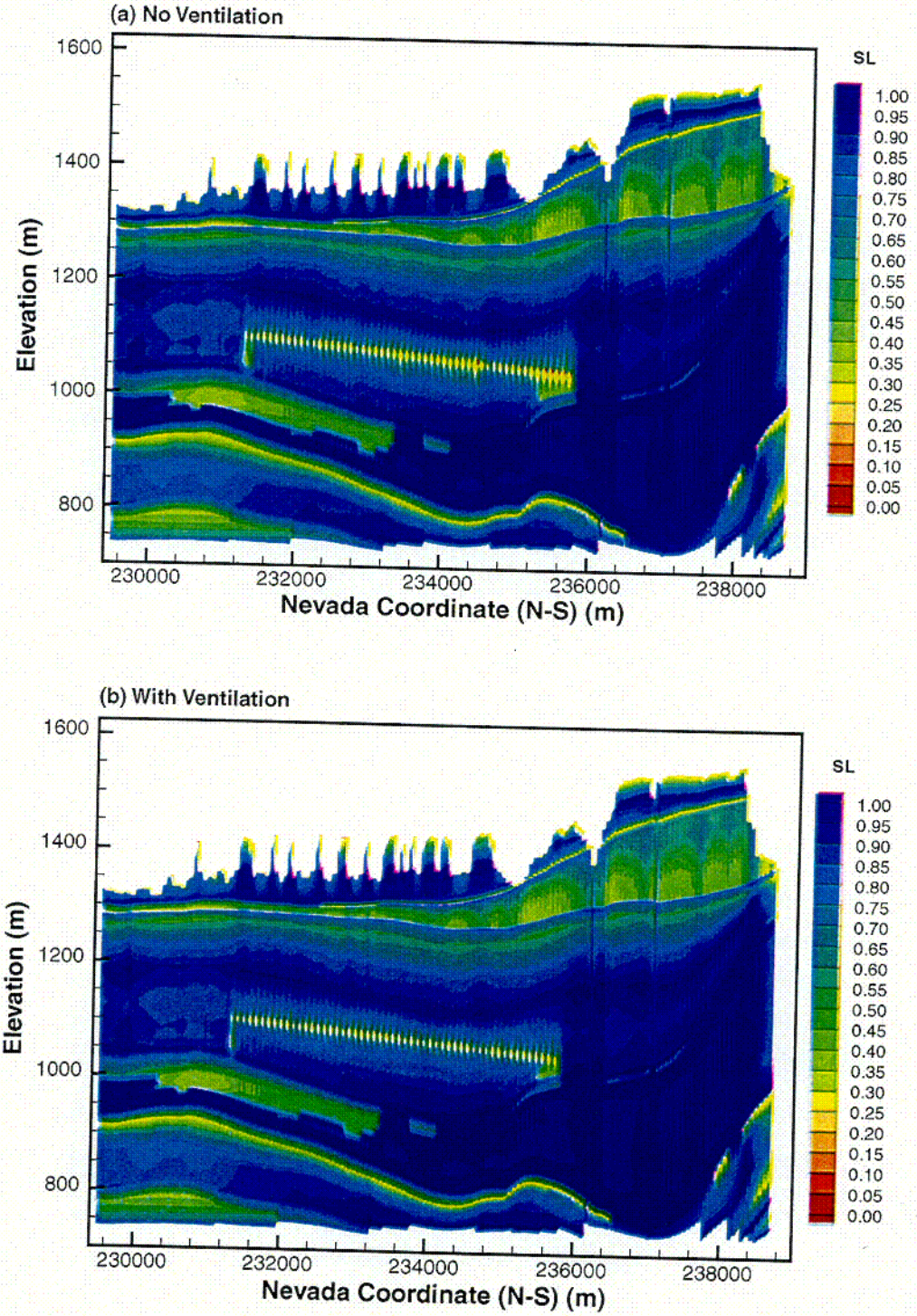

Figure 3.12-8. Matrix Liquid Saturation (SI) along NS#2 Cross-Section Grid at 1,000 Years (a) No Ventilation, (b) with Ventilation (Adapted from CRWMS M&O 2000, U0105, Figures 50 and 64).

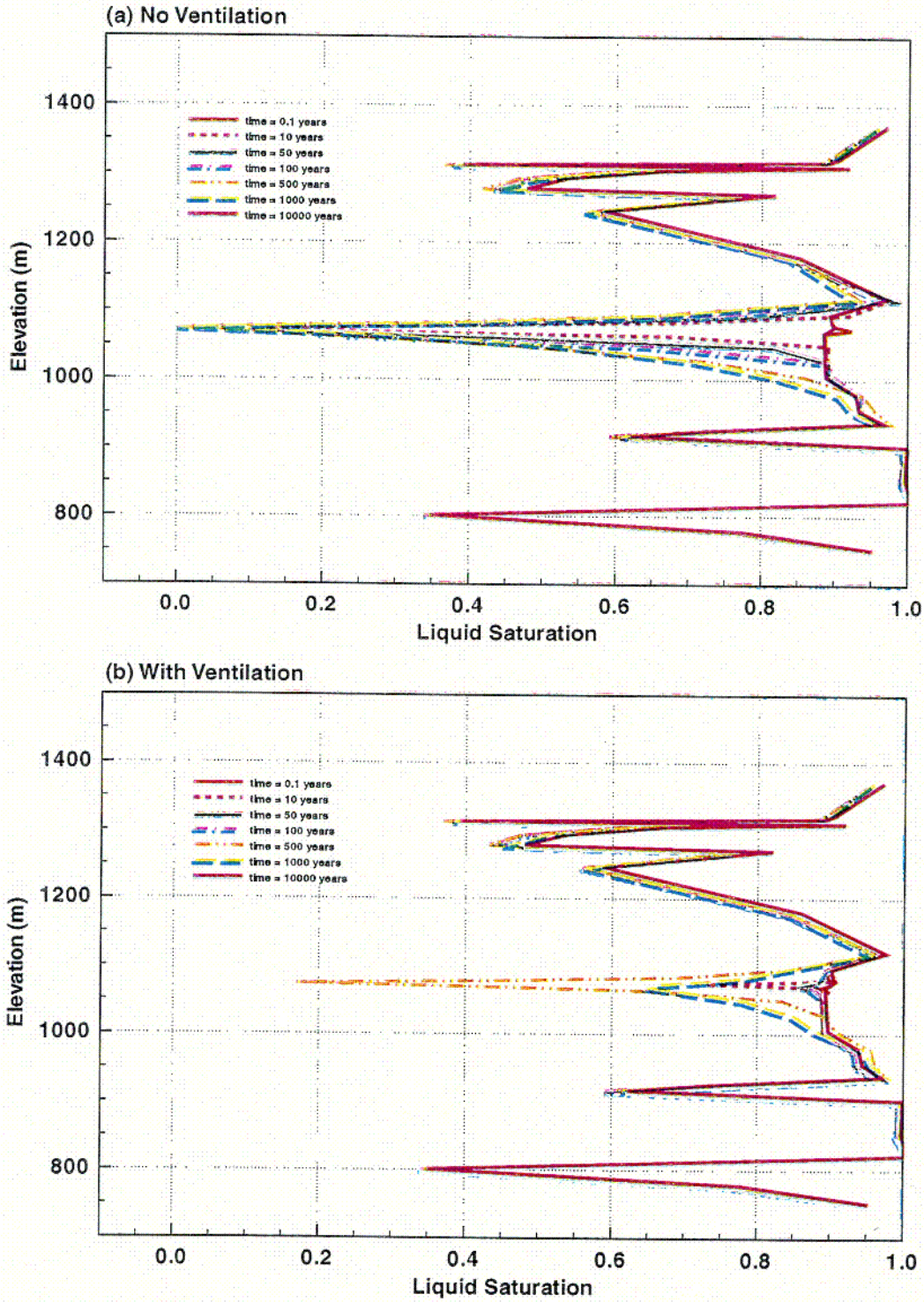

Figure 3.12-9. Matrix Liquid Saturation at Location#1, NS#2 Cross-Section Grid (a) No Ventilation, (b) with Ventilation (Adapted from CRWMS M&O 2000, U0105, Figures 51 and 65).

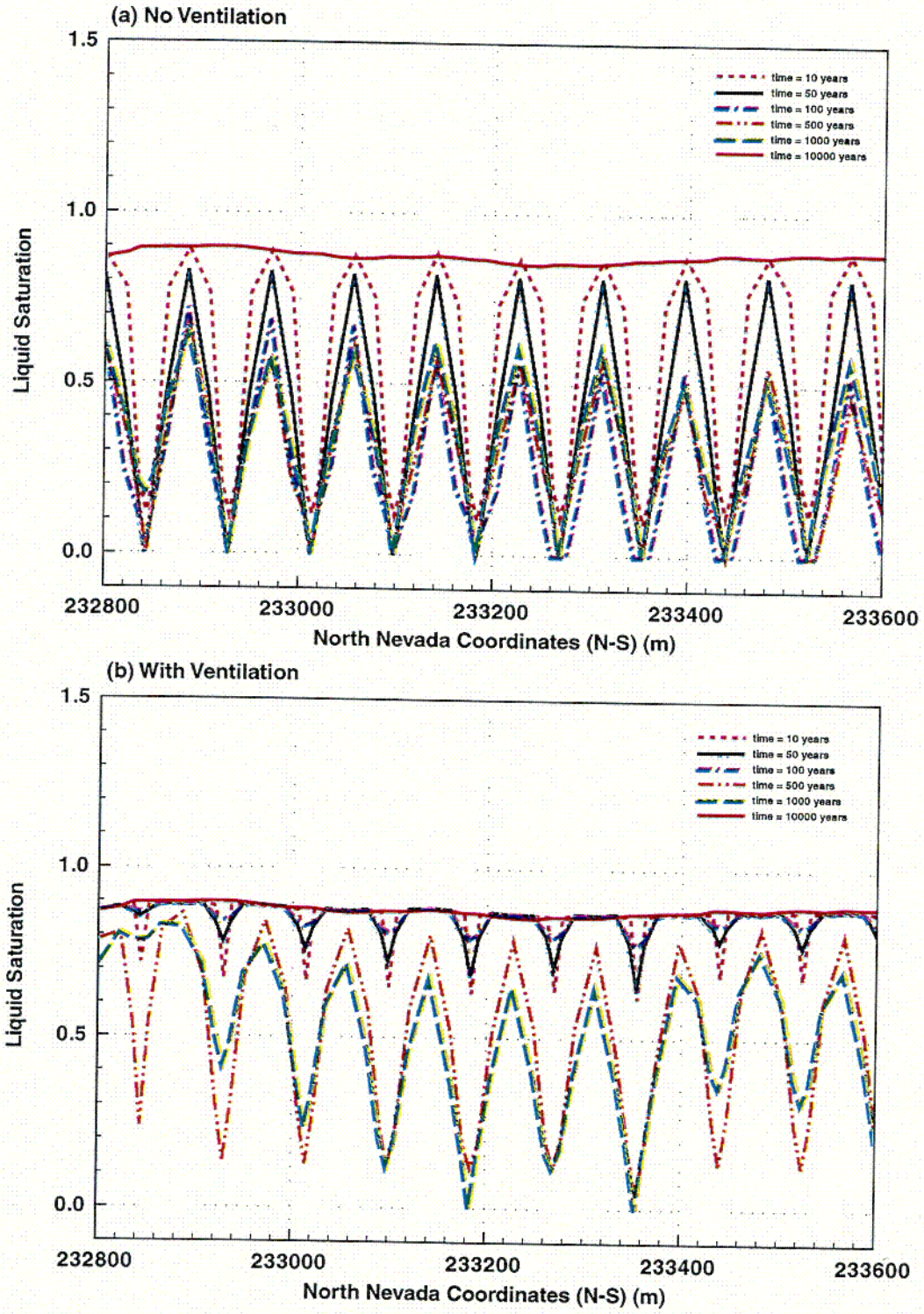

Figure 3.12-10. Matrix Liquid Saturation along a Section of the Potential Repository Horizon, NS#2 Cross-Section Grid (a) No Ventilation, (b) with Ventilation (Adapted from CRWMS M&O 2000, U0105, Figures 52 and 66).

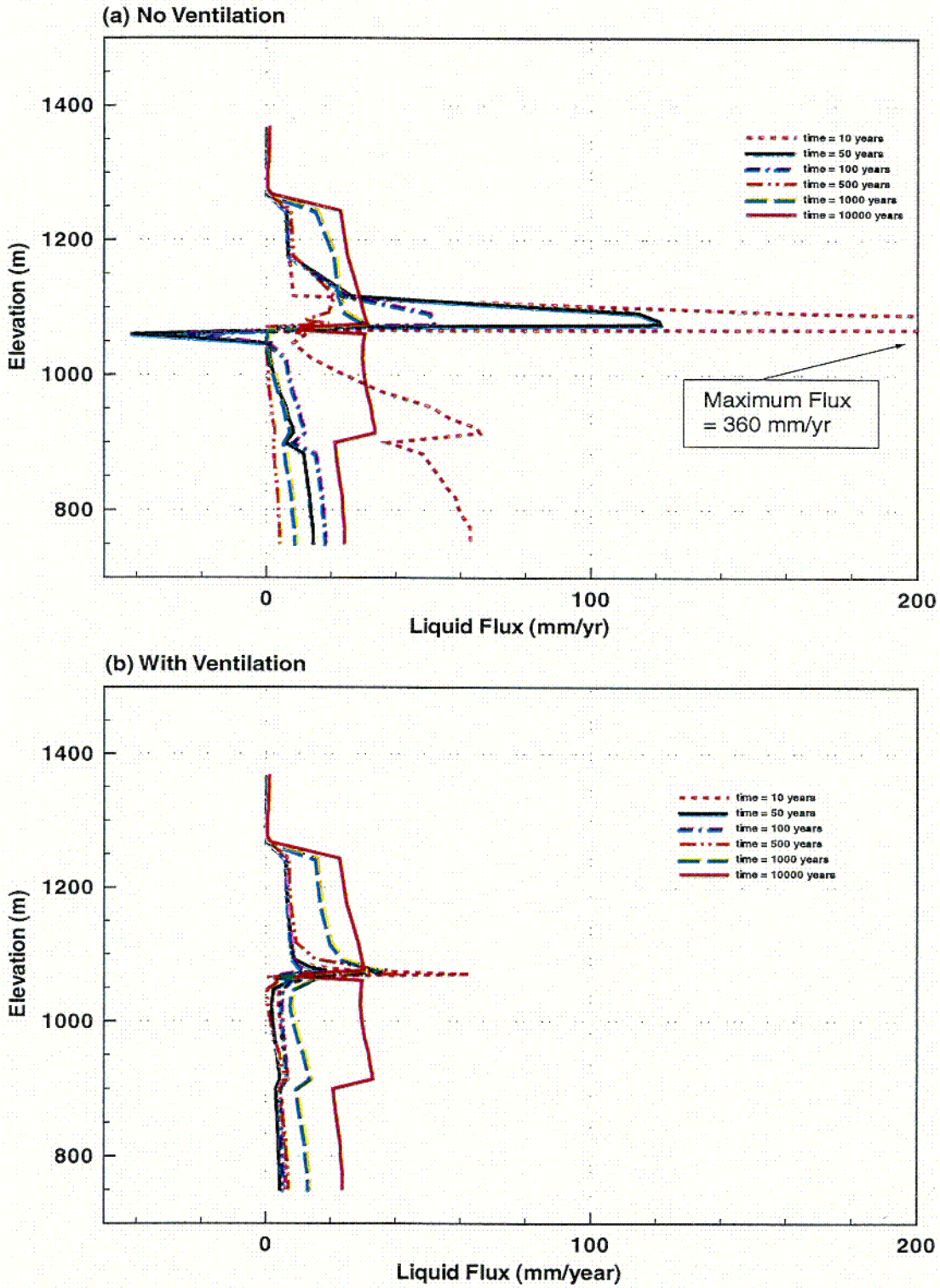

Figure 3.12-11. Fracture Liquid Flux at Location #1,NS#2 Cross-Section Grid (a) No Ventilation, (b) With Ventilation (Adapted from CRWMS M&O 2000, U0105, Figures 53 and 67).

C132

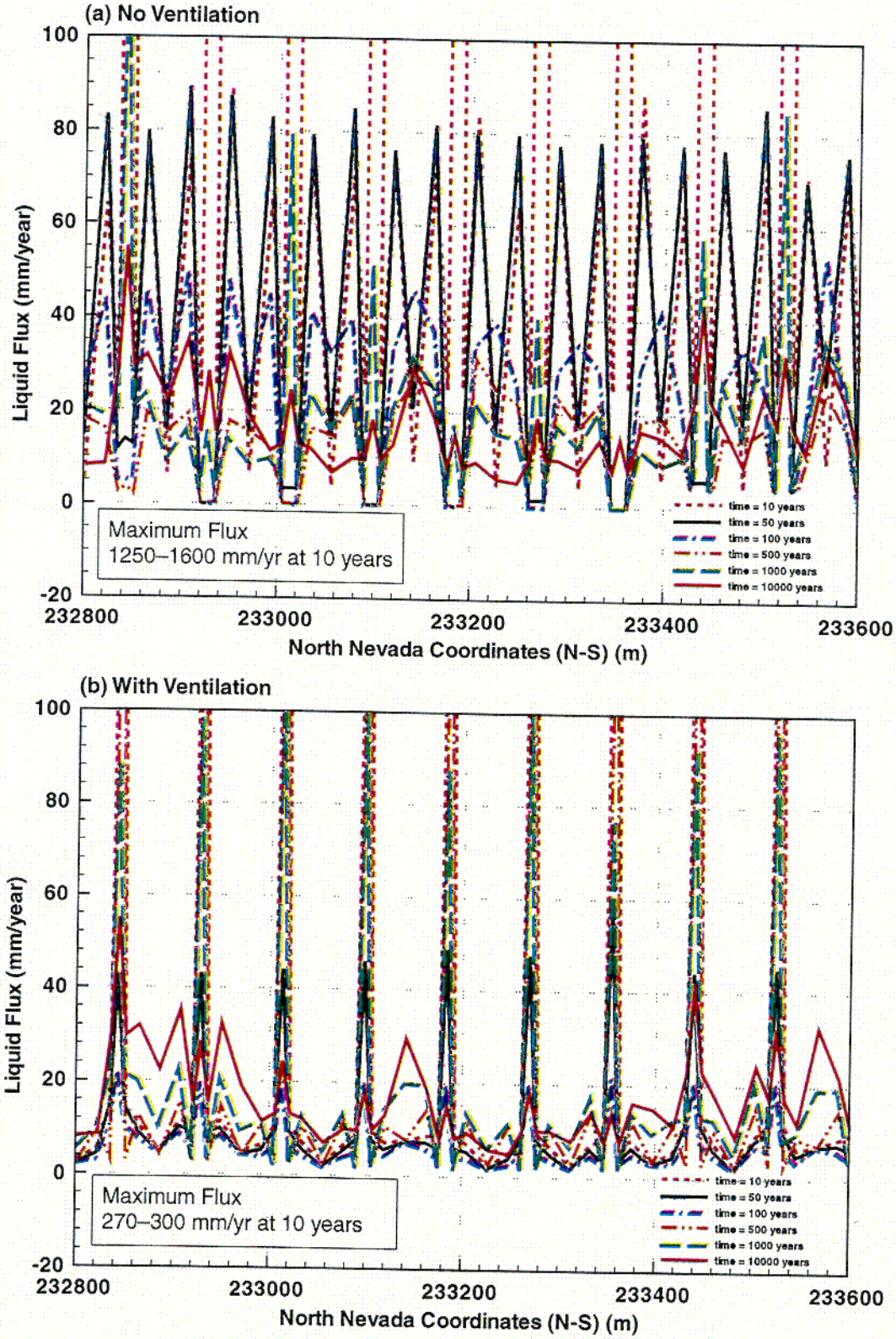

Figure 3.12-12. Fracture Liquid Flux along a Section of the Potential Repository Horizon, NS#2 Cross-Section Grid (a) No Ventilation, (b) with Ventilation (Adapted from CRWMS M&O 2000, U0105, Figures 55 and 69).

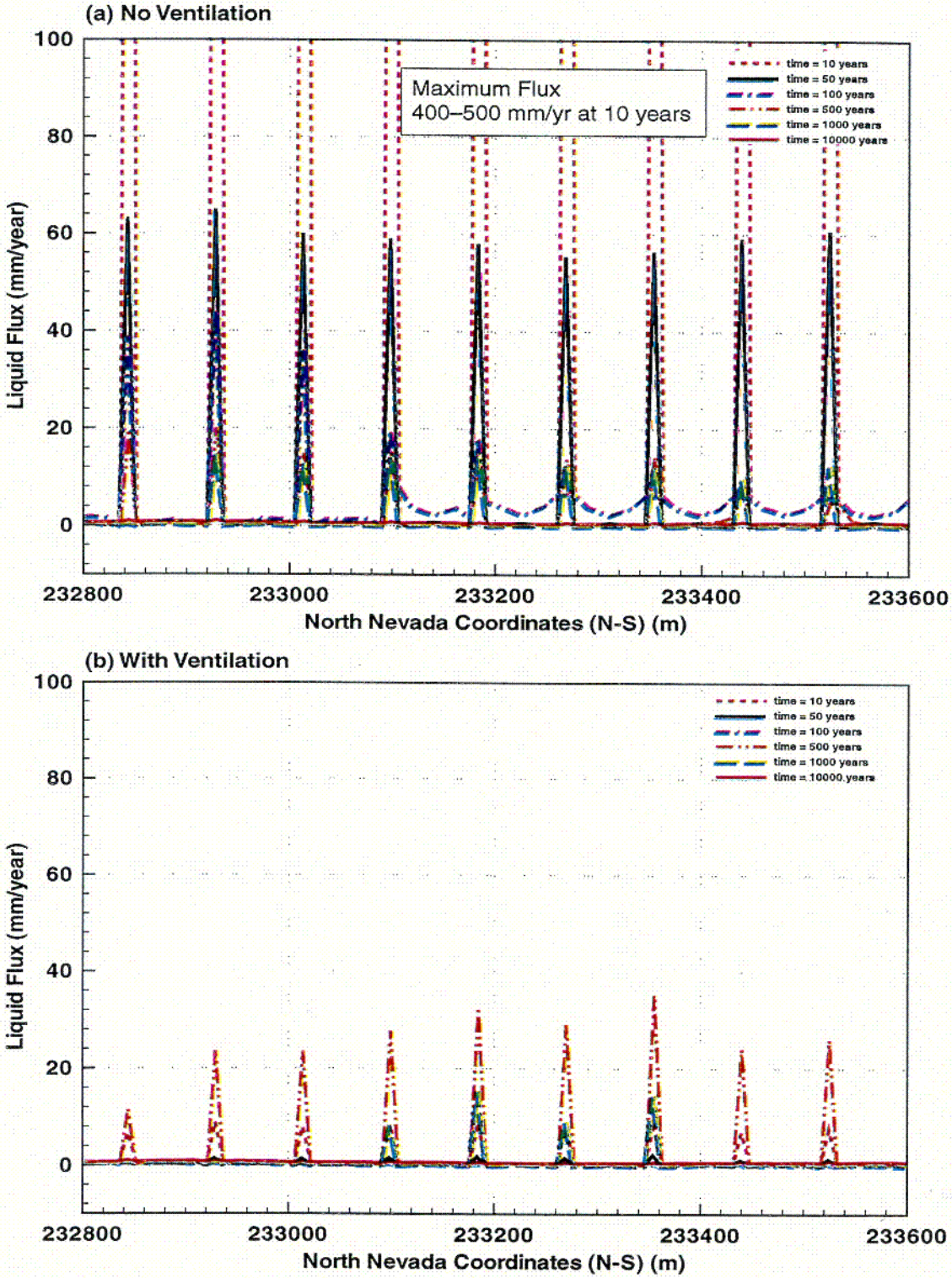

Figure 3.12-13. Matrix Liquid Flux along a Section of the Potential Repository Horizon, NS#2 Cross-Section Grid (a) No Ventilation, (b) with Ventilation (Adapted from CRWMS M&O 2000, U0105, Figures 56 and 70).

C134

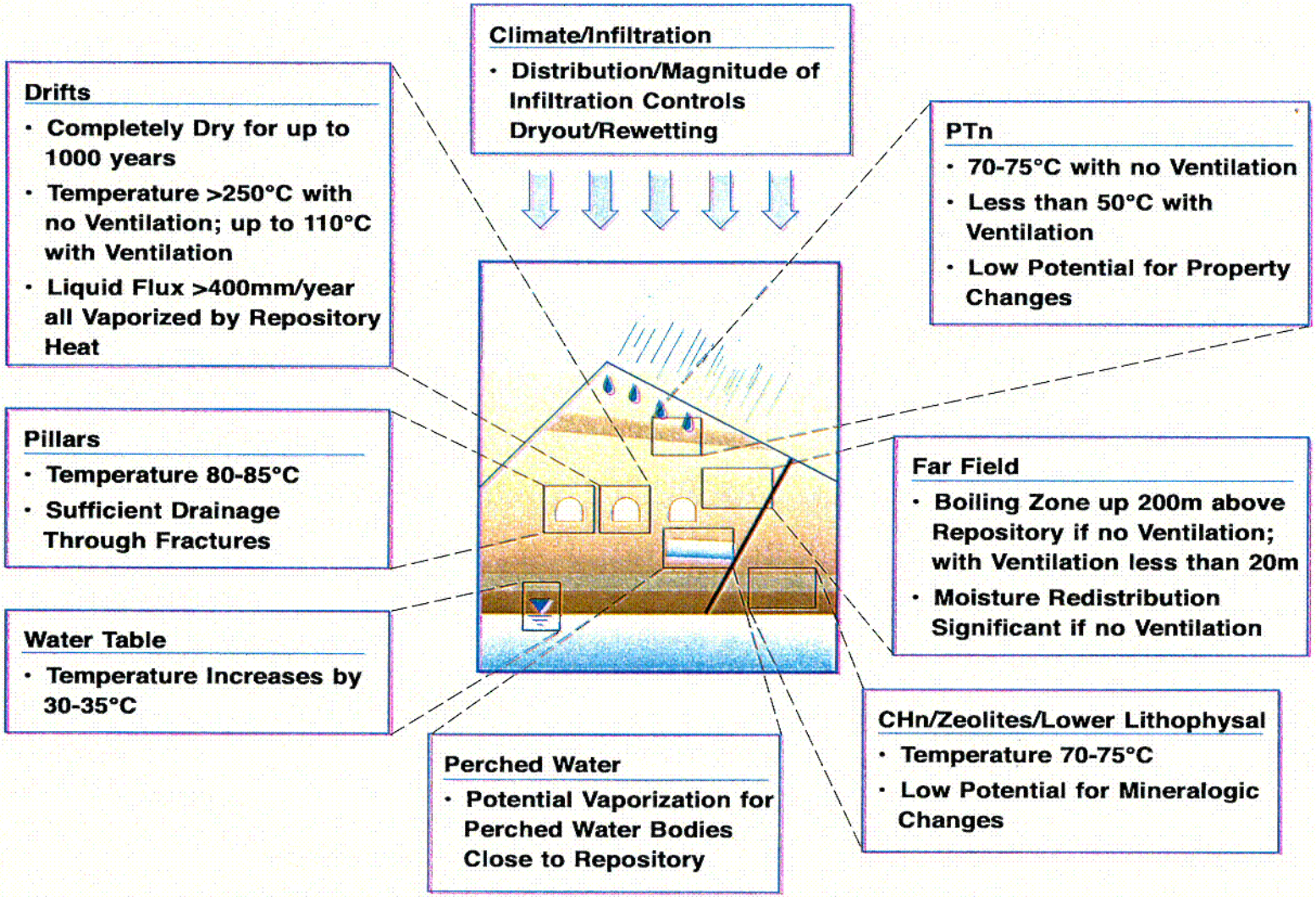

Figure 3.12-14. Summary of TH Model Results

C/35

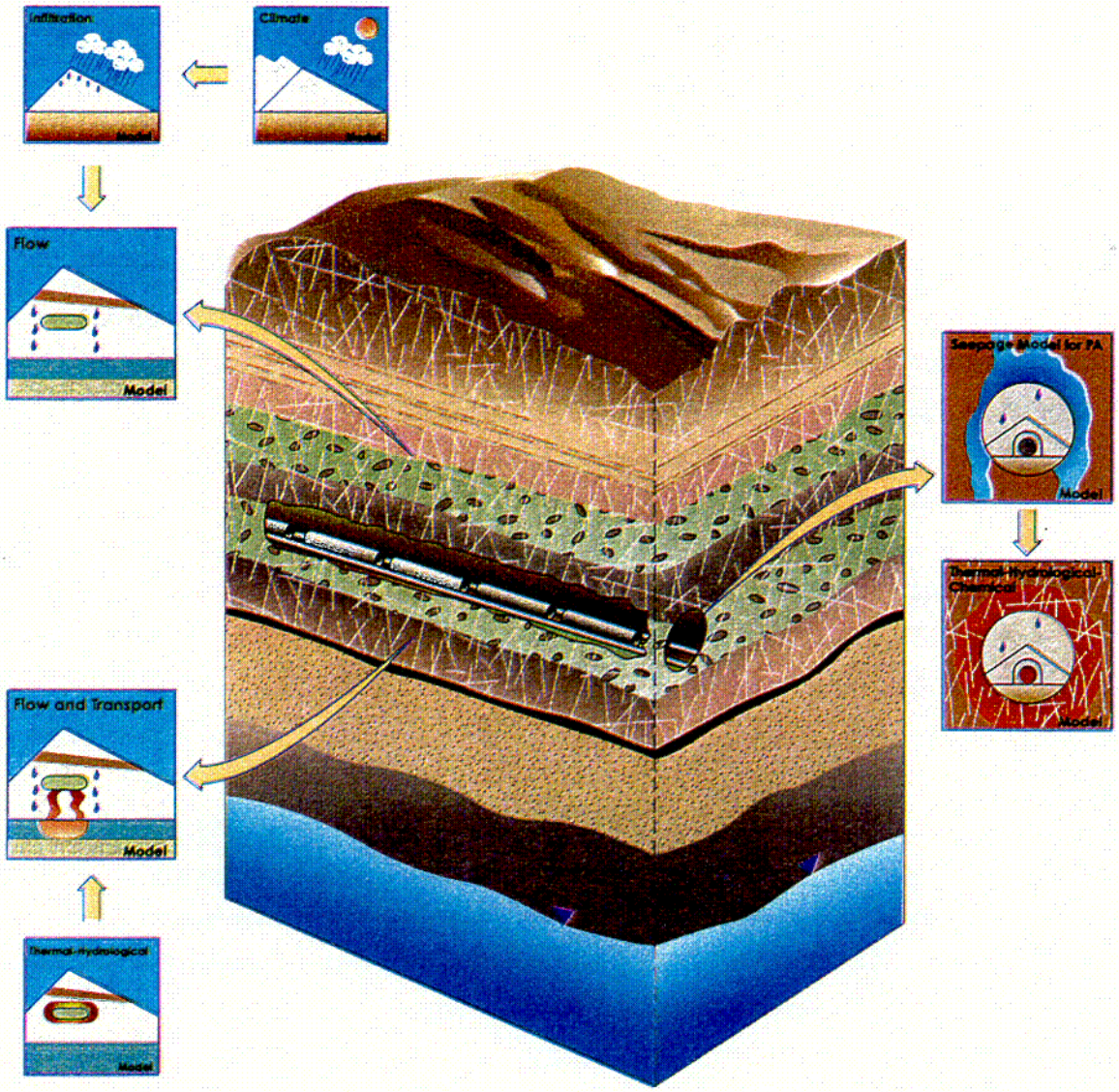

Figure 5.1-1. Conceptual Sketch of the UZ with Icons Representing Major Model Components

C136

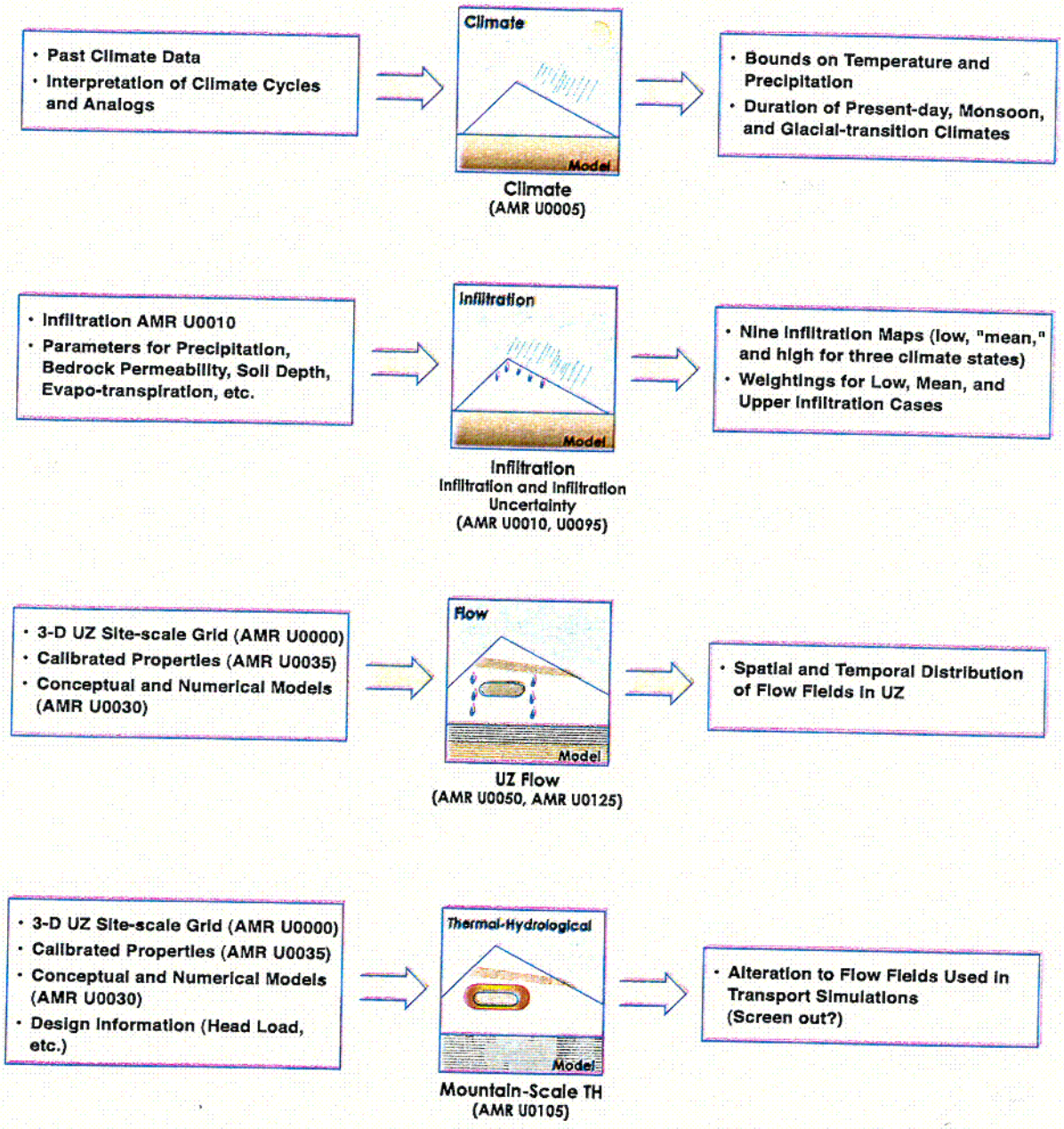

Figure 5.1-2. Schematic of Major Inputs and Outputs for UZ Flow Model and its Submodels

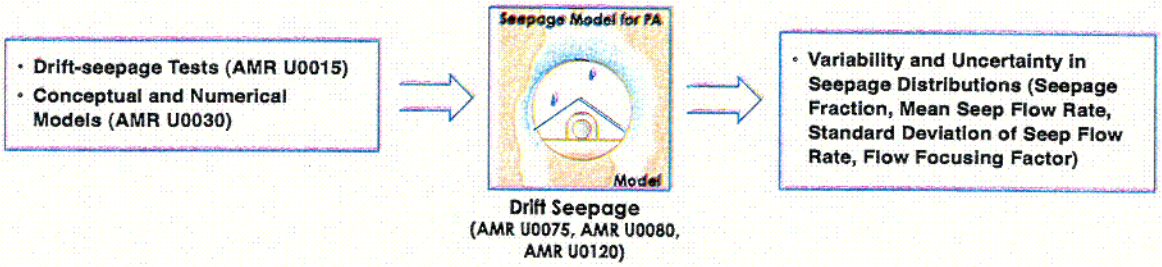

Figure 5.1-3. Schematic of Major Inputs and Outputs of the Drift Seepage Models

C138

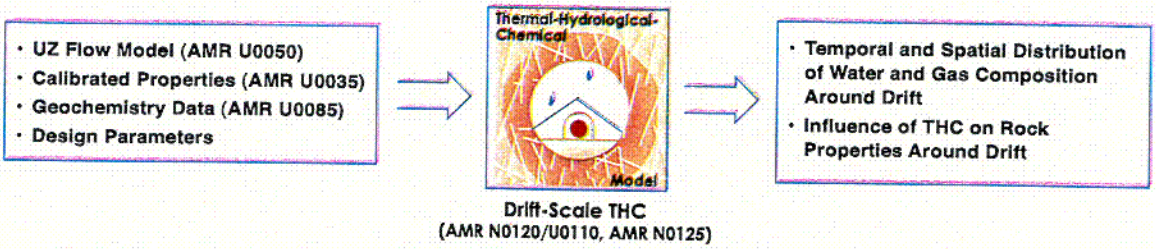

Figure 5.1-4. Schematic of Major Inputs and Outputs of the Drift-Scale THC Models

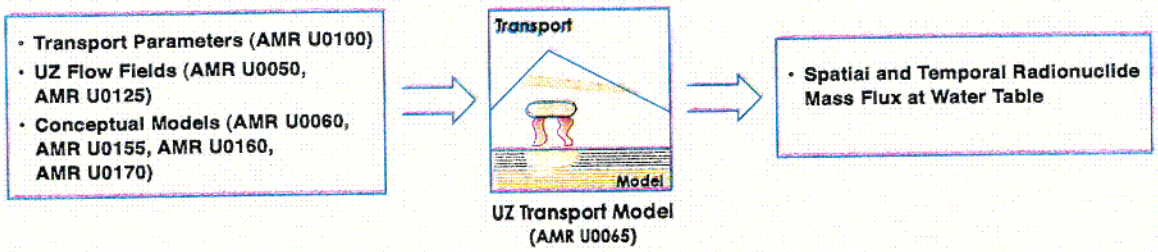

Figure 5.1-5. Schematic of Major Inputs and Outputs of the UZ Transport Models

C140